Copyright 2001

Dirk Schweitzer

Biomimetic Models of the Active Site of the Metalloenzyme Nitrile Hydratase

by

Dirk Schweitzer

A dissertation submitted in partial fulfillment of the
requirements for the degree of

Doctor of Philosophy

University of Washington

2001

Program Authorized to Offer Degree: Chemistry

This is to certify that I have examined this copy of a doctoral dissertation by

Dirk Schweitzer

and have found that it is complete and satisfactory in all respects,
and that any and all revisions required by the final
examining committee have been made.

Chair of Supervisory Committee:

_____

Julia A. Kovacs

Reading Committee:

_____

Craig C. Beeson

_____

Heinz-Günter Floss

Date: _____

In presenting this dissertation in partial fulfillment of the requirements for the Doctoral degree at the University of Washington, I agree that the Library shall make its copies freely available for inspection. I further agree that extensive copying of the dissertation is allowable only for scholarly purposes, consistent with "fair use" as prescribed in the U.S. Copyright Law. Requests for copying or reproduction of this dissertation may be referred to Bell and Howell Information and Learning, 300 North Zeeb Road, P. O. Box 1346, Ann Arbor, MI 48106-1346, to whom the author has granted "the right to reproduce and sell (a) copies of the manuscript in microform and/or (b) printed copies of the manuscript made from microform."

Signature _____

Date _____

University of Washington

Abstract

Biomimetic Models of the Active Site of the Metalloenzyme Nitrile Hydratase

by Dirk Schweitzer

Chairperson of the Supervisory Committee

Professor Julia A. Kovacs
Department of Chemistry

An Fe(III)-NO-bound model compound, $[Fe(III)S_2^{Me2}N_3(Pr,Pr)(NO)]PF_6$ (**1-NO**), is prepared. Its electronic properties are nearly identical to those of the active site in NO-inactivated NHase. Therefore, the assignment of the active site in NO-inactivated NHase as being $\{FeNO\}^6$ is supported. The stability of **1-NO** demonstrates that the 'claw' structure observed in NHase is not necessary to stabilize an Fe(III)-NO species.

To examine how small structural changes influence the reactivity of metal complexes, a series of related Fe(III) thiolate complexes was synthesized and characterized. A hexacoordinated Fe(III) complex containing an η^2-coordinated persulfide is described, $[Fe(III)(S_2^{Me2}N_3(Et,Pr))\text{-}S^{pers}]PF_6$ (**4**). It is the first structurally characterized, first row transition metal-η^2-persulfide complex. This complex is a model for the possible interaction between cysteine persulfide (thiocysteine, cysteine perthiolate) and Fe(III) in biological systems. The extra

persulfide sulfur can be removed to afford a pentacoordinated compound, $[Fe(III)S_2^{Me2}N_3(Et,Pr)]PF_6$ (**5**), which possesses a more open binding site than the previously reported, pentacoordinated model compound $[Fe(III)S_2^{Me2}N_3(Pr,Pr)]PF_6$ (**1**). A comparison of the reaction of **1** and **5** with azide provides a model system for the concept of entatic state.

Further, the Fe(III) coordination chemistry of N,N'-1,2-ethanediylbis[2-mercapto-2-methyl-propanamide] was investigated. Thereby, two compounds, $(NMe_4)_2[(Fe(III)S_2^{Me2}N_2^{amide}(Et))_2]$ (**6**) and $(NMe_4)[Fe(III)S_2^{Me2}N_2^{amide}(Et)(Py)]$ (**7**), were isolated that contain deprotonated carboxamide nitrogens coordinated to Fe(III). The deprotonated carboxamide nitrogens provide significant stabilization to the + 3 oxidation state of the Fe(III) ion, as indicated by the reduction potential. A comparison of pentacoordinated, carboxamide nitrogen-coordinated **7** with another pentacoordinated, imine nitrogen-coordinated model compound provides evidence that an imine group is a valid structural and electronic model for a carboxamide.

TABLE OF CONTENTS

	Page
List of Figures.....	v
List of Tables.....	ix
Numbered Compounds.....	x
Chapter I: Introduction.....	1
Bioinorganic Chemistry.....	1
Nitrile Hydratase - Its Physiological Role.....	3
Nitrile Hydratase - Structure of the Active Site.....	4
Nitrile Hydratase - Possible Mechanisms of Nitrile Hydration.....	12
Other Model Compounds of Nitrile Hydratase.....	14
Challenges of Fe(III)/Co(III)-Thiolate Chemistry.....	18
Chapter II: A Model Compound of the Active Site of the NO-Inactivated Form of Nitrile Hydratase.....	20
Introduction.....	20
Synthesis of Model Compound.....	21
Properties of the Model Compound and Relevance to the Active Site of Nitrile Hydratase.....	22
Electronic Structure of Model Compounds.....	29
Abbreviated Qualitative MO Diagram of the $\mathbf{1}^+$ Ion.....	30
Abbreviated Qualitative MO Diagram of the $\mathbf{1\text{-}NO}^+$ Ion.....	34

Chapter III: The Influence of a Small Structural Change on the Reactivity of Metal Complexes..... 38
Introduction..... 38
Synthesis and Characterization of **4**..... 38
Synthesis and Characterization of **5**..... 47
Synthesis and Characterization of **5-N$_3$**..... 54
Thermodynamic Equilibrium Study of Azide Binding..... 63
The Concept of Entatic State..... 66
Comparing the Reactivity of **1** and **5** - A Model for the Entatic State..... 68
Chapter IV: Fe(III) Complexes of an $(N_{amide})_2(S_{thiolate})_2$ Ligand..... 72
Introduction..... 72
Synthesis and Crystal Structure of Dimeric **6**..... 73
Reactivity Studies of Dimeric **6**..... 77
Synthesis and Crystal Structure of Monomeric Pyridine-Bound **7**..... 80
Comparison of Physical Properties of Dimeric **6** and Monomeric Pyridine-Bound **7**..... 83

Chapter V: Experimental Section..... 93

General Methods..... 93

X-ray Data Collection and

Structure Solution and Refinement..... 95

Magnetic Measurements..... 95

Azide Binding Studies..... 98

Titration of **6** with Pyridine..... 99

Synthesis and Characterization of

3-chloro-3-methyl-2-butanone..... 100

Synthesis and Characterization of

3-mercapto-3-methyl-2-butanone..... 101

Synthesis and Characterization of

$[Fe(III)S_2^{Me2}N_3(Pr,Pr)]PF_6$ (**1**)..... 102

Synthesis and Characterization of

$[Fe(III)S_2^{Me2}N_3(Pr,Pr)(NO)]PF_6$ (**1-NO**)..... 108

Synthesis and Characterization of

$[Fe(III)S_2^{Me2}N_3(Pr,Pr)(N_3)]$ (**1-N$_3$**)..... 112

Synthesis and Characterization of

$[Co(III)(S_2^{Me2}N_3(Pr,Pr))]PF_6$ (**2**)..... 113

Synthesis and Characterization of

$[Co(III)(S^{Me2}(S^{Me2}(O)_2)N_3(Pr,Pr))]PF_6$ (**2-O$_2$**)..... 115

Synthesis and Characterization of

$[Co(III)((\eta^2\text{-}S^{Me2}O)(S^{Me2}(O)_2)N_3(Pr,Pr))]PF_6$ (**2-O$_3$**)..... 115

Synthesis and Characterization of

$[Fe(III)(S_2^{Me2}N_3(Et,Pr))\text{-}S^{pers}]PF_6$ (**4**)..... 117

Synthesis and Characterization of
$[Fe(III)S_2^{Me2}N_3(Et,Pr)]PF_6$ (**5**)..... 119
Synthesis and Characterization of
$[Fe(III)S_2^{Me2}N_3(Et,Pr)(N_3)]$ (**5-N$_3$**)..... 123
Synthesis and Characterization of
N,N'-1,2-Ethanediylbis[2-mercapto-2-methyl-propanamide]... 125
Synthesis and Characterization of
$(NMe_4)_2[(Fe(III)S_2^{Me2}N_2^{amide}(Et))_2]$ (**6**)..... 127
Synthesis and Characterization of
$(NMe_4)[Fe(III)S_2^{Me2}N_2^{amide}(Et)(Py)]$ (**7**)..... 130
Chapter VI: Summary and Conclusions..... 132
References..... 134
Bibliography..... 163

LIST OF FIGURES

Number		*Page*
1-1	Biological pathways to convert nitriles to carboxylic acids...	3
1-2	Absorption spectrum of active and NO-inactivated NHase..	6
1-3	Proposed structure of the active site of NHase prior to the publication of the first crystal structure in 1997.....	7
1-4	Activity dependence of Fe-containing NHase.....	8
1-5	Schematic representation of the structure of the active site of Fe-containing NHase.....	10
1-6	Reasonable mechanisms for the hydration of nitriles by NHase	12
1-7	Other model compounds of NHase.....	14
1-8	Visible absorption spectrum of active Fe-containing NHase.	15
1-9	Visible absorption spectrum of $[Fe(III)(ADIT)_2]^+$.....	15
1-10	Thermal ellipsoid plot of the cation of **2-O$_3$**.....	16
2-1	Synthesis of **1-NO** from **1**.....	21
2-2	Absorption spectrum of **1-NO**.....	23
2-3	Thermal ellipsoid plot of the cation of **1-NO**.....	25
2-4	Coordinate systems for **1**$^+$ and **1-NO**$^+$.....	29
2-5	General qualitative MO diagram of a metal complex.....	31
2-6	Abbreviated qualitative MO diagram of the **1**$^+$ ion.....	33
2-7	Abbreviated qualitative MO diagram of the **1-NO**$^+$ ion.....	35

2-8 Graphical representation of the formation of a σ and π bond between Fe and NO..... 36
2-9 MO diagram of NO..... 36
3-1 Syntheses of **1** and **4**..... 40
3-2 Thermal ellipsoid plot of **3**..... 41
3-3 Thermal ellipsoid plot of the cation of **4**..... 43
3-4 Solid state effective paramagnetic magnetic moment of **4**..... 45
3-5 EPR spectrum of **4**..... 46
3-6 UV/Vis absorption spectrum of **4**..... 46
3-7 Synthesis of **5** from **4**..... 47
3-8 Thermal ellipsoid plot of the cation of **1**..... 48
3-9 Thermal ellipsoid plot of the cation of **5**..... 49
3-10 Solid state effective paramagnetic magnetic moment of **1** and **5** 52
3-11 EPR spectra of **1** and **5**..... 53
3-12 UV/Vis absorption spectra of **1** and **5**..... 53
3-13 Synthesis of **5-N$_3$** from **5**..... 54
3-14 Thermal ellipsoid plot of **1-N$_3$**..... 56
3-15 Thermal ellipsoid plot of **5-N$_3$**..... 57
3-16 Solid state effective paramagnetic magnetic moment of **1-N$_3$** and **5-N$_3$**..... 60
3-17 EPR spectra of **1-N$_3$** and **5-N$_3$**..... 61
3-18 UV/Vis absorption spectra of **1-N$_3$** and **5-N$_3$**..... 62
3-19 UV/Vis absorption spectra showing the temperature dependent equilibrium **5** + N_3^- = **5-N$_3$** + PF_6^- in MeOH..... 63

3-20 Van't Hoff plot for the binding of azide to **1** and **5** in MeOH at I = 0.06 mol/l..... 66

3-21 Reaction coordinate of a single-step chemical reaction..... 67

4-1 Synthesis of dimeric **6**..... 73

4-2 Thermal ellipsoid plot of the anion of **6**..... 74

4-3 Synthesis of **7** from **6**..... 80

4-4 Titration of a solution of **6** in CH_2Cl_2 with pyridine..... 81

4-5 Diagram showing the absorbance at 487 nm as a function of the ratio pyridine/dimer (**6**)..... 82

4-6 Thermal ellipsoid plot of the anion of **7**..... 83

4-7 Solid state effective paramagnetic magnetic moment of **6** and **7** 84

4-8 EPR spectra of **6** and **7**..... 86

4-9 Electronic absorption spectra of **6** and **7**..... 87

4-10 Abbreviated qualitative MO diagram of the anion of **7**..... 88

4-11 Structures of the anion of **7** and its N_{imine}-containing analogue. 89

4-12 Diagram showing the two possible resonance structures of a deprotonated, N-coordinated carboxamido group..... 90

5-1 Setup for Evans method..... 97

5-2 UV/Vis absorption spectrum of **1**..... 105

5-3 ^{1}H NMR spectrum of **1** in MeCN at RT..... 107

5-4 Details of ^{1}H NMR spectrum of **1** in MeCN at RT..... 107

5-5 ^{1}H NMR spectrum of **1-NO** in MeCN at RT..... 109

5-6 Details of ^{1}H NMR spectrum of **1-NO** in MeCN at RT..... 110

5-7 IR spectrum of **1-NO**..... 111

5-8 IR spectrum of **4**..... 119

5-9 Thermal ellipsoid plot of the cation of **5**. The disorder about the imposed two-fold axis is shown..... 121

5-10 IR spectrum of **5**..... 122

5-11 IR spectrum of **5-N_3**..... 125

5-12 IR spectrum of N,N'-1,2-ethanediylbis[2-mercapto-2-methyl-propanamide]..... 126

5-13 IR spectrum of **6**..... 128

5-14 IR spectrum of **7**..... 131

LIST OF TABLES

Number		*Page*
1-1	Selected bond distances and angles of the active site of Fe-containing NO-inactivated nitrile hydratase.....	11
2-1	EXAFS parameters of NO-inactivated NHase and of **1-NO**	21
2-2	Comparison of 'NO' parameters.....	24
2-3	Selected bond distances and angles of **1-NO**.....	27
3-1	Selected bond distances and angles of **4**.....	44
3-2	Selected bond distances and angles of **3**, **5**, and **1**.....	50
3-3	Selected bond distances and angles of **1-N$_3$** and **5-N$_3$**.....	58
3-4	Equilibrium constants for the reaction of **1** and **5** with azide in MeOH at I = 0.06 mol/l.....	65
3-5	Thermodynamic parameters of azide binding to **1** and **5** in MeOH at I = 0.06 mol/l.....	69
4-1	Selected bond distances and angles of **6** and **7**.....	75
4-2	Summary of **6** reactivity studies.....	78
5-1	Crystallographic data for **1-NO** and **4**.....	116
5-2	Crystallographic data for **5** and **5-N$_3$**.....	122
5-3	Crystallographic data for **6** • 2 MeOH and **7** • 2 MeOH.....	129

NUMBERED COMPOUNDS

1	$[Fe(III)S_2^{Me2}N_3(Pr,Pr)]PF_6$
1-NO	$[Fe(III)S_2^{Me2}N_3(Pr,Pr)(NO)]PF_6$
1-N$_3$	$[Fe(III)S_2^{Me2}N_3(Pr,Pr)(N_3)]$
2	$[Co(III)(S_2^{Me2}N_3(Pr,Pr))]PF_6$
2-O$_2$	$[Co(III)(S^{Me2}(S^{Me2}(O)_2)N_3(Pr,Pr))]PF_6$
2-O$_3$	$[Co(III)((\eta^2\text{-}S^{Me2}O)(S^{Me2}(O)_2)N_3(Pr,Pr))]PF_6$
3	$[Fe(II)S_2^{Me2}N_3(Et,Pr)]$
4	$[Fe(III)(S_2^{Me2}N_3(Et,Pr))\text{-}S^{pers}]PF_6$
5	$[Fe(III)S_2^{Me2}N_3(Et,Pr)]PF_6$
5-N$_3$	$[Fe(III)S_2^{Me2}N_3(Et,Pr)(N_3)]$
6	$(NMe_4)_2[(Fe(III)S_2^{Me2}N_2^{amide}(Et))_2]$
7	$(NMe_4)[Fe(III)S_2^{Me2}N_2^{amide}(Et)(Py)]$

Acknowledgements

First of all, I would like to thank the Chemistry Department for accepting me into the graduate program. I would like to thank my research advisor, Prof. Julie Kovacs, for giving me this interesting project. Also, I would like to thank my former advisors Prof. Ernst-Gottfried Jäger, Prof. Jonathan Sessler, and Prof. Rolf Hilgenfeld for their influence on my scientific development and their advice. Further, I would like to thank my fifth cousin Prof. George Schweitzer for his advice and for first exposing me to the educational system in the United States of North America.

I would like to thank the following former Kovacs group members for their friendship and help throughout the previous years: Drew Nienstedt, Dr. Jeff Ellison, Henry Jackson, Irene Kung, Jennifer Nehring, Wendy Taylor, Dr. Durrell Rittenberg, as well as my former undergraduate students Suzanna Hugo and Elisabeth May. During my time here several other people in the department also provided valuable help. They include Dr. Martin Sadílek, Dr. Scott Lovell, Dr. Werner Kaminsky, James Law, Dr. Tamara Okonogi, Prof. Daniel Gamelin, Pavle Radovanovic, Byron Gates, Dr. Sang-Hyun Park, and Dr. Ziyi Zhong.

On a personal level, I first want to thank my parents for raising me, for educating me to the person I am, and for their ongoing support. Then, I would like to thank my wife, Erin Robinson, as well as her sister and mother, for their support and encouragement throughout this difficult time period. I also would like to thank the people that I met at FIUTS and a number of 'little girls.' They provided me with much needed distraction from my work in the laboratory.

I would like to dedicate this dissertation to my parents: Sabine Schweitzer, née Kogel, and Dietrich Schweitzer, and to my grandparents: Marie Antonie Johanne Kogel, née Schneider, Günther Ernst Heinrich Hugo Kogel, Anna Martha Elisabeth Schweitzer, née Krauße, and Johann Gottfried Benjamin Schweitzer.

Faust. Wohin der Weg?

Mephistopheles. Kein Weg! Ins Unbetretene.

Chapter I: Introduction

Bioinorganic Chemistry

Bioinorganic chemistry is a discipline of chemistry that investigates the functions and roles of 'non-organic' elements within biological systems. This discipline emerged in the 1960's. It was the rapid development of analytical methods which enabled scientists to recognize that metal ions play significant roles in biological systems. For example, it was found that many proteins require one or more metal ions to exercise their biological activity. This includes such essential functions as the charge separation in chlorophyll, the oxidation of water by the oxygen-evolving complex, the transport of oxygen by hemoglobin and myoglobin, and several steps in the mitochondrial electron transport chain.[1,2] Consequently, an important aspect of bioinorganic chemistry involves the study of how a metal ion influences the biological activity of an enzyme. The research described herein attempts to contribute to an understanding of some aspects of this question.

The influence of a metal ion on the biological activity of an enzyme can be investigated in two possible ways. Either the enzyme, its mutants, and forms of the enzyme in which the naturally occurring metal ion has been replaced by another metal ion can be studied, or model compounds can be studied. The study of low molecular mass model compounds is referred to as the 'synthetic analogue approach.' It involves the synthesis and characterization of small compounds that model the spectroscopic, structural, and ultimately reactivity properties of an enzyme. This is the approach utilized in this dissertation. By systematically altering the structure of the low molecular mass model compounds, a deeper understanding of the structure-reactivity relationship in the enzyme is gained.

Scientists want to understand important structural features and requirements for the functionality of the metal site, and they want to estimate the influence of the protein environment on the intrinsic nature of the incorporated metal ions. Ultimately, it is hoped that this knowledge will enable scientists to design novel catalysts which can perform reactions that are not found in biological systems.

One of the metals most commonly present in the active centers/sites of enzymes is iron. Iron can occur in an active site as a heme unit (e. g., cytochrome P450), as a diiron-carboxylate unit (e. g., hemerythrin), as an iron-sulfur cluster (e. g., ferredoxins and nitrogenase), or as a mononuclear iron center.[1,2] Only a small number of mononuclear iron centers are known to contain iron in a mixed nitrogen/oxygen/sulfur coordination environment. They include nitrile hydratase,[3,4] center II of desulfoferrodoxin (*dfx*/*rbo*),[5] and neelaredoxin.[6] Nitrile hydratase is the focus of this dissertation.

The active site of neelaredoxin and center II of desulfoferrodoxin is an octahedral $FeN_4S_1X_1$ site, with the cysteine being opposite to the open coordination site. The symbol X is used to denote an open coordination site, which might be occupied by a water molecule or by a substrate molecule. The iron ions in desulfoferrodoxin and neelaredoxin are always high-spin. Desulfoferrodoxin and neelaredoxin have superoxide reductase activity.[7-9] They reduce the reactive, and therefore toxic, superoxide ion (O_2^-) to peroxide ion (O_2^{2-}). Peroxide is then converted to oxygen and water by the action of catalase or it is used by a peroxidase.[1,2] Another enzyme, thiocyanate hydrolase, exhibits a high sequence homology to nitrile hydratase,[10,11] and thus might also contain a mononuclear iron or cobalt site in a mixed nitrogen/sulfur coordination environment.

Nitrile Hydratase - Its Physiological Role

Nitrile hydratase (NHase) is a bacterial enzyme.[3,4,12] Its physiological role is to catalyze the hydration of nitriles to the corresponding terminal amides. This is necessary to remove toxic nitriles,[13] to use nitriles as a source of carbon and nitrogen,[14] and to synthesize plant hormones.[15] Nitriles are potentially toxic since they can be hydroxylated in the α position by P450 to form cyanhydrins.[16] Cyanhydrins are known to decompose to form HCN and aldehydes.[17] Cyanhydrins also occur naturally in the form of cyanogenic glycosides.[13,17] The production of plant hormones by bacteria seems to be essential for symbiosis between bacteria and plants. Most NHases exhibit a large substrate variability.

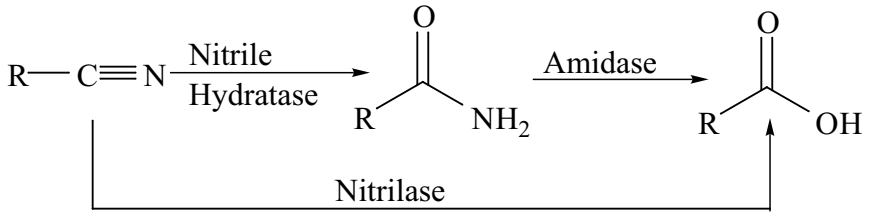

Figure 1-1: Biological pathways to convert nitriles to carboxylic acids.

Related chemical transformations are catalyzed by nitrilase[18] and amidase.[19] Nitrilase hydrolyzes nitriles to their corresponding acids and ammonia. Amidase hydrolyzes amides to their corresponding acids and ammonia. Cysteine is the catalytically active residue in nitrilase,[18] while it is either cysteine[19] or serine[20] in amidase. In contrast to NHase, neither nitrilase nor amidase require any metal ion to exercise their catalytic activity.

NHase is used in a variety of applications. Immobilized *Rhodococcus rhodochrous* J1 cells, which contain NHase, are used in an industrial 30,000 t/y

production process to hydrate acrylonitrile to acrylamide.[21] NHase was shown to be effective in the removal of nitriles from waste[22] and in the degradation of nitrile-containing herbicides.[23] Because the nitrile hydration reaction occurs under very mild conditions, NHase has the potential to be employed in many industrial and laboratory scale chemical processes.[24] NHase has also been used in the regioselective[25] and enantiospecific[26-28] synthesis of amides.[17]

NHase is known to occur either as an Fe- or as a Co-containing enzyme. Fe-containing NHases have been isolatedfrom a number of bacterial species. They include *Rhodococcus sp.* N-771,[29] *Rhodococcus sp.* R312 (= *Brevibacterium* R312),[30] *Comamonas testosteroni* NI1,[31] and *Pseudomonas chlororaphis* B23.[32] Organisms that are known to express the Co-containing enzyme are *Rhodococcus rhodochrous* J1,[33] *Pseudomonas putida* NRRL-18668,[34] and *Agrobacterium tumefaciens*.[15] An organism can express both the Fe- and the Co-containing enzyme simultaneously.[15] The investigated Co-containing NHases have a higher activity and a higher stability than the investigated Fe-containing NHases.[35,36] For completeness, it should be mentioned that there are also mutant[37,38] and Zn-containing[39] enzymes that display NHase activity. It is also known that nitriles which are activated by electron withdrawing groups are catalytically hydrated to the corresponding amides using 2-mercaptoethanol in an aqueous phosphate buffer at pH = 9.[40]

Nitrile Hydratase - Structure of the Active Site

Studies on NHase from *Rhodococcus* N-771 indicate that NHase is an $\alpha\beta$ heterodimer, with the α and β subunit each having approximately a molecular mass

of 27.5 and 28 kDa, respectively.[29] In NHase from *Rhodococcus* N-774, the α subunit is comprised of 207 amino acids and the β subunit is comprised of 212 amino acids.[41] The Fe-containing center is located on the α subunit.[42] Sequence alignment indicates that the α subunit of NHase contains a conserved sequence: -Cys-Thr/Ser-Leu-Cys-Ser-Cys-Tyr/Thr-.[26,34,43,44] This sequence is conserved in both Fe- and Co-containing NHases. In the crystal structure of NHase from *Rhodococcus* sp. R312, one iron ion was located in the active center.[41]

NHase contains in its active center either a low-spin (S = 1/2) Fe(III)[45] or a low-spin (S = 0) Co(III).[34] The assignment of a low-spin Fe(III) in the active site of active Fe-containing NHase is based upon the EPR spectrum (g_{max} = 2.284, g_{mid} = 2.140, g_{min} = 1.971).[45] To date, NHase is the only non-heme enzyme known to contain a low-spin Fe(III). It is remarkable that NHase, which catalyzes a reaction in which water attacks a substrate, contains Fe(III) or Co(III) in its active site, instead of Zn(II) as do most hydrolytic enzymes.[1,2]

Fe-containing NHase has a maximum activity at about pH = 7.8, and above 50 % activity between pH = 6.5 and 9.0.[29] However, below pH = 5.5 and above pH = 8.5 activity is gradually lost.[29] In comparison, Co-containing NHase has a maximum activity at around pH = 7.5, and above 50 % activity between pH = 6.0 and 8.5.[34]

The visible absorption spectrum of active Fe-containing NHase is characterized by a shoulder at around 400 nm and an intense band with sulfur to iron charge transfer[46] character at around 700 nm ($\varepsilon \sim 1100\ M_{Fe}^{-1}cm^{-1}$).[43,47] The absorption at 700 nm causes the green color. NO-inactivated Fe-containing NHase displays an absorption maximum at 370 nm, which has also sulfur to iron charge

transfer character.[48] In comparison, active Co-containing NHase appears pink with an absorption maximum at 410 nm and broad absorption between 400 and 600 nm.[49]

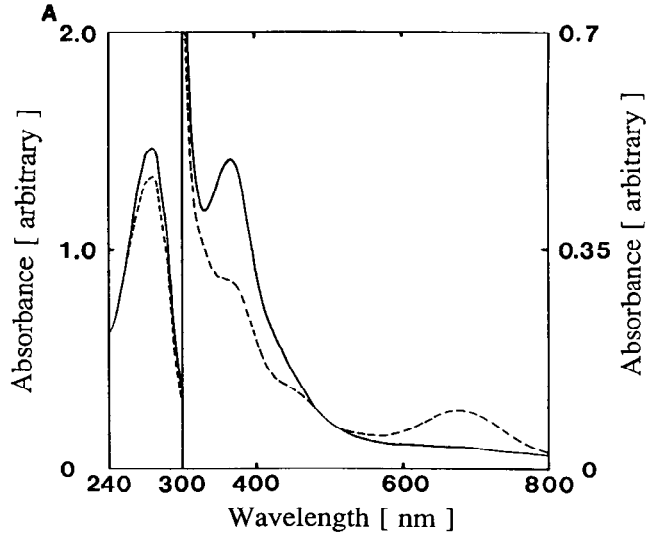

Figure 1-2: Absorption spectrum of active (---) and NO-inactivated (-) NHase.[29] Permission was granted by Academic Press (Orlando, FL) to use this Figure (Christine Smith, February 8th, 2001).

An immense number of articles have been published in which studies of the active center of NHase were reported. Among the techniques that were used to gain information about the active center of NHase are UV/Vis, FTIR, EPR, XAS, EXAFS, ENDOR, resonance Raman, Mößbauer, mass spectrometry, X-ray crystallography, light irradiation, and mutagenesis studies.

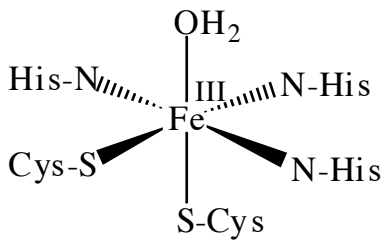

Figure 1-3: Proposed structure of the active site of NHase prior to the publication of the first crystal structure in 1997.

Before X-ray crystallography was performed, the spectroscopic data was interpreted in such a way that the metal ion in NHase was assigned to a mixed histidine-cysteine coordination environment. This coordination environment was proposed to contain two cysteine-sulfurs, three histidine-imidazole-nitrogens, and an open coordination site, which is occupied by a water molecule or, depending upon the pH, a hydroxide ion.[43,45,47,50-53] It was with this knowledge about the active center of NHase that the projects described in Chapters II and III were initiated. In contrast to the interpretation of the spectroscopic data, the X-ray structures, vide infra, show the iron in the active center to be coordinated by three sulfurs and two amide nitrogens.[41,54]

When Fe-containing NHases were studied, it was found that they exist in an active and in an inactive form. The NHase activity in cells decreased over time, but was restored upon exposure of the cells to white light. In addition, the purified inactive enzyme could be activated upon exposure to white light. In contrast to this, the purified active enzyme did not lose activity over time.

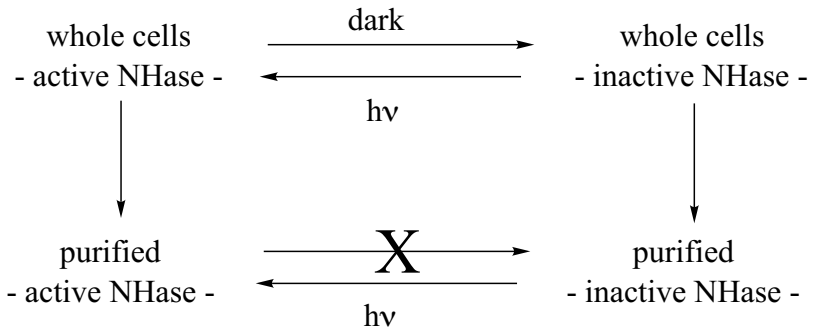

Figure 1-4: Activity dependence of Fe-containing NHase.[29]

Natural Fe-containing NHase (^{14}N (natural abundance)) has an IR absorption maximum at 1855 cm^{-1} while ^{15}N labeled NHase has an IR absorption maximum at 1820 cm^{-1}. Based upon the energy of this IR absorption, and its response to ^{15}N-labeling, it was proposed that NO (nitric oxide, nitrogen monoxide) is bound to the active site iron in the inactive form of NHase.[55] Subsequently, it was shown that light irradiation of inactive NHase produces NO and active NHase. The released NO was trapped by a spin trap that upon NO binding becomes EPR active.[56] In further studies active NHase was deactivated by the addition of NO gas.[48,56] A detailed study showed that active NHase can be inactivated by the addition of an NO solution or by NO produced in situ by NO synthase.[31] An iron K-edge X-ray absorption (XAS) study confirmed the 1:1 stoichiometry of NO bound to low-spin Fe(III) in NO-inactivated NHase.[57] The bound NO was also detected in the crystal structure of the NO-inactivated form of NHase.[54] Recently, as discussed in Chapter II of this dissertation, an NO-bound Fe(III)-containing model compound, $[Fe(III)S_2^{Me2}N_3(Pr,Pr)(NO)]PF_6$ (**1-NO**), was reported that models the spectroscopic properties of NO-inactivated Fe-containing NHase.[57,58]

In comparison, no interaction between NO and Co-containing NHase is known to date.

Two crystal structures of NHase were solved by X-ray diffraction.[41,54] In the first structure,[41] data up to a resolution of 2.65 Å was included in the refinement. The final model had R = 26.4 % and R_{free} = 28.9 %. The enzyme crystallized as an αβ heterodimer with an extensive interface between two heterodimers, suggesting that in solution an $\alpha_2\beta_2$ tetramer might be in equilibrium with the αβ heterodimer. The active center is located within the conserved sequence[26,34,43,44] -Cys-Thr/Ser-Leu-Cys-Ser-Cys-Tyr/Thr- on the α subunit. The active site is situated in a cavity that is located at the interface between the α and β subunit. The donor atoms to the iron ion are the sulfurs of three cysteines and two peptide amide (carboxamide) nitrogens. The three sulfur donor atoms are in a facial (*fac*) arrangement. The five donor atoms are located at five corners of an octahedron, while the sixth position is unoccupied. Given the relatively low resolution of the crystal structure, it is understandable that no electron density corresponding to oxidized cysteines, as found in the second crystal structure, and a metal-coordinated water molecule or hydroxide ion was detected.

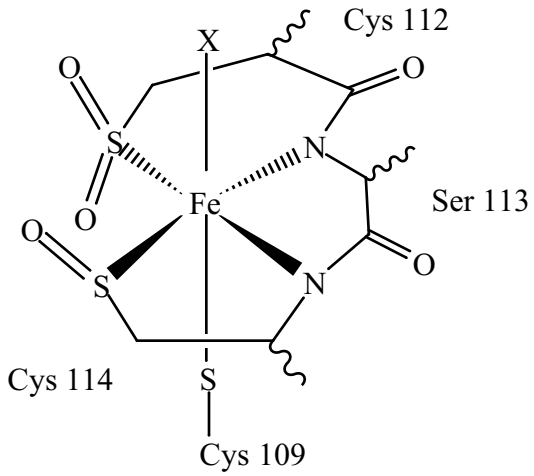

Figure 1-5: Schematic representation of the structure of the active site of Fe-containing NHase (active form: X = OH^-/H_2O; NO-inactivated form: X = NO).

The second crystal structure[54] was solved at a better resolution of 1.7 Å. The final model had R = 17.9 % and R_{free} = 22.8 %. Like expected, it revealed the iron ion in the active site of NO-inactivated NHase to be coordinated by two amide nitrogens and one NO ligand. The NO is coordinated via the nitrogen, as it is the case in $[Fe(III)S_2^{Me2}N_3(Pr,Pr)(NO)]PF_6$ (**1-NO**), see Chapter II for complete details. Unexpectedly, two of the three cysteine thiolate ligands were found to be modified to a sulfone (sulfinato) (-S(O_2)-) and a sulfoxide (sulfenato) (-S(O)-)! The two modified cysteines are the equatorial cysteines; they are accessible to solvent. The sulfone and sulfoxide oxygens participate in extensive hydrogen bonding to two of the arginine residues in the β subunit. A mutation of any one of these arginine residues results in the loss of activity.[4,59] Mass spectrometric studies confirmed the presence of the sulfone modification in the active enzyme, while proof for the sulfoxide modification remains elusive.[54,60-63] It has been shown that the sulfone modification is posttranslational and essential for catalytic activity.[62,63] It is

possible that the sulfoxide modification observed in the crystal structure was generated by a reaction with NO, since it has been shown that NO can react with cysteine to form cysteine-sulfenic acid (R-S-OH) and N_2O.[64]

No crystal structure of Co-containing NHase has been reported. However, since both Fe- and Co-containing NHase contain the same active site sequence,[26,34,43,44] it can be assumed that the active site structure of Co-containing NHase is very similar to that of Fe-containing NHase. This is supported by EXAFS data.[65] Additionally, it was found that the substitution of cobalt into Fe-containing NHase affords an enzyme with properties similar to native Co-containing NHase.[4,62]

Table 1-1: Selected bond distances and angles of the active site of Fe-containing NO-inactivated nitrile hydratase.[54]

bond	distance (Å)	angle	(°)
Fe-S (Cys 109)	2.30	Fe-N-O	158.6
Fe-$S(O)_2$ (Cys 112)	2.26	S(114)-Fe-N(113)	171.1
Fe-S(O) (Cys 114)	2.33	S(112)-Fe-N(114)	175.6
Fe-N (Ser 113)	2.09	S(109)-Fe-N(NO)	172.3
Fe-N (Cys 114)	2.05		
Fe-N (NO)	1.65		
S-O	1.41 - 1.51		

NHase is the second enzyme in which the coordination of an amide (carboxamide) nitrogen to a metal ion has been observed. The other example occurs in the P-cluster of nitrogenase.[66] Based upon the crystal structure, it cannot be

said whether or not the amide nitrogens are deprotonated. However, studies on model compounds show that the coordination of a deprotonated carboxamide nitrogen, which is negatively charged, to an Fe(III)[67-74] or a Co(III)[68,75-78] ion forms a stable structure. This is described in more detail in Chapter IV. Such a coordination mode significantly stabilizes the +3 oxidation state. That means, the reduction potential is shifted to more negative values.

Nitrile Hydratase - Possible Mechanisms of Nitrile Hydration

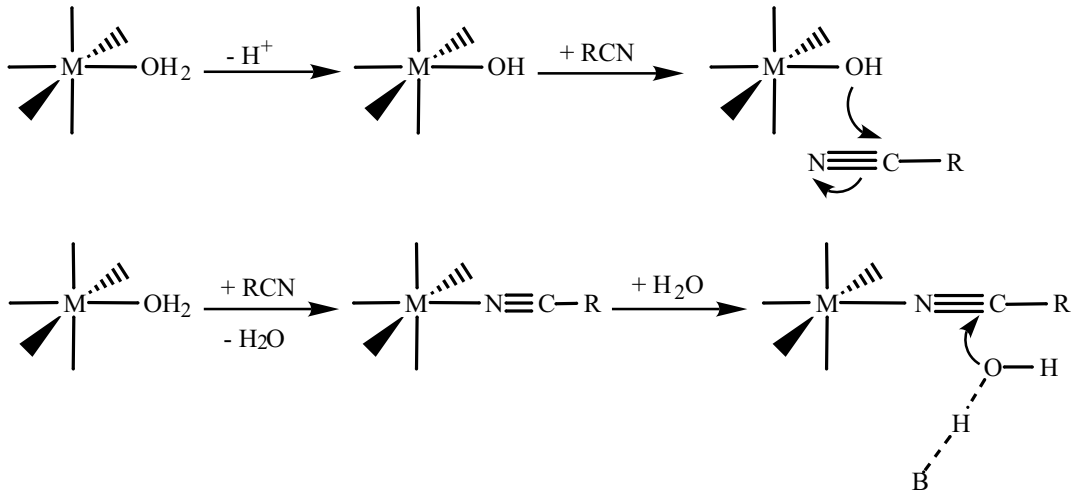

Figure 1-6: Reasonable mechanisms for the hydration of nitriles by NHase (M = Fe(III) or Co(III)).[41]

There are two plausible mechanisms according to which NHase could catalyze the hydration of nitriles to amides. The attack on the nitrile could be performed by a metal-bound hydroxide ion as it is usually the case in Zn-containing hydrolytic enzymes.[1,2,41,79] A hydroxide ion bound to a transition metal ion with a completely or partly filled d shell ($L_nM\text{-}(OH)^{q+}$) is expected to have a higher

nucleophilicity than a proton-bound hydroxide ion (H-OH).[80] A NHase model compound in which a Co(III)-bound hydroxide ion (p*K*a(H_2O-M) = 8.3) catalyzes the hydration of nitriles is known, vide infra.[75] ENDOR has shown that a competitive inhibitor, butyric acid, binds in a well defined geometry close to the metal-bound hydroxide ion.[81] After the slowly reacting substrate *i*-butyronitrile was added, no butyric acid remained near the active site. "This suggests that *i*-butyronitrile is capable of displacing butyric acid without binding to the ferric ion."[81] There *i*-butyronitrile is either attacked by the metal-bound hydroxide ion or it has to undergo a positional change so that it is bound to the active site iron.

The other reasonable mechanism involves a base-assisted attack of a water molecule on a metal-bound nitrile.[41,82,83] For example, it was observed that the hydration under basic conditions of a nitrile to form an amide is accelerated by a factor of 10^6 upon coordination of the nitrile to $Co(NH_3)_5^{3+}$.[82] This mechanism seems probable considering the fact that NHase contains Fe(III) or Co(III) in its active site instead of Zn(II) as do most hydrolytic enzymes.[1,2] A possible explanation for this might be that iron and cobalt are the only readily biologically accessible metals that can form a +3 oxidation state in aqueous solution. If one assumes that the nitrile substrate must be polarized prior to the nucleophilic attack upon the nitrile carbon, then it is understandable that a metal ion in a +3 oxidation state is required for NHase to exercise its catalytic function. A metal ion with a +3 oxidation state is a much stronger Lewis acid than a metal ion with a +2 oxidation state. It would be interesting to measure the activity of NHase when the Fe(III) or Co(III) ion is replaced by divalent metal ions. To the best of the author's knowledge, this kind of experiment has not been reported.

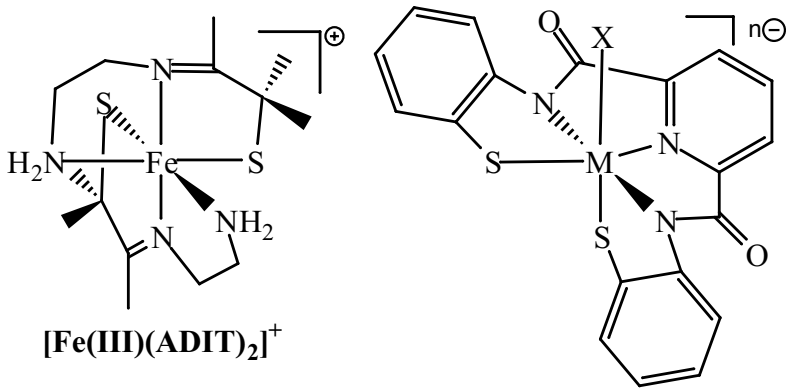

[Fe(III)(ADIT)$_2$]$^+$

[M(III)(PyPS)(X)]$^{n-}$

Figure 1-7: Other model compounds of NHase: [Fe(III)(ADIT)$_2$]$^+$,[84] [Co(III)(PyPS)(OH)]$^{2-}$,[75] and [Fe(III)(PyPS)(OH)]$^{2-}$.[74]

Other Model Compounds of Nitrile Hydratase

There are a number of Fe(III) complexes that contain two cis thiolate donors perpendicular to two trans imine or amide nitrogen donors in a N_4S_2 donor set (the $Fe(S)_2$ plane is perpendicular to the $Fe(N_{imine/amide})_2$ plane).[58,67,74,84-91] Some of them, including [Fe(III)(ADIT)$_2$]$^+$, which was first reported by the Kovacs group in 1995, and [Fe(III)(PyPS)(OH)]$^{2-}$, see Figure 1-7, model the spectroscopic and electronic properties (UV/Vis, EPR, spin state) of the active site of NHase surprisingly well. For example, [Fe(III)(ADIT)$_2$]$^+$[84] has g values of 2.19, 2.13, 2.01 and a low energy electronicabsorption maximum at 718 nm with an ε of 1400 $M^{-1}cm^{-1}$ while the corresponding parameters of [Fe(III)(PyPS)(OH)]$^{2-}$[74] are g = 2.31, 2.12, 1.93 and 790(700). The visible absorption spectrum of [Fe(III)(ADIT)$_2$]$^+$, see Figure 1-9, has a striking resemblance to that of active Fe-containing NHase, see Figures 1-2 and 1-8. [Fe(III)(ADIT)$_2$]$^+$ has an absorption maximum at 438 nm, while the spectrum of NHase contains a shoulder at ~ 400 nm.

Both $[Fe(III)(ADIT)_2]^+$ and active Fe-containing NHase are green since they have a broad absorption maximum at about 700 nm. Interestingly, the replacement of the terminal NH_2 group in $[Fe(III)(ADIT)_2]^+$ with pyridine or imidazole yields also hexacoordinated compounds with very similar physical properties.[90]

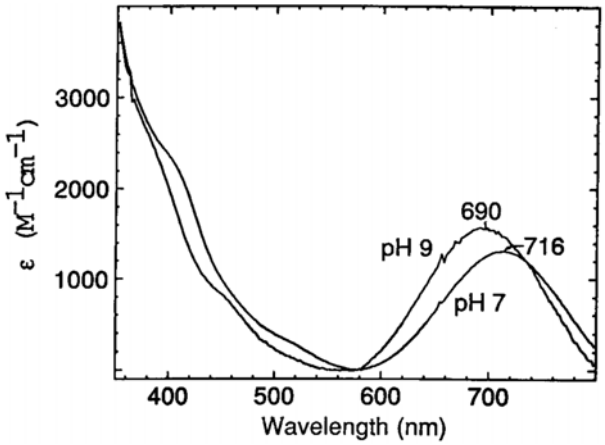

Figure 1-8: Visible absorption spectrum of active, Fe-containing NHase. The spectrum was provided by Dr. Mark Nelson.

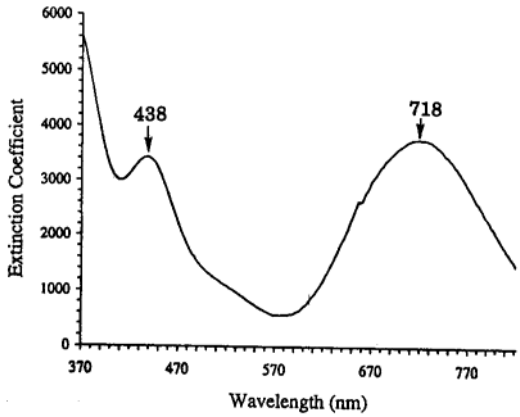

Figure 1-9: Visible absorption spectrum of $[Fe(III)(ADIT)_2]^+$ in MeCN.

The sulfone coordination mode found in the active site of NHase is not unprecedented. Several Fe(III),[68] Co(III),[68,76,78,92-95] Pd(II),[96] and Ni(II)[96-98] sulfone (sulfinato, $M\text{-}S(O)_2\text{-}R$) complexes are known. Metal sulfoxide (sulfenato,

M-S(O)-R) complexes are also known.[93,95,96,99] Furthermore, a Co(III) complex, $[Co(III)((\eta^2\text{-}S^{Me2}O)(S^{Me2}(O)_2)N_3(Pr,Pr))]PF_6$ (**2-O$_3$**), containing an η^2-coordinated sulfoxide and a sulfone was recently described by Kung and co-workers.[100] The η^2 coordination mode of the sulfoxide has only been observed once before![101]

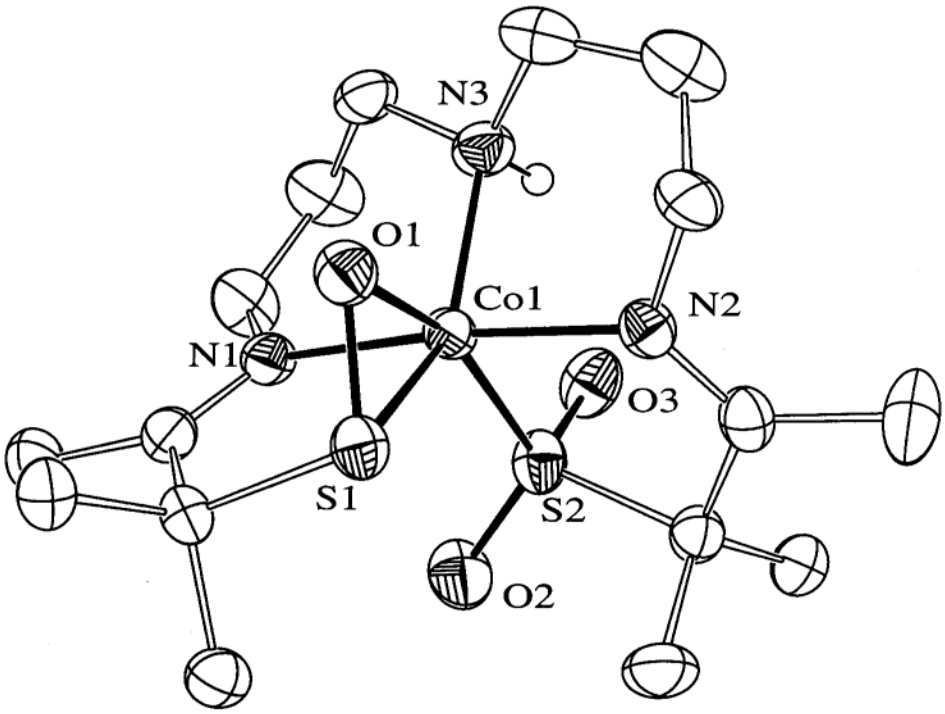

Figure 1-10: Thermal ellipsoid plot (50 % probability level) of the cation of **2-O$_3$**. H atoms, except for the H-N_{amine}, are omitted for clarity. Selected bond lengths (Å) and angles (°): Co-N1, 1.957(3); Co-N2, 1.943(3); Co-N3, 1.993(3); Co-O1, 2.042(2); Co-S1, 2.132(1); Co-S2, 2.118(1); S1-O1, 1.548(3); S2-O2, 1.454(3); S2-O3, 1.464(3); N1=C(imine), 1.281(5); N2=C(imine), 1.279(5); N1-Co-N2, 173.6(1); N1-Co-N3, 95.2(1); N1-Co-O1, 89.7(1); N1-Co-S1, 87.0(1); N1-Co-S2, 90.8(1); N2-Co-N3, 89.0(1); N2-Co-O1, 94.5(1); N2-Co-S1, 92.6(1); N2-Co-S2,

83.5(1); N3-Co-O1, 99.7(1); N3-Co-S1, 143.2(1); N3-Co-S2, 102.3(1); O1-Co-S1, 43.5(8); O1-Co-S2, 157.8(9); S1-Co-S2, 114.4(5).[100]

Compound **2-O$_3$** can be prepared in either of two ways. When a solution of [Co(III)($S_2^{Me2}N_3$(Pr,Pr))]PF_6 (**2**) is stirred on air for three days, [Co(III)(S^{Me2}(S^{Me2}(O)$_2$)N_3(Pr,Pr))]PF_6 (**2-O$_2$**) is formed in a clean reaction. Complex **2-O$_2$** contains a coordinated sulfone and a coordinated thiolate. Upon treatment of a solution of **2-O$_2$** with 30 % H_2O_2, **2-O$_3$** is formed in a clean reaction. Alternatively, **2-O$_3$** can be synthesized in a clean reaction by the treatment of a solution of **2** with 30 % H_2O_2.

This reactivity of **2** provides a model for how the active site of NHase could be assembled. After transcription and translation, the protein is folded. Then an auxiliary protein inserts the metal ion.[61,62] By reaction with air, one of the thiolate ligands is oxidized to a sulfone thereby generating the active enzyme.[62,63] In the presence of an oxidizing agent (NHase: NO; **2-O$_2$**: H_2O_2), the other solvent accessible thiolate can be oxidized to a sulfoxide. It is known that NO can react with thiols to form a sulfenic acid (R-S-OH) and N_2O.[64] Compound **2-O$_2$** did not react with NO under the conditions investigated.

Recently, Noveron et al. reported a Co(III)-containing model compound, [Co(III)(PyPS)(OH)]$^{2-}$ in Figure 1-7, of NHase that displays NHase activity.[75,102] This is the first example of an Fe(III) or Co(III) complex in a mixed nitrogen/sulfur coordination environment displaying NHase activity. The reported Co(III) complex contains one pyridine nitrogen, two carboxamide nitrogens, and two thiolate sulfurs as donor atoms. There is also a coordinated H_2O molecule with a p*K*a of 8.3. The bound H_2O/OH^- is trans to a thiolate donor. At pH = 9.5, the

complex catalyzes 15 turnovers of the hydration of acetonitrile within 2 hours via a mechanism that is proposed to involve the attack of the metal-bound hydroxide ion onto the nitrile. This model compound and NHase hydrate nitriles under much milder conditions than typical laboratory procedures. In a typical laboratory procedure, the nitrile is either refluxed with acid or base.[103] In most cases, the hydrolysis product, that is, the corresponding acid, is isolated from these reactions.

Challenges of Fe(III)/Co(III)-Thiolate Chemistry

The synthesis of compounds containing Fe(III) or Co(III) in a thiolate sulfur coordination environment provides several challenges. Firstly, the combination of Fe(III) or Co(III) and thiolates is usually thermodynamically unstable with respect to the formation of the divalent metal ion and disulfide.[104-109] This reaction proceeds via a rate-determining intramolecular electron transfer, that is, a redox reaction, followed by a radical recombination.[107,110] In agreement with this, it has been observed that in the synthesis of the model compounds reported herein a relatively large amount of side-products is formed.[111] The compounds should, whenever possible, be stored at a low temperature, preferably as a solid, since they are unstable in solution.[112]

Secondly, compounds containing thiolates (RS^-) are susceptible to oxidation by oxygen present in the air. This could, for example, result in the formation of disulfide (RS-SR)[113] and iron oxide. Also, a sulfoxide (-S(O)-) and/or a sulfone ($-S(O)_2-$) could be formed. Therefore, metal thiolate compounds have to be handled in a glovebox or on a Schlenk line under an atmosphere of nitrogen or argon to exclude oxygen.

Thirdly, coordinatively unsaturated compounds containing thiolates can be unstable with respect to oligomerization via thiolate bridges.[114] In addition, a single multidentate ligand can coordinate to a metal ion in a variety of coordination modes. For example, by varying the anion and the reaction conditions, Brand and Vahrenkamp have isolated six different zinc complexes of a single tridentate ligand![115]

Chapter II: A Model Compound of the Active Site of the NO-Inactivated Form of Nitrile Hydratase[58]

Introduction

As it was mentioned above, NHase exists in an active and in an inactive form. The inactive form was found to be formed by the binding of NO (nitric oxide, nitrogen monoxide) to the active center of active NHase. NO binding and release, thus, regulate the activity of NHase.

Within the last several years a constantly increasing number of biological functions of NO have been found.[116,117] They include the regulation of blood pressure by NO. NO binds to the iron in the heme group of guanylate cyclase, thus causing a conformational change which activates guanylate cyclase. Guanylate cyclase is then converting GTP (guanosine triphosphate) into cGMP (guanosine 3',5'-monophosphate). cGMP acts as a secondary messenger molecule to activate protein kinases which ultimately results in the relaxation of smooth muscle, thus widening the blood vessel. NO acts further as a neurotransmitter and is produced as a part of the immune response mediated by macrophages. Here, the function of NO is to inhibit enzymes of the antigen (e. g., invading bacteria) and to cause destructive radical reactions.

NO is produced in biological systems by the enzyme NO synthase, a heme protein. It converts arginine to citrulline and NO in a five electron oxidation process that requires O_2 and NAPDH (reduced nicotinamide adenine dinucleotide phosphate).

The NO-inactivated form of NHase is X-band EPR silent. Therefore, it does not possess an odd number of unpaired electrons. It has an absorption

maximum at 370 nm, see Figure 1-2. As discussed in Chapter I, the crystal structure of the NO-inactivated form of NHase was solved.[54] Relevant bond lengths and angles of the active site of itare given in Table 1-1. Before the crystal structure was solved, EXAFS analysis indicated the bond lengths shown in Table 2-1.

Table 2-1: EXAFS parameters of NO-inactivated NHase and of **1-NO**.[57]

	NO-inactivated NHase		**1-NO**
$n_{NO}/n_N/n_S$	1/2/3	1/3/2	1/3/2
r(Fe-NO) (Å)	1.680(27)	1.684(27)	1.680(23)
r(av. Fe-N) (Å)	1.968(25)	1.977(20)	1.998(34)
r(av. Fe-S) (Å)	2.265(11)	2.267(11)	2.267(20)
∠Fe-N-O (°)	163(13)	166(12)	165(12)

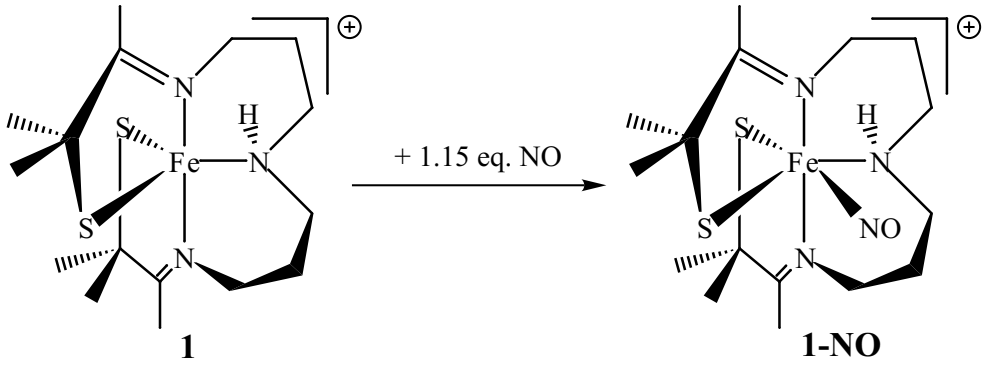

Figure 2-1: Synthesis of **1-NO** from **1**.

Synthesis of Model Compound

The addition of a small excess of NO gas to a solution of pentacoordinated $[Fe(III)S_2^{Me2}N_3(Pr,Pr)]PF_6$ (**1**), see Chapter III for more details about **1**, results in

the formation of hexacoordinated $[Fe(III)S_2^{Me2}N_3(Pr,Pr)(NO)]PF_6$ (**1-NO**) in a clean reaction. This reaction is performed by adding 1.15 equivalents of NO gas on a Schlenk line to a frozen MeCN solution of **1**. Upon warming to room temperature, the NO dissolves in the solution and **1-NO** is formed. In the glovebox, the solution is then overlayered with Et_2O. After standing for several days at - 35 °C, crystals of **1-NO** can be isolated. In comparison, it was not possible to obtain clean **1-NO** by bubbling NO gas through an MeCN solution of **1**. It is not possible to use MeOH as the solvent since **1** decomposes in MeOH under N_2 with an estimated rate of 15 % / 24 h in the dark at room temperature.

Properties of the Model Compound and Relevance to the Active Site of Nitrile Hydratase

It was hoped that NO would bind to the iron in **1** in a fashion which resembles the binding mode of NO to the active site iron of NHase. If this is the case then the electronic and structural properties of **1-NO** should match those of the NO-inactivated form of NHase. One can then investigate the electronic and structural properties of **1-NO**, the analogue of NO-inactivated NHase, at a level of detail which is impossible to achieve in the enzyme. Such a detailed investigation is difficult to achieve in the enzyme since the properties of the large 'protein ligand' mask the properties of the active site metal ion and its immediate coordination sphere.

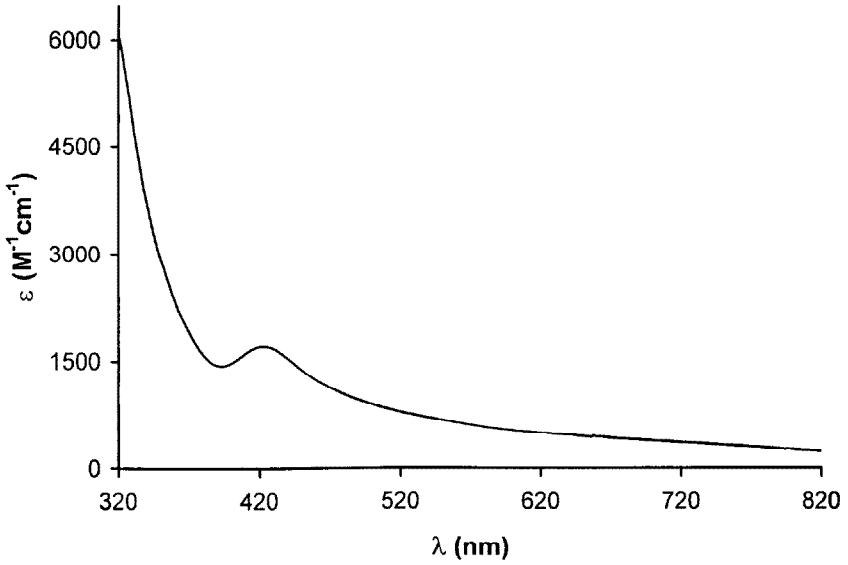

Figure 2-2: Absorption spectrum of $[Fe(III)S_2^{Me2}N_3(Pr,Pr)(NO)]PF_6$ (**1-NO**).

The visible absorption spectrum of **1-NO** is characterized by a single maximum at 422 nm, see Figure 2-2. A comparison of the absorption spectra shows that the absorption spectrum of **1-NO**, see Figure 2-2, matches the one of NO-inactivated Fe-containing NHase, see Figure 1-2, very closely. Within the range of 320 - 800 nm, NO-inactivated NHase and **1-NO** each have a single absorption maximum at 370 and 422 nm, respectively. The electronic absorption band at 370 nm in NO-inactivated NHase has sulfur to iron charge transfer character.[48] An explanation for the disappearance of the absorption band at 700 nm, when going from active to NO-inactivated NHase, is given below.

Compound **1-NO** is formed by the reaction between Fe(III) and NO•. Therefore, it is an $\{FeNO\}^6$ complex according to the nomenclature of Enemark and Feltham.[118,119] $\{FeNO\}^6$ means that a total number of six electrons are associated with the iron d and the NO π* orbitals. An $\{FeNO\}^6$ complex is

formally composed of the three resonance structures 'Fe(II) and NO^+', 'Fe(III) and NO•', and 'Fe(IV) and NO^-'. "The bonding in the $M(NO)_x$ moieties of metal nitrosyl complexes is largely of a covalent nature, and ... the electron distribution in the M-NO unit is more or less evenly distributed in this group. As a result, it is unreasonable to assign formal oxidation states to the metal and the nitrosyl ligand in M-NO complexes."[119] The IR data for both **1-NO** and NO-inactivated NHase fall into the range expected for an $\{FeNO\}^6$ system.[119-121] A comparison of the data in Table 2-2 suggests that the dominant resonance structure in both NO-inactivated NHase and **1-NO** is 'Fe(III)-NO•'.

Table 2-2: Comparison of 'NO' parameters.[119-121]

	NO^+	NO•	NO^-	'NO'-inactivated NHase	'NO' in **1-NO**
r(N-O) (Å)	1.06	1.15	1.26	N/A	1.161(4)
ν_{N-O} (cm^{-1})	2377	1875	1470	1853	1823

$[Fe(III)S_2^{Me2}N_3(Pr,Pr)(NO)]PF_6$ (**1-NO**) is diamagnetic (S = 0) as shown in the NMR Figures in Chapter V. Since NO• and **1**, at temperatures below 100 K, see Figure 3-10, each have a spin of 1/2, an electron pairing must be occurring in addition to the σ bond formation between the filled lone pair orbital on the nitrogen and an empty orbital of the iron. Therefore, the Fe-NO bond must have a double bond character. This double bond character is expressed in the considerably shorter Fe-NO bond length (1.676(3) Å) as compared to the other Fe-N bonds (mean: 2.0(1) Å) in **1-NO**. Also, the Fe-NO distance in NO-inactivated NHase is shorter than the other Fe-N distances, see Tables 2-1 and 1-1. The Fe-NO distance in **1-NO** falls within the range (1.62 - 1.68 Å) expected for $\{FeNO\}^6$ systems.[122] An

MO explanation for the spin pairing is given below. The MO in which this newly formed electron pair is located is distributed throughout the molecule.

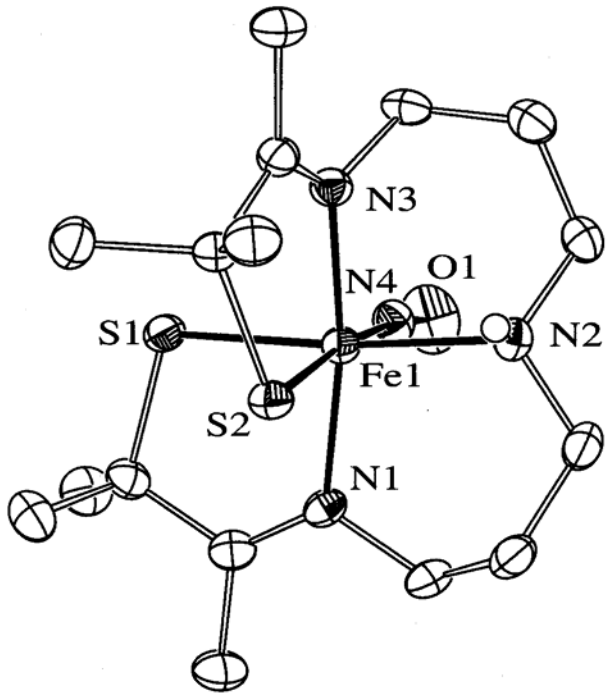

Figure 2-3: Thermal ellipsoid plot (50 % probability level) of the cation of **1-NO**. H atoms, except for the H-N_{amine}, are omitted for clarity.

As shown by the X-ray crystallographic analysis, the iron ion in **1-NO** is in a near ideal octahedral coordination environment. Transangles vary from 165.9(1)° to 174.29(8)° and cis angles vary from 83.0(1)° to 102.5(1)°. The NO ligand in **1-NO** is bound trans to one of the thiolate sulfurs (S2) and it is inserted into the wider N-Fe-S angle (N2-Fe-S1 = 132.3(1)°) of **1** on the site opposite to the amine nitrogen hydrogen. The binding of NO causes the N2-Fe-S1 angle to open from 132.3(1)° in **1** to 174.29(8)° in **1-NO**. The Fe-NO distance (Fe-N4 = 1.676(3) Å) is short, which indicates a double bond character. The Fe-N-O angle is nearly linear

(172.3(3)°), which is expected for an $\{FeNO\}^6$ system.[118,121] A comparison of the structural parameters of **1-NO** as determined by EXAFS,[57] see Table 2-1, and by X-ray crystallography, see Table 2-3, shows that both are very similar. This shows that EXAFS can provide accurate structural information. In addition, a comparison of the structural parameters of **1-NO**, see Tables 2-1 and 2-3, and of NO-inactivated NHase, see Tables 2-1 and 1-1, shows that they are very similar. This is the case even though **1-NO** does not contain oxidized sulfurs and amide nitrogens as does NO-inactivated NHase.

Table 2-3: Selected bond distances and angles of**1-NO**.

bond	distance (Å)	angle	(°)
Fe-S1	2.2603(9)	Fe-N4-O1	172.3(3)
Fe-S2	2.2604(9)	N1-Fe-N2	101.0(1)
Fe-N1 (imine)	1.993(3)	N1-Fe-N3	165.9(1)
Fe-N2 (amine)	2.108(3)	N1-Fe-N4	91.1(1)
Fe-N3 (imine)	1.979(3)	N1-Fe-S1	84.68(8)
Fe-N4 (NO)	1.676(3)	N1-Fe-S2	83.57(8)
N4-O1	1.161(4)	N2-Fe-N3	83.0(1)
N1=C (imine)	1.281(4)	N2-Fe-N4	88.9(1)
N3=C (imine)	1.289(4)	N2-Fe-S1	174.29(8)
		N2-Fe-S2	89.02(7)
		N3-Fe-N4	102.5(1)
		N3-Fe-S1	91.35(8)
		N3-Fe-S2	83.01(8)
		N4-Fe-S1	91.6(1)
		N4-Fe-S2	173.8(1)
		S1-Fe-S2	91.09(3)

Another hexacoordinated derivative of **1** has been synthesized. It is [Fe(III)$S_2^{Me2}N_3$(Pr,Pr)(N_3)] (**1-N_3**),[89] see Chapter III for more details, in which azide instead of NO is bound to the iron center through the N2-Fe-S1 angle. The iron in **1-N_3** is in the low-spin (S = 1/2) state. A comparison of corresponding bond lengths in **1-NO**, see Table 2-3, and **1-N_3**, see Table 3-3, shows the Fe-S bonds in **1-NO** to be slightly (0.06 Å) elongated and the Fe-N_{amine} bond in **1-NO** to be

slightly shortened (0.05 Å). This can be explained if one assumes, like it is done in the discussion below, that the orbital 'yz', which contains the unpaired electron in **1**, which pairs with the unpaired NO π* electron, has σ* Fe-S character. The resulting doubly occupied MO would thus be bonding with respect to Fe-NO, but slightly antibonding with respect to Fe-S and N-O. The weaker interaction between sulfur and iron would decrease the sulfur's trans influence which would result in a stronger interaction between N_{amine} and iron, and thus a shorter Fe-N_{amine} bond. Note that the Fe-N_{imine} distances in **1-NO** and **1-N$_3$** are very similar.

NHase binds NO reversibly. In NO-inactivated NHase, all NO is completely dissociated after photolysis with white light (500 W) for 15 minutes.[56] Also, in the case of **1-NO**, a photolytic cleavage of the Fe-NO bond to form **1** and NO occurs. However, the reaction is not reversible owing to the subsequent photodecomposition of **1**.

The Mößbauer parameters of **1-NO**,[123] $\delta = 0.0924$ mm/s and $\Delta E_o = 1.0078$ mm/s, are similar to those of NO-inactivated NHase,[124,125] $\delta = 0.02$ mm/s and $\Delta E_o = 1.49$ mm/s. They fall in the range expected for a low-spin Fe(III), which is in a very unsymmetrical electron environment.[126]

Based upon the fact that NO-inactivated NHase is formed by the reaction between NHase (Fe(III)) and NO, and based upon the similarities (UV/Vis, IR, magnetism, EXAFS, and Mößbauer) between **1-NO** and NO-inactivated NHase, the Fe-NO moiety in NO-inactivated NHase is assigned as being $\{FeNO\}^6$. The fact that **1-NO**, which contains two unmodified cis thiolates perpendicular to two imine nitrogens (the $Fe(S)_2$ plane is perpendicular to the $Fe(N_{imine})_2$ plane), is a very good spectroscopic model of the active site of NO-inactivated NHase suggests that NHase only contains one posttranslationally modified thiolate. If only the sulfone

modification is present, as indicated by mass spectrometric measurements,[54,60-63] then the remaining two unmodified cis thiolates are perpendicular to the two amide nitrogens (the $Fe(S)_2$ plane is perpendicular to the $Fe(N_{amide})_2$ plane). This characteristic structural motif of two cis thiolates perpendicular to two trans imine or amide nitrogens is also present in a number of good spectroscopic model compounds of active Fe-containing NHase.[67,74,84-91] As discussed in Chapter IV, the imine group models one of the tautomeric forms of an amide group.

Electronic Structure of Model Compounds

In order to be able to give a molecular orbital (MO) description, a coordinate system has to be defined. The coordinate system which was chosen for the cation of **1**, $[Fe(III)S_2^{Me2}N_3(Pr,Pr)]^+$ (**1**$^+$), is shown in Figure 2-4. For the cation of **1-NO**, $[Fe(III)S_2^{Me2}N_3(Pr,Pr)(NO)]^+$ (**1-NO**$^+$), a coordinate system was constructed in which the NO ligand binds along the y axis. By using the y axis for the NO ligand, the coordinate systems of **1**$^+$ and **1-NO**$^+$ are as similar as possible. Note that both ions are of C_1 symmetry.

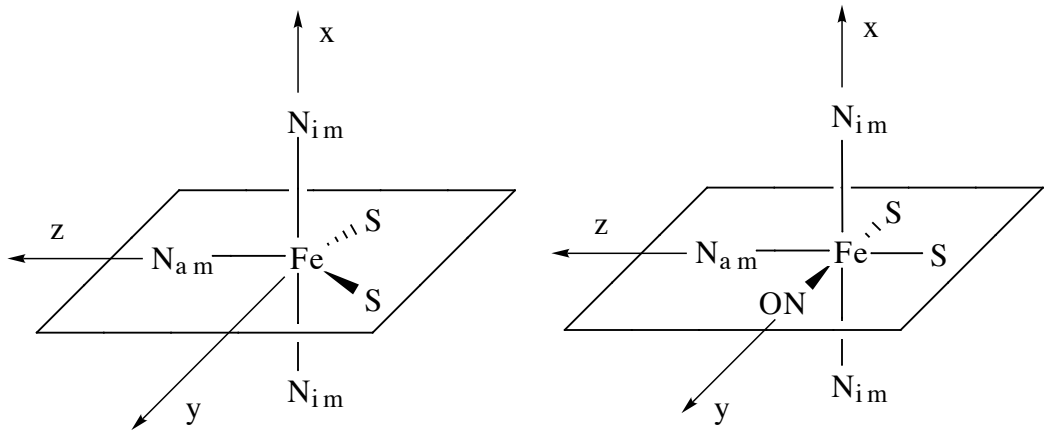

Figure 2-4: Coordinate systems for the cation of **1**, $[Fe(III)S_2^{Me2}N_3(Pr,Pr)]^+$ (**1**$^+$), and the cation of **1-NO**, $[Fe(III)S_2^{Me2}N_3(Pr,Pr)(NO)]^+$ (**1-NO**$^+$).

Herein, an abbreviated qualitative molecular orbital description will be presented. Since both imine nitrogens and both sulfurs are in an identical chemical environment, it cannot be assumed that only one metal orbital interacts with only one ligand orbital. In a detailed qualitative molecular orbital diagram, one would have to construct mixed metal orbitals so that both metal-imineN and both metal-S interactions are equivalent. The level of approximation chosen for the MO diagrams is sufficient to explain the spin state of 1/2 at temperatures below 100 K, see Figure 3-10, of the cation of **1**, $[Fe(III)S_2^{Me2}N_3(Pr,Pr)]^+$ (**1**$^+$), and the spin-pairing upon binding NO. Density function calculations, which will provide a quantitative description of the shapes and energies of the molecular orbitals of the cation of **1**, are currently in progress in the research group of Professor Solomon at Stanford University.[127]

Abbreviated Qualitative MO Diagram of the $[Fe(III)S_2^{Me2}N_3(Pr,Pr)]^+$ (1$^+$) Ion

In the molecular orbital diagram of the cation of **1**, $[Fe(III)S_2^{Me2}N_3(Pr,Pr)]^+$ (**1**$^+$), only σ interactions are considered. Also, only the higher energy orbitals that are involved in bonding are considered. The atomic orbitals of iron, which are involved in bonding, are higher in energy than the atomic orbitals of the ligands, which are involved in bonding.[46] Therefore, one can assume that the σ molecular orbitals have mainly ligand character, while the σ* and non-bonding (n) molecular orbitals have mainly metal character. Thus, the molecular orbitals are denoted as, for example, d 'yz', indicating that the molecular orbital d 'yz' has approximately the same shape (angular dependence function) as the atomic orbital d yz. In other words, the contributions of other atomic orbitals to the molecular orbital d 'yz' are close to zero.

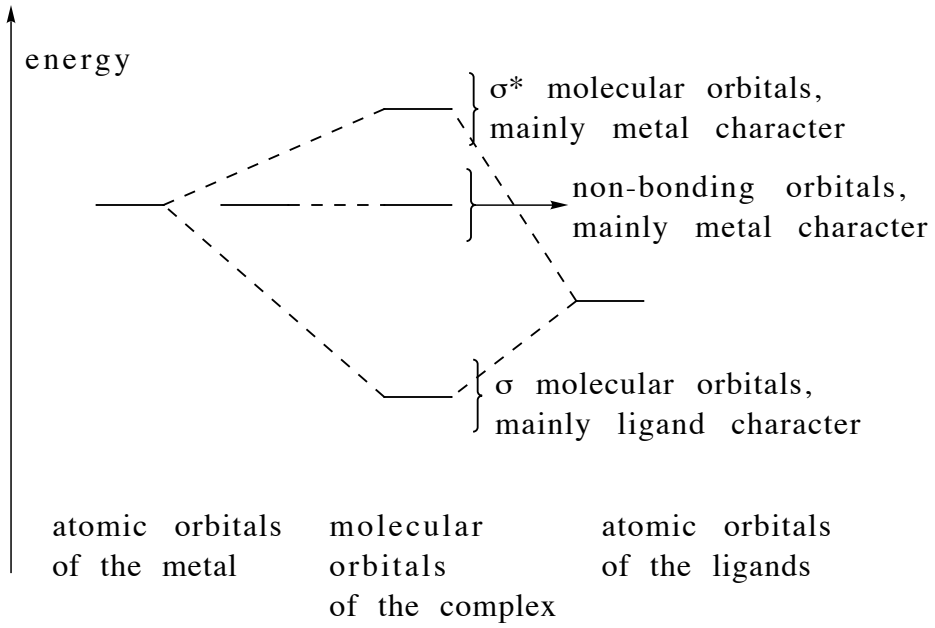

Figure 2-5: General qualitative MO diagram of a metal complex.[46]

If one considers the orientations of the metal-based 3d and 4p orbitals within the coordinate system of the cation of **1**, one can conclude that the d 'xy', d 'xz', and p 'y' molecular orbitals are non-bonding. This is the case sincethey are not directly pointing at any donor atom. Likewise, since they are pointing at at least one donor atom, one can conclude that the d 'yz', d 'z^2', d 'x^2-y^2', p 'z', and p 'x' molecular orbitals are anti-bonding (σ*). Crystal field arguments indicate that the d 'xz' orbital is higher in energy than the d 'xy' orbital because the d 'xz' orbital interacts in its plane with three donor atoms, while the d 'xy' orbital interacts in its plane with only two donor atoms. Crystal field arguments further indicate the following order according to increasing energy: d'yz' < d 'z^2' < d 'x^2-y^2'. The d 'x^2-y^2' MO is higher in energy than the d 'z^2' MO, since d 'x^2-y^2' points directly at two donor atoms, while d 'z^2' points directly at only one donor atom. The d 'yz' MO is

lower in energy since it only points indirectly at the two sulfur donor atoms. Because the 4p atomic orbitals are higher in energy than the 3d atomic orbitals, the 'p' molecular orbitals must also be higher in energy than the 'd' molecular orbitals. Since the molecular orbital p 'y' is non-bonding, it must be lower in energy than the p 'x' and p 'z' molecular orbitals. The five σ molecular orbitals are completely filled using the ten electrons which are contributed by the donor atoms of the ligand to the formation of bonds (two imine nitrogens with two electrons each, one amine nitrogen with two electrons, and two sulfurs with two electrons each). Therefore, all five 3d electrons of Fe(III) are used to fill the 'd' molecular orbitals. This MO diagram explains the fact that the cation of **1**, $[Fe(III)S_2^{Me2}N_3(Pr,Pr)]^+$ (**1**$^+$), has a spin of S = 1/2, if one assumes that the energy difference between the d 'xz' orbital and the d 'z^2' orbital is larger than the spin pairing energy. Only the HOMO/LUMO region is shown in the MO diagram.

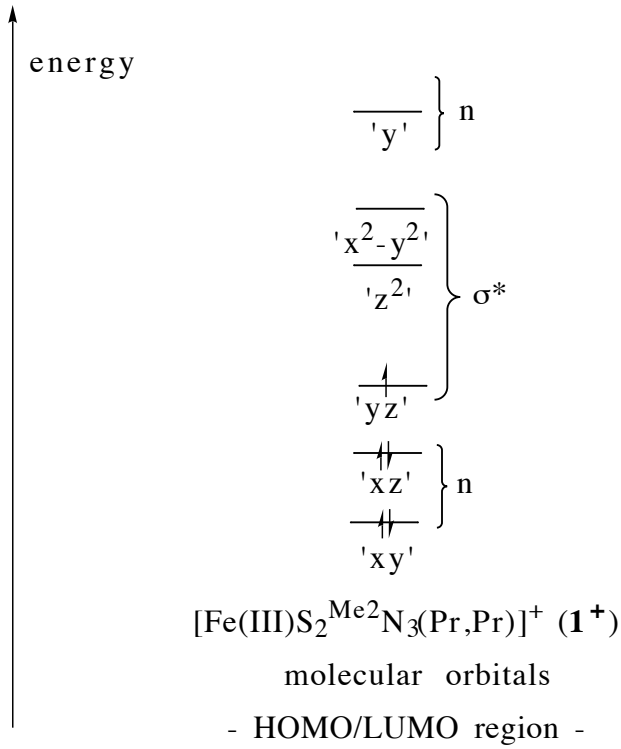

Figure 2-6: Abbreviated qualitative MO diagram of the cation of **1**.

Abbreviated Qualitative Molecular Orbital Diagram of the 1-NO$^+$ Ion

For NO to bind to pentacoordinated $[Fe(III)S_2^{Me2}N_3(Pr,Pr)]^+$ (**1**$^+$), an empty non-bonding orbital must point in the direction of the incoming NO ligand. This condition is satisfied by the presence of the non-bonding p 'y' orbital. The p 'y' orbital of iron interacts with the filled lone pair orbital σ_2 on the nitrogen of the NO ligand to form a σ bond. Since the cation of **1-NO**, **1-NO**$^+$, is diamagnetic, S = 0, a spin pairing between the unpaired electron spin of **1**$^+$ and NO must occur. This can be achieved either if the orbitals of **1**$^+$ and NO that contain the unpaired electron interact to form two molecular orbitals, that is a bond, or if antiferromagnetic coupling occurs. Since iron and NO are directly interacting and the orbitals are properly aligned, it is assumed that a π interaction between the **1**$^+$ d 'yz' σ* orbital

and the NO π* orbital containing the unpaired electron occurs. This π interaction results in the formation of a new bonding and a new anti-bonding orbital between iron and NO. The σ and π interactions are shown in the following MO diagram. Only the HOMO/LUMO region and the molecular orbitals of NO that are involved in Fe-NO binding are shown. The MO diagram of NO is shown in Figure 2-9. About 60 % of the spin density of the unpaired electron in NO is located on the nitrogen atom in a π symmetry orbital.[119] In a more detailed description of the cation of **1-NO**, $[Fe(III)S_2^{Me2}N_3(Pr,Pr)(NO)]^+$ (**1-NO**$^+$), one also would have to consider a π interaction between the filled d 'xy' orbital and the empty NO π* orbital. This would be called a π "back-bonding" or a π "back-donation".[46] A graphical representation of the formation of the σ and π bond between Fe and NO is shown in Figure 2-8.

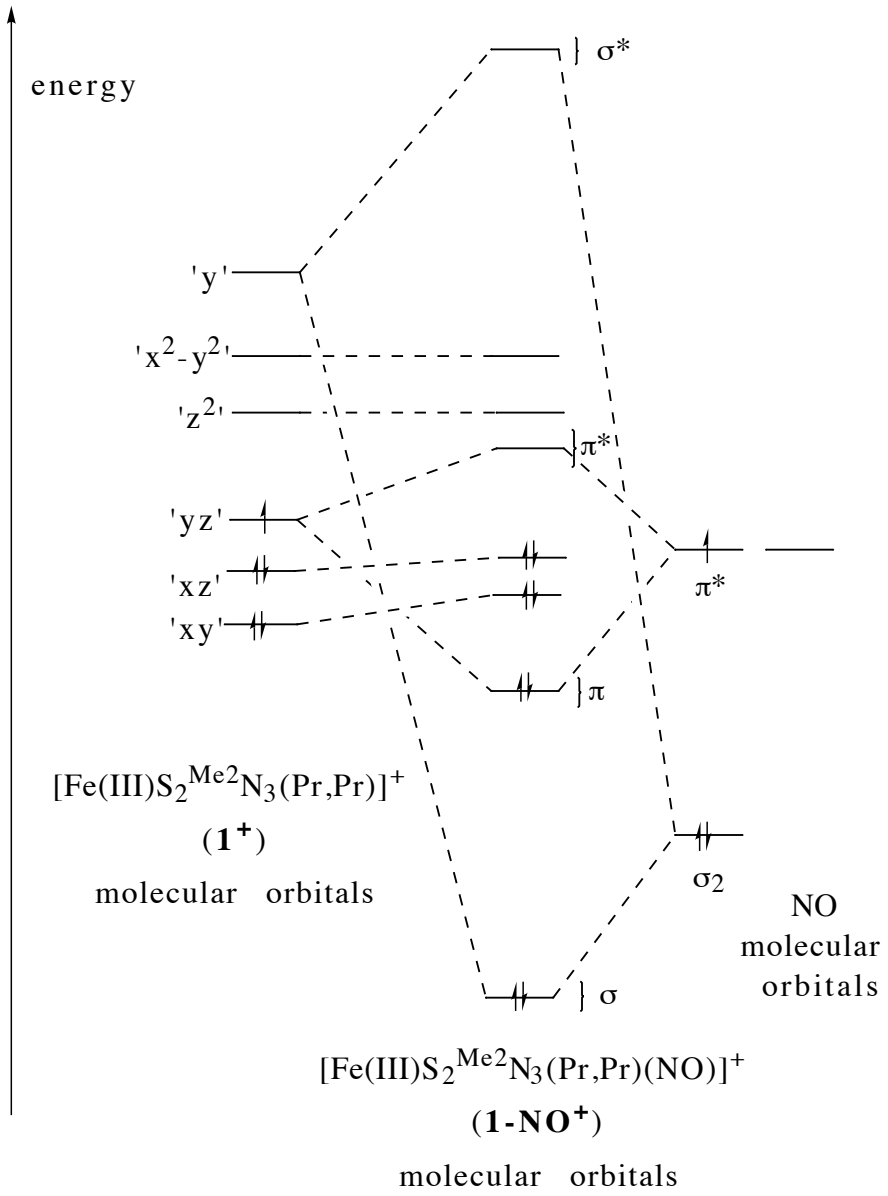

Figure 2-7: Abbreviated qualitative MO diagram of the cation of **1-NO**.

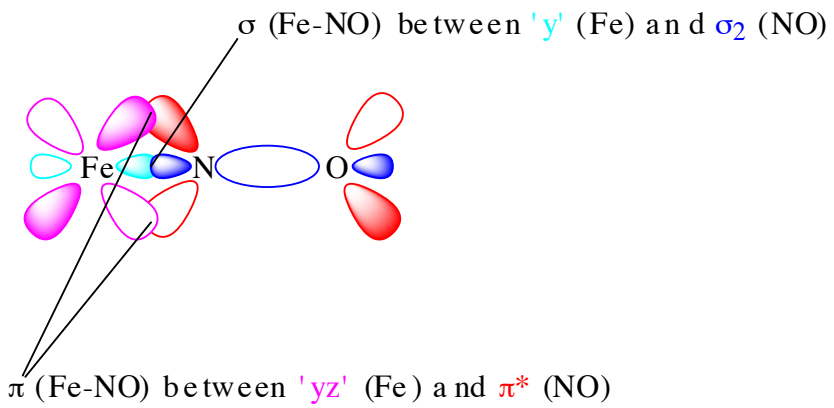

Figure 2-8: Graphical representation of the formation of a σ and π bond between Fe and NO.

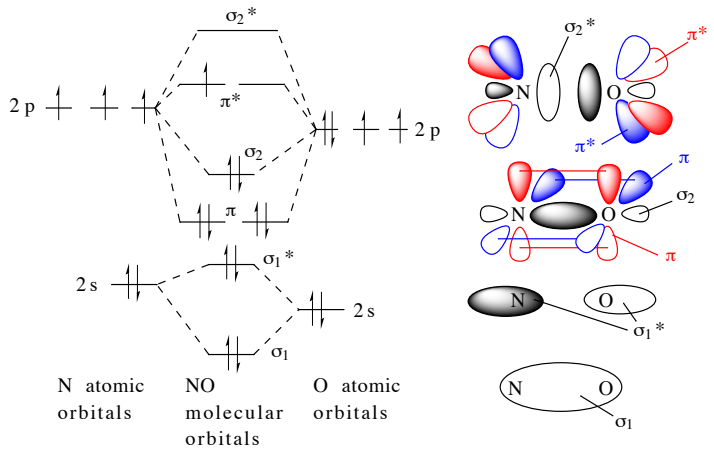

Figure 2-9: MO diagram of NO.[119]

The energy of the newly formed π* orbital in Fe-NO complexes is below that of the unfilled metal d 'z^2' and d 'x^2-y^2' orbitals.[128] It is this orbital which in $\{Fe\text{-}NO\}^7$ complexes contains the extra electron. Since this orbital is mainly N-based, $\{Fe\text{-}NO\}^7$ complexes contain a bent Fe-NO unit. In comparison, in CO

compounds this π* orbital is always higher in energy than the 'd' orbitals, therefore one never worries about it.

It has been observed that hexacoordinated compounds, such as [Fe(III)$S_2^{Me2}N_3$(Pr,Pr)(N_3)] (**1-N_3**)[89] or [Fe(III)$S_2^{Me2}N_3$(Et,Pr)(N_3)] (**5-N_3**), see Chapter III for more details, containing two cis thiolate donors perpendicular to two trans imine or amide nitrogen donors give rise to intense absorption bands at about 400 and 700 nm (the $Fe(S)_2$ plane is perpendicular to the $Fe(N_{imine/amide})_2$ plane).[67,74,84-91] In NHase, these absorption bands have sulfur to iron charge transfer character.[43,47,48] In comparison, in [Fe(III)$S_2^{Me2}N_3$(Pr,Pr)(NO)]PF_6 (**1-NO**) only the absorption band at around 400 nm is present. A likely explanation for this is that the d 'yz' orbital, which contains the electron that undergoes spin pairing with the unpaired electron on the NO ligand, that is, π bond formation, is the orbital into which the sulfur lone pair electron is promoted in the 700 nm electron transition. After binding NO, this orbital is filled because of the accompanying spin pairing. Therefore, the 700 nm electron transition can no longer occur.

Chapter III: The Influence of a Small Structural Change on the Reactivity of Metal Complexes[91]

Introduction

Previous research in the Kovacs group resulted in the isolation of a pentacoordinated compound, $[Fe(III)S_2^{Me2}N_3(Pr,Pr)]PF_6$ (**1**).[89] It possesses a Pr,Pr ligand backbone derived from N-(3-aminopropyl)-1,3-propanediamine (Pr,Pr-amine). Azide[89] and, as it was discussed in the previous Chapter, NO[58] bind at the open binding site of **1**. Thereby hexacoordinated Fe(III) complexes are generated that are good spectroscopic models (spin states and electronic absorption spectra) of the active site in Fe-containing NHase.

The open binding site of **1** is within the angle S1-Fe-N_{amine} = 132.3(1)°. To study how the length of the ligand backbone influences the reactivity of the resulting metal complexes, N-(2-aminoethyl)-1,3-propanediamine(Et,Pr-amine) was used instead of Pr,Pr-amine in a reaction analogous to the synthesis of **1**. This change of the amine results in the shortening of the ligand backbone by one methylene unit. It is expected that the different ligand backbone will result in a distortion of the coordination sphere relative to **1** and hence also a different reactivity.

Synthesis and Characterization of 4

Previous research in the Kovacs group has shown that a Schiff base condensation of Pr,Pr-amine with two equivalents of the sodium salt of 3-mercapto-3-methyl-2-butanone on an Fe(II) template, followed by oxidation, results in the formation of pentacoordinated $[Fe(III)S_2^{Me2}N_3(Pr,Pr)]PF_6$ (**1**), see Figure 3-1.[89] Interestingly, it was found in the present research that the removal of

a methylene unit from the amine source in this Schiff base condensation, after oxidation, results in the formation of a hexacoordinated persulfide-containing complex, **4**, instead of the expected pentacoordinated complex. That is, a very stable Fe(III)-thiolate complex, $[Fe(III)(S_2^{Me2}N_3(Et,Pr))\text{-}S^{pers}]PF_6$ (**4**), which contains an η^2-coordinated alkyl persulfide ligand, can be isolated, after oxidation, from the Fe(II)-templated Schiff base condensation of Et,Pr-amine with the sodium salt of 3-mercapto-3-methyl-2-butanone, see Figure 3-1. Alternatively, **4** can be prepared by the reaction between Fe(III), the sodium salt of 3-mercapto-3-methyl-2-butanone, and Et,Pr-amine.

There are only a small number of metal complexes known that contain an η^2-coordinated alkyl persulfide ($R\text{-}S_2^-$) ligand.[129-136] Most of them were prepared by alkylation of the disulfido ligand (S_2^{2-}).[129,130,133-135] Of the known η^2-alkyl persulfide complexes, only three were stable enough to be isolated in crystalline form so that their crystal structure could be determined.[129,136,137] Those three complexes contain 2nd (Mo) or 3rd (W, Os) row transition metals.

In comparison, if two methylene units are removed from the amine source, that is, Et,Et-amine is used, then only a hexacoordinated complex can be isolated which contains two meridional (*mer*) tridentate ligands.[138] Each one of the tridentate ligands contains as donor groups one thiolate, one imine, and one secondary amine. The ligand also contains an unbound primary amine; in other words, only one of the primary amine units of Et,Et-amine participated in a Schiff base condensation.

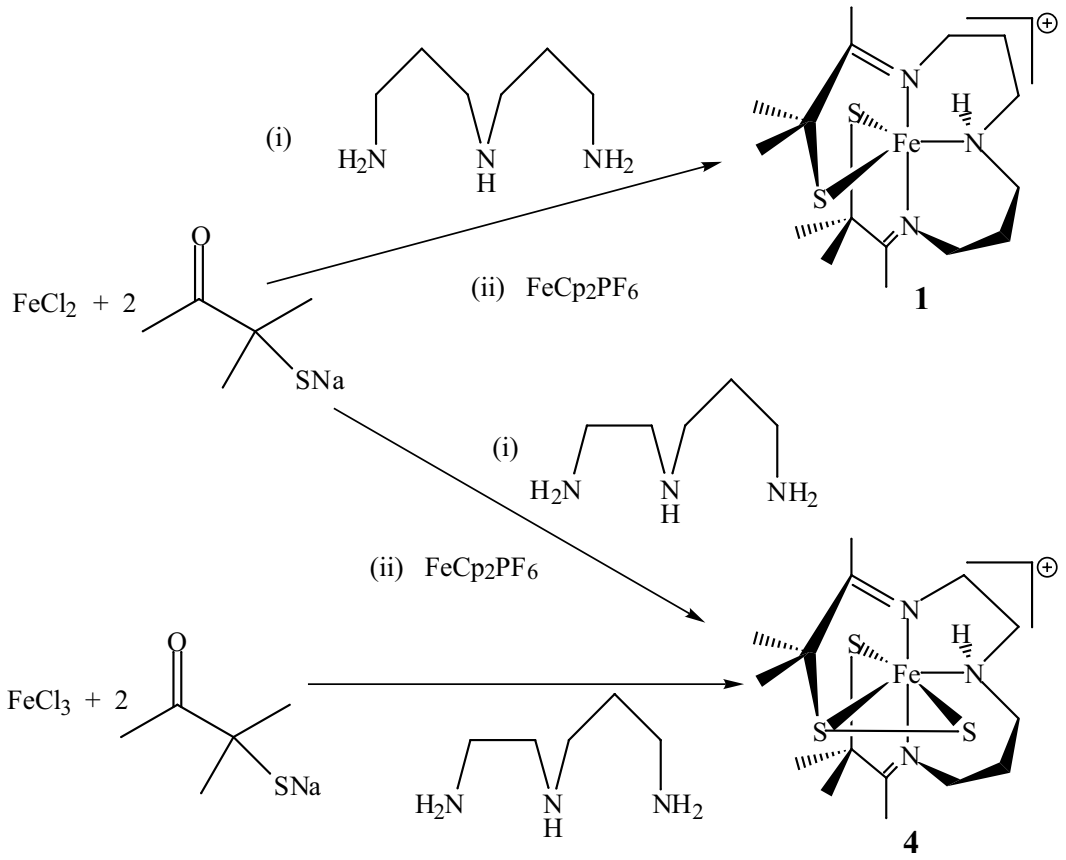

Figure 3-1: Syntheses of **1** and **4**.

During the formation of the alkyl persulfide containing **4**, a C-S bond cleavage must occur. The mechanism of this reaction in the present system is currently not understood. However, it is known that C-S bond cleavage can occur on low-valent metal complexes,[139,140] on metal surfaces,[141] or during hydrodesulfurization.[142] C-S bond cleavage during reduction is well documented.[143,144] It is interesting to note that in the present case C-S bond cleavage, that is the formation of **4**, was observed both in the reaction starting from Fe(II) as well as in the reaction starting from Fe(III). In the reaction starting from

Fe(II) a somewhat higher yield is observed. This is attributed to the formation of [Fe(II)$S_2^{Me2}N_3$(Et,Pr)] (**3**) at the Fe(II) stage, which is then oxidized to the Fe(III) form. Presumably, in the reaction starting from Fe(III), some of the substance is lost due to the formation of Fe(II) and disulfide. Conducting the reaction in the presence of excess thiol or thiolate did not result in a significant increase in yield.

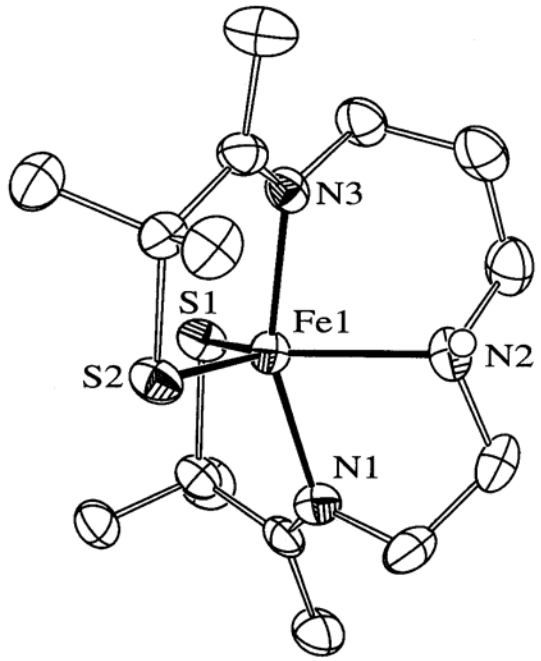

Figure 3-2: Thermal ellipsoid plot (50 % probability level) of **3**. H atoms, except for the H-N_{amine}, are omitted for clarity.

When the reaction to synthesize **4** while starting on Fe(II) was worked up before adding the oxidizing agent, it was possible to isolate a small amount of crystals of the pentacoordinated Fe(II) analogue [Fe(II)$S_2^{Me2}N_3$(Et,Pr)] (**3**), see Figure 3-2 and Table 3-2. However, due to its high oxygen sensitivity, it was not possible to isolate sufficient quantities of this substance that could have permitted a full characterization. This compound is mentioned here, since its existence suggests

that the persulfide formation, that is C-S bond cleavage, occurs at the Fe(III) stage and not at the Fe(II) stage. However, it should also be noted that in another system C-S bond cleavage was proposed to occur at the Fe(II) stage.[145]

The present Fe(III)-containing, η^2-alkyl persulfide coordinated compound $[Fe(III)(S_2^{Me2}N_3(Et,Pr))\text{-}S^{pers}]PF_6$ (**4**) may represent a model for an intermediate in the assembly of Fe-S clusters. Cysteine persulfide (thiocysteine, cysteine perthiolate) is found in biological systems. It has been shown that NifS catalyzes the desulfurization of cysteine to form alanine and a NifS-bound cysteine persulfide.[146] This cysteine persulfide-containing enzyme may then interact with Fe(II) or Fe(III) to form Fe-S clusters.[147] Also, a NifS homolog enzyme[148] and a cystine lyase[149] are able to direct Fe-S cluster assembly. A cysteine persulfide, which is coordinated end-on to an iron (Fe-S = 2.48 Å), was found in the prismane protein.[150] The intermediate enzyme-sulfur complex of rhodanese also contains the extra sulfur bound to cysteine in the form of a persulfide.[151] It should also be noted that cystine lyases are able to cleave one of the C-S bonds in cystine to produce cysteine persulfide.[149,152] Cysteine persulfide has also been found as an unexpected result of mutagenesis studies[153,154] and of the purification procedure.[155]

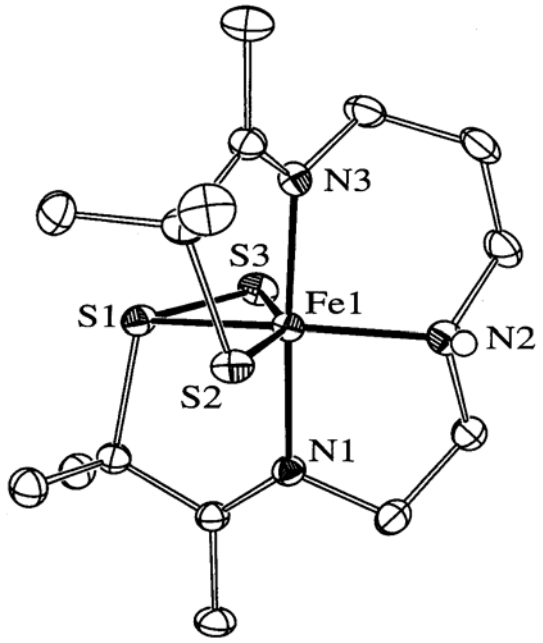

Figure 3-3: Thermal ellipsoid plot (50 % probability level) of the cation of **4**. H atoms, except for the H-N_{amine}, are omitted for clarity.

The Fe-S1,2 distances (average = 2.20(3) Å) in **4** are similar to those observed in other hexacoordinated low-spin (S = 1/2) Fe(III) complexes with nitrogen and sulfur donor atoms.[67,74,84-91,156] In comparison, a typical high-spin (S = 5/2) Fe(III)-thiolate distance is about 2.3 Å.[157] The S-S distance within the η^2-coordinated alkyl persulfide (S1-S3 2.011(1) Å) is similar to those (mean = 2.021(6) Å) observed in the other three structurally characterized η^2-alkyl persulfide-containing complexes.[129,136,137] It is, however, slightly shorter than the average S-S distance (2.05(1) Å) in α-S_8.[104] The extra persulfide sulfur is bound at the site that in the pentacoordinated compound **5**, see below, is the open binding site. Compound **4** contains its iron ion in a highly distorted octahedral coordination environment. Trans angles vary from 149.86(9)° to 175.6(1)° and cis

angles vary from 51.85(3)° to 108.25(9)°. The structure of **4** is illustrated in Figure 3-3 and important bond lengths and angles are provided in Table 3-1.

Table 3-1: Selected bond distances and angles of [Fe(III)($S_2^{Me2}N_3$(Et,Pr))-S^{pers}]PF_6 (**4**).

bond	distance (Å)	angle	(°)
Fe-S1	2.2209(9)	N1-Fe-N2	85.2(1)
Fe-S2	2.1694(8)	N1-Fe-N3	175.6(1)
Fe-S3	2.3687(9)	N1-Fe-S1	84.99(8)
Fe-N1 (imine)	1.944(2)	N1-Fe-S2	92.35(8)
Fe-N2 (amine)	1.993(3)	N1-Fe-S3	87.13(8)
Fe-N3 (imine)	1.971(2)	N2-Fe-N3	92.1(1)
S1-S3	2.011(1)	N2-Fe-S1	149.86(9)
N1=C (imine)	1.285(4)	N2-Fe-S2	108.25(9)
N3=C (imine)	1.290(4)	N2-Fe-S3	99.23(9)
		N3-Fe-S1	99.07(8)
		N3-Fe-S2	85.13(8)
		N3-Fe-S3	96.80(8)
		S1-Fe-S2	100.57(3)
		S1-Fe-S3	51.85(3)
		S2-Fe-S3	152.38(4)
		Fe-S1-S3	67.87(3)
		Fe-S3-S1	60.29(3)

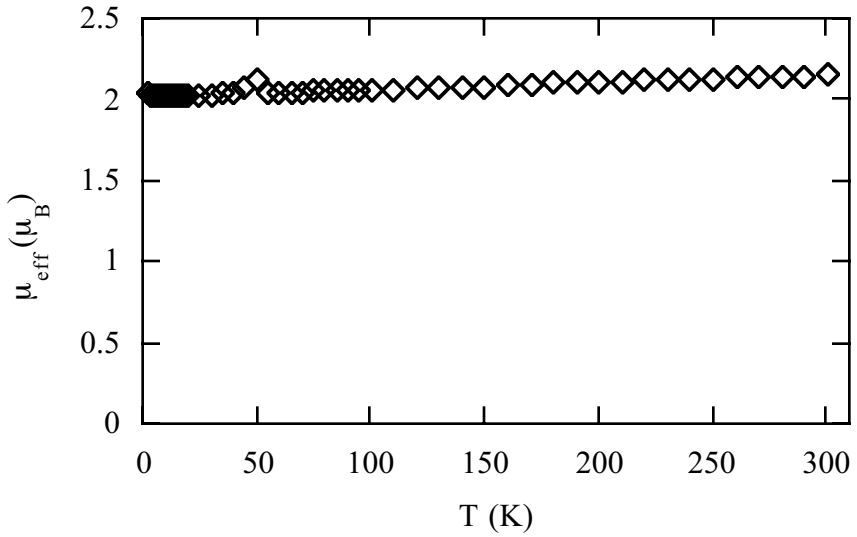

Figure 3-4: Solid state effective paramagnetic magnetic moment of $[Fe(III)(S_2^{Me2}N_3(Et,Pr))\text{-}S^{pers}]PF_6$ (**4**).

Based upon solid state effective paramagnetic magnetic moment measurements, see Figure 3-4, complex **4** is in the low-spin state (S = 1/2) in the temperature range of 2 - 300 K. An EPR spectrum of **4**, see Figure 3-5, confirms this assignment. Hexacoordinated **4** gives rise to a characteristic Fe(III) low-spin rhombic EPR signal with g-values of 2.165, 2.106, and 1.994. This spin state is consistent with earlier findings that hexacoordinated Fe(III) complexes containing two cis thiolate donors perpendicular to two trans imine nitrogens donors are in the low-spin state in the temperature range of 2 - 300 K.[84,89,90]

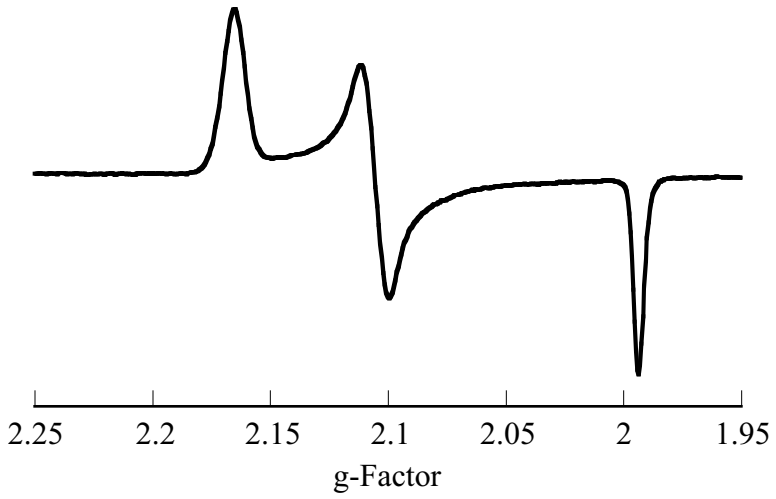

Figure 3-5: EPR spectrum (MeOH/EtOH 9/1; 141 K) of **4**.

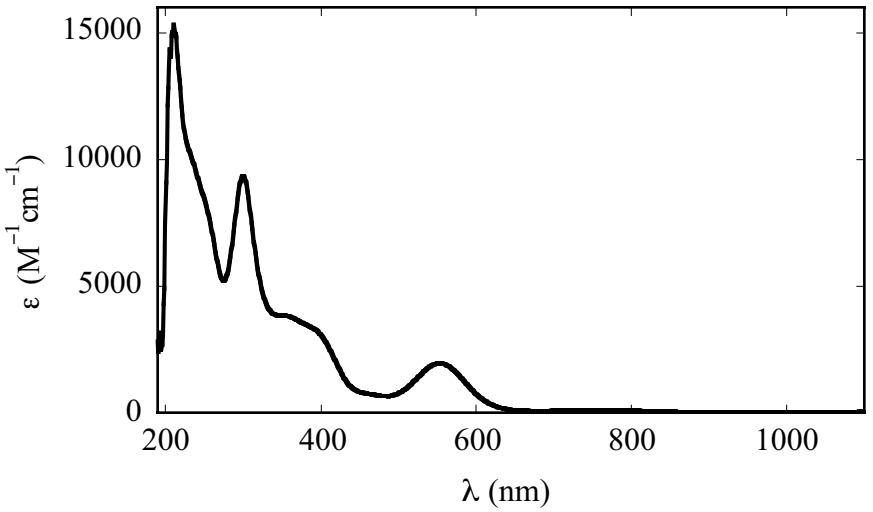

Figure 3-6: UV/Vis absorption spectrum of $[Fe(III)(S_2^{Me2}N_3(Et,Pr))\text{-}S^{pers}]PF_6$ (**4**) in MeOH.

Complex **4** dissolves in solvents such as CH_2Cl_2, MeOH, and MeCN to give an intensely pink colored solution. This is due to the absorption of green light. The extinction coefficient of the absorption band at 553 nm (ε = 1950 $M^{-1}cm^{-1}$) is characteristic of a charge transferelectron excitation. The reduction potential ($E_{irrev.\ Red.}$ = - 790 mV (vs. SCE)) of hexacoordinated **4** compares well with that of other hexacoordinated Fe(III)-containing compounds.[69,90] The fact that the reduction of **4** is irreversible suggests the corresponding Fe(II) persulfide compound decomposes within the time frame of one cyclic voltammetry scan (~ 5 s).

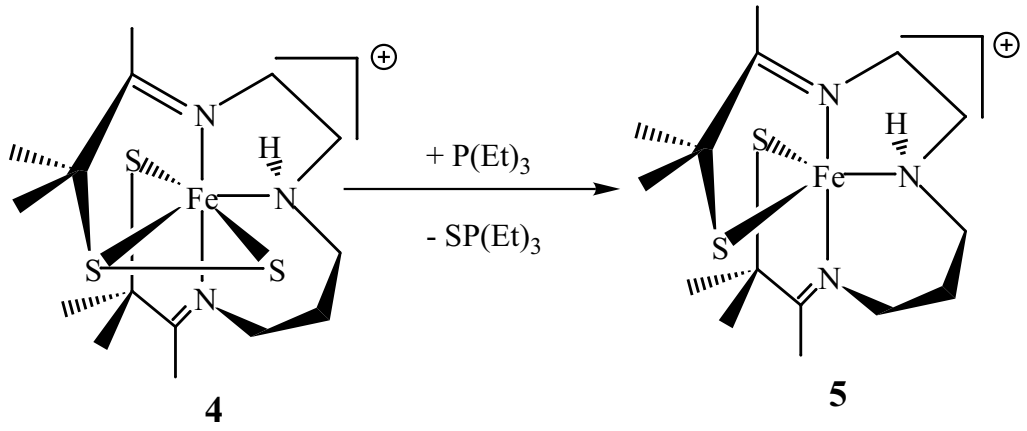

Figure 3-7: Synthesis of **5** from **4**.

Synthesis and Characterization of 5

Using $P(Et)_3$ to abstract the extra persulfide sulfur, it was possible to convert hexacoordinated $[Fe(III)(S_2^{Me2}N_3(Et,Pr))\text{-}S^{pers}]PF_6$ (**4**) into pentacoordinated $[Fe(III)S_2^{Me2}N_3(Et,Pr)]PF_6$ (**5**) in a clean reaction. Evaporation of the ether from the extraction yielded a white solid that was identified as $SP(Et)_3$ by mass spectrometry and NMR. The same reaction was observed when $P(Ph)_3$ was used. However, it was found that **4** is stable in the presence of $(Me)_3SiSi(Me)_3$ and EtMgBr. Surprisingly, pentacoordinated **5** is stable in solution. In MeCN and

CH_2Cl_2 as the solvent it is stable for days, while in a MeOH solution about 10 % decomposition is observed within 40 hours. It was not possible to convert **5** back into **4** by the addition of thiols or sodium thiolates to a solution of **5**.

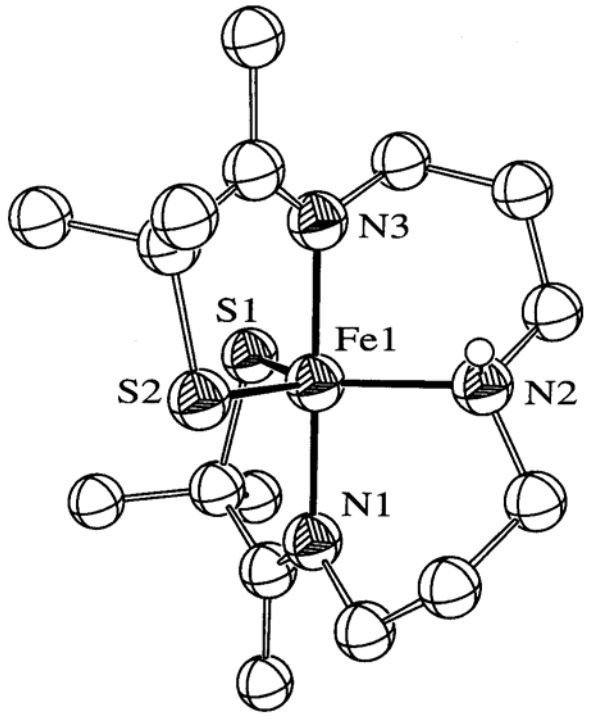

Figure 3-8: Thermal ellipsoid plot (50 % probability level) of the cation of **1**. H atoms, except for the H-N_{amine}, are omitted for clarity.[89]

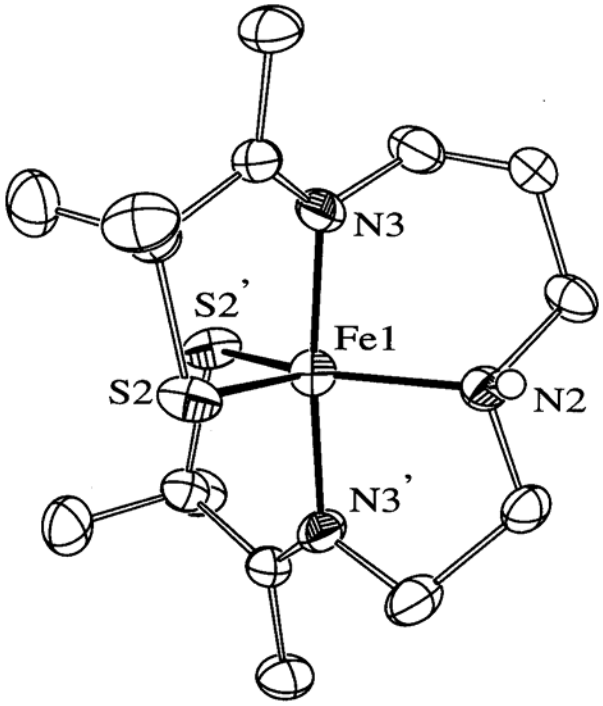

Figure 3-9: Thermal ellipsoid plot (50 % probability level) of the cation of **5**. H atoms, except for the H-N_{amine}, are omitted for clarity.

The bond distances in pentacoordinated $[Fe(III)S_2^{Me2}N_3(Et,Pr)]PF_6$ (**5**), see Figure 3-9 and Table 3-2, are slightly shorter than those in pentacoordinated $[Fe(III)S_2^{Me2}N_3(Pr,Pr)]PF_6$ (**1**), see Figure 3-8 and Table 3-2.[89] Specifically, the mean Fe-S bond distance shortens by 0.030 Å, the mean Fe-N_{imine} bond distance shortens by 0.037 Å, and the Fe-N_{amine} bond distance shortens by 0.039 Å. The bond distances in **1** are slightly longer than those in **5** since at the temperature (183 K) of the structure determination of **1** higher spin states are partially occupied, see Figure 3-10. In comparison, **5** is low-spin (S = 1/2) at the temperature (161 K) of its structure determination. In most cases, higher spin states cause an increase of the metal-ligand bond distances since antibonding orbitals are occupied. The most

significant difference between the structures of **1** and **5** is the increase of the S1/2'-Fe-N2 angle from 132.3(1)° in **1** (∠ S1-Fe-N2) to 141.8(1)° in **5** (∠ S2'-Fe-N2). It is at this open binding site where **1** binds azide and NO.[58,89] This opening of the binding site can also be characterized by the change in τ; τ is defined as the difference between the largest and the second largest angle divided by 60°: $\tau = (\alpha - \beta)/60° = 0$ for ideal C_{4v}, and $\tau = 1$ for ideal D_{3h}.[158] The parameter τ is 0.763 in the case of **1** and 0.538 in the case of **5**. This indicates that the removal of a methylene unit from the ligand backbone of **1** causes a significant distortion: **5** is more square pyramidal than **1**, thereby the reactive site is more open. As it is discussed below, azide binds to the iron at this site. Preliminary results indicate that even nitriles and MeOH can bind through this site.[159]

Table 3-2: Selected bond distances (Å) and angles (°) of $[Fe(II)S_2^{Me2}N_3(Et,Pr)]$ (**3**), $[Fe(III)S_2^{Me2}N_3(Et,Pr)]PF_6$ (**5**),[#] and $[Fe(III)S_2^{Me2}N_3(Pr,Pr)]PF_6$ (**1**).[89]

	3 • MeCN	**5**[#]	**1**
Fe-S1	2.342(1)	2.117(1)	2.133(2)
Fe-S2	2.317(1)	2.117(1)	2.161(2)
Fe-N1 (imine)	2.123(4)	1.924(2)	1.967(4)
Fe-N2 (amine)	2.216(4)	2.010(4)	2.049(4)
Fe-N3 (imine)	2.116(4)	1.924(2)	1.954(4)
N1=C (imine)	1.271(6)	1.271(3)	1.279(9)
N3=C (imine)	1.270(6)	1.271(3)	1.279(9)
N1-Fe-N2	77.0(1)	86.4(1)	94.2(2)
N1-Fe-N3	157.8(1)	174.1(1)	178.1(2)

N1-Fe-S1	81.6(1)	86.69(7)	86.7(1)
N1-Fe-S2	108.4(1)	96.90(7)	95.2(1)
N2-Fe-N3	81.0(1)	87.9(1)	86.2(2)
N2-Fe-S1	123.0(1)	141.8(1)	132.3(1)
N2-Fe-S2	114.0(1)	112.5(1)	106.5(1)
N3-Fe-S1	108.5(1)	96.90(7)	91.6(1)
N3-Fe-S2	83.1(1)	86.68(7)	86.4(1)
S1-Fe-S2	122.84(5)	105.67(5)	121.0(1)
τ	0.580	0.538	0.763

[#] Due to the crystallographically imposed two-fold axis, see Chapter V for more details, S2' and N3' in **5** correspond to S1 and N1 in the other compounds.

The bond distances in pentacoordinated $[Fe(III)S_2^{Me2}N_3(Et,Pr)]PF_6$ (**5**), as compared to those of pentacoordinated $[Fe(II)S_2^{Me2}N_3(Et,Pr)]$ (**3**), show a clear trend that one would expect when replacing Fe(II) by Fe(III) in an identical coordination environment. Because of the higher charge at the central metal ion, shorter metal-ligand distances are observed. In this case, the mean Fe-S distance shortens by 0.213 Å, the mean Fe-N_{imine} distance shortens by 0.196 Å, while the Fe-N_{amine} distance shortens by 0.206 Å.

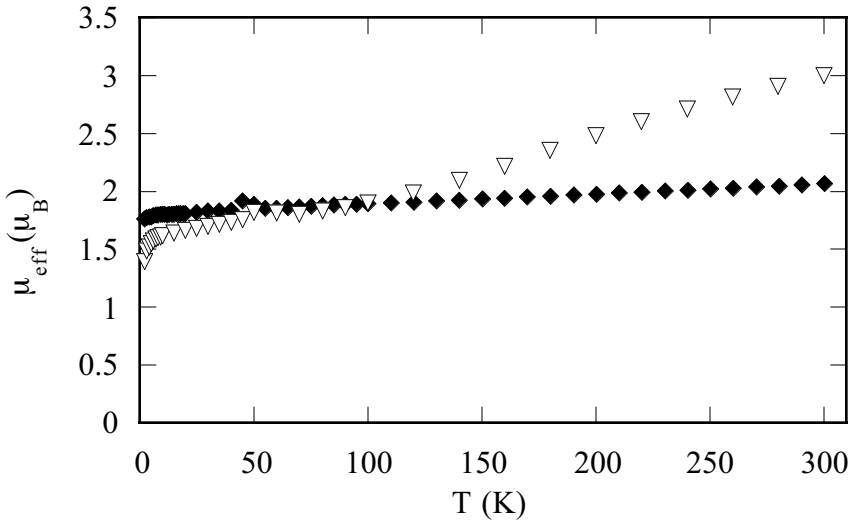

Figure 3-10: Solid state effective paramagnetic magnetic moment of [Fe(III) $S_2^{Me2}N_3$(Pr,Pr)]PF_6 (**1**) (∇) and [Fe(III)$S_2^{Me2}N_3$(Et,Pr)]PF_6 (**5**) (♦).

Solid state effective paramagnetic magnetic moment data, see Figure 3-10, indicates that in the temperature range of 2 - 300 K complex [Fe(III)$S_2^{Me2}N_3$(Et,Pr)]PF_6 (**5**) is in the spin state S = 1/2 (low-spin). Its magnetic behavior is different from that of [Fe(III)$S_2^{Me2}N_3$(Pr,Pr)]PF_6 (**1**).[89] Higher spin states become partially populated in **1** at temperatures above 100 K. Figure 3-11 shows the EPR spectra of pentacoordinated **1** and **5**. Complexes **1** and **5** are characterized by pseudo-rhombic Fe(III) S = 1/2 EPR signals with g-values of 2.14, 2.07, and 2.01 (**1**) and 2.12, 2.07, and 2.02 (**5**). The additional feature with a g value maximum of 2.20 (**1**) or 2.17 (**5**) is presumably caused by an intermolecular interaction since it becomes less intense if a less concentrated solution is measured.

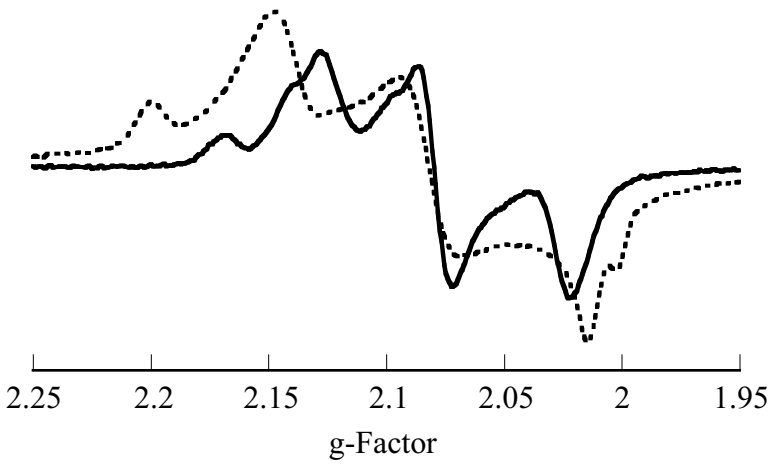

Figure 3-11: EPR spectra of $[Fe(III)S_2^{Me2}N_3(Pr,Pr)]PF_6$ (**1**) (···) and $[Fe(III)S_2^{Me2}N_3(Et,Pr)]PF_6$ (**5**) (-) in CH_2Cl_2/Toluene 1/1 (**1**: 125 K, **5**: 150 K).

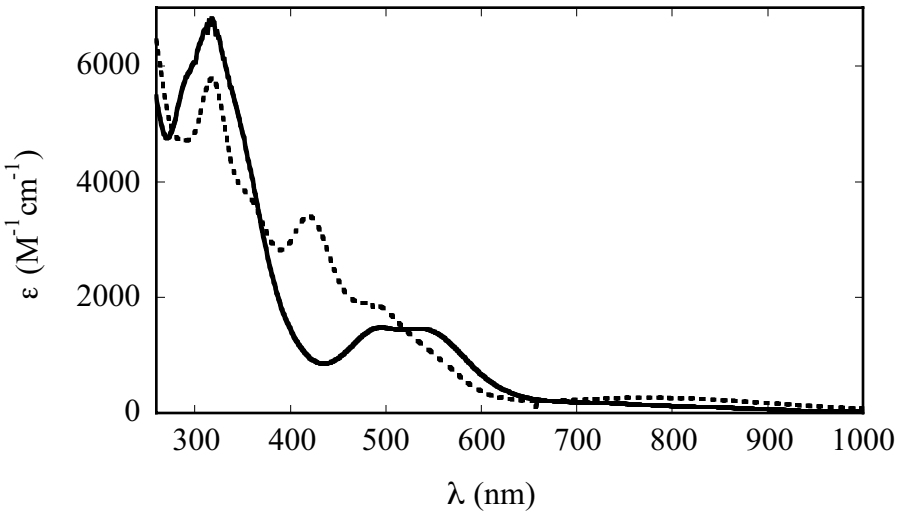

Figure 3-12: UV/Vis absorption spectra of **1** (···) and **5** (-) in CH_2Cl_2.

Complex **5** is soluble in solvents such as CH_2Cl_2, MeOH, and MeCN to give an intensely pink colored solution. This is due to the absorption of green light. The extinction coefficients (~ 1500 $M^{-1}cm^{-1}$) of the absorption bands at 493 and 532 nm are characteristic of a charge transfer electron excitation. In comparison, **1** gives rise to absorption bands at around 319 and 420 nm. The Fe(III) oxidation state in pentacoordinated **5** is stabilized, that is, its redox potential is more negative, by 55 mV as compared to the Fe(III) oxidation state in pentacoordinated **1**.[58]

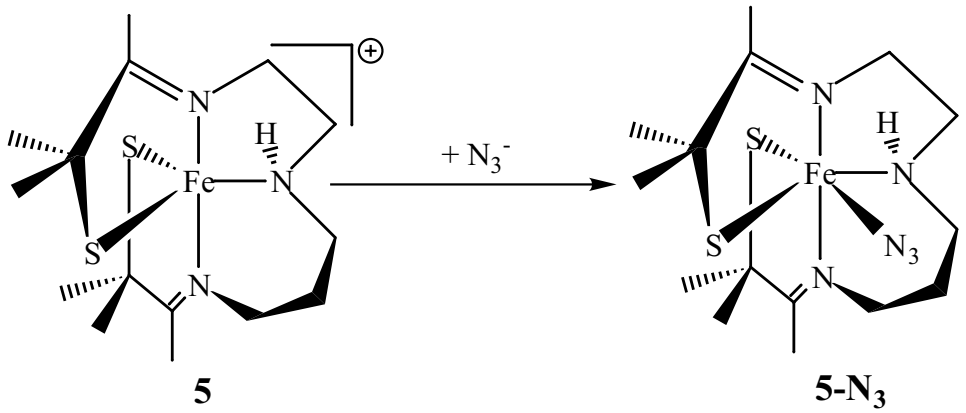

Figure 3-13: Synthesis of **5-N$_3$** from **5**.

Synthesis and Characterization of 5-N$_3$

The addition of soluble azide salts, such as tetra(*n*-butyl)ammonium azide or tetramethylammonium azide, to pentacoordinated $[Fe(III)S_2^{Me2}N_3(Et,Pr)]PF_6$ (**5**) results in the binding of azide to the iron at the open binding site of **5** to form hexacoordinated $[Fe(III)S_2^{Me2}N_3(Et,Pr)(N_3)]$ (**5-N$_3$**), see Figure 3-13. Azide coordination to **5** causes the absorption band at 532 nm to disappear, the absorption band at 493 nm to shift to 475 nm, and the appearance of the absorption band at 760 nm, see Figure 3-19. In solvents such as MeCN and CH_2Cl_2, the addition of 1.5 equivalents of azide at room temperature results in complete azide

binding. In comparison to this, it was found that when MeOH is used as the solvent the equilibrium is shifted so that significant amounts of both pentacoordinated **5** and azide-bound **5-N_3** are present. Besides azide, a number of other 'substrates' bind to **5**. They include SCN^- ($\lambda_{max,\ low\ energy\ absorption}$ = 800 nm, MeCN RT), cyclohexylisonitrile (888 nm, CH_2Cl_2 RT), MeCN (830 nm, CH_2Cl_2 - 90 °C), Cl^- (744 nm, CH_2Cl_2 - 90 °C), CN^- (818 nm, CH_2Cl_2 RT), and MeOH (758 nm, CH_2Cl_2 - 90 °C). In comparison, **1** also binds N_3^- (720 nm, CH_2Cl_2 RT), SCN^- (778 nm, CH_2Cl_2 RT), cyclohexylisonitrile (739 nm, CH_2Cl_2 RT), and CN^- (760 nm, CH_2Cl_2 RT). But no binding of Cl^-, MeCN, and MeOH to **1** was observed under the conditions investigated. Furthermore, it was found that the addition of H_2O and of $N[(CH_2)_3CH_3]_4OH \cdot 30\ H_2O$ in CH_2Cl_2 to **1** or **5** results in decomposition of the metal-containing complexes.

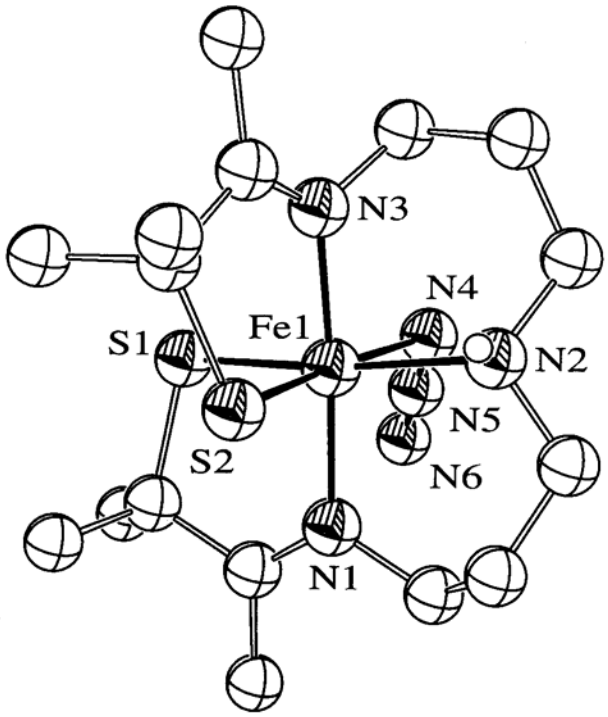

Figure 3-14: Thermal ellipsoid plot (50 % probability level) of **1-N$_3$**. H atoms, except for the H-N$_{amine}$, are omitted for clarity.[89]

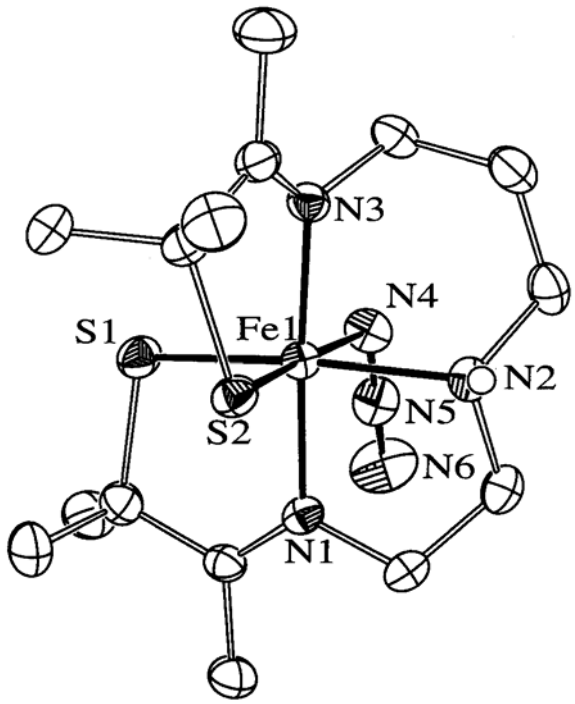

Figure 3-15: Thermal ellipsoid plot (50 % probability level) of **5-N$_3$**. H atoms, except for the H-N$_{amine}$, are omitted for clarity.

The Fe(III) ion in both azide-ligated **1-N$_3$**, see Figure 3-14 and Table 3-3, and azide-ligated **5-N$_3$**, see Figure 3-15 and Table 3-3, is in a near ideal octahedral coordination environment. In **1-N$_3$**, trans angles vary from 172.5(1)° to 174.9(1)° and cis angles vary from 82.2(1)° to 99.7(1)°, while in **5-N$_3$**, trans angles vary from 167.85(5)° to 175.62(6)° and cis angles vary from 82.38(7)° to 99.15(6)°. As it was observed for azide-bound **1-N$_3$**,[89] the azide ligand in **5-N$_3$** is bound trans to one of the thiolate sulfurs (S2). Azide is inserted into the wider N-Fe-S angle (∠ S2'-Fe-N2 = 141.8(1)°) of **5** on the side opposite to the amine nitrogen hydrogen. The binding of azide causes the N2-Fe-S2' angle to open from 141.8(1)° in **5** to 167.85(5)° in **5-N$_3$** (Δ∠ = 26.05°). This structural rearrangement is less than that

which occurs upon azide binding to **1**. In the case of **1**, the N2-Fe-S1 angle opens from 132.3(1)° in **1** to 172.5(1)° in **1-N$_3$** ($\Delta\angle$ = 40.20°). As shown in Table 3-3, the angles in **1-N$_3$** and **5-N$_3$** are nearly identical. All angles are within 6.5° of each other, except for the N1-Fe-N2 angle. This angle changes from 99.7(1)° in **1-N$_3$** to 86.28(7)° in **5-N$_3$**. This change is caused by the replacement of a six-membered ring by a five-membered ring due to the shortening of the ligand backbone from propylene to ethylene. As expected, the azide ligand in both **1-N$_3$** and **5-N$_3$** is bound with an Fe-N$_3$ angle of about 120° and it is nearly linear.

Table 3-3: Selected bond distances (Å) and angles (°) of [Fe(III)S$_2^{Me2}$N$_3$(Pr,Pr)(N$_3$)] (**1-N$_3$**)[89] and [Fe(III)S$_2^{Me2}$N$_3$(Et,Pr)(N$_3$)] (**5-N$_3$**).

	1-N$_3$	**5-N$_3$**
Fe-S1	2.196(1)	2.2226(7)
Fe-S2	2.209(1)	2.1994(6)
Fe-N1 (imine)	1.978(3)	1.916(2)
Fe-N2 (amine)	2.157(3)	2.061(2)
Fe-N3 (imine)	1.970(3)	1.963(2)
Fe-N4 (azide)	2.061(4)	2.093(2)
N4-N5	1.189(5)	1.197(3)
N5-N6	1.162(5)	1.164(3)
N1=C (imine)	1.289(1)	1.284(3)
N3=C (imine)	1.289(1)	1.277(3)
N1-Fe-N2	99.7(1)	86.28(7)
N1-Fe-N3	174.9(1)	173.20(8)
N1-Fe-N4	88.8(1)	89.14(7)

N1-Fe-S1	84.8(1)	86.57(6)
N1-Fe-S2	90.8(1)	90.97(5)
N2-Fe-N3	82.2(1)	88.69(7)
N2-Fe-N4	82.9(1)	82.38(7)
N2-Fe-S1	172.5(1)	167.85(5)
N2-Fe-S2	90.6(1)	93.25(5)
N3-Fe-N4	96.2(1)	94.73(8)
N3-Fe-S1	93.7(1)	99.15(6)
N3-Fe-S2	84.4(1)	84.74(6)
N4-Fe-S1	91.3(1)	87.70(6)
N4-Fe-S2	173.3(1)	175.62(6)
S1-Fe-S2	95.3(1)	96.68(3)
Fe-N4-N5	118.5(3)	119.5(2)
N4-N5-N6	179.7(5)	179.1(2)

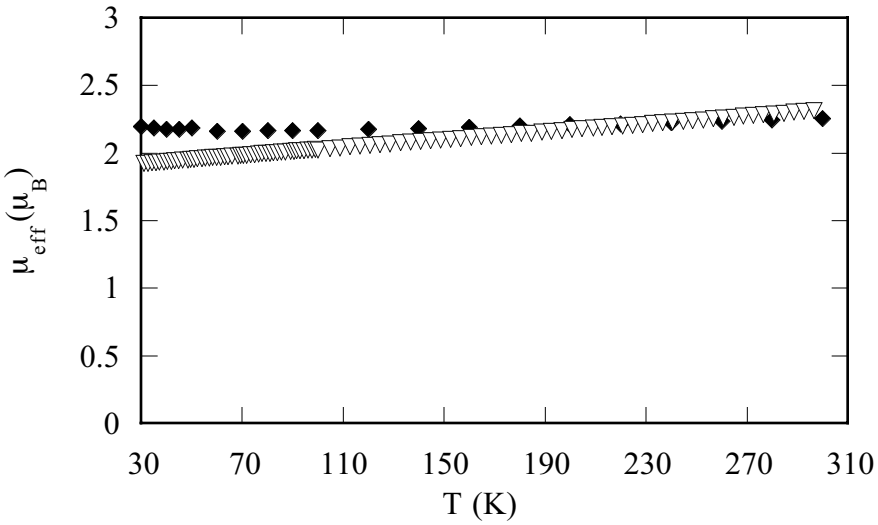

Figure 3-16: Solid state effective paramagnetic magnetic moment of [Fe(III)$S_2^{Me2}N_3$(Pr,Pr)(N_3)] (**1-N$_3$**) (∇) and [Fe(III)$S_2^{Me2}N_3$(Et,Pr)(N_3)] (**5-N$_3$**) (♦).

Solid state effective paramagnetic magnetic moment data shows that in the temperature range of 30 - 300 K both azide-bound complexes are in the spin state S = 1/2 (low-spin). A similar spin state behavior was observed in other hexacoordinated Fe(III) complexes containing two cis thiolate donors perpendicular to two trans imine nitrogen donors.[84,89,90]

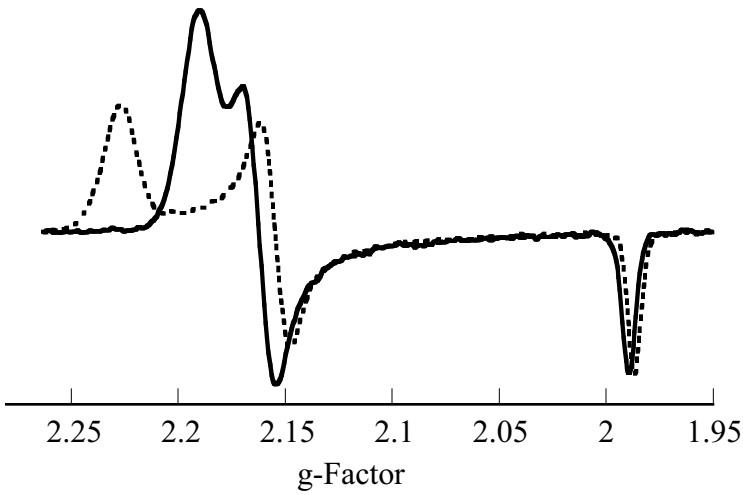

Figure 3-17: EPR spectra of [Fe(III)$S_2^{Me2}N_3$(Pr,Pr)(N_3)] (**1-N_3**) (···) and [Fe(III)$S_2^{Me2}N_3$(Et,Pr)(N_3)] (**5-N_3**) (-) in CH_2Cl_2/Toluene 1/1 at 131 K.

The S = 1/2 spin state of **1-N_3** and **5-N_3** is supported by the X-band EPR spectra shown in Figure 3-17. Both compounds give rise to characteristic Fe(III) low-spin rhombic EPR signals with g-values of 2.226, 2.155, and 1.987 (**1-N_3**) and 2.190, 2.162, and 1.989 (**5-N_3**).

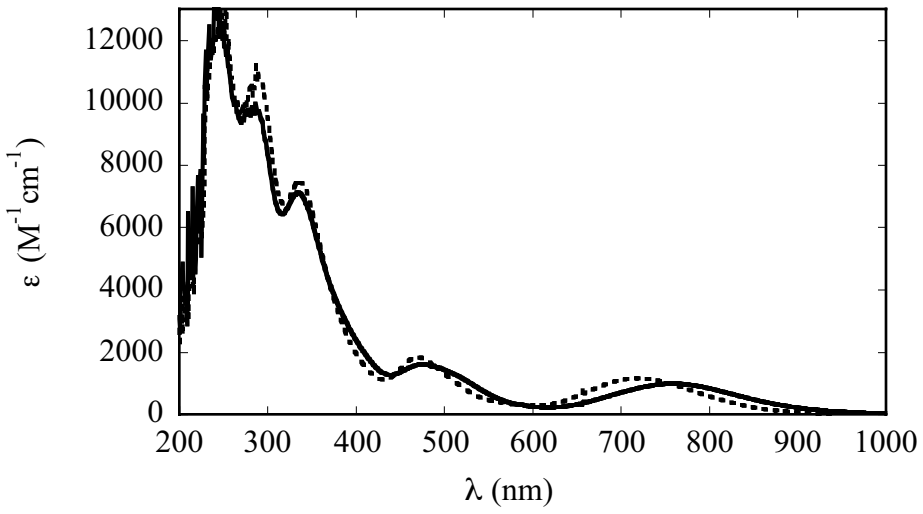

Figure 3-18: UV/Vis absorption spectra of **1-N$_3$** (···) and **5-N$_3$** (-) in CH_2Cl_2.

Complex **5-N$_3$** dissolves in solvents such as CH_2Cl_2, MeCN, THF, and even Et_2O to give an intensely orange-brown colored solution. This is due to intense absorption bands at 475 and 760 nm. In comparison, **1-N$_3$** gives rise to intense absorption bands at 470 and 720 nm. Since the absorption band at around 700 nm in active Fe-containing NHase has substantial sulfur to iron charge transfer character,[43,47] it is reasonable to assume that the absorption bands at 720 and 760 nm in **1-N$_3$** and **5-N$_3$**, respectively, also have substantial sulfur to iron charge transfer character. This assignment is supported by their high extinction coefficients (~ 1000 $M^{-1}cm^{-1}$). The reduction potential of azide-bound **5-N$_3$** (E(irrev. Red.) = - 590 mV (vs. SCE)) compares well with that of azide-bound **1-N$_3$** ($E_{1/2}$(reversible) = - 545 mV (vs. SCE)). The fact that the reduction of **5-N$_3$** is irreversible suggests that the corresponding Fe(II)-containing compound decomposes within the time frame of one cyclic voltammetry scan (~ 5 s).

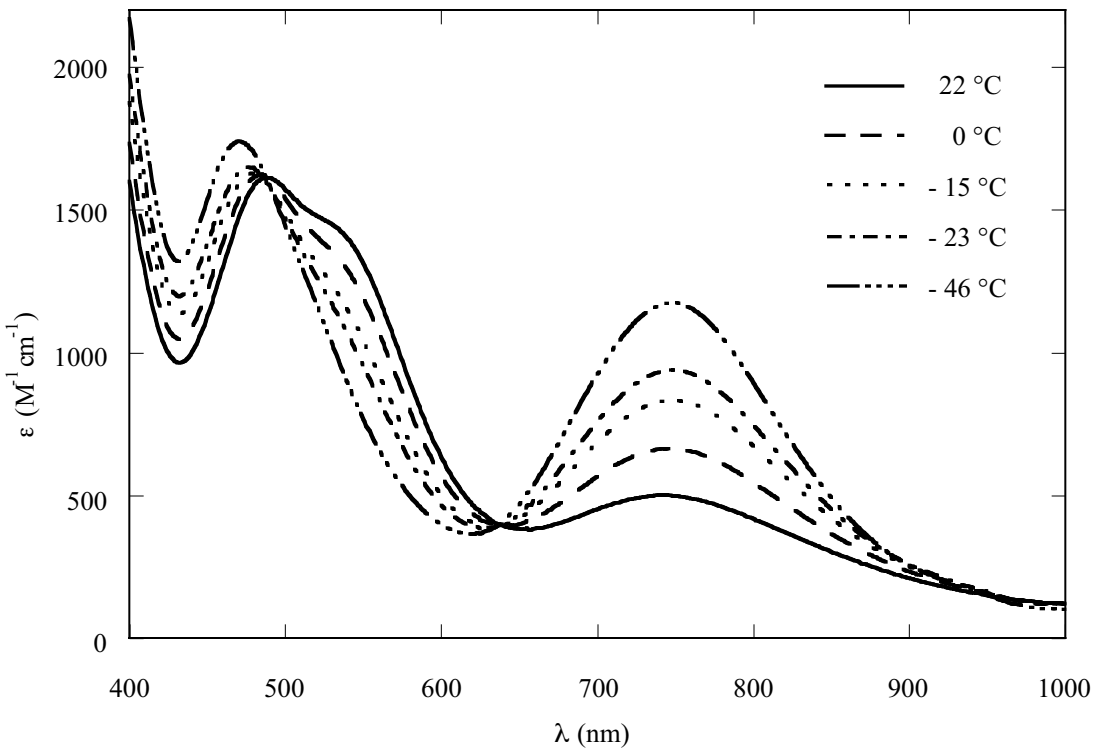

Figure 3-19: UV/Vis absorption spectra showing the temperature dependent equilibrium $[Fe(III)S_2^{Me2}N_3(Et,Pr)]PF_6$ (**5**) + N_3^- = $[Fe(III)S_2^{Me2}N_3(Et,Pr)(N_3)]$ (**5-N$_3$**) + PF_6^- in MeOH ($[c\mathbf{5}]_0$ = 1.0 10^{-3} mol/l, $[cN_3^-]_0$ = 5.0 10^{-3} mol/l, I = 0.06 mol/l). As the solution is cooled, azide binds to **5** to form **5-N$_3$** (22 °C, 34 %; 0 °C, 49 %; - 15 °C, 67 %; - 23 °C, 75 %; and - 46 °C, 95 % bound). The increasing amount of **5-N$_3$** is indicated by the appearance of an absorption band at 470 nm, the disappearance of the shoulder at 550 nm, and by the appearance of an absorption band at 760 nm.

Thermodynamic Equilibrium Study of Azide Binding

Azide binds reversibly to **1** and **5** in MeOH. To quantify the influence that ligand constraints, in this case the length of the ligand backbone, have on the reactivity of pentacoordinated **1** and **5**, a study was undertaken to determine the

thermodynamic parameters of azide binding to $[Fe(III)S_2^{Me2}N_3(Et,Pr)]PF_6$ (**5**) and compare them to those of azide binding to $[Fe(III)S_2^{Me2}N_3(Pr,Pr)]PF_6$ (**1**). The thermodynamic parameters of azide binding to **1**, ΔH = - 5.2 ± 0.5 kcal/mol = - 21.9 ± 2.2 kJ/mol and ΔS = - 12.4 ± 2.2 cal/(mol K) = - 51.8 ± 9.4 J/(mol K), were measured in a previous study.[89]

To ensure that the equilibrium constants for azide binding to **5** are comparable to those for the reaction of **1** with azide, the equilibrium constants for azide binding to **5** were measured at the same ionic strength (I = 0.06 mol/l) and in the same solvent (MeOH) as for **1**. This was done spectrophotometrically. Equilibrium constants were determined at five different temperatures, see Figure 3-19 and Table 3-4. The enthalpy change (ΔH = - 7.5 ± 0.6 kcal/mol = - 31.5 ± 2.7 kJ/mol) and entropy change (ΔS = - 16.6 ± 2.5 cal/(mol K) = - 69.6 ± 10.4 J/(mol K)) associated with azide binding to **5** were calculated from a van't Hoff plot ($\ln K_{eq} = -\Delta H/R\ (1/T) + \Delta S/R$), see Figure 3-20.

Table 3-4: Equilibrium constants for the reaction of **1**[89] and **5** with azide in MeOH at I = 0.06 mol/l.

Temperature (°C)	K_{eq} (M^{-1}): **1** + $\mathbf{N_3^-}$ = **1-N$_3$**	K_{eq} (M^{-1}): **5** + $\mathbf{N_3^-}$ = **5-N$_3$**
22	ND	110 ± 20
0	23 ± 3	210 ± 40
- 15	66 ± 7	470 ± 90
- 23	ND	720 ± 140
- 41	200 ± 20	ND
- 46	ND	4950 ± 990
- 77	1200 ± 120	ND*

ND = not determined; * Compound **5** significantly (> 10 %) binds MeOH at temperatures below - 46 °C,[159] therefore K_{eq} at - 77 °C could not be determined.

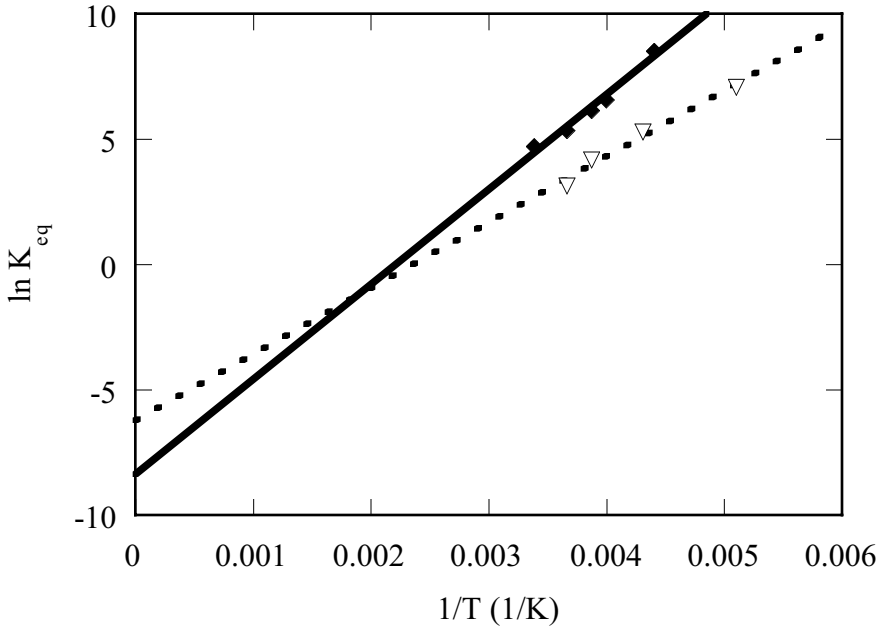

Figure 3-20: Van't Hoff plot for the binding of azide to **1** (∇)[89] and **5** (♦) in MeOH at I = 0.06 mol/l.

The Concept of Entatic State

Generally, according to transition state theory, it is assumed that enzymes catalyze reactions by lowering the energy of the transition state, that is, the transition state is stabilized; this is illustrated by case **B** in Figure 3-21.[104] Thereby, the energy needed to reach the transition state is reduced and the reaction proceeds faster. Conceptually, the energy needed to reach the transition state can also be reduced if the reactant is forced by the enzyme into a conformation that is close to the transition state of the reaction to be catalyzed. The concept of destabilizing the ground state of a reactant in an enzymatic reaction is known as entatic (entasis) or rack state.[160-163] A more general term is energised state.[161]

The reactant, which is forced by the protein into an entatic state, can be the active site of an enzyme or the substrate of the enzymatic reaction while being bound to the catalytically active site, that is, the enzyme-substrate complex. "In all cases when structure is obviously deviant from expectation based on simple models, the energisation can be called entatic."[161] Putting the reactant into an unstable conformation causes its energy to increase, that is, the ground state is destabilized. Besides a reduction of the energy needed to reach the transition state, the destabilization of the reactant also results in a larger energy difference between the enzyme-bound reactant and the unbound product, as it is illustrated by case **C** in Figure 3-21. This larger energy difference between enzyme-bound reactant and unbound product is reflected by an increase of K_{eq} ($K_{eq}^{\#}$ versus K_{eq}).

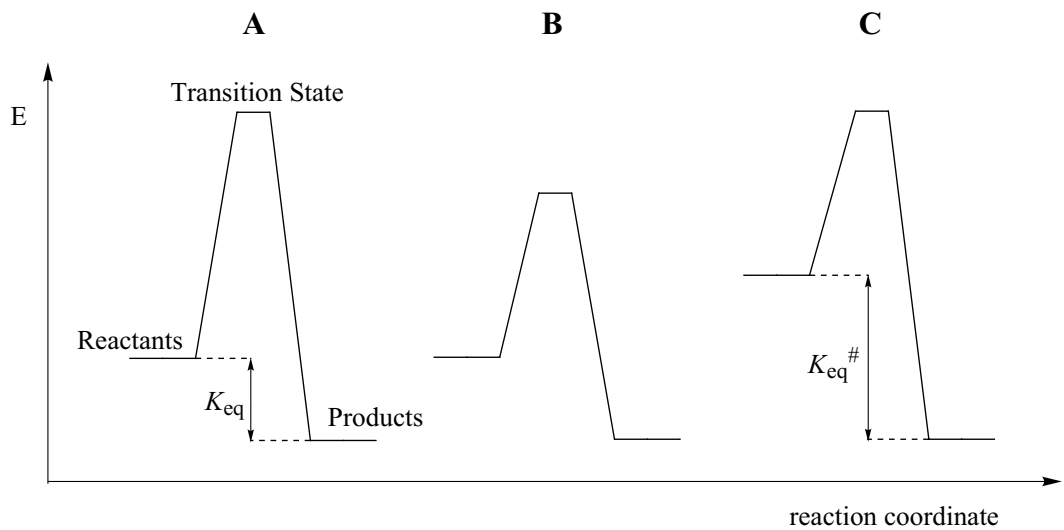

Figure 3-21: Reaction coordinate of a single-step chemical reaction: uncatalyzed case (**A**), traditional enzymatic catalysis by lowering the energy of the transition state (**B**), and catalysis by entasis (**C**).

The classic example of a metalloenzyme in an entatic state is that of blue copper proteins.[164] In blue copper proteins the metal ion is held by the protein in a constrained and distorted conformation that lowers the reorganization energy required upon electron transfer. Another example in which entasis may play a role is that of lysozyme.[165] It is discussed that protein constraints in lysozyme force the substrate to adopt a half-chair conformation which lowers the activation energy to the formation of the carbocation intermediate.

Low molecular mass compounds that encompass a metal ion in a distorted and destabilized geometry are inherently unstable. Therefore, only a few model compounds are known to contain a metal ion in a highly distorted coordination geometry which models the entatic state of a metalloenzyme.[166-172] However, there are numerous examples in the literature of ligand constraints influencing the structure, electronic properties, and/or reactivity of the resulting metal complexes.[173-191]

Comparing the Reactivity of 1 and 5 - a Model for the Entatic State

For the reaction of $[Fe(III)S_2^{Me2}N_3(Pr,Pr)]PF_6$ (**1**) and $[Fe(III)S_2^{Me2}N_3(Et,Pr)]PF_6$ (**5**) with azide in MeOH, a large difference in K_{eq} was observed. It was found, see Table 3-4, that at each temperature the equilibrium constant of the reaction of **5** with azide is shifted by approximately one order of magnitude to the product side as compared to the reaction of **1** with azide. For example, at 0 °C, a five-fold excess of azide causes 49 % of Et,Pr-containing **5** to convert to the azide-bound **5-N$_3$**, but only 10 % of Pr,Pr-containing **1** to be azide-bound. At 0 °C, the K_{eq} for the reaction of **5** with azide is 210 ± 40 M^{-1}, while it is only 23 ± 3 M^{-1} for the reaction of **1** with azide.

Table 3-5: Thermodynamic parameters of azide binding to **1**[89] and **5** in MeOH at I = 0.06 mol/l.

	ΔH (kcal/mol)	ΔS (cal/(mol K))
(Pr,Pr) **1** + N_3^- = **1-N$_3$**	- 5.2 ± 0.5	- 12.4 ± 2.2
(Et,Pr) **5** + N_3^- = **5-N$_3$**	- 7.5 ± 0.6	- 16.6 ± 2.5

Utilizing a van't Hoff plot, see Figure 3-20 and Table 3-5, the thermodynamic parameters for the binding of azide to **1** and **5** in MeOH at I = 0.06 mol/l were determined. As expected, the entropy changes associated with azide binding to **1** and **5** are identical within the error limits. This is not surprising since both reactions involve a similarly associative process, which is combined with a similar change in the solvent sphere around the reacting molecules.

A comparison of the enthalpy change associated with azide binding to **1** and **5** shows that 2.3 kcal/mol more are released by the azide binding to **5**. This change in enthalpy corresponds to a change in the equilibrium constant, at any given temperature, of more than one order of magnitude.[192] The experimentally observed equilibrium constants, see Table 3-4, confirm this prediction. This significant difference in ΔH provides a quantitative measure of the change of reactivity that is associated with the removal of just one methylene unit from the ligand backbone when going from $[Fe(III)S_2^{Me2}N_3(Pr,Pr)]PF_6$ (**1**) to $[Fe(III)S_2^{Me2}N_3(Et,Pr)]PF_6$ (**5**).

The larger released enthalpy in the case of **5** could be a consequence of an increase of the enthalpy of **5** relative to **1**, a decrease of the enthalpy of **5-N$_3$** relative to **1-N$_3$**, or some combination of both. It was found that **1-N$_3$** and **5-N$_3$**

have a very similar electronic absorption spectrum, see Figure 3-18, a very similar magnetic behavior, see Figure 3-16, and very similar structural parameters, see Table 3-3. In contrast, it was found that the electronic absorption spectrum, see Figure 3-12, the magnetic behavior, see Figure 3-10, and the structural parameters, see Table 3-2, of **1** are very different from those of **5**. Therefore, it is assumed that the enthalpy difference between **1-N$_3$** and **5-N$_3$** is much smaller than the enthalpy difference between **1** and **5**. This means that the increase in released enthalpy is primarily due to a destabilization of **5** relative to **1**. In other words, **5** is higher in enthalpy, by about 2.3 kcal/mol, as compared to **1**.

In this sense, compound **5** is a model for the entatic state of a reactant. The removal of only one methylene unit from the ligand backbone when going from Pr,Pr-ligated **1** to Et,Pr-ligated **5** results in a significant structural distortion as it is indicated by the opening of the S1/2'-Fe-N2 angle from 132.3(1)° in **1** to 141.8(1)° in **5**. This structural distortion causes **5** to increase in enthalpy relative to **1**. Therefore, the relationship between **1** and **5** can be seen as a model for the relationship between an unbound reactant and its enzyme-bound form during an entatic enzyme catalysis, see Figure 3-21. Structural distortions cause the enzyme-bound form, which is represented by **5**, to be higher in enthalpy than the unbound reactant or ground state, which is represented by **1**. Alternatively, the reactivity difference between **1** and **5** shows that ligand constraints (= protein constraints), in the present case represented by the shorter ligand backbone, can force a metal ion (= active site) into a more reactive state (= entatic state).

The difference in enthalpy between the reactions of $[Fe(III)S_2^{Me2}N_3(Et,Pr)]PF_6$ (**5**) and $[Fe(III)S_2^{Me2}N_3(Pr,Pr)]PF_6$ (**1**) with azide can also be explained by another line of reasoning. In both systems, energy is released owing to the formation of the new Fe-N bond. It is reasonable to assume that this

energy is nearly identical in both cases. Energy is needed in both reactions to desolvate the pentacoordinated cation and the azide anion as well as for the structural rearrangement of the ligand backbone upon converting the pentacoordinated complex (cation of **5** or **1**) to the hexacoordinated azide-bound complex. The desolvation energy is approximately equal since both reactions involve a similarly associative process; this is supported by the nearly identical entropy change. However, the energy needed for rearrangement is not identical in both systems. In the reaction of azide binding to **5**, there is less conformational change required as compared to the reaction of azide binding to**1**. In the Pr,Pr case (**1** / **1-N$_3$**) a structural rearrangement of the S1/2'-Fe-N2 angle by 40.20° (132.3° to 172.5°) has to occur while it is only 26.05° (141.80° to 167.85°) in the Et,Pr case (**5** / **5-N$_3$**). Hence, in the Et,Pr system, more of the energy from the Fe-azide bond formation is released to the environment, that is, a more negative ΔH is observed. It has been observed that both **5** and **1** bind azide quantitatively in MeCN and CH_2Cl_2. This behavior can be explained by the fact that ions in such solvents are not solvated very much. Therefore, very little energy is needed for desolvation.

Chapter IV: Fe(III) Complexes of an $(N_{amide})_2(S_{thiolate})_2$ Ligand[193]

Introduction

As it was discussed in the introduction, NHase is only the second enzyme in which the coordination of an amide (carboxamide) nitrogen to a metal ion has been observed.[3,4] The other example occurs in the P-cluster of nitrogenase.[66] To gain an understanding of the nature of the metal-amide bond, and its significance with respect to the active site of NHase, metal complexes with amide donor ligands have to be prepared and studied. Several other researchers have studied metal complexes containing an Fe(III)[67-74] or a Co(III)[68,75-78] ion bound to an amide nitrogen donor atom. To study how Fe(III) behaves in a coordination environment close to that of NHase, the Fe(III) coordination chemistry of the known ligand N,N'-1,2-ethanediylbis[2-mercapto-2-methyl-propanamide][189] was investigated. N,N'-1,2-ethanediylbis[2-mercapto-2-methyl-propanamide] serves as a first generation amide/thiolate-containing ligand, since it provides two amide nitrogen donor atoms and two thiolate sulfur donor atoms. In comparison, the metal ion (Fe(III) or Co(III)) in NHase is coordinated by two amide nitrogen donor atoms and three sulfur donor atoms derived from cysteine thiolate.[3,4]

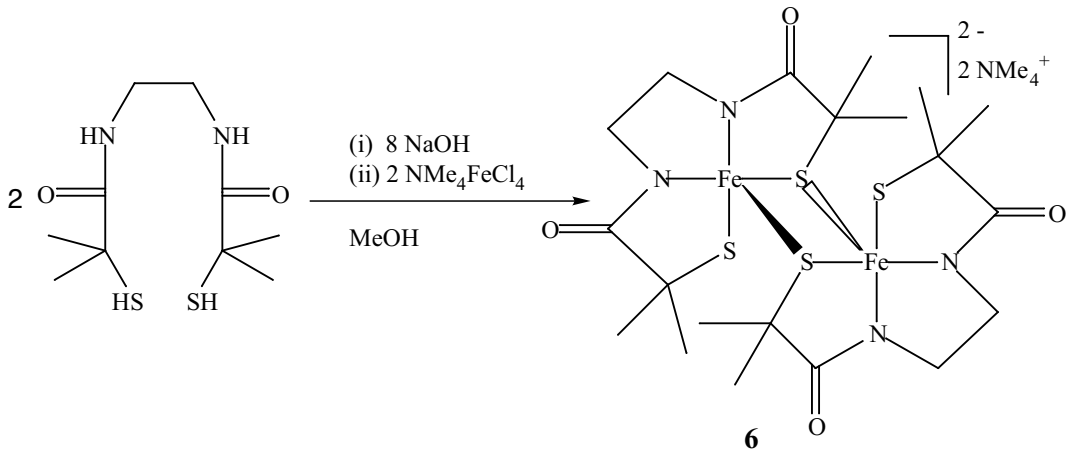

Figure 4-1: Synthesis of dimeric **6**.

Synthesis and Crystal Structure of Dimeric 6

The addition of a MeOH solution containing four equivalents of base and one equivalent of the ligand N,N'-1,2-ethanediylbis[2-mercapto-2-methyl-propanamide] to a MeOH solution of one equivalent of Fe(III) resulted in the immediate formation of a brown color. After filtration and crystallization, crystalline $(NMe_4)_2[(Fe(III)S_2^{Me2}N_2^{amide}(Et))_2]$ (**6**) was obtained. Four equivalents of base are needed, since both of the amides and both of the thiolates need to be deprotonated. NMe_4FeCl_4 proved to be a convenient starting material. It is a nonhygroscopic source of Fe(III) as compared to $FeCl_3$. Furthermore, it provides a stoichiometric amount of a tetraalkylammonium cation which is needed to increase the solubility of the dimeric dianion of **6**.

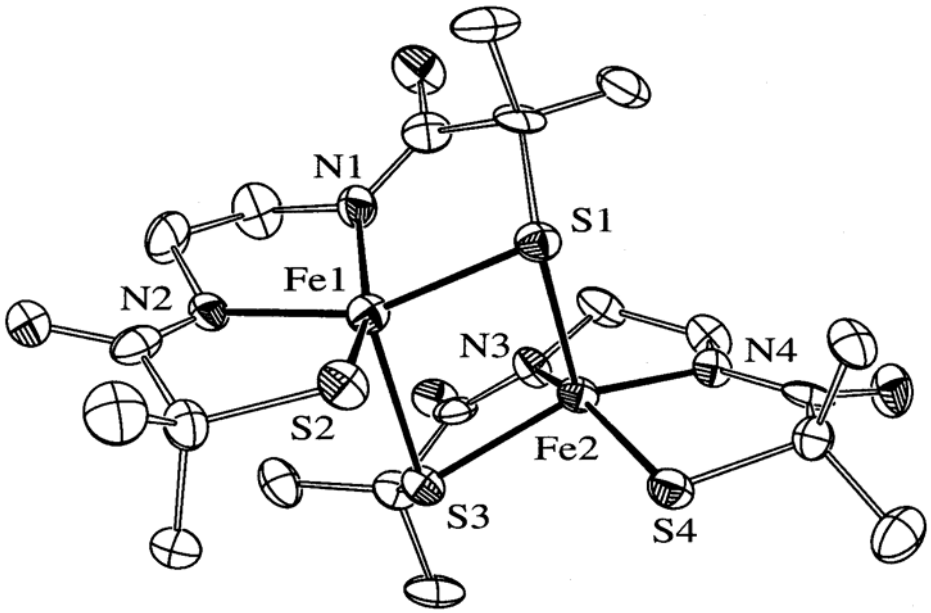

Figure 4-2: Thermal ellipsoid plot (50 % probability level) of the anion of **6**. H atoms are omitted for clarity.

An ORTEP of the dianion of **6** is shown in Figure 4-2. The dianion contains two Fe(III) ions. Each Fe(III) ion is coordinated by two deprotonated amide nitrogens and three thiolates. One (N2, N4) of the coordinated amides is bound to a terminal thiolate (S2, S4), while the other (N1, N3) coordinated amide is bound to a bridging thiolate (S1, S3). There are also two molecules of MeOH in the crystal structure which are H-bonded to the oxygens of the amides that are bound to the bridging thiolates. One (S2, S4) of the coordinated thiolates is terminal, that means it is only bound to one Fe(III). The other thiolate (S1, S3) of the ligand is bridging the two iron ions of the dianion. Therefore, each Fe(III) is coordinated by not only the two thiolates of its own ligand, but also by a bridging thiolate provided by the ligand of the other Fe(III). Hence, each Fe(III) is pentacoordinated. The τ parameters of the irons are 0.0167 (Fe1) and 0.0050 (Fe2). This indicates a near

ideal square pyramidal coordination environment about each Fe(III) ion. The plane of the square pyramid is formed by the two deprotonated amide nitrogens and the two thiolates of the iron's own ligand, while the apex is being provided by the bridging thiolate of the other iron's ligand. The iron ions are displaced from the plane of the square pyramid towards the apex by about 0.448(2) Å. The angle between the two square pyramidal planes is 4.7(2)°. The Fe(III)-N_{amide} distances are 1.91(2) Å, while the Fe(III)-$S_{terminal}$ distances are 2.207(6) Å, the Fe(III)-$S_{bridging\ own\ ligand}$ distances are 2.253(4) Å, and the Fe(III)-$S_{bridging\ other\ ligand}$ distances are 2.449(3) Å. Hence, the thiolate bridges are very unsymmetrical.

Table 4-1: Selected bond distances (Å) and angles (°) of $(NMe_4)_2$ $[(Fe(III)S_2^{Me2}N_2^{amide}(Et))_2]$ (**6**) and $(NMe_4)[Fe(III)S_2^{Me2}N_2^{amide}(Et)(Py)]$ (**7**).

	6	**7**
Fe1-S1	2.252(3)	2.203(1)
Fe1-S2	2.204(3)	2.215(1)
Fe1-S3	2.449(3)	N/A
Fe2-S1	2.449(3)	N/A
Fe2-S3	2.253(3)	N/A
Fe2-S4	2.210(3)	N/A
Fe1-N1	1.912(7) (amide)	1.900(3) (amide)
Fe1-N2	1.917(7) (amide)	1.919(3) (amide)
Fe1-N3	N/A	2.165(3) (pyridine)
Fe2-N3	1.920(7) (amide)	N/A
Fe2-N4	1.894(7) (amide)	N/A
N1-C(O) (amide)	1.332(12)	1.335(5)

N2-C(O) (amide)	1.306(12)	1.331(5)
N3-C(O) (amide)	1.340(12)	N/A
N4-C(O) (amide)	1.324(11)	N/A
Fe1···Fe2 (within dimer)	2.997	N/A
Fe···Fe (shortest between anions)	8.974	7.798
N1-Fe1-N2	83.3(3)	83.0(1)
N1-Fe1-N3	N/A	99.1(1)
N1-Fe1-S1	85.2(2)	86.3(1)
N1-Fe1-S2	153.7(3)	159.2(1)
N1-Fe1-S3	113.1(3)	N/A
N2-Fe1-N3	N/A	102.3(1)
N2-Fe1-S1	154.7(2)	153.8(1)
N2-Fe1-S2	85.7(2)	87.0(1)
N2-Fe1-S3	106.1(2)	N/A
N3-Fe1-S1	N/A	102.97(9)
N3-Fe1-S2	N/A	100.8(1)
S1-Fe1-S2	95.0(1)	94.86(4)
S1-Fe1-S3	99.10(9)	N/A
S2-Fe1-S3	92.9(1)	N/A
N3-Fe2-N4	82.9(3)	N/A
N3-Fe2-S1	112.1(2)	N/A
N3-Fe2-S3	85.3(2)	N/A
N3-Fe2-S4	154.3(2)	N/A
N4-Fe2-S1	106.8(2)	N/A
N4-Fe2-S3	154.0(2)	N/A

N4-Fe2-S4	85.6(2)	N/A
S1-Fe2-S3	99.05(9)	N/A
S1-Fe2-S4	93.3(1)	N/A
S3-Fe2-S4	95.46(9)	N/A
Fe1-S1-Fe2	79.08(9)	N/A
Fe1-S3-Fe2	79.06(9)	N/A
Fe1-(plane of N1, N2, S1, S2)	0.4486(13)	0.4043(13)
Fe2-(plane of N3, N4, S3, S4)	0.4470(13)	N/A
∠ between plane of N1, N2, S1, S2 and plane of N3, N4, S3, S4	4.66 (18)	N/A
τ	0.0167 (Fe1) & 0.0050 (Fe2)	0.0900

Reactivity Studies of Dimeric 6

Since the two iron ions of **6** are connected via a weak bridge, it was reasoned that it should be possible to cleave the dimer using a strong ligand. Thereby, dimeric **6** should be converted into monomeric complexes. For this purpose, a number of cleaving experiments have been performed. They are summarized in Table 4-2. In the cleaving experiments, **6** was treated with various anions/molecules. The progress of the reaction was judged by observing the electronic absorption spectrum. If no change occurred, that is only the absorption bands of **6** (MeOH: 208, 301, 420, 467 nm and MeCN: 197, 306, 497 nm) were present, it was concluded that no reaction occurred.

Table 4-2: Summary of $(NMe_4)_2[(Fe(III)S_2^{Me2}N_2^{amide}(Et))_2]$ (**6**) reactivity studies.

dimeric **6** + what reagent	RT, 1 h	55 °C, 1 h
100 % MeOH	λ_{max} = 208, 301, 420, and 467 nm	
100 % MeCN	λ_{max} = 197, 306, and 497 nm	
NaS-tertButyl / MeOH	N.R.	not tried
NaOH / MeOH	N.R.	N.R.
NaN_3 / MeOH	N.R.	decomposition
NMe_4S-tertButyl / MeOH	N.R.	N.R.
KSCN / MeOH	N.R.	N.R.
NaCN / MeOH	N.R.	N.R.
NaSEt / MeOH	N.R.	N.R.
H_2O_2 (3 %) / MeOH	decomposition (formation of gas and insoluble precipitate)	
air / MeOH	decomposition (formation of insoluble precipitate within days)	
Cyclohexylisonitrile / MeOH	N.R.	not tried
Cyclohexylisonitrile / MeCN	N.R.	not tried
Pyridine (100 %) or Pyridine / MeOH (1/2, v/v)	Only shift of highest wavelength maximum from 467 to 487 nm. Upon pumping to dryness and redissolving in MeOH the 467 nm absorption band is restored.	
air / (Pyridine (100 %) or Pyridine / MeOH (1/2, v/v))	Only shift of highest wavelength maximum from 467 to 487 nm. No further reaction within two weeks at RT.	

H_2O_2 (3 %) / Pyridine	decomposition (formation of gas and insoluble precipitate)	
NaSPh / MeOH	N.R.	N.R.
NaOPh / MeOH	N.R.	N.R.
NB_4SCN / MeCN	N.R.	N.R.
NMe_4Cl / MeOH	N.R.	N.R.
NMe_4Cl / MeCN	N.R.	N.R.
NB_4N_3 / MeCN	N.R.	N.R.
NB_4CN / MeCN (NB_4SCN + excess NaCN)	N.R.	N.R.
$S{=}C(NH_2)_2$ / MeOH	N.R.	N.R.
Pyridine *N*-oxide / MeOH	N.R.	N.R.
$P(Ph)_3$ / MeOH	N.R.	N.R.
$P(Ph)_3$ / MeCN	N.R.	decomposition

N.R. = no reaction.

As can be seen in the cleaving experiments table, in most cases dimeric **6** remains unchanged. In a number of cases, decomposition is observed as judged by the disappearance of the absorption bands of **6** and the formation of insoluble precipitate. An attempt was also made to trap an intermediate in the formation of **6** by performing the synthesis of **6** in the presence of an excess of several potentially binding anions ($^-$SEt, $^-$OPh, $^-$SPh, and $^-$Cl). These experiments only resulted in the formation of **6**. It was further attempted to prepare the Fe(II) complex of N,N'-1,2-ethanediylbis[2-mercapto-2-methyl-propanamide] and then oxidize it with air to obtain a μ-oxo bridged dimer[194] and/or an oxidized sulfur derivative. As judged

by UV/Vis absorption spectroscopy, only **6** was formed in this reaction. In other reactions, a dimer splitting was attempted by using the alkylating agents iodoacetamide,[195,196] benzylbromide,[197] and iodoacetic acid.[198] In all of those reactions decomposition was observed. A reaction between **6** and NO was also attempted. The addition of 2.3 equivalents of NO to an MeCN solution of **6** resulted in the formation of a greenish-brown color. However, during the attempted crystallization, decomposition was observed. In comparison, no reaction was observed when **7** (**6** in Pyridine / MeOH (1/2, v/v)) was treated with NO.

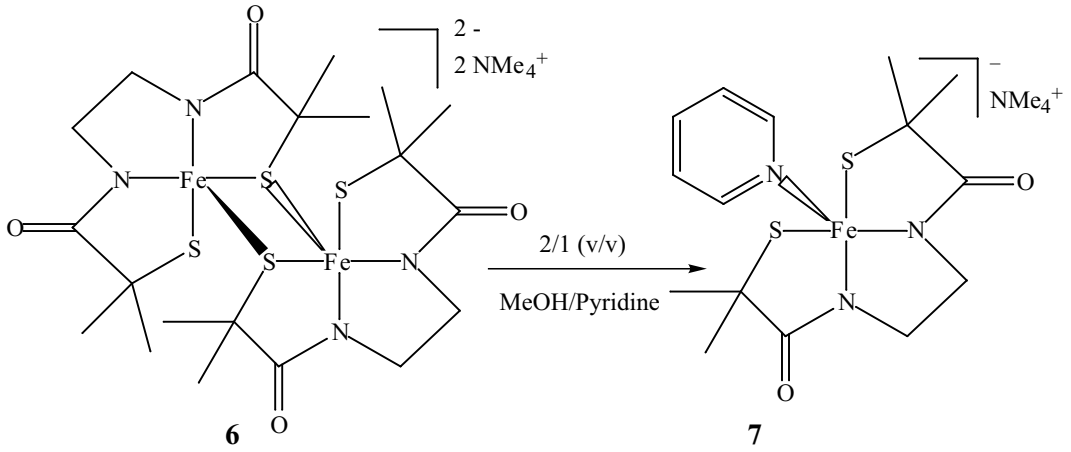

Figure 4-3: Synthesis of **7** from **6**.

Synthesis and Crystal Structure of Monomeric Pyridine-Bound 7

Since a small change in the absorption spectrum was observed when dimeric **6** was dissolved in solutions containing pyridine, it was decided to crystallize **6** from a MeOH/pyridine mixture. To do this, **6** was dissolved in 2/1 (v/v) MeOH/pyridine and the solution was overlayered with Et_2O. After standing for several days at - 35 °C, the inside of the flask was covered with well formed red crystals. An X-ray structure analysis showed the crystals to be a new compound.

It is the monomeric Fe(III) complex $(NMe_4)[Fe(III)S_2^{Me2}N_2^{amide}(Et)(Py)]$ (**7**). Based upon electronic absorption spectroscopy measurements, it was determined that a MeOH solution containing at least 25 % pyridine contains only monomeric **7**. An attempt was also made to crystallize **6** from MeCN. However, thereby only an amorphous powder was obtained.

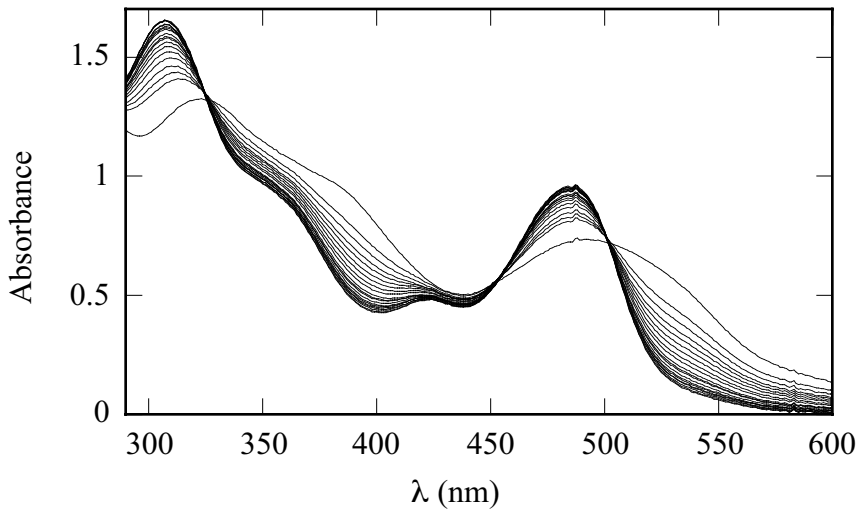

Figure 4-4: Titration of a solution of **6** in CH_2Cl_2 with pyridine.

A titration experiment, see Figure 4-4, was performed to learn how many equivalents of pyridine are needed to convert dimeric **6** in CH_2Cl_2 into monomeric pyridine-bound **7**. To do this a cation exchange was performed to obtain the $N[(CH_2)_3CH_3]_4^+$ salt of **6**. This was dissolved in CH_2Cl_2, and a solution of pyridine in CH_2Cl_2 was titrated into it. As shown in Figure 4-5, about six equivalents of pyridine are needed to completely convert dimeric **6** into monomeric pyridine-bound **7**. This means three moles of pyridine are necessary per mole of iron in **6**.

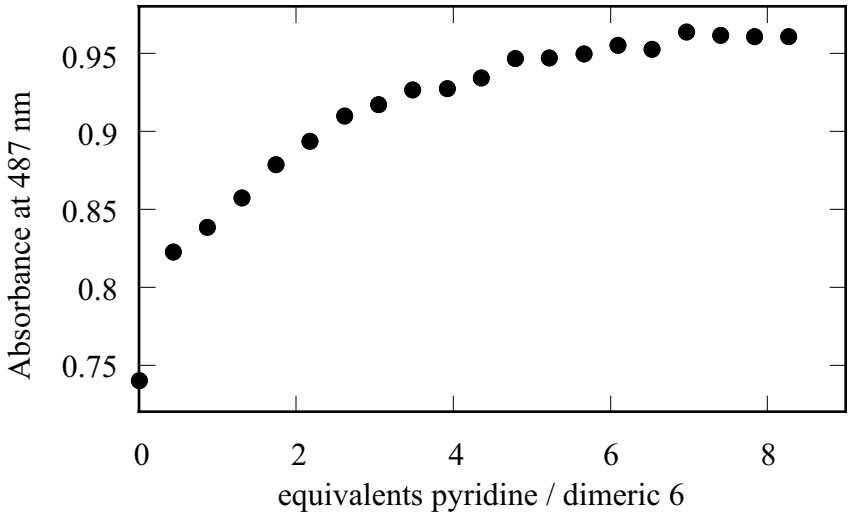

Figure 4-5: Diagram showing the absorbance at 487 nm as a function of the ratio pyridine/dimer (**6**).

As shown by the crystal structure analysis, compound **7** contains the Fe(III) as part of an anion, which is shown in Figure 4-6. Each anion contains one Fe(III) ion. The Fe(III) ion is coordinated by two deprotonated amide nitrogens, two thiolates, and one pyridine-based nitrogen. This shows, see also Figure 4-4, that **7** is produced by the cleavage of the dimer **6** with pyridine. Each Fe(III) is pentacoordinated. The τ parameter of the iron is 0.0900. This indicates a near ideal square pyramidal coordination environment about the Fe(III) ion. The plane of the square pyramid is formed by the two deprotonated amide nitrogens and the two thiolates of the ligand N,N'-1,2-ethanediylbis[2-mercapto-2-methyl-propanamide], while the apex is provided by the nitrogen of the pyridine ligand. The iron ion is displaced from the plane of the square pyramid towards the apex by about 0.404(1)

Å. The Fe(III)-N_{amide} distances are 1.91(1) Å, the Fe(III)-thiolate distances are 2.21(1) Å, and the Fe(III)-$N_{pyridine}$ distance is 2.165(3) Å.

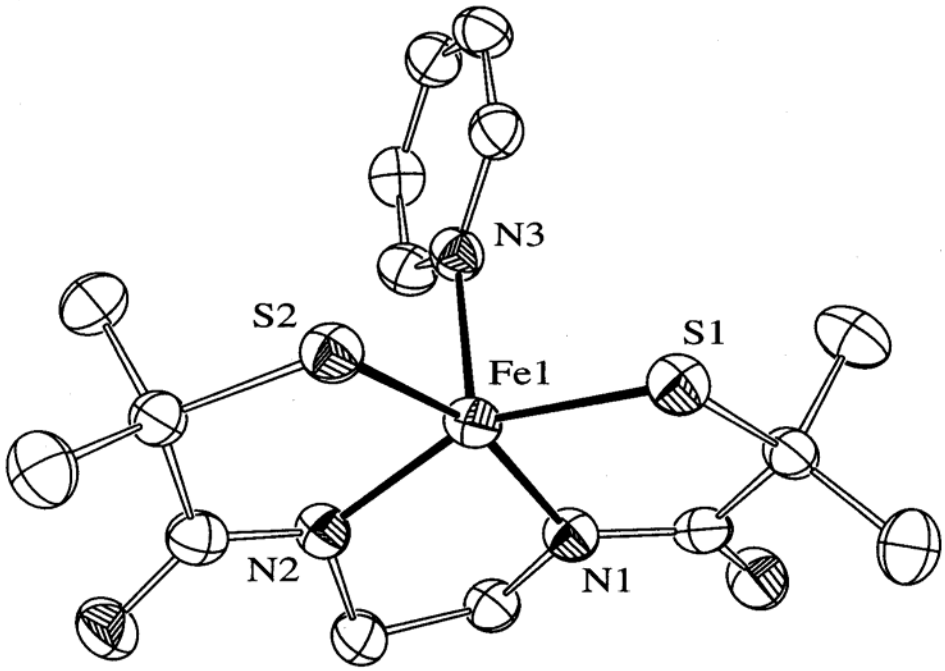

Figure 4-6: Thermal ellipsoid plot (50 % probability level) of the anion of **7**. H atoms are omitted for clarity.

Comparison of Physical Properties of Dimeric 6 and Monomeric Pyridine-Bound 7

Solid state magnetic susceptibility measurements of compounds **6** and **7** show that both compounds contain Fe(III) in the S = 3/2 spin state in the temperature range of 5 - 300 K. Figure 4-7 shows plots of the effective paramagnetic magnetic moment of **6** and **7** as a function of temperature. For both compounds, the high temperature value is characteristic of an S = 3/2 system. In the case of **6**, the effective paramagnetic magnetic moment at 300 K is 5.94μ_B. The expected spin-only value for two non-interacting S = 3/2 centers in one molecule is

5.48 μ_B (μ_{eff} = g * (3/2 * (3/2 + 1) + 3/2 * (3/2 + 1))$^{1/2}$ with g = 2). When the temperature dependence of the effective paramagnetic magnetic moment of **6** is fit to a spin system containing two interacting S = 3/2 spins, equation 1,[199] the following parameters are obtained: J = - 1.14(3) cm^{-1} and g = 2.192(4) with r = 0.958.

$$\mu_{eff} = 2.8279 \cdot \sqrt{0.375145836 \cdot m2 \cdot m2 \cdot \frac{2e^{2(m1/T)} + 10e^{6(m1/T)} + 28e^{12(m1/T)}}{1 + 3e^{2(m1/T)} + 5e^{6(m1/T)} + 7e^{12(m1/T)}}} \quad (1)$$

(m1 = J/k and m2 = g)

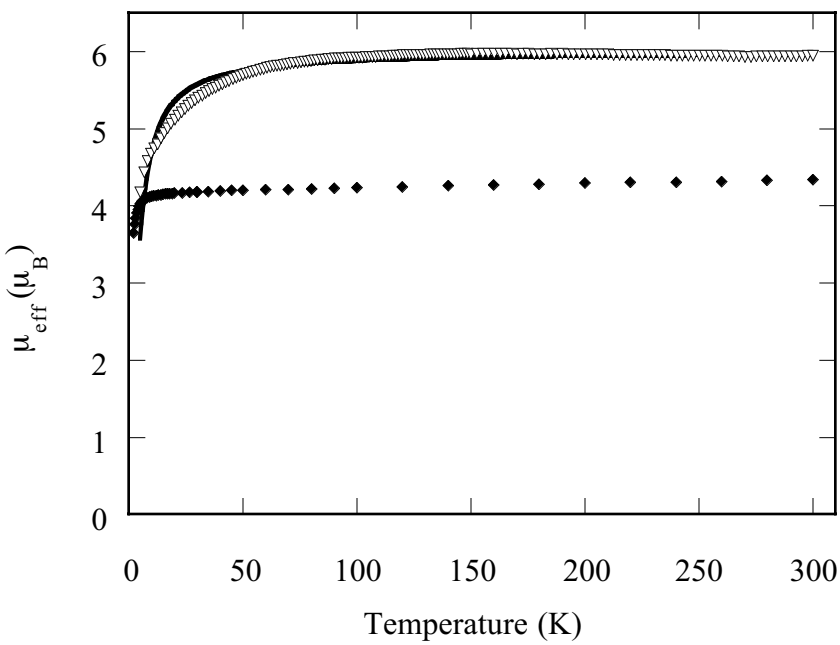

Figure 4-7: Solid state effective paramagnetic magnetic moment of $(NMe_4)_2[(Fe(III)S_2^{Me2}N_2^{amide}(Et))_2]$ (**6**) (∇) and $(NMe_4)[Fe(III)S_2^{Me2}N_2^{amide}(Et)(Py)]$ (**7**) (♦).

The low J value indicates that the Fe(III) ions in the dianion of **6** are nearly independent of each other. At temperatures above 50 K, they are in an S = 3/2 spin state. Only at low temperatures do they experience weak antiferromagnetic coupling and zero-field splitting as indicated by the decrease of μ_{eff}. The low antiferromagnetic coupling via two -S(alkyl)- bridges in**6** is not unexpected. It has been observed that the protonation of an oxo bridge reduces the antiferromagnetic coupling between two S = 5/2 Fe(III) ions by one order of magnitude (-O- bridge: J = - 121 cm^{-1}; -O(H)- bridge: J = - 17 cm^{-1} (for both complexes: g = 2.0)).[200] In this system, the protonation of the oxo bridge causes the average Fe-O_{bridge} bond distance to increase by 0.172 Å.[200] Other researchers described an alkoxy-bridged dimeric Fe(III) complex in which the two S = 5/2 Fe(III) ions are antiferromagnetically coupled with J = - 12 cm^{-1}.[201] In **6**, the Fe-S-Fe angles are close to 90° (79.1 (1)°) and the Fe(III)-$S_{bridging\ other\ ligand}$ distances are fairly long (2.449(3) Å). Therefore, there is little overlap and hence the electron spins of the two Fe(III) ions do not couple very much. Also, the Fe···Fe distance (2.997 Å) within the dimer of **6** is too long for a direct bond. In the case of **7**, the effective paramagnetic magnetic moment at300 K is 4.34 μ_B. The expected spin-only value for one S = 3/2 center is 3.87 μ_B ($\mu_{eff} = g * (3/2 * (3/2 + 1))^{1/2}$ with g = 2). The decrease of μ_{eff} of **7** at temperatures below 20 K is caused by zero-field splitting as commonly observed in compounds containing an Fe(III) ion in an S = 3/2 spin state.[202] Based upon an analysis of the EPR spectrum, with $g_{mid}/g_{min} \sim 2.2$, the axial zero-field splitting parameter D of **7** is estimated to be about + 0.077 cm^{-1} ($\Delta E = g\beta H + 2D$; ν = 9.365 GHz, g = 2.2, H for g = 4.35).

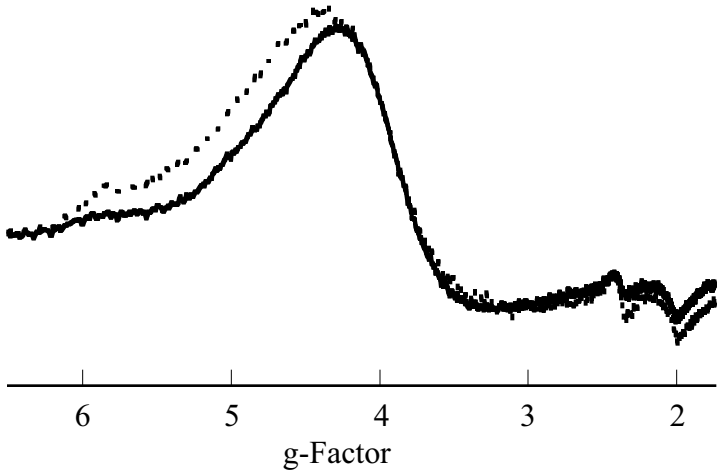

Figure 4-8: EPR spectra of $(NMe_4)_2[(Fe(III)S_2^{Me2}N_2^{amide}(Et))_2]$ (**6**) (-) and $(NMe_4)[Fe(III)S_2^{Me2}N_2^{amide}(Et)(Py)]$ (**7**) (···) in MeOH/EtOH 9/1 at 130 K.

The similar spin state of both compounds, and the fact that **6** contains two nearly independent S = 3/2 centers, is confirmed by EPR measurements. Both compounds give rise to a g_{max} in the EPR, see Figure 4-8, characteristic[202] of an S = 3/2 system (**6**: g_{max} = 4.28 and **7**: g_{max} = 4.35).

Both compounds, see Figure 4-9, give rise to a very similar electronic absorption spectrum. In MeOH as the solvent, **6** exhibits absorption maxima at 301 (16400), 420 (5700), and 465 (6000) nm, while **7** exhibits absorption maxima at 307 (8000), 425 (2600), and 487 (4800) nm in pyridine as the solvent. This again shows that the Fe(III) ions in **6** and **7** are in a similar electronic environment. The molar extinction coefficients of **6** are about twice as large as those of **7**, since **6** contains two moles of Fe(III) ions per mole of substance, whereas **7** only contains one mole of Fe(III) ion per mole of substance.

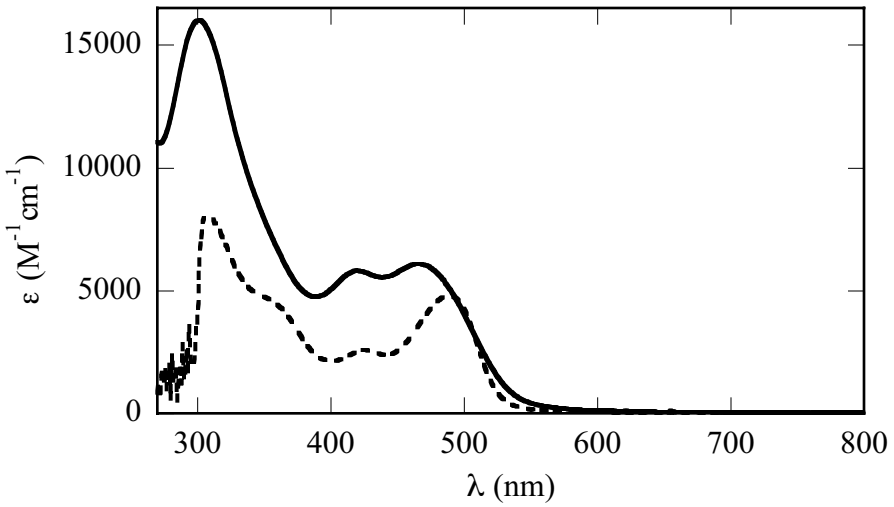

Figure 4-9: Electronic absorption spectra of $(NMe_4)_2[(Fe(III)S_2^{Me2}N_2^{amide}(Et))_2]$ (**6**) (-, MeOH) and $(NMe_4)[Fe(III)S_2^{Me2}N_2^{amide}(Et)(Py)]$ (**7**) (···, pyridine).

A comparison of the Fe-N_{amide} and Fe-$S_{terminal}$ distances of **6** and **7**, see Table 4-1, shows that they are identical within the error limits. This is the case since both compounds contain an Fe(III) ion with an S = 3/2 spin state.

A comparison of the Fe-S distances (2.21(1) Å) in **7** with those (2.21(2) Å) in **1-N$_3$** and **5-N$_3$** shows that they are very similar, although the compounds have different spin states. Surprisingly, the Fe-N_{amide} distances (1.91(1) Å) in **7** are shorter than those (1.954(2) Å) in $[Fe(III)(PyPepS)_2]^-$, $PyPepSH_2$ = *N*-2-mercaptophenyl-2'-pyridinecarboxamide, which has an S = 1/2 spin state![67] However, as expected since a higher spin state causes the population of antibonding orbitals, the Fe(III)-$N_{pyridine}$ distance (2.165(3) Å) in **7** is longer than those (2.02(4) Å) in model compounds with an S = 1/2 spin state.[67,85,90] These observations can be explained if **7** is placed into a coordinate system so that the z axis is aligned

along the Fe-$N_{pyridine}$ vector and the x and y axes point towards the sulfur and N_{amide} donor atoms. Thereby, the abbreviated qualitative molecular orbital diagram shown in Figure 4-10 is obtained.

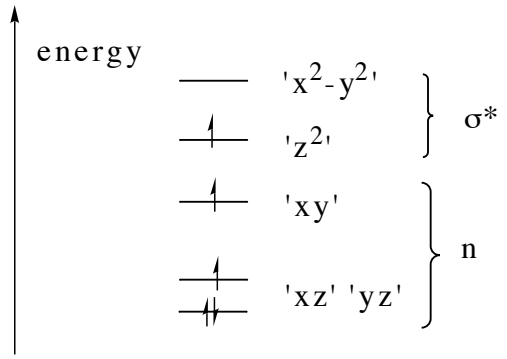

$[Fe(III)S_2^{Me2}N_2^{amide}(Et)(Py)]^-$ (**7**$^-$)
molecular orbitals
- HOMO/LUMO region -

Figure 4-10: Abbreviated qualitative MO diagram of the anion of **7** (**7**$^-$).

According to this abbreviated qualitative molecular orbital diagram, the antibonding d 'x^2-y^2' orbital does not contain any electrons. Therefore, shorter than expected Fe-S and Fe-N_{amide} bond distances are observed in **7**. Since the antibonding d 'z^2' orbital is half populated, a longer Fe-$N_{pyridine}$ bond distance is present in **7**. On the one hand, compound **7** is not in an S = 1/2 spin state since the energy difference between the d 'xz' or d 'yz' orbital and the d 'z^2' orbital is smaller than the spin pairing energy. On the other hand, compound **7** is not in an S = 5/2 spin state since the energy difference between the d 'yz' or d 'xz' orbital and the d 'x^2-y^2' orbital is larger than the spin pairing energy. It is interesting to note that another pentacoordinated complex, the pentacoordinated precursor of $[Fe(III)(PyPS)(OH)]^{2-}$ in Figure 1-7, with the same donor atoms as **7**, but a

different spacial arrangement, τ = 0.401167, is in the high spin state, S = 5/2, even at 4 K![74] This shows how sensitive the energies of the orbitals are to the spacial arrangement of the donor atoms. In addition, two other pentacoordinated complexes with two carboxamide nitrogens and two thiolate sulfurs forming the plane of a square pyramid, that means τ is close to zero, have been described. As it is the case for **7**, they are in an S = 3/2 spin state at all investigated temperatures even though they contain a chlorine[70] or an oxygen[71] donor atom at the apex instead of a $N_{pyridine}$ as does **7**.

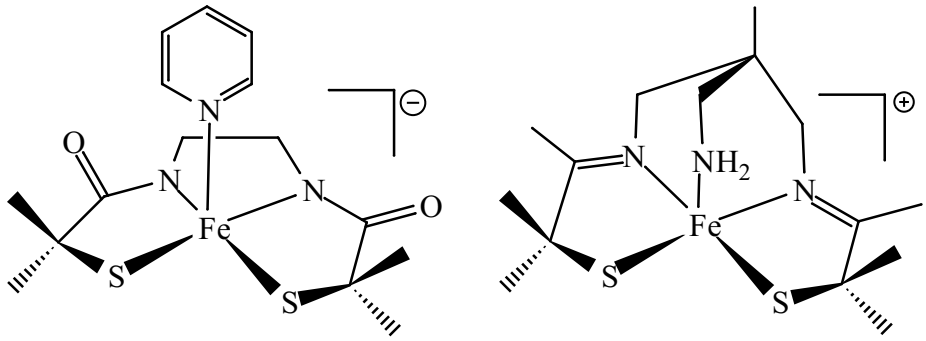

7$^-$ **[Fe(III)(N$_3$(tame)S$_2^{Me2}$)]$^+$**

Figure 4-11: Structures of the anion of **7** (**7**$^-$) and its N_{imine}-containing analogue.

An interesting comparison can be made between **7** and the structurally related compound $[Fe(III)(N_3(tame)S_2^{Me2})]^+$.[203] This compound also contains Fe(III) and it is pentacoordinated with a τ of 0.0117.[203] It contains two imine nitrogens as donor atoms instead of two amide nitrogen donor atoms. The plane of the square pyramid is formed by two cis imine nitrogens and by two cis thiolate sulfurs, while the apex is being provided by an NH_2 group. In comparison, the plane of the square pyramid in **7** is formed by two cis deprotonated carboxamido nitrogens and by two cis thiolate sulfurs, while the apex is being provided by the

nitrogen of the pyridine ligand. Both N_{amide}-containing **7**, see Figure 4-7, and N_{imine}-containing $[Fe(III)(N_3(tame)S_2^{Me2})]^+$ are in an S = 3/2 spin state over the entire temperature range of 5 to 300 K. This shows that a coordinated N_{imine} is a good structural and electronic model of a deprotonated, coordinated N_{amide}. A coordinated N_{imine} models the 'imine' resonance form, **B** in Figure 4-12, of a deprotonated, coordinated N_{amide}.

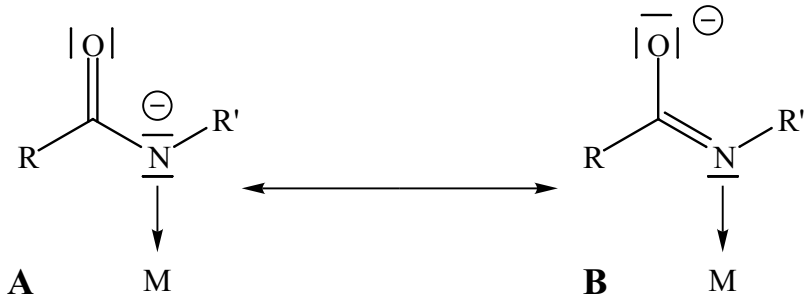

Figure 4-12: Diagram showing the two possible resonance structures of a deprotonated, N-coordinated carboxamido group (**A**: 'amide' form; **B**: 'imine' form).

Recent calculations support the finding that N-coordinated imines and N-coordinated carboxamides are electronically very similar.[204] The C-N bond orders and partial charge distributions calculated for several N-coordinated carboxamide Fe(III) model compounds show a considerable contribution of the 'imine' resonance structure. For N-coordinated carboxamide, it was found that the C-N bond has substantial double character and that there is negative charge delocalized onto the oxygen atom.

A comparison of the carboxamido carbonyl stretching frequency (ν_{CO}) in the free ligand with that of the metal complexes provides further evidence for a participation of the 'imine' resonance structure **B**. Upon complexation, ν_{CO} shifts from 1641 cm^{-1} in the free ligand to 1576 cm^{-1} in **7** and 1583 cm^{-1} (terminal) and

1550 cm^{-1} (bridging) in **6**. This shift to lower energies is indicative of a contribution of resonance structure **B** in the metal complexes. A similar bathochromic shift was observed in other Fe(III)[67,72,74] and Cu(II)[174] coordination complexes.

It is interesting to note that the active site of NHase, which holds an Fe(III) ion in an S = 1/2 spin state, contains as the donor atoms two carboxamido nitrogens perpendicular to two cis thiolate sulfurs, provided that only the sulfone modification is present (the $Fe(S)_2$ plane is perpendicular to the $Fe(N_{amide})_2$ plane).[41,54,60-63] As it was discussed above, the coordination of two cis imine/amide nitrogens and two cis thiolate sulfurs to an Fe(III) ion in the same plane affords an S = 3/2 as opposed to an S = 1/2 spin state. In comparison to this, the arrangement of two cis thiolate sulfur donor atoms perpendicular to two trans imine nitrogens,[74,84-91] e. g., **1-N$_3$** and **5-N$_3$**, or two trans amide nitrogens[67] as donor atoms gives rise to an S = 1/2 spin state of the coordinated Fe(III) ion (the $Fe(S)_2$ plane is perpendicular to the $Fe(N_{imine/amide})_2$ plane). This similarity in the coordination environment between the model compounds and the active site of NHase can be seen as additional evidence to support the notion that only the sulfone modification, but not the sulfoxide modification, is present in active NHase. Furthermore, the arrangement of two cis thiolate donors perpendicular to two imine/amide nitrogen donors (the $Fe(S)_2$ plane is perpendicular to the $Fe(N_{imine/amide})_2$ plane) seems to be essential for the S = 1/2 spin state of a coordinated Fe(III) and the low energy absorption maximum at around 700 nm.

NHase is the second enzyme in which the coordination of an amide (carboxamide) nitrogen to a metal ion has been observed. The other example occurs in the P-cluster of nitrogenase.[66] Based upon the crystal structure, it cannot be said whether or not the amide nitrogens are deprotonated. However, the present

study, as well as work by other authors,[67-74] shows that the coordination of a deprotonated amide nitrogen, which is negatively charged, to an Fe(III) ion forms a stable structure. This is the case even though at the pH required to deprotonate an uncoordinated carboxamide nitrogen, the insoluble"iron(III) hydroxide" is the most stable form of Fe(III) in an aqueous environment.[72,104] The coordination of a deprotonated carboxamide nitrogen to Fe(III) significantly stabilizes the +3 oxidation state, as it is indicated by the shift of the reduction potential to more negative potentials (**6**: $E_{irr.}$(MeOH, vs. SCE) = - 1.10 V and **7**: $E_{1/2}$(py, vs. SCE) = - 1.34 V). A similarly negative reduction potential was found in other Fe(III) amide coordination compounds.[67-74]

Chapter V: Experimental Section

General Methods

All reactions involving oxygen and/or water sensitive compounds were performed in a Vacuum Atmospheres glove box or on a high vacuum line using Schlenk techniques under dry nitrogen at room temperature. In the glove box, it proved to be useful to add solids to a flask via a funnel that fits through the joint into the flask. The balance boat and the funnel were thereafter washed with the appropriate solvent. Generally in the glove box, liquid reactants were weighted out on the balance into a glass container. This glass container was then filled with approximately 1 ml of the appropriate solvent. The solution was mixed with a pipette and added to the flask. Then the glass vial was washed with 2 ml of solvent. In synthetic procedures, this will be listed as "a g of b were added employing 3 ml of c". All solvent ratios are in v/v. Stirring was always achieved by means of a magnetic stirring bar. Customary, in reactions using metal complexes, the solvents were removed by evaporation under vacuum on a Schlenk line. All chemicals, except when stated otherwise, were used as received from commercial suppliers. Solvents were dried before use. Sodium was added to methanol, and it was then distilled under nitrogen. Acetonitrile was distilled from calcium hydride under nitrogen. Dichloromethane, toluene, and tetrahydrofuran were dried by standing over $MgSO_4$. Pyridine was dried by standing over KOH.

Infrared (4400 - 400 cm^{-1}) spectra were recorded as KBr pellets on a Perkin-Elmer 1600 FTIR spectrometer. Electronic (190 - 1100 nm) spectra were recorded on a Hewlett-Packard 8450 spectrometer. ^1H NMR spectra were recorded on either an AC200 or an AF300 spectrometer at room temperature. Chemical shifts

are reported in ppm relative to TMS. ^{31}P NMR spectra were recorded on an AF300 spectrometer at room temperature. Chemical shifts are cited relative to 85 % H_3PO_4 (^{31}P, external, coaxial capillary). For Mößbauer measurements (natural abundance, ~ 2.25 % ^{57}Fe) approximately 35 mg of substance were ground with 15 mg of BN in a mortar and placed into a Mößbauer sample holder. The sample was then shipped to Prof. Huynh at Emory University for analysis. Elemental analyses were performed by Atlantic Microlab, Norcross, GA.

Cyclic voltammetry data in MeCN for **1-NO** was collected in a cell using a 0.01 M $AgNO_3$ (containing 0.1 M electrolyte)/Ag electrode as the reference electrode, a platinum disc working electrode, and a platinum wire auxiliary electrode. As the internal reference, the redox couple $Fe(Cp)_2^{+/0}$ (0.003 M, + 0.1 M electrolyte) was used. $N[(CH_2)_3CH_3]_4(PF_6)$ was used as the electrolyte. A Bioanalytical Systems electrochemical analyzer was used in the measurements. All reported potentials were obtained with a scan rate of 100 mV/s. For $Fe(Cp)_2^{+/0}$ in MeCN, it was found that $E_{1/2}$ = + 86 mV versus 0.01 M $AgNO_3$/Ag. Cyclic voltammetry for all other compounds was performed by using a EG&G Princeton Applied Research 273 potentiostat with a glassy carbon working electrode, a platinum wire auxiliary electrode, and a saturated KCl calomel reference electrode (SCE) ($E_{1/2}$ = + 0.2412 V versus NHE).[205] A 0.1 M solution of $N[(CH_2)_3CH_3]_4(PF_6)$ supporting electrolyte was used. In MeCN as the solvent, the $Fe(Cp)_2^{+/0}$ couple was + 400 mV. Thus, the following equations have to be used to convert the redox potentials into each other: $E_{1/2}(SCE) = E_{1/2}(Ag^+/Ag) + 314$ mV; $E_{1/2}°$ ($E_{1/2}$ versus NHE) = $E_{1/2}(Ag^+/Ag) + 555$ mV; and $E_{1/2}°$ ($E_{1/2}$ versus NHE) = $E_{1/2}(SCE) + 0.241$ mV. It was recommended by IUPAC to report redox potentials obtained in non-aqueous solvents versus the $Fe(Cp)_2^{+/0}$ redox couple.[206]

To do this, the potential of the $Fe(Cp)_2^{+/0}$ redox couple is set to zero. The $E_{1/2}$ versus $Fe(Cp)_2^{+/0}$ ($E_{1/2}(Fc)$) in MeCN is calculated by $E_{1/2}(Fc) = E_{1/2}(Ag^+/Ag) - 86$ mV and $E_{1/2}(Fc) = E_{1/2}(SCE) - 400$ mV.

In MeOH as the solvent, the $Fe(Cp)_2^{+/0}$ couple was + 360 mV. Thus, the following equations have to be used to convert the redox potentials into each other: $E_{1/2}°$ ($E_{1/2}$ versus NHE) = $E_{1/2}(SCE) + 0.241$ mV and $E_{1/2}(Fc) = E_{1/2}(SCE) - 360$ mV.

In pyridine as the solvent, the $Fe(Cp)_2^{+/0}$ couple was + 520 mV. Thus, the following equations have to be used to convert the redox potentials into each other: $E_{1/2}°$ ($E_{1/2}$ versus NHE) = $E_{1/2}(SCE) + 0.241$ mV and $E_{1/2}(Fc) = E_{1/2}(SCE) - 520$ mV.

X-ray Data Collection and Structure Solution and Refinement

Suitable crystals were immersed in Paratone 8277 oil (Exxon). After examination under a microscope, a crystal was mounted onto a glass fiber and immediately placed into a low-temperature $N_2(g)$ stream. X-ray data for **1-NO**, **4**, **5**, **5-N$_3$**, and **6** was collected at 161 K and X-ray data for **7** was collected at 130 K using a Nonius Kappa CCD diffractometer (Mo Kα, λ = 0.71070 Å). The structures were solved by direct methods (SIR 92)[207] and refined with SHELXL97.[208] H atoms were placed with idealized geometry and refined with a riding model. A short discussion of each crystal structure that was obtained by the author of this dissertation is included with the synthesis of each compound. Relevant crystallographic information is summarized in Tables.

Magnetic Measurements[209,210]

Magnetic susceptibility measurements in the solid state (polycrystalline sample) were performed using a Quantum Design MPMS SQUID susceptometer

(B = 1000 G) at Michigan State University (East Lansing, MI) or in the Chemistry Department at the University of Washington. Data was manipulated with either MS Excel or KaleidaGraph. Firstly, the measured magnetic moment (A) has to be divided by the employed magnetic field (B) to obtain the raw susceptibility (C) [C = A / B]. Secondly, the diamagnetic contribution (~ - 5.06 10^{10} / $mg_{(of\ gelcap)}$) of the gelcap (D) has to be subtracted [E = C - D]. Thirdly, the molar paramagnetic susceptibility of the measured compound ($\chi_{M,para}$) is calculated [$\chi_{M,para}$ = E ∗ (MM / $m_{(of\ complex\ used)}$) - $\chi_{M,dia}$]. The values for the diamagnetic susceptibilities ($\chi_{M,dia}$) of the complexes (**1**: - 291.26 10^{-6} emu/mol; **1-N$_3$**: - 238.09 10^{-6}; **4**: - 294.40 10^{-6}; **5**: - 279.40 10^{-6}; **5-N$_3$**: - 226.23 10^{-6}; **6**: - 447.48 10^{-6}; **7**: - 293.79 10^{-6}) were calculated based on Pascal's constants.[211] The effective paramagnetic magnetic moment ($\mu_{eff,para}$) can then be calculated [$\mu_{eff,para} = 2.8279 * (\chi_{M,para} * T)^{1/2}$]. All magnetic moments reported in this thesis are effective paramagnetic magnetic moments.

Solution magnetic moments were determined on an AF300 NMR spectrometer using the Evans method, as modified for superconducting solenoids.[212,213] Van Geet's method was used to determine the temperature of the measurement (spin ≥ 20 min; NMR of 1 ml D_3COD + 1 drop regular MeOH; T ~ $\Delta\nu$).[214] For the Evans method, a stock solution of ~ 3 ml D_3CCN and 2 drops TMS was prepared (solution A). This solution was used to dissolve an exact amount, ~ 5 mg, of the compound to be investigated in a 2 ml volumetric flask (solution B; m = concentration of compound in g/ml). As shown in Figure 5-1, a capillary containing solution A was then placed within an NMR tube containing solution B. The white plastic holder for the capillary was obtained from VWR. A similar setup was used for ^{31}P NMR. After spinning for ≥ 20 min, an NMR spectrum was recorded. The mass susceptibility (χ_g (emu/g)) of the dissolved

substance is given by: $\chi_g = ((-3\ \Delta\nu)/(4\ \pi\ \nu\ m)) + \chi_0 + (\chi_0\ (\rho_0 - \rho_s)/m)$.[212] After correction, the molar susceptibility (χ_M (emu/mol)) of the dissolved substance is calculated: $\chi_M = \chi_g * MM$.[213] It consists of a paramagnetic and a diamagnetic part: $\chi_M = \chi_{M,para} + \chi_{M,dia}$. The paramagnetic part is used to calculate the effective paramagnetic magnetic moment ($\mu_{eff,para}$) [$\mu_{eff,para} = 2.8279 * (\chi_{M,para} * T)^{1/2}$].

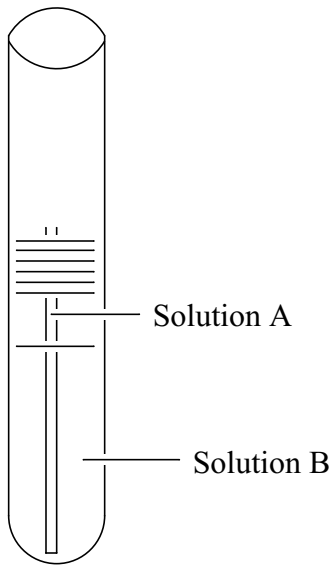

Figure 5-1: Setup for Evans method.

EPR spectra were recorded on an EPX Bruker using the following glasses and temperatures: **1**: CH_2Cl_2/toluene (1/1), 125 K; **5**: CH_2Cl_2/toluene (1/1), 150 K; **1-N$_3$** and **5-N$_3$**: CH_2Cl_2/toluene (1/1), 130 K; **4**: MeOH/EtOH (9/1), 141 K. The following parameters were utilized: microwave frequency: 9.395 GHz for **1**, 9.380 GHz for **1-N$_3$**, 9.404 GHz for **4**, 9.390 GHz for **5**, 9.375 GHz for **5-N$_3$**, 9.355 GHz for **6**, 9.365 GHz for **7**; microwave power: 6.331 mW for **1**, **1-N$_3$**, and **5**, 12.631 mW for **4**, 0.633 mW for **5-N$_3$**, 25.20 mW for **6**, 31.73 mW for **7**; modulation amplitude: 5.00 G for **1**, **1-N$_3$**, **5**, and **5-N$_3$**, 3.00 G for **4**, 1.00 G for **6** and **7**;

modulation frequency: 10.00 kHz for **1**, **1-N$_3$**, **5**, **5-N$_3$**, **6**, and **7**, 100.00 kHz for **4**; receiver gain: 1.59 10^5 for **1** and **5**, 1.26 10^5 for **1-N$_3$** and **5-N$_3$**, 1.00 10^5 for **4**, 7.096 10^5 for **6** and **7**.

Azide Binding Studies

Azide binding studies were performed using freshly prepared solutions in MeOH. Typically, about a 1 mM solution of **5** in MeOH was prepared. This solution was used to dissolve and transfer a known amount of tetra(*n*-butyl)ammonium azide into a volumetric flask containing an appropriate amount of tetra(*n*-butyl)ammonium nitrate. Tetra(*n*-butyl)ammonium nitrate was used to achieve a constant ionic strength of I = 0.06 M. After mixing, the solution was then transferred into a custom-designed low-temperature quartz optical Dewar. The Dewar was similar to the ones available from HSMARTIN. Equilibrium constants were determined at five different temperatures (22 °C, 0 °C, -15 °C, -23 °C, and -46 °C). After recording the spectrum at room temperature, the Dewar was cooled stepwise using the appropriate cooling bath (ice water (0 °C), ethylene glycol/CO_2 (-15 °C), CCl_4/CO_2 (-23 °C), and MeCN/CO_2 (-46 °C)). The spectrum was recorded at each of those temperatures. Concentrations for all low-temperature measurements were corrected for changes in the density of MeOH upon cooling.[215] The following concentration correction factors were used: c(0 °C) = c(22 °C) ∗ 1.0261285; c(- 15 °C) = c(22 °C) ∗ 1.0438974; c(- 23 °C) = c(22 °C) ∗ 1.053415; c(- 46 °C) = c(22 °C) ∗ 1.0811576. To minimize error, electronic spectral data at the wavelength (551 nm) which displays the greatest difference in absorbance for the two complexes of interest, **5** and **5-N$_3$**, was used in the calculations. The amount of tetra(*n*-butyl)ammonium azide was chosen so that 20

% to 80 % of the iron complex was azide bound. This range gave the least amount of error. The 551 nm extinction coefficient of **5** at I = 0.06 mol/l was found to be 1590 ± 35 $M^{-1}cm^{-1}$ at 22 °C, 0 °C, and - 15 °C. It was 1567 ± 30 $M^{-1}cm^{-1}$ at - 23 °C and 1475 ± 45 $M^{-1}cm^{-1}$ at - 46 °C. The 551 nm extinction coefficient of **5-N$_3$** was determined by using 60 equivalents of tetra(*n*-butyl)ammonium azide, that is I = 0.06 mol/l. At - 46 °C, - 23 °C, and - 15 °C complete azide binding was observed. The value at these temperatures, 693 ± 25 $M^{-1}cm^{-1}$, was used at all temperatures. Equilibrium constants were calculated using equations 2 and 3,[126] and determined to be K_{eq}(22 °C) = 110 ± 20 M^{-1}, K_{eq}(0 °C) = 210 ± 40 M^{-1}, K_{eq}(- 15 °C) = 470 ± 90 M^{-1}, K_{eq}(- 23 °C) = 720 ± 140 M^{-1}, and K_{eq}(- 46 °C) = 4950 ± 990 M^{-1}. Thermodynamic parameters, ΔH = - 7.5 ± 0.6 kcal/mol = - 31.5 ± 2.7 kJ/mol and ΔS = - 16.6 ± 2.5 cal/(mol K) = - 69.6 ± 10.4 J/(mol K), were determined from a van't Hoff plot.

$$[\mathbf{5-N_3}] = \frac{A - \varepsilon_5[\mathbf{5}]_0}{\varepsilon_{5-N3} - \varepsilon_5} \tag{2}$$

$$K_{eq} = \frac{[\mathbf{5\text{-}N_3}]}{([\mathbf{5}]_0 - [\mathbf{5\text{-}N_3}])([N_3^-]_0 - [\mathbf{5\text{-}N_3}])} \tag{3}$$

Titration of 6 with Pyridine

Since the NMe_4^+ salt of **6** is insoluble in CH_2Cl_2 a cation exchange had to be performed. To do this, 100 mg of $(NMe_4)_2[(Fe(III)S_2^{Me2}N_2^{amide}(Et))_2]$ (**6**) (0.118 mmol) and 100 mg of $N[(CH_2)_3CH_3]_4(PF_6)$ (0.258 mmol) were dissolved in 20 ml of MeCN in a 100 ml sidearm flask. After stirring for 30 min, 20 ml of Et_2O were added. The mixture was stirred for another 30 min and then filtered through Celite into a 100 ml sidearm flask. An additional 30 ml of MeCN/Et_2O (1/1) were used to

wet the Celite and for washing. Upon pumping to dryness, a red, CH_2Cl_2 soluble powder, $(N[(CH_2)_3CH_3]_4)_2[(Fe(III)S_2^{Me2}N_2^{amide}(Et))_2]$, was obtained. The ε of **6** in CH_2Cl_2 was estimated by measuring the electronic absorption spectrum of a solution of **6** in CH_2Cl_2 before and after the addition of an excess of pyridine (20 μl for 5 ml of solution). Since the ε of pyridine-bound **7** was known, the ε of **6** in CH_2Cl_2 could be calculated.

Five ml of a solution of **6** in CH_2Cl_2 were transferred into an UV/Vis cell equipped with a Kontes joint. Based upon the absorption at 488 nm, the concentration of **6** was calculated to be 1.13855 10^{-4} mol/l ($n_{\mathbf{6}}$ = 5.69275 10^{-7} mol). Thereafter, a solution of 200 μl of pyridine in 200 ml of CH_2Cl_2 was prepared in the glove box (c_{py} = 1.23964 10^{-2} mol/l). Now the pyridine solution was added in 20 μl aliquots (n_{py} = 2.47929 10^{-7} mol) to the solution of **6** in the UV/Vis cell. After each addition, the solution was mixed 'by going up and down in a pipette,' and the electronic absorption spectrum was recorded.

Synthesis and Characterization of 3-chloro-3-methyl-2-butanone[216]

Under nitrogen and cooling with ice/rock salt, predistilled SO_2Cl_2 (0.6 mol) was added dropwise using a pressure equalized dropping funnel to a 500 ml three-necked flack containing stirred 3-methyl-2-butanone (0.6 mol). After the addition was completed, the reaction was stirred for 12 h at room temperature. Upon distillation of the crude reaction mixture, aclear, colorless liquid was obtained (T_b = 24 °C / p = ~ 7 Torr). ^{1}H NMR spectroscopy indicated that less than 5 % impurities were present. The starting material 3-methyl-2-butanone accounted for most of the impurities; if a small excess, 10 %, of SO_2Cl_2 was used, then no 3-methyl-2-butanone was present in the product. The ^{1}H NMR spectrum ($CDCl_3$)

of 3-chloro-3-methyl-2-butanone contains two peaks: 1.675 ppm [$CH_3COCCl(C\underline{H}_3)_2$] and 2.374 ppm [$C\underline{H}_3COCCl(CH_3)_2$]. The reaction performed on a 0.6 mol scale gave an isolated yield of 75 %.

Synthesis and Characterization of 3-mercapto-3-methyl-2-butanone[217]

A with ice/rock salt cooled magnetically stirred solution of 2.15 equivalents of NaOH in 260 ml of H_2O was saturated with H_2S. It was essential for the success of the reaction that throughout the entire course of the reaction the contents of the flask were held at ice/rock salt temperature. While H_2S was continued to be introduced into the solution, one equivalent of 3-chloro-3-methyl-2-butanone was added dropwise. The addition funnel was washed with 5 ml of MeOH. The solution was then stirred for 2 h at low temperature without H_2S being introduced. Using diluted H_2SO_4, the pH of the solution was adjusted to 4. The system was extracted twice using 70 ml of CH_2Cl_2 each time. The combined CH_2Cl_2 phase was washed with saturated $NaHCO_3$, washed with water, and then dried over Na_2SO_4. The drying agent was removed by filtration, and the CH_2Cl_2 was destilled off at normal pressure. ^{1}H NMR spectroscopy of the remaining colorless liquid indicated that less than 5 % impurities were present. Dichloromethane and 3-methyl-2-butanone accounted for most of the impurities. In many cases the product was sufficiently pure at this stage, if not it was destilled (T_b = 100 °C / p = ~ 20 Torr). Typically, the reaction gave an isolated yield of 85 %. Equally well, the reaction can also be performed using NaSH • 2 H_2O in H_2O. The ^{1}H NMR spectrum ($CDCl_3$) of 3-mercapto-3-methyl-2-butanone contains 3 peaks: 1.517 ppm [$CH_3COCSH(C\underline{H}_3)_2$], 2.040 ppm [$CH_3COCS\underline{H}(CH_3)_2$], and 2.326 ppm [$C\underline{H}_3COCSH(CH_3)_2$].

Synthesis and Characterization of $[Fe(III)S_2^{Me2}N_3(Pr,Pr)]PF_6$ (1)[89]

The purification of this substance proved to be an extreme challenge. A gray powder with an absorption maximum at around 210 nm, but no other features, possesses very similar solubility properties as the desired product. It was found that the desired product could only be separated from this impurity by mechanical means as described below. The exact identity of this impurity is not known. It is speculated that this gray powder is an 'Fe-S-containing' compound since it gives rise to an absorption in Mößbauer spectroscopy. Earlier Mößbauer measurements of an unclean sample of **1** indicated the presence of three Fe-containing impurities: 0.86/3.39, 0.47/1.32, and 0.65/1.96 ($\delta/\Delta E_Q$ in mm/s). Those impurities are not pyrite whose Mößbauer parameters are $\delta = 0.314$ mm/s and $\Delta E_Q = 0.614$ mm/s.[218] The following procedure, provided that the purification is successful, yields a reasonably clean compound. All steps were performed in a glove box. In a 50 ml sidearm flask, 400 mg of NaOH (10 mmol) were dissolved in 10 ml ofMeOH under stirring. The 3-mercapto-3-methyl-2-butanone (1.182 g, 10 mmol) was added dropwise employing 3 ml of MeOH. This solution was stirred for 30 min. In an 100 ml sidearm flask, 634 mg (5 mmol) of $FeCl_2$ were dissolved in 10 ml of MeOH. The sodium thiolate solution was then added dropwise to the stirring $FeCl_2$ solution. Initially, the solution is green-brown, after approximately two thirds of the sodium thiolate solution were added, suddenly, an orange solid began to precipitate. After 20 min stirring, 656 mg (5 mmol) of N-(3-aminopropyl)-1,3-propanediamine were added dropwise employing 3 ml of MeOH. After 10 min stirring, the solution turned green-brown. After stirring overnight at room temperature, 1.820 g (5.5 mmol) of $Fe(Cp)_2PF_6$ were added as a solid to the stirring

solution. The balance boat and funnel were washed with 10 ml of MeCN. The solution was stirred for 10 min at room temperature. The flask with the reaction mixture was then stored at - 35 °C for 4 h. The reaction mixture was then filtered through Celite (wet with MeCN) on a C-frit into a 200 ml flask without washing. Once the solvent was evaporated off, the solid was washed several times with Et_2O until the Et_2O remained nearly colorless. This removed most of the $Fe(Cp)_2$. The solid was then dissolved in 15 ml of MeCN. To this stirring solution 7.5 ml of Et_2O were added dropwise. This mixture was filtered after 5 min stirring through Celite (wet with 1/1 MeCN/Et_2O) on a C-frit into a 100 ml flask. By doing this a brown impurity was separated from the desired product. This step can be repeated using 15 ml of MeCN and 10 ml of Et_2O to ensure that all of this impurity has been separated. After all of the solvent was evaporated off, the solid was dissolved in 7 ml of MeCN and overlayered with 18 ml of Et_2O. After 2 d at - 35 °C, the mother liquid was decanted while the flask was still cold. The black crystals that remained in the flask where washed several times with Et_2O in the following way. All of the solid in the flask was suspended in Et_2O. Since the black crystals had a higher density they sunk to the ground of the flask. In the Et_2O layer a gray solid remained suspended. Using a pipette the Et_2O containing the suspended gray solid was then separated from the desired product. This mechanical separation was the crucial step in the purification process. The black crystals were then poured into another flask and the last recrystallization and the Et_2O suspension purification were repeated to increase the purity of the product. By following this procedure, **1** was obtained (250 mg, 9 % yield) in 95 % purity as estimated by Mößbauer spectroscopy.

Alternatively, **1** can be prepared using $FeSO_4 \cdot 7\ H_2O$ as the iron source. In this case, 440 mg of NaOH (11 mmol) were dissolved in 10 ml of MeOH under

stirring in a 50 ml sidearm flask. The 3-mercapto-3-methyl-2-butanone (1.182 g, 10 mmol) was added dropwise employing 3 ml of MeOH. After stirring for 20 min, the sodium thiolate solution was added dropwise to a suspension of $FeSO_4 \cdot 7\ H_2O$ (1.390 g, 5 mmol) in 10 ml of MeOH in a 100 ml sidearm flask. After 40 min stirring, 656 mg (5 mmol) of N-(3-aminopropyl)-1,3-propanediamine were added dropwise employing 3 ml of MeOH. After stirring overnight at room temperature, 1.820 g (5.5 mmol) of $Fe(Cp)_2PF_6$ were added as a solid to the stirring solution. The balance boat and funnel were washed with 10 ml of MeCN. The solution was stirred for 10 min at room temperature. The flask with the reaction mixture was then stored at - 35 °C for 4 h. The reaction mixture was then filtered through Celite (wet with MeCN) on a C-frit into a 200 ml flask without washing. Once the solvent was evaporated off, the solid was washed several times with Et_2O until the Et_2O remained nearly colorless. This removed most of the $Fe(Cp)_2$. The solid was then filtered without pulling vacuum through Celite into a 200 ml sidearm flask using about 100 ml of 100 % CH_2Cl_2. Thereafter, a gray-brown solid remained on the frit. After evaporation to dryness, the residue was washed portionwise with Et_2O and again filtered using CH_2Cl_2 without applying vacuum. The solvent was then removed, the residue washed with Et_2O and dissolved in 15 ml of MeCN. To this stirring solution 10 ml of Et_2O were added dropwise. This mixture was filtered after 5 min stirring through Celite (wet with 1/1 MeCN/Et_2O) on a C-frit into a 200 ml flask. About 30 ml of 1/1 MeCN/Et_2O were used for washing. After all of the solvent was evaporated off, the residue was washed again with Et_2O. Using 15 ml of MeCN, it was then transferred into a 100 ml sidearm flask and overlayered with 95 ml of Et_2O. After standing at room temperature for 4 d, the mother liquid was decanted. The black crystalline solid was washed several times with Et_2O. To do this, all of the solid in the flask was made loose using a spatula. The crystalline

solid was suspended in Et_2O and the Et_2O layer was removed using a pipette. After pumping vacuum for 15 min, clean **1** was obtained.

Electronic absorption spectrum in MeCN, see Figure 5-2, λ_{max}, nm (ε, M^{-1} cm^{-1}): 230 (9900), 316 (6040), 418 (4140), 770 (300). Electronic absorption spectrum in CH_2Cl_2, see Figure 3-12, λ_{max}, nm (ε, M^{-1} cm^{-1}): 231 (10200), 319 (6100), 420 (3400), 770 (300).

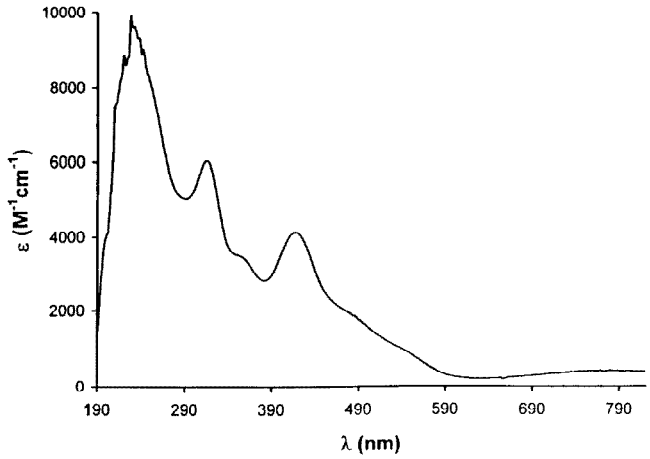

Figure 5-2: UV/Vis absorption spectrum of **1** in MeCN.

The reduction potential of $[Fe(III)S_2^{Me2}N_3(Pr,Pr)]^{+/0}$ ($\mathbf{1}^{+/0}$) in MeCN, which is attributed to a change of the iron oxidation state from +3 to +2, is $E_{1/2}(Ag^+/Ag)$ = - 714 mV, $E_{1/2}$(SCE) = - 400 mV, $E_{1/2}°$ = - 159 mV, and $E_{1/2}$(Fc) = - 800 mV.[58] To evaluate the influence of the α-methyl groups upon the stability of **1**, one has to compare the reduction potential of **1** with the oxidation potential of $[Fe(II)S_2N_3(Pr,Pr)]$. The oxidation potential of $[Fe(II)S_2N_3(Pr,Pr)]^{0/+}$ in MeCN, which is attributed to a change of the iron oxidation state from +2 to +3, is $E_{1/2}$(SCE) = - 260 mV, $E_{1/2}°$ = - 19 mV, and $E_{1/2}$(Fc) = - 660 mV.[219] Those results show that the α-methyl groups donate electron density (+I effect) via the sulfurs to

the iron. Thus, the equilibrium Fe(III) + e^- = Fe(II) is shifted by 140 mV to the left side in $[Fe(III)S_2^{Me2}N_3(Pr,Pr)]^+$ (**1**$^+$) as compared to $[Fe(II)S_2N_3(Pr,Pr)]$ [Nernst equation: $E = E° - (RT/nF) \ln (a_{right}/a_{left})$, therefore $E° = (RT/nF) \ln (a_{right}/a_{left})$]. In other words, because of the increased electron density at the iron in **1**, it becomes more difficult to add another electron to Fe(III). One can say that the Fe(III) in **1** is stabilized by the presence of the α-methyl groups. Note that the more negative the reduction potential, the more the equilibrium Fe(III) + e^- = Fe(II) is shifted to the left side (Fe(II) becomes a stronger reducing agent and Fe(III) becomes a weaker oxidizing agent).

In summary, it can be said that the α-methyl groups provide two mechanisms to stabilize $[Fe(III)S_2^{Me2}N_3(Pr,Pr)]^+$ (**1**$^+$) as compared to $[Fe(II)S_2N_3(Pr,Pr)]$. Firstly, they provide a steric protection against oxidation by O_2 at the sulfur and against disulfide formation. Secondly, they donate electron density to the iron. Thereby, they cause an electronic stabilization of the +3 oxidation state of iron.

Magnetic moment: 3.00 μ_B (300 K, solid state, see Figure 3-10). The paramagnetism of **1** is confirmed by its ^{1}H NMR spectrum, see Figures 5-3 and 5-4. EPR (CH_2Cl_2/Toluene 1/1; 125 K): g = 2.14, 2.07, 2.01 (see Figure 3-11). Mößbauer parameters: δ = 0.21 mm/s and ΔE_Q = 3.01 mm/s. The other characterization data is identical to that reported in the literature.[89]

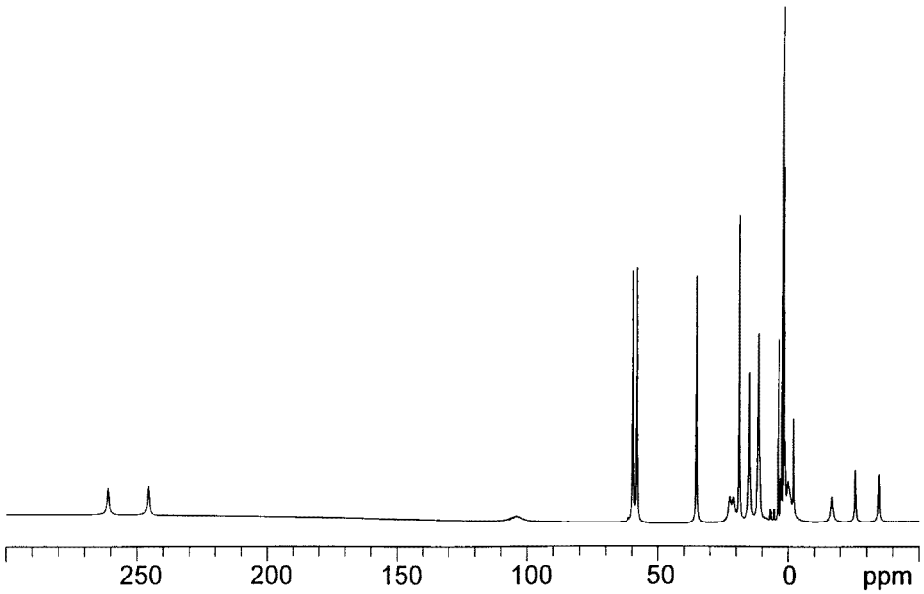

Figure 5-3: ^{1}H NMR spectrum of **1** in MeCN at RT.

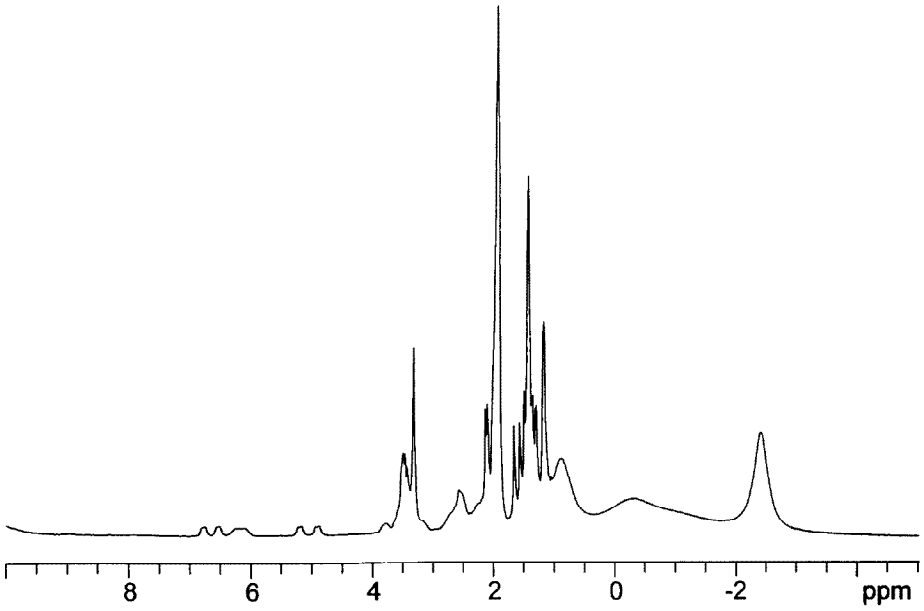

Figure 5-4: Details of ^{1}H NMR spectrum of **1** in MeCN at RT.

Synthesis and Characterization of [Fe(III)$S_2^{Me2}N_3$(Pr,Pr)(NO)]PF_6 (1-NO)[58]

Approximately 75 mg of **1** were dissolved in 10 ml of MeCN to give a red solution. On a high vacuum line using a constant volume bulb, 1.15 equivalents of NO were added. The NO was allowed to condense in the liquid nitrogen cooled reaction vessel for 1 h. After this the reaction vessel was allowed to warm to room temperature under stirring. The reaction system was then taken into a glove box. There, the green-brown solution was poured into a 100 ml flask that did not contain a magnetic stirring bar. The solution was overlayered with 90 ml of Et_2O and stored at - 35 °C for 2 d. The mother liquid was decanted and the remaining black crystals were washed with Et_2O several times. The solid was dried by applying high vacuum for 20 min. The crystals obtained in this way were of X-ray quality. Before some of the solid was dissolved in D_6-MeCN to prepare an NMR sample, the solid was dried for an additional 40 min under high vacuum. To measure the extinction coefficients the reaction was performed in a vessel to which a UV/Vis cell was attached. **1-NO** is stable as a solid in the dark under nitrogen at - 35 °C for weeks.

1-NO is diamagnetic as proven by ^{1}H NMR, see Figures 5-5 and 5-6. If the NMR is taken using a wider window, see Figure 5-5, also signals corresponding to paramagnetic **1** can be detected.

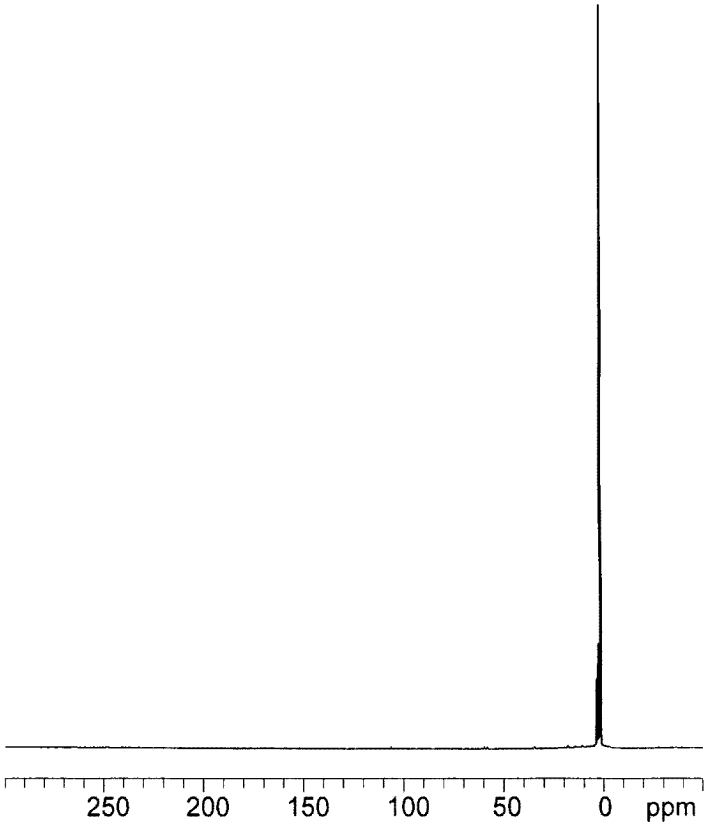

Figure 5-5: ^{1}H NMR spectrum of **1-NO** in MeCN at RT.

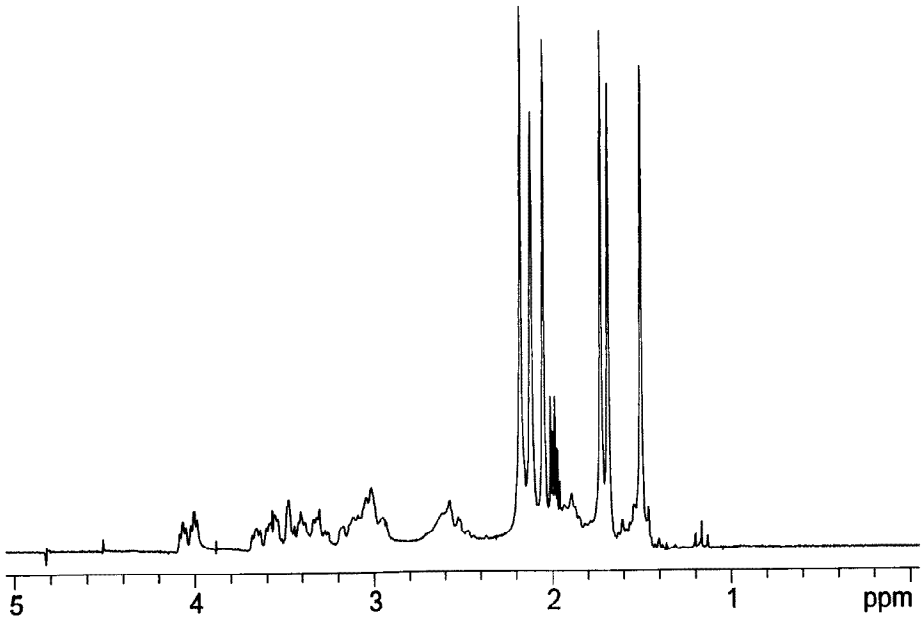

Figure 5-6: Details of ^{1}H NMR spectrum of **1-NO** in MeCN at RT.

EXAFS parameters of **1-NO** are given in Table 2-1. In the range λ = 320 - 820 nm, **1-NO** has a single absorption maximum which is located at λ_{max} = 422 nm (ε = 1710 l/(mol cm)), for details see Figure 2-2. IR spectroscopy of **1-NO** crystals showed the ν_{NO} to be at 1823 cm^{-1} and the $\nu_{C=N}$ to be at 1610 cm^{-1}, see Figure 5-7. It should be noted that two additional peaks at 1770 and 1721 cm^{-1} were observed when the IR spectrum was recorded of the residue that was obtained when the MeCN solvent was evaporated under vacuum immediately after completion of the reaction with NO gas. These two additional absorptions could be caused by an O-bound (η^1-O) and a side-on-bound (η^2-N,O) linkage isomer of the NO ligand as it was observed in other $\{MNO\}^6$ systems.[220,221] Compound **1-NO** was found to be crystallized in the centrosymmetric space group $P2_1/n$ (No. 14) (R = 5.68 %). Both the molecule and its mirror image are present in a 1:1 ratio in the crystal

lattice. The asymmetric unit contains one complete molecule. When the structure was refined using an Fe-O-N arrangement, the R factor was about 5 units higher. Therefore, it was decided that the NO is coordinated to the iron via its nitrogen as opposed to via its oxygen. The ORTEP, selected structural parameters, and relevant crystallographic information of **1-NO** are shown in Figure 2-3, Table 2-3, and Table 5-1, respectively.

The reduction potential of **1-NO**$^{+/0}$ in MeCN, which is attributed to a change of the iron oxidation state from +3 to +2, is $E_{1/2}(Ag^{+}/Ag)$ = - 769 mV, $E_{1/2}$(SCE) = - 455 mV, $E_{1/2}°$ = - 214 mV, and $E_{1/2}$(Fc) = - 855 mV. From these reduction potentials one can conclude that the Fe(III) in **1-NO** is stabilized by 55 mV as compared to the Fe(III) in **1**. Mößbauer parameters: δ = 0.0924 mm/s and ΔE_Q = 1.0078 mm/s. The other characterization data was identical to that reported in the literature.[58]

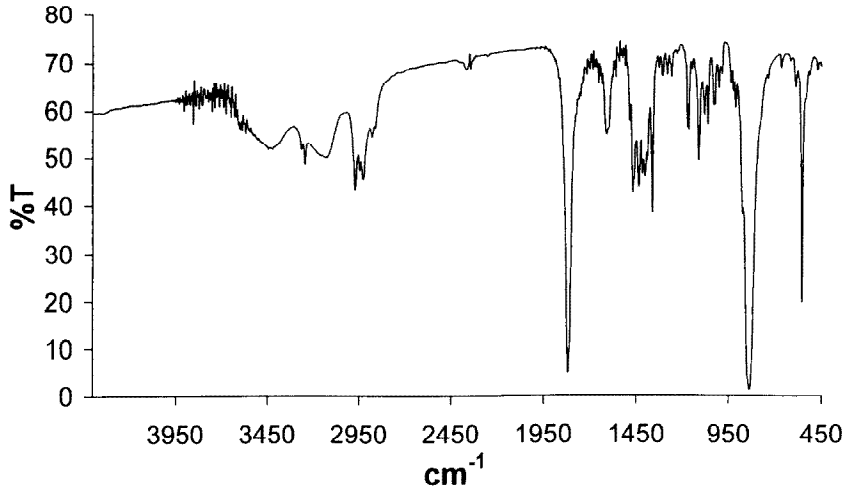

Figure 5-7: IR spectrum (KBr pellet) of **1-NO**.

The photolytic behavior of **1-NO** was also studied. It was not possible to observe any formation of **1** when **1-NO** was exposed to light and/or stored at room

temperature for several days. The following experiments, all, except for the EPR study, at room temperature, have been performed. When solid **1-NO** was exposed to light, no formation of **1** or decomposition of **1-NO** was observed by EPR.[123] An unidentified diamagnetic ^{1}H NMR spectrum was observed in a sample of **1-NO**, which was stored as a CD_3CN solution in the dark for two weeks in a closed NMR tube. Irradiation (UV/Vis) of a CD_3CN solution of **1-NO** in a closed NMR tube for two hours resulted in the presence of another unidentified diamagnetic ^{1}H NMR spectrum. Compound **1-NO**, in an MeCN solution under a N_2 atmosphere in the dark, showed considerable decomposition after 4 hours, as judged by UV/Vis spectroscopy. Irradiation (UV/Vis) of an MeCN solution of **1-NO** under a N_2 atmosphere showed decomposition of **1-NO** within 3 hours, as judged by UV/Vis spectroscopy. Further, it was shown that **1** in an MeCN solution does not significantly decompose within two weeks if stored in the dark. However, exposure of an MeCN solution of **1** to UV/Vis radiation causes considerable decomposition within 4 hours. Mass spectrometric analysis of headspace gases after photolysis (6 h, 25 °C, Hg lamp) of an MeCN solution of **1-NO** show the presence of NO. From these results it must be concluded that the photolytic cleavage of **1-NO** in solution to form **1** and NO does occur, however the reaction is not reversible owing to the subsequent photodecomposition of **1**.

Synthesis and Characterization of [Fe(III)$S_2^{Me2}N_3$(Pr,Pr)(N_3)] (1-N_3)[89]

Compound **1** (486 mg, 0.92 mmol) was weighted out into a 20 ml vial. Into another vial $N[(CH_2)_3CH_3]_4N_3$ (391 mg, 1.38 mmol) was weighted out. MeCN (1.5 ml; 1 pipette = 1.5 ml) was used to dissolve the $N[(CH_2)_3CH_3]_4N_3$. This MeCN solution was then added to the solid **1** in the 20 ml vial. After that, an additional 3

ml of MeCN were used to wash the vial in which the $N[(CH_2)_3CH_3]_4N_3$ was originally. This solution was also added to the vial with **1**. To ensure that all **1** was dissolved the solution was mixed 'by going up and down in a pipette.' The solution was then overlayered with 9 ml of Et_2O and carefully placed into a refrigerator (T = - 35 °C). After 3 d, the mother liquid was decanted and the remaining black crystalline solid was washed repeatedly by suspending it in Et_2O. The solid was dried by inserting a needle that was connected to vacuum through a rubber septum that was placed headover onto the vial. Yield: 183 mg (0.59 mmol, 65 %). Electronic absorption spectrum in CH_2Cl_2, see Figure 3-18, λ_{max}, nm (ε, M^{-1} cm^{-1}): 244 (15000), 287 (12000), 336 (8700), 470 (1900), 720 (1200). Reduction potential in MeCN: $E_{1/2}$(SCE) = - 545 mV, $E_{1/2}°$ = - 304 mV, and $E_{1/2}$(Fc) = - 945 mV. Magnetic moment: 2.32 μ_B (297 K, solid state). EPR (CH_2Cl_2/Toluene 1/1; 131 K): g = 2.226, 2.155, 1.987 (see Figure 3-17). The other characterization data was identical to that reported in the literature.[89]

Synthesis and Characterization of $[Co(III)(S_2^{Me2}N_3(Pr,Pr))]PF_6$ (2)[100]

Even though the reaction was performed in the glove box, the flask had to be closed with a rubber septum whenever possible since the Co(II) compound is extremely O_2 sensitive. NaOH (440 mg, 11 mmol) was dissolved in a 50 ml sidearm flask in 15 ml of MeOH. Using ~ 3 ml of MeOH, 1.182 g (10 mmol) of 3-mercapto-3-methyl-2-butanone were added. $CoCl_2 \cdot 6\ H_2O$ (1.190 g, 5 mmol) was dissolved in 15 ml of MeOH in a 100 ml sidearm flask. After the Co(II) solution was stirred for 15 min the sodium thiolate solution was added pipettewise to it. The 50 ml flask was washed with MeOH. After stirring for another 15 min, 656 mg of N-(3-aminopropyl)-1,3-propanediamine (5 mmol) were added using 3 ml of

MeOH. The flask was closed with a rubber septum and stirred for 24 h at RT. $Fe(Cp)_2PF_6$ (1.738 g, 5.25 mmol) was then added using 10 ml of MeCN. The flask was closed with a rubber septum and stirred for an additional 24 h at RT. Thereafter, the solution was filtered through Celite (wet with MeCN) on a C frit into a 200 ml sidearm flask. Washing was performed using MeCN. The solution was then pumped to dryness under the hood. The flask was then taken into the glove box, and the solid in it was extracted portionwise with about 120 ml of Et_2O. Between each extraction, the Et_2O was allowed to sit over the solid for at least a few minutes. The solid was dissolved in 20 ml of MeCN and 10 ml of Et_2O were added to the stirring solution. After stirring for 5 min the mixture was filtered through Celite (wet with 2/1 MeCN/Et_2O) on a C frit into a 100 ml sidearm flask. Washing was performed using 2/1 MeCN/Et_2O. The solution was pumped to dryness, and the remaining solid was extracted portionwise with about 50 ml of Et_2O. The remaining solid was dissolved in 12 ml of MeCN, transferred into a 50 ml pearshaped flask, and overlayered with 40 ml of Et_2O. The flask was put into the refrigerator (- 35 °C) for crystallization. After several days the mother liquid was decanted and the remaining black crystalline solid was washed with Et_2O. Yield: 1.28 g (2.4 mmol, 48 %). Electronic absorption spectrum in MeCN, λ_{max}, nm (ε, M^{-1} cm^{-1}): 239 (7600), 358 (5200), 445 (2200), 522 (2100), 797 (50). Elemental analysis, calculated for $C_{16}H_{31}N_3CoF_6PS_2$: C, 36.02; H, 5.86; N, 7.88. Found: C, 35.96; H, 5.72; N, 8.03. The other characterization data was identical to that reported in the literature.[100]

Synthesis and Characterization of

[Co(III)(S^{Me2}(S^{Me2}(O)$_2$)N_3(Pr,Pr))]PF_6 (2-O_2)[100]

All operations were performed on the benchtop. An MeCN (25 ml) solution of **2** was stirred for 3 d exposed to air. Each day the side of the glass was washed to ensure that nothing is above the liquid level and does not react. Upon pumping to dryness, it formed a foam. The remaining residue was dissolved in MeCN (10 ml), transferred into a 50 ml pear-shaped flask, and then overlayered with Et_2O (40 ml). The flask was allowed to stand at RT for crystallization. After several days the mother liquid was decanted. There were black crystals and a red powder. Washing with Et_2O was performed several times so that the red powder was suspended and could be decanted while the black crystals remained in the flask. Visible electronic absorption spectrum in MeCN, λ_{max}, nm (ε, M^{-1} cm^{-1}): 414 (2700), 805 (290). The other characterization data was identical to that reported in the literature.[100]

Synthesis and Characterization of

[Co(III)((η^2-S^{Me2}O)(S^{Me2}(O)$_2$)N_3(Pr,Pr))]PF_6 (2-O_3)[100]

All operations were performed on the benchtop.

Method A. **2-O_2** was dissolved in Me_2CO (15 ml). After H_2O (10 ml) was added, 30 % H_2O_2 (25 ml) was added, and the solution was stirred at RT for 2 h. Thereafter, the solution was poured into culture dishes so that they were half filled. Besides the red solution, there was also a red powder-like solid. This red powder was dissolved in a minimum amount of Me_2CO and added to the culture dishes. Also, any red powder present in the culture dishes was dissolved by using a minimal amount of Me_2CO. It was efficiently dissolved by 'going up and down

with a pipette.' The culture dishes were left to stand in the lab (not under the hood, evaporation is too fast there) for at least 24 h. There were red crystals in a red mother liquid. The mother liquid was decanted, the crystals were washed with H_2O, and then dried under high vacuum. Electronic absorption spectrum in MeCN, λ_{max}, nm (ε, M^{-1} cm^{-1}): 226 (12500), 281 (7100), 338 (9800), 480 (450). Elemental analysis, calculated for $C_{16}H_{31}N_3CoF_6O_3PS_2$: C, 33.05; H, 5.37; N, 7.23. Found: C, 33.18; H, 5.19; N, 7.24. The solubility in MeOH is ~ 15 mg/25 ml. The other characterization data was identical to that reported in the literature.[100]

Method B. Alternatively, **2-O$_3$** can be prepared if **2** is used instead of **2-O$_2$** in a reaction under identical conditions. The product of this reaction is spectroscopically identical to the product of method A.

Table 5-1: Crystallographic data for $[Fe(III)S_2^{Me2}N_3(Pr,Pr)(NO)]PF_6$ (**1-NO**)[58] and $[Fe(III)(S_2^{Me2}N_3(Et,Pr))\text{-}S^{pers}]PF_6$ (**4**).[91]

	1-NO	**4**
formula	$C_{16}H_{31}F_6FeN_4OPS_2$	$C_{15}H_{29}F_6FeN_3PS_3$
molecular mass	560.39	548.42
crystal color, habit	red, cube	red, plate
T (K)	161(2)	161(2)
crystal system	monoclinic	monoclinic
space group	$P2_1/n$ (No. 14)	Cc (No. 9)
a (Å)	12.863(1)	17.9869(6)
b (Å)	14.149(1)	11.8622(2)
c (Å)	13.621(1)	11.3417(4)
α (°)	90	90

β (°)	109.379(1)	110.444(1)
γ (°)	90	90
V (Å^3)	2338.6(3)	2267.5(1)
Z	4	4
$\rho_{calc.}$ (g cm^{-3})	1.586	1.606
μ(Mo Kα) (mm^{-1})	0.955	1.068
Θ range (°)	3 - 28	2 - 31
collected reflections	32521	24625
unique reflections	5011	6001
number of parameters	280	263
GOF[a] on F^2	1.088	1.079
R_1[b] (wR_2[c]) (%)	5.68 (16.56)	3.92 (10.51)
absolu. struc. param.	N/A	0.491(14)

[a] GOF = $\{\Sigma[w(F_o^2 - F_c^2)^2]/(M - N)\}^{1/2}$ (M = number of reflections, N = number of parameters refined). [b] $R_1 = \Sigma||F_o| - |F_c||/\Sigma|F_o|$ for $I > 2\sigma(I)$. [c] $wR_2 = \{\Sigma[w(F_o^2 - F_c^2)^2]/\Sigma[w(F_o^2)^2]\}^{1/2}$ using all data.

Synthesis and Characterization of [Fe(III)($S_2^{Me2}N_3$(Et,Pr))-S^{pers}]PF_6 (4)[91]

Method A. A MeOH solution (30 ml) of NaOH (800 mg, 20 mmol) and 3-mercapto-3-methyl-2-butanone (2.364 g, 20 mmol) was added dropwise to a MeOH solution (40 ml) of $FeCl_2$ (1.266 g, 10 mmol). N-(2-aminoethyl)-1,3-propanediamine (1.172 g, 10 mmol) was added after 15 min of stirring. After the mixture was stirred for 5 h, $Fe(Cp)_2PF_6$ (3.476 g, 10.5 mmol) was added using MeCN (~ 20 ml). After stirring for ~ 60 h, the mixture was evaporated to dryness under vacuum. The residue was extracted with a solution containing Et_2O/MeOH

in a ratio of 2/1 until the liquid phase was weakly red. The residue was dissolved in MeCN and filtered through Celite. After the solution was evaporated to dryness under vacuum, the residue was again extracted with 2/1 Et_2O/MeOH. The remaining residue was dissolved in a solution containing Et_2O/MeCN in a ratio of 1/1 and then filtered through Celite. The solution was again evaporated to dryness and extracted with 2/1 Et_2O/MeOH. The residue was then dissolved in CH_2Cl_2 and filtered through Celite. After the evaporation of the solvent, crystals of **4** were grown by slow diffusion of Et_2O (105 ml) into an MeCN (15 ml) solution at room temperature. The obtained crystals were washed by suspending them several times in Et_2O and dried under vacuum. The crystals obtained in this way were of X-ray quality. Yield: 0.990 g (1.8 mmol, 27 % based on S). Electronic absorption spectrum in MeOH, see Figure 3-6, λ_{max}, nm (ε, M^{-1} cm^{-1}): 211 (15500), 300 (9400), 553 (1950). Elemental analysis, calculated for $C_{15}H_{29}N_3F_6FePS_3$: C, 32.85; H, 5.33; N, 7.66. Found: C, 32.91; H, 5.13; N, 7.62. Reduction potential in MeCN: E(vs. SCE)(irreversible reduction) = - 790 mV, E°= - 549 mV, E(Fc) = - 1190 mV. Magnetic moment: 2.02 μ_B (301 K, MeCN solution) and 2.15 μ_B (300 K, solid state). EPR (MeOH/EtOH 9/1; 141 K): g = 2.165, 2.106, 1.994 (see Figure 3-5). Compound **4** was found to be crystallized in a non-centrosymmetric space group (*Cc*, No. 9) (R = 3.92 %). However, its absolute structure parameter is 0.491(14), which indicates racemic twinning. This means the lattices of both enantiomers are grown into each other. The asymmetric unit contains one complete molecule. The ORTEP, selected structural parameters, and relevant crystallographic information of **4** are shown in Figure 3-3, Table 3-1, and Table 5-1, respectively.

Method B. A MeOH solution (30 ml) of NaOH (800 mg, 20 mmol) and 3-mercapto-3-methyl-2-butanone (2.364 g, 20 mmol) was added dropwise to a

MeOH solution (40 ml) of $FeCl_3$ (1.622 g, 10 mmol). N-(2-aminoethyl)-1,3-propanediamine (1.172 g, 10 mmol)was added after 15 min of stirring. Thereafter, KPF_6 (2.1 g, 11.4 mmol) was added. After the mixture was stirred for ~ 90 h, it was evaporated to dryness under vacuum and worked up as described in method A. Yield: 0.680 g (1.24 mmol, 19 % based on S). This material is spectroscopically identical to the product of method A.

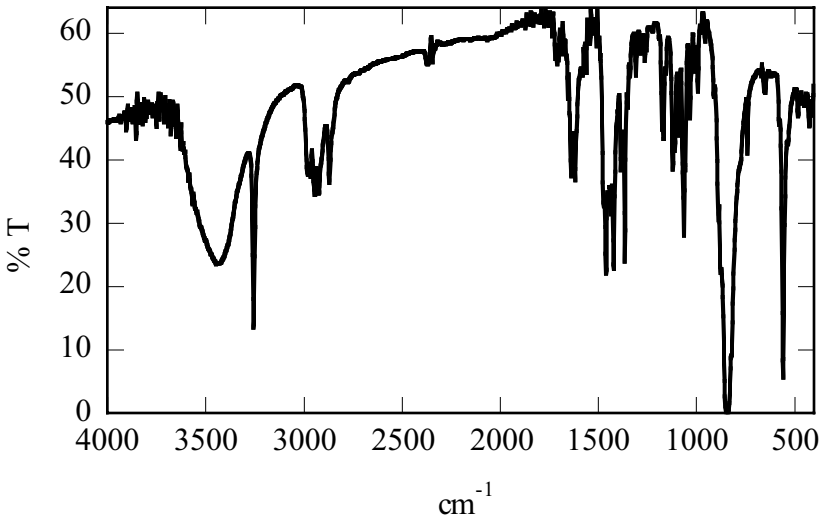

Figure 5-8: IR spectrum (KBr pellet) of **4**.

Synthesis and Characterization of $[Fe(III)S_2^{Me2}N_3(Et,Pr)]PF_6$ (5)[91]

Four equivalents of $P(Et)_3$ (8.0 mmol, 8 ml of a 1.0 M solution in THF) were added to a solution of **4** (1.1 g, 2.0 mmol) in MeCN (~ 25 ml). After the mixture was stirred for 24 h, it was evaporated to dryness under vacuum. The residue was extracted with Et_2O. To remove all of the remaining $SP(Et)_3$, the solid was dissolved in MeCN (~ 10 ml) and added dropwise to the rapidly stirring Et_2O (~ 150 ml). The precipitate was filtered off and washed with Et_2O. Thereafter, the

precipitate was dissolved in CH_2Cl_2 and filtered. After the evaporation of the solvent, crystals of **5** were grown by slow diffusion of Et_2O (105 ml) into a CH_2Cl_2 (15 ml) solution at room temperature. The obtained crystals were washed by suspending them several times in Et_2O and dried under vacuum. Yield: 0.730 g (1.4 mmol, 70 %). ^{31}P NMR was used to verify the absence of any $SP(Et)_3$ [$^{31}P\{^1H\}$ NMR (MeCN): $\delta(SP(Et)_3)$ 57 (s), $\delta(PF_6^-)$ -142 ppm (m)]. Electronic absorption spectrum in MeOH, λ_{max}, nm (ε, M^{-1} cm^{-1}): 207 (15400), 316 (7300), 493 (1530), 532 (1520). The absorptions bands at 316, 493, and 532 nm have the same λ_{max} and ε in MeOH, MeCN, and CH_2Cl_2 as the solvent. Elemental analysis, calculated for $C_{15}H_{29}N_3F_6FePS_2$: C, 34.89; H, 5.66; N, 8.14. Found: C, 34.72; H, 5.50; N, 8.00. Reduction potential in MeCN: $E_{1/2}$(vs. SCE)(reversible) = - 455 mV, $E_{1/2}°$ = - 214 mV, $E_{1/2}$(Fc) = - 855 mV. Magnetic moment: 2.19μ_B (301 K, MeCN solution) and 2.07 μ_B (300 K, solid state). EPR (CH_2Cl_2/Toluene 1/1; 150 K): g = 2.12, 2.07, 2.02 (see Figure 3-11). Crystals for X-ray analysis were obtained by slow diffusion of Et_2O into an MeCN solution at room temperature. Compound **5** was found to be crystallized in a centrosymmetric space group (*Pccn*, No. 56) (R = 4.44 %). Therefore, both enantiomers are present in a 1:1 ratio. In the case of this compound, see Figure 5-9, the cation was located on a two-fold axis going through Fe1 and a point halfway between N2 and N2'. Therefore, the cation was found to be disordered in a way that the ethyl and propyl groups in the ligand backbone occupy the same region of space 50 % of the time. Thus, the cation and its symmetry equivalent molecule are superimposed onto each other in the refinement. Disordered atoms N2, C7, C14, and C15 as well as Fe1 on the two-fold axis were given 0.5 occupancy factors, while atoms C1 - C6, N3, and S2 were given site occupancies of 1. The remaining atoms of the cation are related to these by two-

fold symmetry. One of the symmetry equivalent molecules contains the ligand backbone: C6, C14, C15, N2, C7', and C6'. In this molecule, the H on N2 points towards the reader. The open angle is S2'-Fe1-N2 = 141.8(1)°, while the angle S2-Fe1-N2 is 112.5(1)°. This is the molecule shown in Figure 3-9. In the other symmetry equivalent molecule, the ligand backbone is: C6, C7, N2', C15', C14', and C6'. In this molecule, the H on N2' points away from the reader. The open angle is S2-Fe1-N2' = 141.8(1)°, while the angle S2'-Fe1-N2' is 112.5(1)°. Owing to the imposed two-fold axis, there is half a molecule in the asymmetric unit. The ORTEP, selected structural parameters, and relevant crystallographic information of **5** are shown in Figure 3-9, Table 3-2, and Table 5-2, respectively.

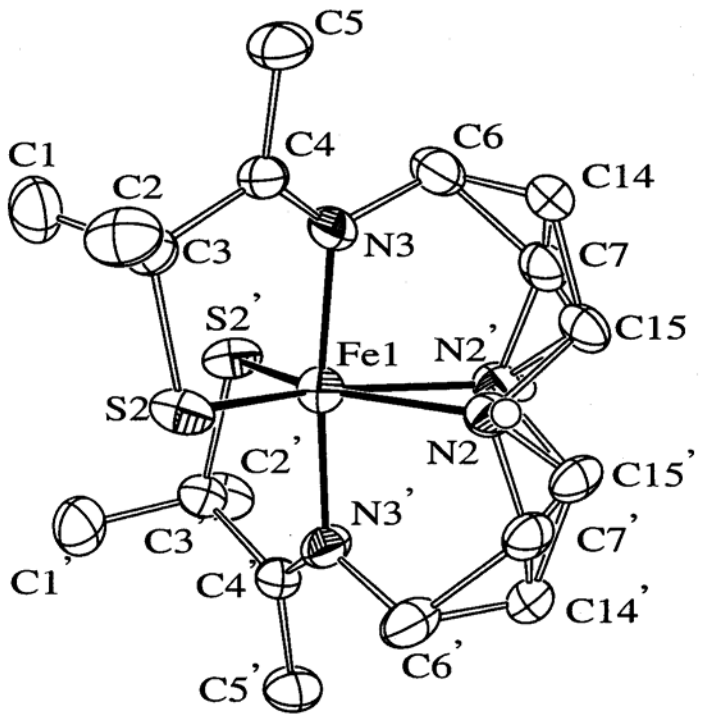

Figure 5-9: Thermal ellipsoid plot (50 % probability level) of the cation of **5**. H atoms, except for the H-N_{amine}, are omitted for clarity. The disorder about the imposed two-fold axis is shown.

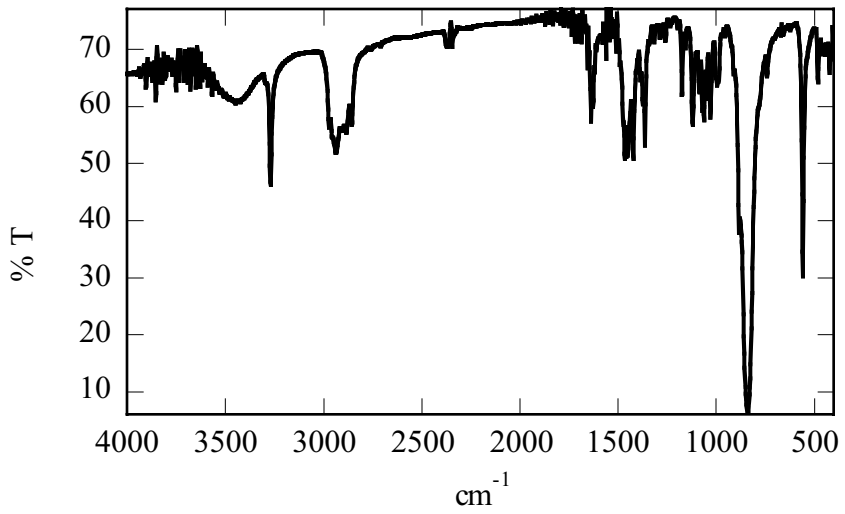

Figure 5-10: IR spectrum (KBr pellet) of **5**.

Table 5-2: Crystallographic data for $[Fe(III)S_2^{Me2}N_3(Et,Pr)]PF_6$ (**5**) and $[Fe(III)S_2^{Me2}N_3(Et,Pr)(N_3)]$ (**5-N$_3$**).[91]

	5	**5-N$_3$**
formula	$C_{15}H_{29}F_6FeN_3PS_2$	$C_{15}H_{29}FeN_6S_2$
molecular mass	516.36	413.42
crystal color, habit	red, plate	red, prism
T (K)	161(2)	161(2)
crystal system	orthorhombic	orthorhombic
space group	*Pccn* (No. 56)	*Pbca* (No. 61)
a (Å)	8.8920(4)	11.0237(2)
b (Å)	13.4838(3)	11.5374(3)
c (Å)	18.3463(8)	30.8031(7)
α (°)	90	90

β (°)	90	90
γ (°)	90	90
V (Å^3)	2199.7(2)	3917.7(2)
Z	4	8
$\rho_{calc.}$ (g cm^{-3})	1.559	1.402
μ(Mo Kα) (mm^{-1})	1.004	0.993
Θ range (°)	3 - 30	3 - 31
collected reflections	42328	64961
unique reflections	3269	5959
number of parameters	182	219
GOF[a] on F^2	0.937	0.954
R_1[b] (wR_2[c]) (%)	4.44 (12.68)	4.27 (10.86)

[a] GOF = $\{\Sigma[w(F_o^2 - F_c^2)^2]/(M - N)\}^{1/2}$ (M = number of reflections, N = number of parameters refined). [b] $R_1 = \Sigma||F_o| - |F_c||/\Sigma|F_o|$ for $I > 2\sigma(I)$. [c] $wR_2 = \{\Sigma[w(F_o^2 - F_c^2)^2]/\Sigma[w(F_o^2)^2]\}^{1/2}$ using all data.

Synthesis and Characterization of [Fe(III)$S_2^{Me2}N_3$(Et,Pr)(N_3)] (5-N_3)[91]

An MeCN solution (25 ml) containing **5** (506 mg, 0.98 mmol) and $N(Me)_4N_3$ (179 mg, 1.54 mmol) was stirred for 30 min. Thereafter, Et_2O (25 ml) was added and the mixture was stirred for another 30 min. Using Et_2O (20 ml), the mixture was then filtered through Celite. After evaporation to dryness, the residue was extracted with THF (20 ml). The THF solution was filtered and overlayered with Et_2O (105 ml). After standing for 4 d at - 35 °C, the mother liquid was decanted. The black crystalline solid was washed several times by suspending it in Et_2O and dried under vacuum. Yield: 0.150 g (0.36 mmol, 37 %). Electronic

absorption spectrum in CH_2Cl_2, see Figure 3-18, λ_{max}, nm (ε, M^{-1} cm^{-1}): 243 (13000), 285 (10000), 335 (7100), 475 (1600), 760 (1000). Elemental analysis, calculated for $C_{15}H_{29}N_6FeS_2$ • 1/3 THF: C, 44.85; H, 7.30; N, 19.21. Found: C, 44.72; H, 7.55; N, 18.98. Reduction potential in MeCN: E(vs. SCE)(irreversible reduction) = - 590 mV, E° = - 349 mV, E(Fc) = - 990 mV. Magnetic moment: 2.46 μ_B (300 K, MeCN solution) and 2.26 μ_B (300 K, solid state). EPR (CH_2Cl_2/Toluene 1/1; 131 K): g = 2.190, 2.162, 1.989 (see Figure 3-17). IR (KBr): $\nu_a(N_3^-)$ = 2031 cm^{-1}. Crystals for X-ray analysis were obtained by slow diffusion at room temperature of Et_2O into an MeCN solution that contained **5** and an excess of $N[(CH_2)_3CH_3]_4N_3$. Compound **5-N$_3$** was found to be crystallized in the centrosymmetric space group *Pbca* (No. 61) (R = 4.27 %). Both the molecule and its mirror image are present in a 1:1 ratio in the crystal lattice. The asymmetric unit contains one complete molecule. The ORTEP, selected structural parameters, and relevant crystallographic information of **5-N$_3$** are shown in Figure 3-15, Table 3-3, and Table 5-2, respectively.

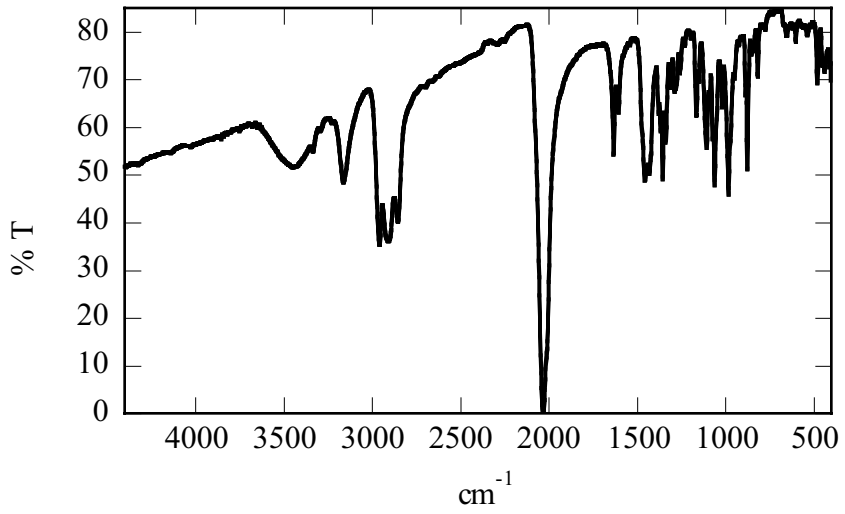

Figure 5-11: IR spectrum (KBr pellet) of **5-N$_3$**.

Synthesis and Characterization of

N,N'-1,2-Ethanediylbis[2-mercapto-2-methyl-propanamide][193]

Into a 250 ml flask equipped with a gas inlet, a 14/20 joint on top, and a 24/40 joint were weighted out 2.6 g (5.85 mmol) of N,N'-1,2-ethanediylbis[2-methyl-2-(phenylmethyl)thio-propanamide].[189] Using the gas inlet, the flask was then flushed with an inert atmosphere (N_2). Then, using an NH_3 condensing apparatus connected to the 14/20 joint, ~ 40 ml of NH_3 were condensed into the flask. During this step a wet piece of Unitest paper was held occasionally to the gas inlet to test for NH_3. During the entire course of the reaction, both the NH_3 condensing apparatus and the 250 ml flask were cooled with acetone/dry ice. Then ~ 0.7 g (30 mmol) of Na were added portionwise through the 24/40 joint, which was otherwise closed with a rubber septum. The mixture was stirred for ~ 45 min while NH_3 was still condensing. During this time a permanent blue color was present.

The NH_3 condensing was stopped and ~ 40 g of powered NH_4Cl were added. Immediately, it became a white suspension. The mixture was stirred under a N_2 stream and open to the atmosphere overnight, during which time all of the NH_3 evaporated. Using ~ 200 ml of acidified H_2O (9/1 H_2O/concentrated HCl) and ~ 100 ml of CH_2Cl_2, all of the white solid was dissolved and transferred into an extraction funnel. After shaking, the phases were separated and the aqueous phase was extracted two more times with each ~ 50 ml of CH_2Cl_2. The combined organic phase was dried over $MgSO_4$ and evaporated to dryness to yield a white powder. Yield: 1.36 g (5.14 mmol, 88 %). Melting point: 133 °C. The ^{1}H NMR spectrum ($CDCl_3$) of N,N'-1,2-Ethanediylbis[2-mercapto-2-methyl-propanamide] contains the following peaks: 1.60 ppm (s) $[CH_2NHCOCSH(C\underline{H}_3)_2]_2$, 2.27 ppm (s) $[CH_2NHCOCS\underline{H}(CH_3)_2]_2$, 3.44 ppm (t) $[C\underline{H}_2NHCOCSH(CH_3)_2]_2$, and 7.35 ppm (s) $[CH_2N\underline{H}COCSH(CH_3)_2]_2$. IR (KBr): ν(CO) = 1641 cm^{-1}.

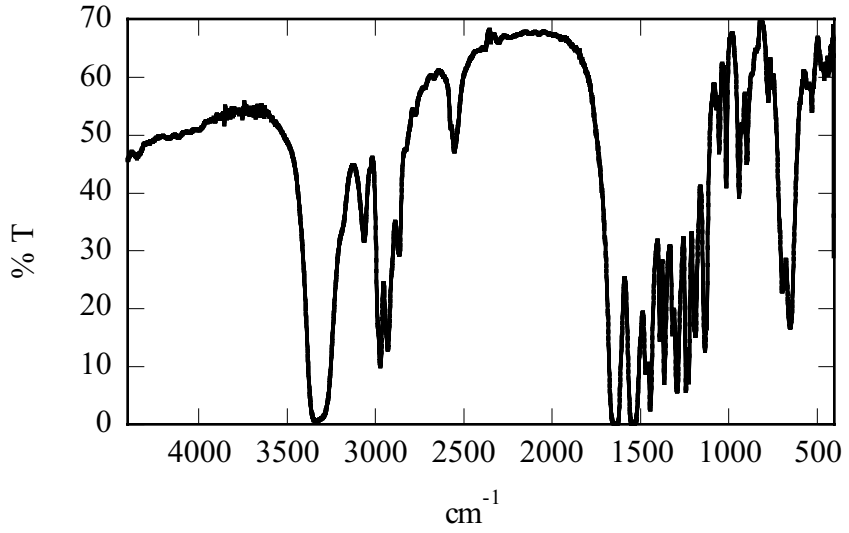

Figure 5-12: IR spectrum (KBr pellet) of N,N'-1,2-ethanediylbis[2-mercapto-2-methyl-propanamide].

Synthesis and Characterization of $(NMe_4)_2[(Fe(III)S_2^{Me2}N_2^{amide}(Et))_2]$ (6)[193]

N,N'-1,2-Ethanediylbis[2-mercapto-2-methyl-propanamide] (400 mg, 1.513 mmol) was dissolved in ~ 10 ml of MeOH in a 50 ml sidearm flask. NaOH (242 mg, 6.052 mmol) was then added using ~ 10 ml of MeOH. While the NaOH was dissolving, a solution of NMe_4FeCl_4 (411 mg, 1.513 mmol) in ~ 15 ml of MeOH in a 100 ml sidearm flask was prepared. Once all NaOH was dissolved, the NaOH/ligand solution was poured all at once into the Fe(III) solution. Washing was performed with MeOH. The color changed immediately to brown. After stirring for 3 h at room temperature, the solution was evaporated to dryness. The residue was extracted with Et_2O. Using ~ 60 ml of MeOH/Et_2O (1/1), the residue was dissolved and filtered through Celite on a C frit into a 100 ml sidearm flask. After evaporation to dryness, the residue was dissolved in MeOH and filtered again through Celite. After removal of the solvent under vacuum, the residue was dissolved and transferred into a 100 ml sidearm flask using 10 ml of MeOH. The solution was overlayered with 110 ml of Et_2O and stored at - 35 °C for several d. After the mother liquid was decanted, the remaining black crystalline solid was washed by suspending it several times in Et_2O and dried under high vacuum. Yield: 0.440 g (0.521 mmol, 69 %). Electronic absorption spectrum in MeOH, see Figure 4-9, λ_{max}, nm (ε, M^{-1} cm^{-1}): 208 (38000), 301 (16400), 420 (5700), 465 (6000). Electronic absorption spectrum in CH_2Cl_2 $\{N[(CH_2)_3CH_3]_4^+$ salt generated by ion exchange with $N[(CH_2)_3CH_3]_4(PF_6)\}$, λ_{max}, nm (ε, M^{-1} cm^{-1}): 232 (22000), 322 (12000), 488 (6500). Elemental analysis, calculated for $C_{28}H_{56}N_6Fe_2O_4S_4$ • 3 MeOH: C, 42.46; H, 7.82; N, 9.58. Found: C, 42.09; H, 7.65; N, 9.51. Reduction potential in MeOH: E(vs. SCE)(irreversible reduction) = - 1.10 V, $E_{1/2}°$ = - 0.86 V,

E(Fc) = - 1.46 V. Magnetic moment: 5.94 μ_B (300 K, solid state). EPR (MeOH/EtOH 9/1; 130 K): g_{max} = 4.28 (see Figure 4-8). IR (KBr): ν(CO) = 1550, 1583 cm^{-1}. Crystals for X-ray analysis were obtained by slow diffusion at room temperature of Et_2O into a MeOH solution. Compound **6** was found to be crystallized in the centrosymmetric space group $P2_1/c$ (No. 14) (R = 6.80 %). Both the molecule and its mirror image are present in a 1:1 ratio in the crystal lattice. The asymmetric unit contains one complete molecule. Also, 2 molecules of MeOH are present in the asymmetric unit. They are H-bonded to the oxygens of the bridging amides. The ORTEP, selected structural parameters, and relevant crystallographic information of **6** are shown in Figure 4-2, Table 4-1, and Table 5-3, respectively.

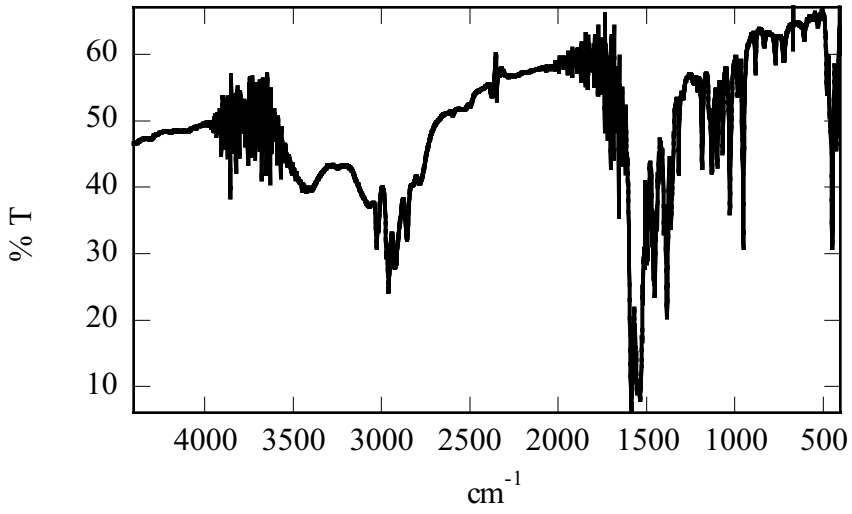

Figure 5-13: IR spectrum (KBr pellet) of **6**.

Table 5-3: Crystallographic data for $(NMe_4)_2[(Fe(III)S_2^{Me2}N_2^{amide}(Et))_2]$ • 2 MeOH (**6** • 2 MeOH) and $(NMe_4)[Fe(III)S_2^{Me2}N_2^{amide}(Et)(Py)]$ • 2 MeOH (**7** • 2 MeOH).[193]

	6 • 2 MeOH	**7** • 2 MeOH
formula	$C_{30}H_{64}Fe_2N_6O_6S_4$	$C_{21}H_{41}FeN_4O_4S_2$
molecular mass	844.83	533.56
crystal color, habit	red, prism	brown, prism
T (K)	161(2)	130(2)
crystal system	monoclinic	monoclinic
space group	$P2_1/c$ (No. 14)	$P2_1/c$ (No. 14)
a (Å)	15.6210(5)	9.0629(3)
b (Å)	11.8659(6)	11.0976(3)
c (Å)	22.8715(10)	26.0129(9)
α (°)	90	90
β (°)	92.556(2)	93.4992(18)
γ (°)	90	90
V (Å^3)	4235.2(3)	2611.4(1)
Z	4	4
$\rho_{calc.}$ (g cm^{-3})	1.237	1.357
μ(Mo Kα) (mm^{-1})	0.596	0.770
Θ range (°)	3 - 21	2 - 25
collected reflections	46010	8596
unique reflections	4412	4448
number of parameters	435	293
GOF[a] on F^2	1.233	0.984

R_1[b] (wR_2[c]) (%)	6.80 (20.96)	4.90 (12.76)

[a] GOF = $\{\Sigma[w(F_o^2 - F_c^2)^2]/(M - N)\}^{1/2}$ (M = number of reflections, N = number of parameters refined). [b] $R_1 = \Sigma||F_o| - |F_c||/\Sigma|F_o|$ for $I > 2\sigma(I)$. [c] $wR_2 = \{\Sigma[w(F_o^2 - F_c^2)^2]/\Sigma[w(F_o^2)^2]\}^{1/2}$ using all data.

Synthesis and Characterization of $(NMe_4)[Fe(III)S_2^{Me2}N_2^{amide}(Et)(Py)]$ (7)[193]

In the glove box, 140 mg of **6** (0.1657 mmol) were dissolved in 15 ml of a 2/1 MeOH/pyridine mixture in a 100 ml sidearm flask. The solution was overlayered with 100 ml of Et_2O and placed into a refrigerator. After standing for several d at - 35 °C, the mother liquid was decanted and the remaining red crystals were washed by suspending them several times in Et_2O and dried under high vacuum. Yield: 0.090 g (0.1687 mmol, 51 %). Electronic absorption spectrum in pyridine in region 300 - 1100 nm, see Figure 4-9, λ_{max}, nm (ε, M^{-1} cm^{-1}): 307 (8000), 425 (2600), 487 (4800). Elemental analysis, calculated for $C_{19}H_{33}FeN_4O_2S_2$ • 1/2 MeOH: C, 48.24; H, 7.27; N, 11.54. Found: C, 47.87; H, 7.15; N, 11.82. Reduction potential in pyridine: $E_{1/2}$(vs. SCE) = - 1.34 V, $E_{1/2}°$ = - 1.10 V, $E_{1/2}$(Fc) = - 1.86 V. Magnetic moment: 4.34 μ_B (300 K, solid state). EPR (MeOH/EtOH 9/1; 130 K): g_{max} = 4.35 (see Figure 4-8). IR (KBr): ν(CO) = 1576 cm^{-1}. The crystals obtained from the crystallization were of X-ray quality. Compound **7** was found to be crystallized in the centrosymmetric space group $P2_1/c$ (No. 14) (R = 4.90 %). Both the molecule and its mirror image are present in a 1:1 ratio in the crystal lattice. The asymmetric unit contains one complete molecule. Also, 2 molecules of MeOH are present in the asymmetric unit. They are H-bonded to the oxygens of the amides. The ORTEP, selected structural parameters, and relevant

crystallographic information of **7** are shown in Figure 4-6, Table 4-1, and Table 5-3, respectively.

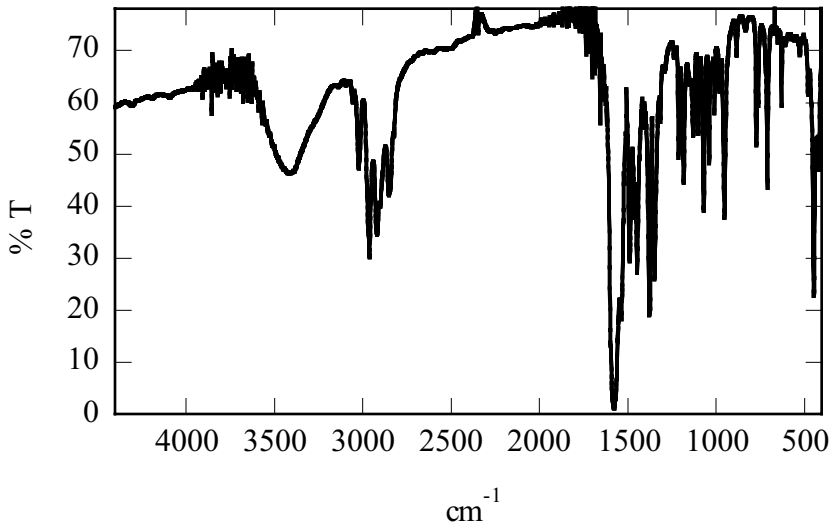

Figure 5-14: IR spectrum (KBr pellet) of **7**.

Chapter VI: Summary and Conclusions

Firstly, it was shown in the present dissertation that small metal complexes with organic ligands can provide valuable insight towards understanding the properties of the active site of a metalloenzyme. The research discussed in Chapter II describes an NO-containing model compound. The striking similarities between the spectroscopic properties of this model compound and the active site of NO-inactivated NHase support the assignment of the active site in NO-inactivated NHase as being $\{FeNO\}^6$. It further shows that a claw arrangement of oxygens is not necessary to stabilize an Fe(III)-NO bond.

Secondly, in Chapter III, it was shown that a small change of the ligand backbone, that is, removal of a methylene unit, can significantly alter the reactivity of the resulting metal complex. A compound was isolated that contains a persulfide ligand coordinated in an η^2 mode to an Fe(III) ion. This compound is the first structurally characterized, first row transition metal η^2-persulfide complex. The Fe(III)-containing, η^2-alkyl persulfide coordinated compound may represent a model for an intermediate in the assembly of Fe-S clusters, since it has been proposed that a cysteine persulfide (thiocysteine, cysteine perthiolate) is involved in their assembly. Upon the removal of the extra persulfide sulfur, a pentacoordinated model compound was generated. A comparison between the reactivity with azide of this pentacoordinated model compound and its analogue containing one more methylene unit in its ligand backboneprovides a model system of how a protein might increase reactivity by holding a metal ion in an entatic state, that is, a distorted geometry. Thereby, it is shown that multidentate ligands can enforce a less stable, distorted coordination geometry. Such a coordination

geometry might not be attainable with monodentate ligands, since they allow the metal ion to arrange the ligands in its preferred coordination geometry.

Thirdly, in Chapter IV, it was shown that the coordination of a deprotonated carboxamide nitrogen to Fe(III) forms a stable structure. The coordinated, deprotonated carboxamide nitrogens provide significant stabilization to the + 3 oxidation state as it is indicated by the reduction potential. A comparison of a pentacoordinated, carboxamide nitrogen-coordinated model compound with a pentacoordinated, imine nitrogen-coordinated model compound provides evidence that an imine group is a valid structural and electronic model for a carboxamide.

Fourthly, it was demonstrated that only Fe(III)-containing model compounds with two cis thiolate sulfur donor atoms in a plane perpendicular to two trans imine nitrogen donor atoms model the electronic properties of Fe-containing NHase well. This similarity can be seen as additional evidence to support the notion that only the sulfone, but not the sulfoxide, modification is present in the active form of NHase.

References

1) Kaim, W. and Schwederski, B.; Bioanorganische Chemie; 1st ed.; B. G. Teubner: Stuttgart, Germany, **1991**.

2) Lippard, S. J. and Berg, J. M.; Principles of Bioinorganic Chemistry; 1st ed.; University Science Books: Mill Valley, CA, U.S.A., **1994**.

3) Endo, I. and Odaka, M.; What Evidences Were Elucidated about Photoreactive Nitrile Hydratase?; *Journal of Molecular Catalysis B: Enzymatic*, **2000**, 10, 81-86.

4) Endo, I.; Nojiri, M.; Tsujimura, M.; Nakasako, M.; Nagashima, S.; Yohda, M.; and Odaka, M.; Fe-Type Nitrile Hydratase; *Journal of Inorganic Biochemistry*, **2001**, 83, 247-253.

5) Coelho, A. V.; Matias, P.; Fulop, V.; Thompson, A.; Gonzalez, A.; and Carrondo, M. A.; Desulfoferrodoxin Structure Determined by MAD Phasing and Refinement to 1.9 Å Resolution Reveals a Unique Combination of a Tetrahedral FeS_4 Centre with a Square Pyramidal $FeSN_4$ Centre; *Journal of Biological Inorganic Chemistry*, **1997**, 2, 680-689.

6) Yeh, A. P.; Hu, Y.; Jenney, F. E., Jr.; Adams, M. W. W.; and Rees, D. C.; Structures of the Superoxide Reductase from *Pyrococcus furiosus* in the Oxidized and Reduced States; *Biochemistry*, **2000**, 39, 2499-2508.

7) Pianzzola, M. J.; Soubes, M.; and Touati, D.; Overproduction of the *rbo* Gene Product from *Desulfovibrio* Species Suppresses All Deleterious Effects of Lack of Superoxide Dismutase in *Escherichia coli*; *Journal of Bacteriology*, **1996**, 178, 6736-6742.

8) Liochev, S. I. and Fridovich, I.; A Mechanism for Complementation of the *sodA sodB* Defect in *Escherichia coli* by Overproduction of the *rbo* Gene Product

(Desulfoferrodoxin) from *Desulfoarculus baarsii*; *Journal of Biological Chemistry*, **1997**, 272, 25573-25575.

9) Lombard, M.; Fontecave, M.; Touati, D.; and Nivière, V.; Reaction of the Desulfoferrodoxin from *Desulfoarculus baarsii* with Superoxide Anion. Evidence for a Superoxide Reductase Activity; *Journal of Biological Chemistry*, **2000**, 275, 115-121.

10) Katayama, Y.; Matsushita, Y.; Kaneko, M.; Kondo, M.; Mizuno, T.; and Nyunoya, H.; Cloning of Genes Coding for The Three Subunits of Thiocyanate Hydrolase of *Thiobacillus thioparus* THI 115 and Their Evolutionary Relationships to Nitrile Hydratase; *Journal of Bacteriology*, **1998**, 180, 2583-2589.

11) Katayama, Y.; Narahara, Y.; Inoue, Y.; Amano, F.; Kanagawa, T.; and Kuraishi, H.; A Thiocyanate Hydrolase of *Thiobacillus thioparus*: A Novel Enzyme Catalyzing The Formation of Carbonyl Sulfide from Thiocyanate; *Journal of Biological Chemistry*, **1992**, 267, 9170-9175.

12) Asano, Y.; Tani, Y.; and Yamada, H.; A New Enzyme "Nitrile Hydratase" Which Degrades Acetonitrile in Combination with Amidase; *Agricultural and Biological Chemistry*, **1980**, 44, 2251-2252.

13) Legras, J. L.; Kaakeh, M. R.; Arnaud, A.; and Galzy, P.; Degradation of Cyanoglucosides by *Brevibacterium sp.* R 312 Strain; *Journal of General and Applied Microbiology*, **1989**, 35, 451-461.

14) Nawaz, M. S.; Chapatwala, K. D.; and Wolfram, J. H.; Degradation of Acetonitrile by *Pseudomonas putida*; *Applied and Environmental Microbiology*, **1989**, 55, 2267-2274.

15) Kobayashi, M.; Suzuki, T.; Fujita, T.; Masuda, M.; and Shimizu, S.; Occurrence of Enzymes Involved in Biosynthesis of Indole-3-Acetic Acid from Indole-3-Acetonitrile in Plant-Associated Bacteria, *Agrobacterium* and *Rhizobium*;

Proceedings of the National Academy of Science of the United States of America, **1995**, 92, 714-718.

16) Sono, M.; Roach, M. P.; Coulter, E. D.; and Dawson, J. H.; Heme-Containing Oxygenases; *Chemical Reviews*, **1996**, 96, 2841-2887.

17) Beyer, H. and Walter, W.; Lehrbuch der Organischen Chemie; 22nd ed.; S. Hirzel Verlag: Stuttgart, Germany, **1991**.

18) Kobayashi, M.; Komeda, H.; Yanaka, N.; Nagasawa, T.; and Yamada, H.; Nitrilase from *Rhodococcus rhodochrous* J1; *The Journal of Biological Chemistry*, **1992**, 267, 20746-20751.

19) Baker, R. T. and Varshavsky, A.; Yeast N-terminal Amidase; *The Journal of Biological Chemistry*, **1995**, 270, 12065-12074.

20) Kobayashi, M.; Goda, M.; and Shimizu, S.; The Catalytic Mechanism of Amidase also Involves Nitrile Hydrolysis; *FEBS Letters*, **1998**, 439, 325-328.

21) Yamada, H. and Kobayashi, M.; Nitrile Hydratase and Its Application to Industrial Production of Acrylamide; *Bioscience, Biotechnology, and Biochemistry*, **1996**, 60, 1391-1400.

22) Wyatt, J. M. and Knowles, C. J.; Microbial Degradation of Acrylonitrile Waste Effluents: the Degradation of Effluents and Condensates from the Manufacture of Acrylonitrile; *International Biodeterioration & Biodegradation*, **1995**, 35, 227-248.

23) Vosáhlová, J.; Pavlu, L.; Vosáhlo, J.; and Brenner, V.; Degradation of Bromoxynil, Ioxynil, Dichlobenil, and Their Mixtures by *Agrobacterium radiobacter* 8/4; *Pesticide Science*, **1997**, 49, 303-306.

24) Meth-Cohn, O. and Wang, M.-X.; An In-Depth Study of the Biotransformation of Nitriles into Amides and/or Acids Using *Rhodococcus rhodochrous* AJ270; *Journal of the Chemical Society, Perkin Transactions I*, **1997**, 1099-1104.

25) Hann, E. C.; Eisenberg, A.; Fager, S. K.; Perkins, N. E.; Gallagher, F. G.; Cooper, S. M.; Gavagan, J. E.; Stieglitz, B.; Hennessey, S. M.; and DiCosimo, R.; 5-Cyanovaleramide Production Using Immobilized *Pseudomonas chlororaphis* B23; *Bioorganic and Medicinal Chemistry*, **1999**, 7, 2239-2245.

26) Bauer, R.; Knackmuss, H.-J.; and Stolz, A.; Enantioselective Hydration of 2-Arylpropionitriles by a Nitrile Hydratase from *Agrobacterium tumefaciens* Strain d3; *Applied Microbiology and Biotechnology*, **1998**, 49, 89-95.

27) Maddrell, S. J.; Turner, N. J.; Kerridge, A.; Willetts, A. J.; and Crosby, J.; Nitrile Hydratase Enzymes in Organic Synthesis: Enantioselective Synthesis of the Lactone Moiety of the Mevinic Acids; *Tetrahedron Letters*, **1996**, 37, 6001-6004.

28) Blakey, A. J.; Colby, J.; Williams, E.; and O'Reilly, C.; Regio- and Stereo-Specific Nitrile Hydrolysis by the Nitrile Hydratase from *Rhodococcus* AJ270; *FEMS Microbiology Letters*, **1995**, 129, 57-62.

29) Nagamune, T.; Kurata, H.; Hirata, M.; Honda, J.; Koike, H.; Ikeuchi, M.; Inoue, Y.; Hirata, A.; and Endo, I.; Purification of Inactivated Photoresponsive Nitrile Hydratase; *Biochemical and Biophysical Research Communications*, **1990**, 168, 437-442.

30) Nagasawa, T.; Ryuno, K.; and Yamada, H.; Nitrile Hydratase of *Brevibacterium* R312; *Biochemical and Biophysical Research Communications*, **1986**, 139, 1305-1312.

31) Bonnet, D.; Artaud, I.; Moali, C.; Pétré, D.; and Mansuy, D.; Highly Efficient Control of Iron-Containing Nitrile Hydratases by Stoichiometric Amounts of Nitric Oxide and Light; *FEBS Letters*, **1997**, 409, 216-220.

32) Nagasawa, T.; Nanba, H.; Ryuno, K.; Takeuchi, K.; and Yamada, H.; Nitrile Hydratase of *Pseudomonas chlororaphis* B23. Purification and Characterization; *European Journal of Biochemistry*, **1987**, 162, 691-698.

33) Nagasawa, T.; Takeuchi, K.; and Yamada, H.; Occurrence of a Cobalt-Induced and Cobalt-Containing Nitrile Hydratase in *Rhodococcus rhodochrous* J1; *Biochemical and Biophysical Research Communications*; **1988**, 155, 1008-1016.

34) Payne, M. S.; Wu, S.; Fallon, R. D.; Tudor, G.; Stieglitz, B.; Turner, I. M., Jr.; and Nelson, M. J.; A Stereoselective Cobalt-Containing Nitrile Hydratase; *Biochemistry*, **1997**, 36, 5447-5454.

35) Ramakrishna, C. and Desai, J. D.; Superiority of Cobalt-Induced Acrylonitrile Hydratase of *Arthrobacter sp.* IPCB-3 for Conversion of Acrylonitrile to Acrylamide; *Biotechnology Letters*, **1993**, 15, 267-270.

36) Nagasawa, T.; Shimizu, H.; and Yamada, H.; The Superiority of the Third-Generation Catalyst, *Rhodococcus rhodochrous* J1 Nitrile Hydratase, for Industrial Production of Acrylamide; *Applied Microbiology and Biotechnology*; **1993**, 40, 189-195.

37) Dufour, É.; Storer, A. C.; and Ménard, R.; Engineering Nitrile Hydratase Activity into a Cysteine Protease by a Single Mutation; *Biochemistry*, **1995**, 34, 16382-16388.

38) Boehlein, S. K.; Rosa-Rodriguez, J. G.; Schuster, S.M.; and Richards, N. G. J.; Catalytic Activity of the N-Terminal Domain of *Escherichia coli* Asparagine Synthetase B Can Be Reengineered by Single-Point Mutation; *Journal of the American Chemical Society*, **1997**, 119, 5785-5791.

39) Maier-Greiner, U. H.; Obermaier-Skrobranek, B. M. M.; Estermaier, L. M.; Kammerloher, W.; Freund, C.; Wülfing, C.; Burkert, U. I.; Matern, D. H.; Breuer, M.; Eulitz, M.; Küfrevioglu, Ö. I.; and Hartmann, G. R.; Isolation and Properties of a Nitrile Hydratase from the Soil Fungus *Myrothecium verrucaria* that is Highly Specific for the Fertilizer Cyanamide and Cloning of its Gene; *Proceedings of the National Academy of Science of the United States of America*; **1991**, 88, 4260-4264.

40) Lee, Y. B.; Goo, Y. M.; Lee, Y. Y.; and Lee, J. K.; Hydrolysis of Various Nitrile Compounds to the Amides by Catalysis of 2-Mercaptoethanol in a Phosphate Buffer; *Tetrahedron Letters*, **1989**, 30, 7439-7440.

41) Huang, W.; Jia, J.; Cummings, J.; Nelson, M.; Schneider, G.; and Lindqvist, Y.; Crystal Structure of Nitrile Hydratase Reveals a Novel Iron Centre in a Novel Fold; *Structure*, **1997**, 5, 691-699.

42) Odaka, M.; Noguchi, T.; Nagashima, S.; Yohda, M.; Yabuki, S.; Hoshino, M.; Inoue, Y.; and Endo, I.; Location ofthe Non-Heme Iron Center on the α Subunit of Photoreactive Nitrile Hydratase from *Rhodococcus* sp. N-771; *Biochemical and Biophysical Research Communications*, **1996**, 221, 146-150.

43) Nelson, M. J.; Jin, H.; Turner, I. M., Jr.; Grove, G.; Scarrow, R. C.; Brennan, B. A.; and Que, L., Jr.; A Novel Iron-Sulfur Center in Nirile Hydratase from *Brevibacterium sp.*; *Journal of the American Chemical Society*, **1991**, 113, 7072-7073.

44) Fallon, R. D.; Stieglitz, B.; and Turner, I., Jr.; A *Pseudomonas putida* Capable of Stereoselective Hydrolysis of Niriles; *Applied Microbiology and Biotechnology*, **1997**, 47, 156-161.

45) Sugiura, Y.; Kuwahara, J.; Nagasawa, T.; and Yamada, H.; Nitrile Hydratase: The First Non-Heme Iron Enzyme with a Typical Low-Spin Fe(III)-Active Center; *Journal of the American Chemical Society*, **1987**, 109, 5848-5850.

46) Miessler, G. L. and Tarr, D. A.; Inorganic Chemistry; 1st ed.; Prentice Hall: Englewood Cliffs, NJ, U.S.A., **1991**.

47) Brennan, B. A.; Cummings, J. G.; Chase, D. B.; Turner, I. M., Jr.; and Nelson, M. J.; Resonance Raman Spectroscopy of Nitrile Hydratase, a Novel Iron-Sulfur Enzyme; *Biochemistry*, **1996**, 35, 10068-10077.

48) Noguchi, T.; Hoshino, M.; Tsujimura, M.; Odaka, M.; Inoue, Y.; and Endo, I.; Resonance Raman Evidence that Photodissociation of Nitric Oxide from the Non-Heme Iron Center Activates Nitrile Hydratase from *Rhodococcus* sp. N-771; *Biochemistry*, **1996**, 35, 16777-16781.

49) Nagasawa, T.; Takeuchi, K.; and Yamada, H.; Characterization of a New Cobalt-Containing Nitrile Hydratase Purified from Urea-Induced Cells of *Rhodococcus rhodochrous* J1; *European Journal of Biochemistry*, **1991**, 196, 581-589.

50) Jin, H.; Turner, I. M., Jr.; Nelson, M. J.; Gurbiel, R. J.; Doan, P. E.; and Hoffman, B. M.; Coordination Sphere of the Ferric Ion in Nitrile Hydratase; *Journal of the American Chemical Society*, **1993**, 115, 5290-5291.

51) Doan, P. E.; Nelson, M. J.; Jin, H.; and Hoffman, B. M.; An Implicit TRIPLE Effect in Mims Pulsed ENDOR: A Sensitive New Technique for Determining Signs of Hyperfine Couplings; *Journal of the American Chemical Society*, **1996**, 118, 7014-7015.

52) Scarrow, R. C.; Brennan, B. A.; Cummings, J. G.; Jin, H.; Duong, D. J.; Kindt, J. T.; and Nelson, M. J.; X-ray Spectroscopy of Nitrile Hydratase at pH 7 and 9; *Biochemistry*, **1996**, 35, 10078-10088.

53) Nelson, M.; The p*K*a of Fe(III)-OH_2 in active Fe-containing NHase is about 7.8, Personal Communication.

54) Nagashima, S.; Nakasako, M.; Dohmae, N.; Tsujimura, M.; Takio, K.; Odaka, M.; Yohda, M.; Kamiya, N.; and Endo, I.; Novel Non-Heme Iron Center of Nitrile Hydratase with a Claw Setting of Oxygen Atoms; *Nature Structural Biology*, **1998**, 5, 347-351.

55) Noguchi, T.; Honda, J.; Nagamune, T.; Sasabe, H.; Inoue, Y.; and Endo, I.; Photosensitive Nitrile Hydratase Intrinsically Possesses Nitric Oxide Bound to the

Non-Heme Iron Center: Evidence by Fourier Transform Infrared Spectroscopy; *FEBS Letters*, **1995**, 358, 9-12.

56) Odaka, M.; Fujii, K.; Hoshino, M.; Noguchi, T.; Tsujimura, M.; Nagashima, S.; Yohda, M.; Nagamune, T.; Inoue, Y.; and Endo, I.; Activity Regulation of Photoreactive Nitrile Hydratase by Nitric Oxide; *Journal of the American Chemical Society*, **1997**, 119, 3785-3791.

57) Scarrow, R. C.; Strickler, B. S.; Ellison, J. J.; Shoner, S. C.; Kovacs, J. A.; Cummings, J. G.; and Nelson, M. J.; X-ray Spectroscopy of Nitric Oxide Binding to Iron in Inactive Nitrile Hydratase and a Synthetic Model Compound; *Journal of the American Chemical Society*, **1998**, 120, 9237-9245.

58) Schweitzer, D.; Ellison, J. J.; Shoner, S. C.; Lovell, S.; and Kovacs, J. A.; A Synthetic Model for the NO-Inactivated Form of Nitrile Hydratase; *Journal of the American Chemical Society*, **1998**, 120, 10996-10997.

59) Piersma, S. R.; Nojiri, M.; Tsujimura, M.; Noguchi, T.; Odaka, M.; Yohda, M.; Inoue, Y.; and Endo, I.; Arginine 56 Mutation in the β Subunit of Nitrile Hydratase: Importance of Hydrogen Bonding to the Non-Heme Iron Center; *Journal of Inorganic Biochemistry*, **2000**, 80, 283-288.

60) Tsujimura, M.; Dohmae, N.; Odaka, M.; Chijimatsu, M.; Takio, K.; Yohda, M.; Hoshino, M.; Nagashima, S.; and Endo, I.; Structure of the Photoreactive Iron Center of the Nitrile Hydratase from *Rhodococcus* sp. N-771. Evidence of a Novel Post-Translational Modification in the Cysteine Ligand; *Journal of Biological Chemistry*, **1997**, 272, 29454-29459.

61) Nojiri, M.; Yohda, M.; Odaka, M.; Matsushita, Y.; Tsujimura, M.; Yoshida, T.; Dohmae, N.; Takio, K.; and Endo, I.; Functional Expression of Nitrile Hydratase in *Escherichia coli*: Requirement of a Nitrile Hydratase Activator and Post-

Translational Modification of a Ligand Cysteine; *Journal of Biochemistry (Tokyo)*, **1999**, 125, 696-704.

62) Nojiri, M.; Nakayama, H.; Odaka, M.; Yohda, M.; Takio, K.; and Endo, I.; Co-Substituted Fe-Type Nitrile Hydratase of *Rhodococcus sp.* N-771; *FEBS Letters*, **2000**, 465, 173-177.

63) Murakami, T.; Nojiri, M.; Nakayama, H.; Odaka, M.; Yohda, M.; Dohmae, N.; Takio, K.; Nagamune, T.; and Endo, I.; Post-Translational Modification is Essential for Catalytic Activity of Nitrile Hydratase; *Protein Science*, **2000**, 9, 1024-1030.

64) DeMaster, E. G.; Quast, B. J.; Redfern, B.; and Nagasawa, H. T.; Reaction of Nitric Oxide with the Free Sulfhydryl Group of Human Serum Albumin Yields a Sulfenic Acid and Nitrous Oxide;*Biochemistry*, **1995**, 34, 11494-11499.

65) Brennan, B. A.; Alms, G.; Nelson, M. J.; Durney, L. T.; and Scarrow, R. C.; Nitrile Hydratase from *Rhodococcus rhodochrous* J1 Contains an Non-Corrin Cobalt Ion with Two Sulfur Ligands; *Journal of the American Chemical Society*, **1996**, 118, 9194-9195.

66) Peters, J. W.; Stowell, M. H. B.; Soltis, S. M.; Finnegan, M. G.; Johnson, M. K.; and Rees, D. C.; Redox-Dependent Structural Changes in the Nitrogenase P-Cluster; *Biochemistry*, **1997**, 36, 1181-1187.

67) Noveron, J. C.; Olmstead, M. M.; and Mascharak, P. K.; Effect of Carboxamido N Coordination to Iron on the Redox Potential of Low-Spin Non-Heme Iron Centers with N,S Coordination: Relevance to the Iron Site of Nitrile Hydratase; *Inorganic Chemistry*, **1998**, 37, 1138-1139.

68) Tyler, L. A.; Noveron, J. C.; Olmstead, M. M.; and Mascharak, P. K.; Oxidation of Metal-Bound Thiolato Sulfur Centers in Fe(III) and Co(III) Complexes with Carboxamido Nitrogens andThiolato Sulfurs as Donors: Relevance to the Active Sites of Nitrile Hydratases; *Inorganic Chemistry*, **1999**, 38, 616-617.

69) Marlin, D. S.; Olmstead, M. M.; and Mascharak, P. K.; Carboxamido Nitrogens Are Good Donors for Fe(III): Syntheses, Structures, and Properties of Two Low-Spin Nonmacrocyclic Iron(III) Complexes with Tetracarboxamido-N Coordination; *Inorganic Chemistry*, **1999**, 38, 3258-3260.

70) Artaud, I.; Chatel, S.; Chauvin, A. S.; Bonnet, D.; Kopf, M. A.; and Leduc, P.; Nitrile Hydratase and Related Non-Heme Iron Sulfur Complexes; *Coordination Chemistry Reviews*, **1999**, 190-192, 577-586.

71) Heinrich, L.; Li, Y.; Vaissermann, J.; Chottard, G.; and Chottard, J.-C.; A Pentacoordinated Di-N-Carboxamidodithiolato-O-Sulfinato-Iron(III) Complex Related to the Metal Site of Nitrile Hydratase; *Angewandte Chemie, International Edition in English*, **1999**, 38, 3526-3528.

72) Marlin, D. S. and Mascharak, P. K.; Coordination of Carboxamido Nitrogen to Tervalent Iron: Insight into a New Chapter of Iron Chemistry; *Chemical Society Reviews*, **2000**, 29, 69-74.

73) Marlin, D. S.; Olmstead, M. M.; and Mascharak, P. K.; Chemistry of Iron(III) Complexes of *N*,*N*'-bis(2-hydroxyphenyl)-pyridine-2,6-dicarboxamide: Seven-coordinate Iron(III) Complexes Ligated to Deprotonated Carboxamido Nitrogens; *Inorganica Chimica Acta*, **2000**, 297, 106-114.

74) Noveron, J. C.; Olmstead, M. M.; and Mascharak, P. K.; A Synthetic Analogue of the Active Site of Fe-Containing Nitrile Hydratase with Carboxamido N and Thiolato S as Donors: Synthesis, Structure, and Reactivities; *Journal of the American Chemical Society*, **2001**, 123, 3247-3259.

75) Noveron, J. C.; Olmstead, M. M.; and Mascharak, P. K.; Co(III) Complexes with Carboxamido N and Thiolato S Donor Centers: Models for the Active Site of Co-Containing Nitrile Hydratases; *Journal of the American Chemical Society*, **1999**, 121, 3553-3554.

76) Tyler, L. A.; Noveron, J. C.; Olmstead, M. M.; and Mascharak, P. K.; Co(III) Complexes with Coordinated Carboxamido Nitrogens and Thiolato Sulfurs as Models for Co-Containing Nitrile Hydratase and Their Conversion to the Corresponding Sulfinato Species; *Inorganic Chemistry*, **2000**, 39, 357-362.

77) Chatel, S.; Rat, M.; Dijols, S.; Leduc, P.; Tuchagues, J. P.; Mansuy, D.; and Artaud, I.; Towards Model Complexes of Co-Containing Nitrile Hydratases: Synthesis, Complete Characterization, and Reactivity toward Ligands such as CN^- and NO of the First Square Planar Co(III) Complex with Two Different Carboxamido Nitrogens and Two Thiolato Sulfur Donors; *Journal of Inorganic Biochemistry*, **2000**, 80, 239-246.

78) Rat, M.; Alves de Sousa, R.; Vaissermann, J.; Leduc, P.; Mansuy, D.; and Artaud, I.; Clean Oxidation of Thiolates to Sulfinates in a Four-Coordinate Co(III) Complex with a mixed carboxamido N-thiolato S donor set: Relevance to Nitrile Hydratase; *Journal of Inorganic Biochemistry*, **2001**, 84, 207-213.

79) Kobayashi, M. and Shimizu, S.; Metalloenzyme Nitrile Hydratase: Structure, Regulation, and Application to Biotechnology; *Nature Biotechnology*, **1998**, 16, 733-736.

80) Caulton, K. G.; Acetaldehyde Hydration by Zinc-Hydroxo Complexes: Coordination Number Expansion during Catalysis; Methylation of Zinc-Bound Thiolates: A Model for Cobalamine Independent Methionine Synthase; *Chemtracts - Inorganic Chemistry*, **1999**, 12, 890-894.

81) Doan, P. E.; Gurbiel, R. J.; Cummins, J. C.; Nelson, M. J.; and Hoffman, B. M.; Inhibitor Binding in Nitrile Hydratase. Determining the Geometry of Enzyme-Bound Butyrate Using ENDOR Spectroscopy; *Journal of Inorganic Biochemistry*, **1999**, 74, 116.

82) Buckingham, D. A.; Keene, F. R.; and Sargeson, A. M.; Base Hydrolysis of Coordinated Acetonitrile; *Journal of the American Chemical Society*, **1973**, 95, 5649-5652.

83) Constable, E. C.; Metals and Ligand Reactivity: An Introduction to the Organic Chemistry of Metal Complexes; 2nd ed.; Verlag Chemie: Weinheim, Germany, **1996**.

84) Shoner, S. C.; Barnhart, D.; and Kovacs, J. A.; A Model for the Low-Spin, Non-Heme, Thiolate-Ligated Iron Site of Nitrile Hydratase; *Inorganic Chemistry*, **1995**, 34, 4517-4518.

85) Noveron, J. C.; Herradora, R.; Olmstead, M. M.; and Mascharak, P. K.; Low-Spin Iron(III) Complexes with N,S Coordination: Syntheses, Structures, and Properties of Bis(N-2-mercaptophenyl-2'-pyridylmethyl-eniminato)iron(III) Tetraphenylborate and Bis(N-2-mercapto-2-methyl-propyl-2'-pyridylmethylenimina-to)iron(III) Tetraphenylborate; *Inorganica Chimica Acta*, **1999**, 285, 269-276.

86) Fallon, G. D. and Gatehouse, B. M.; Crystal and Molecular Structure of an Octahedral Iron(III) Complex with a Sulphur-Containing Schiff-Base Ligand: Bis(2-aminoethylthiosalicylideneiminato)iron(III) Chloride; *Journal of the Chemical Society, Dalton Transactions*, **1975**, 1344-1347.

87) Marini, P. J.; Murray, K. S.; and West, B. O.; Iron Complexes of N-Substituted Thiosalicylideneimines. Part 1. Synthesis and Reactions with Oxygen and Carbon Monoxide; *Journal of the Chemical Society, Dalton Transactions*, **1983**, 143-151.

88) Nivorozhkin, A. L.; Uraev, A. I.; Bondarenko, G. I.; Antsyshkina, A. S.; Kurbatov, V. P.; Garnovskii, A. D.; Turta, C. I.; and Brashoveanu, N. D.; Iron Complexes with an N/S Chromophore Relevant to the Active Site of the Hydrolytic Metalloenzyme Nitrile Hydratase; *Chemical Communications*, **1997**, 1711-1712.

89) Ellison, J. J.; Nienstedt, A.; Shoner, S. C.; Barnhart, D.; Cowen, J. A.; and Kovacs, J. A.; Reactivity of Five-Coordinate Models for the Thiolate-Ligated Fe Site of Nitrile Hydratase; *Journal of the American Chemical Society*, **1998**, 120, 5691-5700.

90) Jackson, H. L.; Shoner, S. C.; Rittenberg, D. K.; Cowen, J. A.; Lovell, S.; Barnhart, D.; and Kovacs, J. A.; Probing the Influence of Local Coordination Environment on the Properties of Fe-Type Nitrile Hydratase Model Complexes; *Inorganic Chemistry*, **2001**, 40, 1646-1653.

91) Schweitzer, D.; Shearer, J.; Rittenberg, D. K.; Shoner, S. C.; Ellison, J. J.; Loloee, R.; Lovell, S.; Barnhart, D.; and Kovacs, J. A.; Enhancing Reactivity via Ligand Constraints; Submitted for Publication.

92) Schubert, M. P.; A New Complex of Cobalt and Cysteine and its Behavior with Hydrogen Peroxide; *Journal of the American Chemical Society*, **1933**, 55, 3336-3342.

93) Sloan, C. P. and Krueger, J. H.; Oxidation of Coordinated Cysteine. Formation of Sulfinato- and Sulfenatocobalt(III) Complexes; *Inorganic Chemistry*, **1975**, 14, 1481-1485.

94) Lange, B. A.; Libson, K.; Deutsch, E.; and Elder, R. C.; Synthesis of a S-Bonded Sulfinic Acid Complex of Cobalt(III) by an Oxidative Route. A Structural Trans Effect in (2-Sulfinatoethylamine-*N*,*S*)bis(ethylenediamine)cobalt(III) Perchlorate Nitrate; *Inorganic Chemistry*, **1976**, 15, 2985-2989.

95) Yamanari, K.; Kawamoto, T.; Kushi, Y.; Komorita, T.; and Fuyuhiro, A.; Sulfenato and Sulfinato Complex Formation via Oxidation of *OC*-6-3'2-Bis{2-[(2-pyridylmethyl)amino]ethanethiolato}cobalt(III) (1+) Complex by Molecular Dioxygen; *Bulletin of the Chemical Society of Japan*, **1998**, 71, 2635-2643.

96) Grapperhaus, C. A. and Darensbourg, M. Y.; Oxygen Capture by Sulfur in Nickel Thiolates; *Accounts of Chemical Research*, **1998**, 31, 451-459, and references therein.

97) Mirza, S. A.; Day, R. O.; and Maroney, M. J.; Oxidation of a Dimeric Nickel Thiolate Complex with O_2; *Inorganic Chemistry*, **1996**, 35, 1992-1995, and references therein.

98) Cocker, T. M. and Bachman, R. E.; Isolation and Crystal Structure of a Novel Dinuclear Ni(II) O-Bound Sulfinate from the Oxidation of 2,2'-Bipyridine-1,2-benzenedithiolatonickel(II); *Chemical Communications*, **1999**, 875-876.

99) Adzamli, I. K.; Libson, K.; Lydon, J. D.; Elder, R. C.; and Deutsch, E.; Synthesis, Characterization, and Reactivity of Coordinated Sulfenic Acids; *Inorganic Chemistry*, **1979**, 18, 303-311.

100) Kung, I.; Schweitzer, D.; Shearer, J.; Taylor, W. D.; Jackson, H. L.; Lovell, S.; and Kovacs, J. A.; How Do Oxidized Thiolate Ligands Affect the Electronic and Reactivity Properties of a Nitrile Hydratase Model Compound?; *Journal of the American Chemical Society*, **2000**, 122, 8299-8300.

101) Cornman, C. R.; Stauffer, T. C.; and Boyle, P. D.; Oxidation of a Vanadium(V)-Dithiolate Complex to a Vanadium(V)-η^2,η^2-Disulfenate Complex; *Journal of the American Chemical Society*, **1997**, 119, 5986-5987.

102) Noveron, J.; In comparison, the iron analogue $[Fe(III)(PyPS)(OH)]^{2-}$ is only stable below -20 °C, at which temperature no nitrile hydration was observed, Personal Communication.

103) March, J.; Advanced Organic Chemistry; 4th ed.; John Wiley & Sons: New York, NY, U.S.A., **1992**.

104) Holleman, A. F. and Wiberg, E.; Lehrbuch der Anorganischen Chemie; 34th ed.; Walter de Gruyter: Berlin, Germany, **1995**.

105) Kolthoff, I. M.; Meehan, E. J.; Tsao, M. S.; and Choi, Q. W.; Oxidation of n-Octyl Mercaptan by Ferricyanide in Acetone-Water Solution; *Journal of Physical Chemistry*, **1962**, 66, 1233-1237.

106) Meehan, E. J.; Kolthoff, I. M.; and Kakiuchi, H.; Reaction between Ferricyanide and 2-Mercaptoethanol; *Journal of Physical Chemistry*, **1962**, 66, 1238-1241.

107) Wallace, T. J.; Reactions of Thiols with Metals. II. Low-Temperature Oxidation by Soluble Metal Salts; *Journal of Organic Chemistry*, **1966**, 31, 3071-3074.

108) Surdhar, P. S. and Armstrong, D. A.; Redox Potentials of Some Sulfur-Containing Radicals; *Journal of Physical Chemistry*, **1986**, 90, 5915-5917.

109) Surdhar, P. S. and Armstrong, D. A.; Reduction Potentials and Exchange Reactions of Thiyl Radicals and Disulfide Anion Radicals; *Journal of Physical Chemistry*, **1987**, 91, 6532-6537.

110) Root, M. J.; Adzamli, I. K.; and Deutsch, E.; Intramolecular Redox Decomposition of $[(en)_2Co(SCH_2CH_2NH_2)]^{2+}$ and Related Complexes; *Inorganic Chemistry*, **1981**, 20, 4017-4019.

111) Based upon Mößbauer measurements of compound **1**, which was only once recrystallized, it is estimated that its chemical yield is less than 60 %.

112) Compound **1**, when dissolved in MeOH under N_2, decomposes with an estimated rate of 15 % / 24 h in the dark at room temperature.

113) Xan, J.; Wilson, E. A.; Roberts, L. D.; and Horton, N. H.; The Absorption of Oxygen by Mercaptans in Alkaline Solution; *Journal of the American Chemical Society*, **1941**, 63, 1139-1141.

114) Hagen, K. S.; Reynolds, J. G.; and Holm, R. H.; Definition of Reaction Sequences Resulting in Self-Assembly of $[Fe_4S_4(SR)_4]^{2-}$ Clusters from Simple Reactants; *Journal of the American Chemical Society*, **1981**, 103, 4054-4063.

115) Brand, U. and Vahrenkamp, H.; A New Tridentate N,N,S Ligand and Its Zinc Complexes; *Inorganic Chemistry*, **1995**, 34, 3285-3293.

116) Butler, A. R. and Williams, D. L. H.; The Physiological Role of Nitric Oxide; *Chemical Society Reviews*, **1993**, 233-241.

117) The complete volumes 268 and 269, both **1996**, of *Methods in Enzymology* are dedicated to NO in biological systems.

118) Enemark, J. H. and Feltham, R. D.; Principles of Structure, Bonding, and Reactivity for Metal Nitrosyl Complexes; *Coordination Chemistry Reviews*, **1974**, 13, 339-406.

119) Richter-Addo, G. B. and Legzdins, P.; Metal Nitrosyls; 1st ed.; Oxford University Press: New York, NY, U.S.A., **1992**.

120) Sellmann, D.; Kunstmann, H.; Moll, M.; and Knoch, F.; Transition Metal Complexes with Sulfur Ligands; *Inorganica Chimica Acta*, **1988**, 154, 157-167.

121) Hauser, C.; Glaser, T.; Bill, E.; Weyhermüller, T.; and Wieghardt, K.; The Electronic Structures of an Isostructural Series of Octahedral Nitrosyliron Complexes $\{Fe\text{-}NO\}^{6,7,8}$ Elucidated by Mössbauer Spectroscopy; *Journal of the American Chemical Society*, **2000**, 122, 4352-4365.

122) A search of the Cambridge Structure Database in March of 1998 showed the Fe-NO distance to be 1.671 +/- 0.057 Å and the FeN-O distance to be 1.166 +/- 0.034 Å. In this analysis only terminal FeNO were considered and all Fe oxidation states were included. When this search was limited to $\{FeNO\}^6$ systems, 13 structures were found. Their Fe-NO bond lengths ranged from 1.62 - 1.68 Å, and their mean N-O distance was 1.143 Å.

123) Huynh, B. H.; Unpublished Results.

124) Nagamune, T.; Honda, J.; Kobayashi, Y.; Sasabe, H.; Endo, I.; Ambe, F.; Teratani, Y.; and Hirata, A.; Mössbauer, Electron Paramagnetic Resonance, and Magnetic Susceptibility Studies of Photosensitive Nitrile Hydratase from *Rhodococcus* sp. N-771; *Hyperfine Interactions*, **1992**, 71, 1271-1274.

125) Honda, J.; Teratani, Y.; Kobayashi, Y.; Nagamune, T.; Sasabe, H.; Hirata, A.; Ambe, F.; and Endo, I.; Light-Induced Oxidation of Iron Atoms in a Photosensitive Nitrile Hydratase; *FEBS Letters*, **1992**, 301, 177-180.

126) Drago, R. S.; Physical Methods for Chemists; 2nd ed.; Saunders College Publishing: Ft. Worth, TX, U.S.A., **1992**.

127) Kennepohl, P.; Schweitzer, D.; Jackson, H.; Kovacs, J.; and Solomon, E.; Studies of the Electronic Structure of Nitrile Hydratase Model Compounds; Manuscript in Preparation.

128) Enemark, J.; Personal Communication.

129) Clark, G. R. and Russell, D. R.; Structural Studies of Complexes Containing the Coordinated Methyldisulphido Ligand: The Crystal Structure of $[Os(\eta^2\text{-}S_2CH_3)(CO)_2(P(C_6H_5)_3)_2]ClO_4$ * 1/2 C_6H_6; *Journal of Organometallic Chemistry*, **1979**, 173, 377-387.

130) Leonard, K.; Plute, K.; Haltiwanger, R. C.; and Rakowski DuBois, M.; Reactions of Metal-Disulfur Complexes with Nucleophiles and Electrophiles; *Inorganic Chemistry*, **1979**, 18, 3246-3251.

131) Migot, J.-L.; Sala-Pala, J.; and Guerchais, J.-E.; Niobium Organometallic Chemistry X. Synthesis of New (η^2-Disulfido) Complexes; Comparison of Their Reactivity with that of (η^2-Dioxo) Derivatives; *Journal of Organometallic Chemistry*, **1983**, 243, 427-436.

132) Legzdins, P. and Sánchez, L.; Insertion of Elemental Sulfur into Tungsten-Carbon Bonds; *Journal of the American Chemical Society*, **1985**, 107, 5525-5526.

133) Floriani, C.; Gambarotta, S.; Chiesi-Villa, A.; and Guastini, C.; Reaction of Elemental Sulphur with Bis(pentamethylcyclopentadienyl)-Vanadium Derivatives: Disulphido and μ-Sulphido Complexes. Crystal Structures of $[V(\eta\text{-}C_5Me_5)_2(S_2)]$ and $[V_2(\eta\text{-}C_5Me_5)_2Cl_2(\mu\text{-}S)_2]$; *Journal of the Chemical Society, Dalton Transactions*, **1987**, 2099-2103.

134) Goh, L. Y.; Hambley, T. W.; and Robertson, G. B.; Chemistry of $[CpCr(CO)_3]_2$. Synthesis of $Cp_2Cr_2(CO)_4S$, $Cp_2Cr_2(CO)_4S_2$, and $Cp_2Cr_2(CO)_5S_2$. Crystal Structure and Reactivity of $Cp_2Cr_2(CO)_4S_2$ and $Cp_2Cr_2(CO)_5S_2$; *Organometallics*, **1987**, 6, 1051-1057.

135) Leblanc, J.-C.; Moise, C.; Volpato, F.; Brunner, H.; Gehart, G.; Wachter, J.; and Nuber, B.; Comparative Studies in the $Cp_2M(\eta^2\text{-}S_2)H$ Series (Cp = t-BuC_5H_4, C_5Me_4Et; M = Nb, Ta) on the Reactivity of Hydride and Disulfide Ligands; *Journal of Organometallic Chemistry*, **1995**, 485, 237-242.

136) Song, L.-C.; Hu, Q.-M.; and Qin, X.-D.; Synthesis of $(\eta^5\text{-}R^1C_5H_4)(CO)_2Mo(\eta^2\text{-}S_2R)$ via Reaction of $(\mu\text{-}RS)(\mu\text{-}p\text{-}MeC_6H_4SO_2S)Fe_2(CO)_6$ with Nucleophiles $(\eta^5\text{-}R^1C_5H_4)(CO)_3MoSeNa$. Crystal Structure of $(\eta^5\text{-}MeO_2C\ C_5H_4)(CO)_2Mo(\eta^2\text{-}S_2Bu^t)$; *Journal of Chemical Research, Synopsis*, **1999**, 84-85.

137) Evans, S. V.; Legzdins, P.; Rettig, S. J.; Sánchez, L.; and Trotter, J.; Crystal Structures of Organotungsten Complexes Formed by Sequential Insertion of Elemental Sulfur into Tungsten-Carbon Bonds; *Organometallics*, **1987**, 6, 7-9.

138) Jackson, H. L.; Unpublished Results.

139) Luh, T.-Y. and Ni, Z.-J.; Transition-Metal-Mediated C-S Bond Cleavage Reactions; *Synthesis*, **1990**, 89-103.

140) Morikita, T.; Hirano, M.; Sasaki, A.; and Komiya, S.; C-S, C-H, and N-H Bond Cleavage of Heterocycles by a Zero-Valent Iron Complex, $Fe(N_2)(depe)_2$ [depe = 1,2-Bis(diethylphosphino)ethane]; *Inorganica Chimica Acta*, **1999**, 291, 341-354.

141) Meagher, K. K.; Bocarsly, A. B.; Bernasek, S. L.; and Ramanarayanan, T. A.; Interaction of Neopentylthiol with Clean and Oxygen-Modified Fe(100) Surfaces; *Journal of Physical Chemistry B*, **2000**, 104, 3320-3326.

142) Carvill, B. T. and Thompson, L. T.; Hydrodesulfurization over Model Sulfide Cluster-Derived Catalysts; *Applied Catalysis*, **1991**, 75, 249-265.

143) Cha, M.; Shoner, S. C.; and Kovacs, J. A.; Nickel-Promoted Reductive C-S Bond Cleavage: A Model for the First Step in the Reaction Promoted by Methyl Coenzyme M Reductase; *Inorganic Chemistry*, **1993**, 32, 1860-1863.

144) Mullen, G. E. D.; Went, M. J.; Wocadlo, S.; Powell, A. K.; and Blower, P. J.; Electron Transfer Induced C-S Bond Cleavage in Rhenium and Technetium Thioether Complexes: Structural and Chemical Evidence forπ Back-Donation to C-S σ^* Orbitals; *Angewandte Chemie, International Edition in English*, **1997**, 36, 1205-1207.

145) Ueno, T.; Ueyama, N.; and Nakamura, A.; Fe-S Cluster Formation by C-S Bond Cleavage Reaction of Mononuclear Fe(II) Cysteine-Containing Peptide Complexes; *Journal of Inorganic Biochemistry*, **1997**, 67, 262.

146) Zheng, L.; White, R. H.; Cash, V. L.; and Dean, D. R.; Mechanism for the Desulfurization of L-Cysteine Catalyzed by the *nifS* Gene Product; *Biochemistry*, **1994**, 33, 4714-4720.

147) Zheng, L. and Dean, D. R.; Catalytic Formation of a Nitrogenase Iron-Sulfur Cluster; *Journal of Biological Chemistry*, **1994**, 269, 18723-18726.

148) Flint, D. H.; *Escherichia coli* Contains a Protein That Is Homologous in Function and N-terminal Sequence to the Protein Encoded by the *nifS* Gene of *Azotobacter vinelandii* and That Can Participate in the Synthesis of the Fe-S Cluster of Dihydroxy-acid Dehydratase; *Journal of Biological Chemistry*, **1996**, 271, 16068-16074.

149) Clausen, T.; Kaiser, J. T.; Steegborn, C.; Huber, R.; and Kessler, D.; Crystal Structure of the Cystine C-S Lyase from *Synechocystis*: Stabilization of Cysteine Persulfide for FeS Cluster Biosynthesis; *Proceedings of the National Academy of Science of the United States of America*, **2000**, 97, 3856-3861.

150) Arendsen, A. F.; Hadden, J.; Card, G.; McAlpine, A. S.; Bailey, S.; Zaitsev, V.; Duke, E. H. M.; Lindley, P. F.; Kröckel, M.; Trautwein, A. X.; Feiters, M. C.; Charnock, J. M.; Garner, C. D.; Marritt, S. J.; Thomson, A. J.; Kooter, I. M.; Johnson, M. K.; van den Berg, W. A. M.; van Dongen, W. M. A. M.; and Hagen, W. R.; The "Prismane" Protein Resolved: X-ray Structure at 1.7 Å and Multiple Spectroscopy of Two Novel 4Fe Clusters; *Journal of Biological Inorganic Chemistry*, **1998**, 3, 81-95.

151) Ploegman, J. H.; Drent, G.; Kalk, K. H.; and Hol, W. G. J.; The Structure of Bovine Liver Rhodanese: II. The Active Site in the Sulfur-Substituted and the Sulfur-Free Enzyme; *Journal of Molecular Biology*, **1979**, 127, 149-162.

152) Ramírez, E. C. and Whitaker, J. R.; Cystine Lyases in Plants: A Comprehensive Review; *Journal of Food Biochemistry*, **1998**, 22, 427-440.

153) Pantoliano, M. W.; Whitlow, M.; Wood, J. F.; Dodd, S. W.; Hardman, K. D.; Rollence, M. L.; and Bryan, P. N.; Large Increases in General Stability for Subtilisin BPN' through Incremental Changes in the Free Energy of Unfolding; *Biochemistry*, **1989**, 28, 7205-7213.

154) Kemper, M. A.; Stout, C. D.; Lloyd, S. E. J.; Prasad, G. S.; Fawcett, S.; Armstrong, F. A.; Shen, B.; and Burgess, B. K.; Y13C *Azotobacter vinelandii* Ferredoxin I: A Designed [Fe-S] Ligand Motif Contains a Cysteine Persulfide; *Journal of Biological Chemistry*, **1997**, 272, 15620-15627.

155) Briggs, R. G. and Fee, J. A.; Sulfhydryl Reactivity of Human Erythrocyte Superoxide Dismutase: on the Origin of the Unusual Spectral Properties of the Protein when Prepared by a Procedure utilizing Chloroform and Ethanol for the Precipitation of Hemoglobin; *Biochimica et Biophysica Acta*, **1978**, 537, 100-109.

156) Koch, W. O.; Schünemann, V.; Gerdan, M.; Trautwein, A. X.; and Krüger, H.-J.; Evidence for an Unusual Thermally Induced Low-Spin (S = 1/2) = Intermediate-Spin (S = 3/2) Transition in a Six-Coordinate Iron(III) Complex: Structure and Electronic Properties of a (1,2-Benzenedithiolato)iron(III) Complex Containing *N*,*N*'-Dimethyl-2,11-diaza[3.3](2,6)pyridinophane as Ligand; *Chemistry - A European Journal*, **1998**, 4, 686-691.

157) Govindaswamy, N.; Quarless, D. A., Jr.; and Koch, S. A.; New Amine Trithiolate Tripod Ligand and Its Iron(II) and Iron(III) Complexes; *Journal of the American Chemical Society*, **1995**, 117, 8468-8469.

158) Addison, A. W.; Rao, T. N.; Reedijk, J.; van Rijn, J.; and Verschoor, G. C.; Synthesis, Structure, and Spectroscopic Properties of Copper(II) Compounds containing Nitrogen-Sulfur Donor Ligands; the Crystal and Molecular Structure of Aqua[1,7-bis(*N*-methylbenzimidazol-2'-yl)-2,6-dithiaheptane]copper(II) Perchlorate; *Journal of the Chemical Society, Dalton Transactions*, **1984**, 1349-1356.

159) Jackson, H. L.; Schweitzer, D.; Rittenberg, D. K.; Kaminsky, W.; Shearer, J.; and Kovacs, J. A.; Manuscript in Preparation.

160) Vallee, B. L. and Williams, R. J. P.; Metalloenzymes: The Entatic Nature of their Active Sites; *Proceedings of the National Academy of Science of the United States of America*, **1968**, 59, 498-505.

161) Williams, R. J. P.; Energised (Entatic) States of Groups and of Secondary Structures in Proteins and Metalloproteins; *European Journal of Biochemistry*, **1995**, 234, 363-381.

162) Lumry, R. and Eyring, H.; Conformation Changes of Proteins; *Journal of Physical Chemistry*, **1954**, 58, 110-120.

163) Malmström, B. G.; Rack-Induced Bonding in Blue-Copper Proteins; *European Journal of Biochemistry*, **1994**, 223, 711-718.

164) Gray, H. B.; Malmström, B. G.; and Williams, R. J. P.; Copper Coordination in Blue Proteins; *Journal of Biological Inorganic Chemistry*, **2000**, 5, 551-559 and references therein.

165) Kirby, A. J.; Mechanism and Stereoelectronic Effects in the Lysozyme Reaction; *CRC Critical Reviews in Biochemistry*, **1987**, 22, 283-315.

166) Balamurugan, R.; Palaniandavar, M.; and Gopalan, R. S.; Trigonal Planar Copper(I) Complex: Synthesis, Structure, and Spectra of a Redox Pair of Novel Copper(II/I) Complexes of Tridentate Bis(benzimidazol-2'-yl) Ligand Framework as Models for Electron-Transfer Copper Proteins; *Inorganic Chemistry*, **2001**, 40, 2246-2255.

167) Comba, P.; Coordination Compounds in the Entatic State; *Coordination Chemistry Reviews*, **2000**, 200-202, 217-245.

168) Börzel, H.; Comba, P.; Hagen, K. S.; Katsichtis, C.; and Pritzkow, H.; A Copper(I) Oxygenation Precursor in the Entatic State: Two Isomers of a Copper(I) Compound of a Rigid Tetradentate Ligand; *Chemistry - A European Journal*, **2000**, 6, 914-919.

169) White, D. J.; Cronin, L.; Parsons, S.; Robertson, N.; Tasker, P. A.; and Bisson, A. P.; Control of Copper(II) Coordination Geometry via Supramolecular Assembly of Ligands in the Solid State; *Chemical Communications*, **1999**, 1107-1108.

170) Warzeska, S. and Krämer, R.; A Dicopper(II) Complex of a New Octaaza Macrocycle: A Receptor in the Entatic State; *Chemical Communications*, **1996**, 499-500.

171) Vogler, C.; Kaim, W.; and Hausen, H.-D.; Zweikernige Bisphosphankupfer(I)-Komplexe mit dem 2,2'-Bipyrimidin-Brückenliganden: Strukturelle Analogie zu "Blauen" Kupferzentren und Reduktion zu Paramagnetischen Spezies; *Zeitschrift für Naturforschung B: A Journal of Chemical Sciences*, **1993**, 48b, 1470-1480.

172) Timmons, J. H.; Martin, J. W. L.; Martell, A. E.; Rudolf, P. R.; and Clearfield, A.; Crystal and Molecular Structure of (5,5,8,8,13,13,16,16-Octamethyl-1,4,9,12-tetraazacyclohexadeca-1,3,9,11-tetraene)copper(I) Perchlorate. A Model for the Entatic State in Blue Copper Proteins; *Inorganic Chemistry*, **1988**, 27, 1638-1640.

173) Lyon, E. J.; Georgakaki, I. P.; Reibenspies, J. H.; and Darensbourg, M. Y.; Coordination Sphere Flexibility of Active Site Models for Fe-Only Hydrogenase: Studies in Intra- and Intermolecular Diatomic Ligand Exchange; *Journal of the American Chemical Society*, **2001**, 123, 3268-3278.

174) Rowland, J. M.; Thornton, M. L.; Olmstead, M. M.; and Mascharak, P. K.; Structure Variation Due to Ligand Flexibility: Synthesesand Structures of the Copper(II) Complexes [Cu(APPy)] and [$Cu_2(AEPy)_2$] Where $APPyH_2$ = Bis[3-(2-pyridinecarboxamido)propyl]-methylamine and $AEPyH_2$ = Bis[3-(2-pyridine-carboxamido)ethyl]-methylamine; *Inorganic Chemistry*, **2001**, 40, 1069-1073.

175) Hubin, T. J.; McCormick, J. M.; Alcock, N. W.; and Busch, D. H.; Topologically Constrained Manganese(III) and Iron(III) Complexes of Two Cross-Bridged Tetraazamacrocycles; *Inorganic Chemistry*, **2001**, 40, 435-444.

176) Chavez, F. A.; Que, L., Jr.; and Tolman, W. B.; Metal Ion Complexation by a New, Highly Sterically Hindered, Bowl-Shaped Carboxylate Ligand; *Chemical Communications*, **2001**, 111-112.

177) Jo, D.-H. and Que, L., Jr.; Tuning the Regiospecificity of Cleavage in Fe(III) Catecholate Complexes: Tridentate Facial versus Meridional Ligands; *Angewandte Chemie, International Edition in English*, **2000**, 39, 4284-4287.

178) Mahadevan, V.; Henson, M. J.; Solomon, E. I.; and Stack, T. D. P.; Differential Reactivity between Interconvertible Side-On Peroxo and Bis-μ-oxodicopper Isomers Using Peralkylated Diamine Ligands; *Journal of the American Chemical Society*, **2000**, 122, 10249-10250.

179) Hagadorn, J. R.; Que, L., Jr.; and Tolman, W. B.; N-Donor Effects on Carboxylate Binding in Mononuclear Iron(II) Complexes of a Sterically Hindered Benzoate Ligand; *Inorganic Chemistry*, **2000**, 39, 6086-6090.

180) Liang, H.-C.; Karlin, K. D.; Dyson, R.; Kaderli, S.; Jung, B.; and Zuberbühler, A. D.; Dioxygen-Binding Kinetics and Thermodynamics of a Series of Dicopper(I) Complexes with Bis[2-(2-pyridyl)ethyl]amine Tridentate Chelators Forming Side-On Peroxo-Bridged Dicopper(II) Adducts; *Inorganic Chemistry*, **2000**, 39, 5884-5894.

181) Lam, B. M. T.; Halfen, J. A.; Young, V. G., Jr.; Hagadorn, J. R.; Holland, P. L.; Lledós, A.; Cucurull-Sánchez, L.; Novoa, J. J.; Alvarez, S.; and Tolman, W. B.; Ligand Macrocycle Structural Effects on Copper-Dioxygen Reactivity; *Inorganic Chemistry*, **2000**, 39, 4059-4072.

182) Gormley, F. K.; Gronbach, J.; Draper, S. M.; and Davis, A. P.; Benzylic Oligothioethers as Ditopic Ligands for Group 6 Transition Metal Carbonyls; *Journal of the Chemical Society, Dalton Transactions*, **2000**, 173-179.

183) Käpplinger, I.; Keutel, H.; and Jäger, E.-G.; Iron(II/III) Complexes of Non-Porphyrin Macrocyclic $[N_4]^{2-}$ Ligands: Structure and Axial Reactivity; *Inorganica Chimica Acta*, **1999**, 291, 190-206.

184) Constable, E. C.; Baum, G.; Bill, E.; Dyson, R.; van Eldik, R.; Fenske, D.; Kaderli, S.; Morris, D.; Neubrand, A.; Neuburger, M.; Smith, D. R.; Wieghardt, K.; Zehnder, M.; and Zuberbühler, A. D.; Control of Iron(II) Spin States in 2,2':6',2"-Terpyridine Complexes through Ligand Substitution; *Chemistry - A European Journal*, **1999**, 5, 498-508.

185) Schneider, J. L.; Carrier, S. M.; Ruggiero,C. E.; Young, V. G., Jr.; and Tolman, W. B.; Influences of Ligand Environment on the Spectroscopic Properties and Disproportionation Reactivity of Copper-Nitrosyl Complexes; *Journal of the American Chemical Society*, **1998**, 120, 11408-11418.

186) Jäger, E.-G.; Schuhmann, K.; and Görls, H.; Steric Effects on Base Adduct Formation and Crystal Structures of Diastereomers of a Nickel(II) Schiff Base Complex; *Chemische Berichte / Recueil*, **1997**, 130, 1643-1646.

187) Jäger, E.-G.; Schuhmann, K.; and Görls, H.; Syntheses, Characterization, Redox Behavior and Lewis Acidity of Chiral Nickel(II) and Copper(II) Schiff Base Complexes; *Inorganica Chimica Acta*, **1997**, 255, 295-305.

188) Sorrell, T. N.; Allen, W. E.; and White, P. S.; Sterically Hindered [Tris(imidazolyl)phosphine]copper Complexes: Formation and Reactivity of a Peroxo-Dicopper(II) Adduct and Structure of a Dinuclear Carbonate-Bridged Complex; *Inorganic Chemistry*, **1995**, 34, 952-960.

189) Krüger, H.-J.; Peng, G.; and Holm, R. H.; Low-Potential Nickel(III,II) Complexes: New Systems Based on Tetradentate Amidate-Thiolate Ligands and the Influence of Ligand Structure on Potentials in Relation to the Nickel Site in [NiFe]-Hydrogenases; *Inorganic Chemistry*, **1991**, 30, 734-742.

190) Hung, Y.; Martin, L. Y.; Jackels, S. C.; Tait, A. M.; and Busch, D. H.; Ring Size Effects among Metal Complexes with Macrocyclic Ligands: Synthesis, Stereochemistry, Spectrochemistry, and Electrochemistry of Co(III) Complexes with Unsubstituted, Saturated Tetraaza Macrocycles; *Journal of the American Chemical Society*, **1977**, 99, 4029-4039.

191) Karlin, K. D. and Lippard, S. J.; Sulfur-Bridged Binuclear Iron(II) Complexes: Effect of Ligand Constraints on Their Physical Properties, Reactions with Carbon Monoxide, and Alkyl Isocyanides; *Journal of the American Chemical Society*, **1976**, 98, 6951-6957.

192) At a given temperature and a constant ΔS, a change of K_{eq} by one order of magnitude corresponds to a change of ΔH by 1.35 kcal/mol.

193) Schweitzer, D.; Rittenberg, D. K.; and Kovacs, J. A.; Manuscript in Preparation.

194) Bag, B.; Mondal, N.; Rosair, G.; and Mitra, S.; The First Thermally-Stable Singly Oxo-Bridged Dinuclear Ni(III) Complex; *Chemical Communications*, **2000**, 1729-1730.

195) Smee, J. J.; Goodman, D. C.; Reibenspies, J. H.; and Darensbourg, M. Y.; Models for Terminal Ni(S-Cysteine) Modification in [NiFe]Hydrogenases by Iodoacetamide and Iodoacetate; *European Journal of Inorganic Chemistry*, **1999**, 539-546.

196) Grapperhaus, C. A.; Bellefeuille, J. A.; Reibenspies, J. H.; and Darensbourg, M. Y.; Synthesis and Dimer Cleavage Reactions of the N_2S Thiolate Bridged Dimer $[(mmp\text{-}dach)_2Ni_2]Cl_2$; *Inorganic Chemistry*, **1999**, 38, 3698-3703.

197) Márquez, V. E.; Anacona, J. R.; Hurtado, R. J.; Díaz de Delgado, G.; and Roque, E. M.; Reactivity of a Binuclear Nickel(II) Sulfur Bridged Complex with

Alkylating Agents, Crystal Structure of $[Ni(L)Br(\mu\text{-}Br)]_2$ (L = 2,6-Bis[(benzyl)mercaptomethyl]pyridine); *Polyhedron*, **1999**, 18, 1903-1908.

198) Goodman, D. C.; Tuntulani, T.; Farmer, P. J.; Darensbourg, M. Y.; and Reibenspies, J. H.; Axial Ligation of Diazacyclooctane-Nickel and -Zinc Complexes; *Angewandte Chemie, International Edition in English*, **1993**, 32, 116-119.

199) O'Connor, C. J.; Magnetochemistry - Advances in Theory and Experimentation; *Progress in Inorganic Chemistry*, **1982**, 29, 203-283.

200) Armstrong, W. H. and Lippard, S. J.; Reversible Protonation of the Oxo Bridge in a Hemerythrin Model Compound: Synthesis, Structure, and Properties of (μ-Hydroxo)bis(μ-acetato)-bis[hydrotris(1-pyrazolyl)borato]diiron(III), $[(HB(pz)_3)Fe(OH)(O_2CCH_3)_2Fe(HB(pz)_3)]^+$; *Journal of the American Chemical Society*, **1984**, 106, 4632-4633.

201) Chen, W. H.; Wei, H. H.; Lee, G. H.; and Wang, Y.; Dimeric Iron(III) Complexes with Salicylaldimine Ligands: Structures, Magnetic Properties, and Activity of H_2O_2 Disproportionation; *Polyhedron*, **2001**, 20, 515-521.

202) Kopf, M.-A.; Varech, D.; Tuchagues, J.-P.; Mansuy, D.; and Artaud, I.; New Intermediate-Spin Chloroiron(III) Complex with a Mixed Nitrogen-Sulfur Coordination Sphere; *Journal of the Chemical Society, Dalton Transactions*, **1998**, 991-998.

203) Schweitzer, D.; Taylor, W. D.; and Kovacs, J. A.; Synthetic Models of the Active Site of Nitrile Hydratase; *Journal of Inorganic Biochemistry*, **1999**, 74, 291.

204) Boone, A. J.; Cory, M. G.; Scott, M. J.; Zerner, M. C.; and Richards, N. G. J.; Investigating the Structural and Electronic Properties of Nitrile Hydratase Model Iron(III) Complexes Using Projected Unrestricted Hartree-Fock (PUHF) Calculations; *Inorganic Chemistry*, **2001**, 40, 1837-1845.

205) Chemical Rubber Company Handbook of Chemistry and Physics; 70th ed.; CRC Press: Boca Raton, FL, U.S.A., **1990**.

206) Gritzner, G. and Kuta, J.; Recommendations on Reporting Electrode Potentials in Nonaqueous Solvents; *Pure & Applied Chemistry*, **1984**, 56, 461-466.

207) Altomare, A.; Cascarano, G.; Giacovazzo, C.; Burla, M. C.; Polidori, G.; and Camalli, M.; SIR; *Journal of Applied Crystallography*, **1994**, 27, 435-442.

208) Sheldrick, G. M.; SHELXL97, A Program for the Refinement of Crystal Structures. University of Göttingen, Germany.

209) Quickenden, T. I. and Marshall, R. C.; Magnetochemistry in SI Units; *Journal of Chemical Education*, **1972**, 49, 114-116.

210) Crooks, J. E.; B or H? A Chemist's Guide to Modern Teachings on Magnetism; *Journal of Chemical Education*, **1979**, 56, 301-303.

211) Mulay, L. N. and Boudreaux, E. A.; Theory and Applications of Molecular Diamagnetism; 1st ed.; John Wiley & Sons: New York, NY, U.S.A.,**1976**.

212) Schubert, E. M.; Utilizing the Evans Method with a Superconducting NMR Spectrometer; *Journal of Chemical Education*, **1992**, 69, 62.

213) Grant, D. H.; Paramagnetic Susceptibility by NMR; *Journal of Chemical Education*, **1995**, 72, 39-40.

214) Van Geet, A. L.; Calibration of the Methanol and Glycol Nuclear Magnetic Resonance Thermometers with a Static Thermistor Probe; *Analytical Chemistry*, **1968**, 40, 2227-2229.

215) Sun, T. F.; Schouten, J. A.; Trappeniers, N. J.; and Biswas, S. N.; Measurements of the Densities of Liquid Benzene, Cyclohexane, Methanol, and Ethanol as Functions of Temperature at 0.1 MPa; *Journal of Chemical Thermodynamics*, **1988**, 20, 1089-1096.

216) Wyman, D. P. and Kaufman, P. R.; The Chlorination of Active Hydrogen Compounds with Sulfuryl Chloride. I. Ketones; *Journal of Organic Chemistry*, **1964**, 29, 1956-1960.

217) Asinger, F.; Thiel, M.; and Esser, G.; Die Herstellung von Thiazolinen-Δ3 durch Gemeinsame Einwirkung von Ammoniak und Oxo-Verbindungen auf α-Mercaptoketone; *Liebigs Annalen der Chemie*, **1957**, 610, 33-49.

218) Greenwood, N. N. and Gibb, T. C.; Mössbauer Spectroscopy; 1st ed.; Chapman & Hall Ltd.: London, U.K., **1971**.

219) Ellison, J. J.; Personal Communication.

220) Carducci, M. D.; Pressprich, M. R.; and Coppens, P.; Diffraction Studies of Photoexcited Crystals: Metastable Nitrosyl-Linkage Isomers of Sodium Nitroprusside; *Journal of the American Chemical Society*, **1997**, 119, 2669-2678.

221) Fomitchev, D. V.; Coppens, P.; Li, T.; Bagley, K. A.; Chen, L.; and Richter-Addo, G. B.; Photo-Induced Metastable Linkage Isomers of Ruthenium Nitrosyl Porphyrins; *Chemical Communications*, **1999**, 2013-2014.

Bibliography

Addison, A. W.; Rao, T. N.; Reedijk, J.; van Rijn, J.; and Verschoor, G. C.; Synthesis, Structure, and Spectroscopic Properties of Copper(II) Compounds containing Nitrogen-Sulfur Donor Ligands; the Crystal and Molecular Structure of Aqua[1,7-bis(*N*-methylbenzimidazol-2'-yl)-2,6-dithiaheptane]copper(II) Perchlorate;*Journal of the Chemical Society, Dalton Transactions*, **1984**, 1349-1356.

Adzamli, I. K.; Libson, K.; Lydon, J. D.; Elder, R. C.; and Deutsch, E.; Synthesis, Characterization, and Reactivity of Coordinated Sulfenic Acids;*Inorganic Chemistry*, **1979**, 18, 303-311.

Altomare, A.; Cascarano, G.; Giacovazzo, C.; Burla, M. C.; Polidori, G.; and Camalli, M.; SIR;*Journal of Applied Crystallography*, **1994**, 27, 435-442.

Arendsen, A. F.; Hadden, J.; Card, G.; McAlpine, A. S.; Bailey, S.; Zaitsev, V.; Duke, E. H. M.; Lindley, P. F.; Kröckel, M.; Trautwein, A. X.; Feiters, M. C.; Charnock, J. M.; Garner, C. D.; Marritt, S. J.; Thomson, A. J.; Kooter, I. M.; Johnson, M. K.; van den Berg, W. A. M.; van Dongen, W. M. A. M.; and Hagen, W. R.; The "Prismane" Protein Resolved: X-ray Structure at 1.7 Å and Multiple Spectroscopy of Two Novel 4Fe Clusters; *Journal of Biological Inorganic Chemistry*, **1998**, 3, 81-95.

Armstrong, W. H. and Lippard, S. J.; Reversible Protonation of the Oxo Bridge in a Hemerythrin Model Compound: Synthesis, Structure, and Properties of (μ-Hydroxo)bis(μ-acetato)-bis[hydrotris(1-pyrazolyl)borato]diiron(III), $[(HB(pz)_3)Fe(OH)(O_2CCH_3)_2Fe(HB(pz)_3)]^+$; *Journal of the American Chemical Society*, **1984**, 106, 4632-4633.

Artaud, I.; Chatel, S.; Chauvin, A. S.; Bonnet, D.; Kopf, M. A.; and Leduc, P.; Nitrile Hydratase and Related Non-Heme Iron Sulfur Complexes; *Coordination Chemistry Reviews*, **1999**, 190-192, 577-586.

Asano, Y.; Tani, Y.; and Yamada, H.; A New Enzyme "Nitrile Hydratase" Which Degrades Acetonitrile in Combination with Amidase;*Agricultural and Biological Chemistry*, **1980**, 44, 2251-2252.

Asinger, F.; Thiel, M.; and Esser, G.; Die Herstellung von Thiazolinen-Δ3 durch Gemeinsame Einwirkung von Ammoniak und Oxo-Verbindungen aufα-Mercaptoketone; *Liebigs Annalen der Chemie*, **1957**, 610, 33-49.

Bag, B.; Mondal, N.; Rosair, G.; and Mitra, S.; The First Thermally-Stable Singly Oxo-Bridged Dinuclear Ni(III) Complex;*Chemical Communications*, **2000**, 1729-1730.

Baker, R. T. and Varshavsky, A.; Yeast N-terminal Amidase;*The Journal of Biological Chemistry*, **1995**, 270, 12065-12074.

Balamurugan, R.; Palaniandavar, M.; and Gopalan, R. S.; Trigonal Planar Copper(I) Complex: Synthesis, Structure, and Spectra of a Redox Pair of Novel Copper(II/I) Complexes of Tridentate Bis(benzimidazol-2'-yl) Ligand Framework as Models for Electron-Transfer Copper Proteins; *Inorganic Chemistry*, **2001**, 40, In Press.

Bauer, R.; Knackmuss, H.-J.; and Stolz, A.; Enantioselective Hydration of 2-Arylpropionitriles by a Nitrile Hydratase from *Agrobacterium tumefaciens* Strain d3; *Applied Microbiology and Biotechnology*, **1998**, 49, 89-95.

Beyer, H. and Walter, W.; Lehrbuch der Organischen Chemie; 22nd ed.; S. Hirzel Verlag: Stuttgart, Germany, **1991**.

Blakey, A. J.; Colby, J.; Williams, E.; and O'Reilly, C.; Regio- and Stereo-Specific Nitrile Hydrolysis by the Nitrile Hydratase from *Rhodococcus* AJ270; *FEMS Microbiology Letters*, **1995**, 129, 57-62.

Boehlein, S. K.; Rosa-Rodriguez, J. G.; Schuster, S. M.; and Richards, N. G. J.; Catalytic Activity of the N-Terminal Domain of *Escherichia coli* Asparagine Synthetase B Can Be Reengineered by Single-Point Mutation; *Journal of the American Chemical Society*, **1997**, 119, 5785-5791.

Bonnet, D.; Artaud, I.; Moali, C.; Pétré, D.; and Mansuy, D.; Highly Efficient Control of Iron-Containing Nitrile Hydratases by Stoichiometric Amounts of Nitric Oxide and Light; *FEBS Letters*, **1997**, 409, 216-220.

Boone, A. J.; Cory, M. G.; Scott, M. J.; Zerner, M. C.; and Richards, N. G. J.; Investigating the Structural and Electronic Properties of Nitrile Hydratase Model Iron(III) Complexes Using Projected Unrestricted Hartree-Fock (PUHF) Calculations; *Inorganic Chemistry*, **2001**, 40, 1837-1845.

Börzel, H.; Comba, P.; Hagen, K. S.; Katsichtis, C.; and Pritzkow, H.; A Copper(I) Oxygenation Precursor in the Entatic State: Two Isomers of a Copper(I) Compound of a Rigid Tetradentate Ligand; *Chemistry - A European Journal*, **2000**, 6, 914-919.

Brand, U. and Vahrenkamp, H.; A New Tridentate N,N,S Ligand and Its Zinc Complexes; *Inorganic Chemistry*, **1995**, 34, 3285-3293.

Brennan, B. A.; Alms, G.; Nelson, M. J.; Durney, L. T.; and Scarrow, R. C.; Nitrile Hydratase from *Rhodococcus rhodochrous* J1 Contains an Non-Corrin Cobalt Ion with Two Sulfur Ligands; *Journal of the American Chemical Society*, **1996**, 118, 9194-9195.

Brennan, B. A.; Cummings, J. G.; Chase, D. B.; Turner, I. M., Jr.; and Nelson, M. J.; Resonance Raman Spectroscopy of Nitrile Hydratase, a Novel Iron-Sulfur Enzyme; *Biochemistry*, **1996**, 35, 10068-10077.

Briggs, R. G. and Fee, J. A.; Sulfhydryl Reactivity of Human Erythrocyte Superoxide Dismutase: on the Origin of the Unusual Spectral Properties of the Protein when Prepared by a Procedure utilizing Chloroform and Ethanol for the Precipitation of Hemoglobin;*Biochimica et Biophysica Acta*, **1978**, 537, 100-109.

Buckingham, D. A.; Keene, F. R.; and Sargeson, A. M.; Base Hydrolysis of Coordinated Acetonitrile;*Journal of the American Chemical Society*, **1973**, 95, 5649-5652.

Butler, A. R. and Williams, D. L. H.; The Physiological Role of Nitric Oxide; *Chemical Society Reviews*, **1993**, 233-241.

Carducci, M. D.; Pressprich, M. R.; and Coppens, P.; Diffraction Studies of Photo-excited Crystals: Metastable Nitrosyl-Linkage Isomers of Sodium Nitro-prusside; *Journal of the American Chemical Society*, **1997**, 119, 2669-2678.

Carvill, B. T. and Thompson, L. T.; Hydrodesulfurization over Model Sulfide Cluster-Derived Catalysts; *Applied Catalysis*, **1991**, 75, 249-265.

Caulton, K. G.; Acetaldehyde Hydration by Zinc-Hydroxo Complexes: Coordination Number Expansion during Catalysis; Methylation of Zinc-Bound Thiolates: A Model for Cobalamine Independent Methionine Synthase; *Chemtracts - Inorganic Chemistry*, **1999**, 12, 890-894.

Cha, M.; Shoner, S. C.; and Kovacs, J. A.; Nickel-Promoted Reductive C-S Bond Cleavage: A Model for the First Step in the Reaction Promoted by Methyl Coenzyme M Reductase; *Inorganic Chemistry*, **1993**, 32, 1860-1863.

Chatel, S.; Rat, M.; Dijols, S.; Leduc, P.; Tuchagues, J. P.; Mansuy, D.; and Artaud, I.; Towards Model Complexes of Co-Containing Nitrile Hydratases: Synthesis, Complete Characterization, and Reactivity toward Ligands such as CN^- and NO of the First Square Planar Co(III) Complex with Two Different Carboxamido Nitrogens and Two Thiolato Sulfur Donors;*Journal of Inorganic Biochemistry*, **2000**, 80, 239-246.

Chavez, F. A.; Que, L., Jr.; and Tolman, W. B.; Metal Ion Complexation by a New, Highly Sterically Hindered, Bowl-Shaped Carboxylate Ligand;*Chemical Communications*, **2001**, 111-112.

Chemical Rubber Company Handbook of Chemistry and Physics; 70th ed.; CRC Press: Boca Raton, FL, U.S.A., **1990**.

Chen, W. H.; Wei, H. H.; Lee, G. H.; and Wang, Y.; Dimeric Iron(III) Complexes with Salicylaldimine Ligands: Structures, Magnetic Properties, and Activity of H_2O_2 Disproportionation; *Polyhedron*, **2001**, 20, 515-521.

Clark, G. R. and Russell, D. R.; Structural Studies of Complexes Containing the Coordinated Methyldisulphido Ligand: The Crystal Structure of $[Os(\eta^2\text{-}S_2CH_3)(CO)_2(P(C_6H_5)_3)_2]ClO_4$ * 1/2 C_6H_6; *Journal of Organometallic Chemistry*, **1979**, 173, 377-387.

Clausen, T.; Kaiser, J. T.; Steegborn, C.; Huber, R.; and Kessler, D.; Crystal Structure of the Cystine C-S Lyase from *Synechocystis*: Stabilization of Cysteine Persulfide for FeS Cluster Biosynthesis;*Proceedings of the National Academy of Science of the United States of America*, **2000**, 97, 3856-3861.

Cocker, T. M. and Bachman, R. E.; Isolation and Crystal Structure of a Novel Dinuclear Ni(II) O-Bound Sulfinate from the Oxidation of 2,2'-Bipyridine-1,2-benzenedithiolatonickel(II); *Chemical Communications*, **1999**, 875-876.

Coelho, A. V.; Matias, P.; Fulop, V.; Thompson, A.; Gonzalez, A.; and Carrondo, M. A.; Desulfoferrodoxin Structure Determined by MAD Phasing and Refinement to 1.9 Å Resolution Reveals a Unique Combination of a Tetrahedral FeS_4 Centre with a Square Pyramidal $FeSN_4$ Centre; *Journal of Biological Inorganic Chemistry*, **1997**, 2, 680-689.

Comba, P.; Coordination Compounds in the Entatic State; *Coordination Chemistry Reviews*, **2000**, 200-202, 217-245.

Constable, E. C.; Baum, G.; Bill, E.; Dyson, R.; van Eldik, R.; Fenske, D.; Kaderli, S.; Morris, D.; Neubrand, A.; Neuburger, M.; Smith, D. R.; Wieghardt, K.; Zehnder, M.; and Zuberbühler, A. D.; Control of Iron(II) Spin States in 2,2':6',2"-Terpyridine Complexes through Ligand Substitution; *Chemistry - A European Journal*, **1999**, 5, 498-508.

Constable, E. C.; Metals and Ligand Reactivity: An Introduction to the Organic Chemistry of Metal Complexes; 2nd ed.; Verlag Chemie: Weinheim, Germany, **1996**.

Cornman, C. R.; Stauffer, T. C.; and Boyle, P. D.; Oxidation of a Vanadium(V)-Dithiolate Complex to a Vanadium(V)-η^2,η^2-Disulfenate Complex; *Journal of the American Chemical Society*, **1997**, 119, 5986-5987.

Crooks, J. E.; B or H? A Chemist's Guide to Modern Teachings on Magnetism; *Journal of Chemical Education*, **1979**, 56, 301-303.

DeMaster, E. G.; Quast, B. J.; Redfern, B.; and Nagasawa, H. T.; Reaction of Nitric Oxide with the Free Sulfhydryl Group of Human Serum Albumin Yields a Sulfenic Acid and Nitrous Oxide; *Biochemistry*, **1995**, 34, 11494-11499.

Doan, P. E.; Gurbiel, R. J.; Cummins, J. C.; Nelson, M. J.; and Hoffman, B. M.; Inhibitor Binding in Nitrile Hydratase. Determining the Geometry of

Enzyme-Bound Butyrate Using ENDOR Spectroscopy; *Journal of Inorganic Biochemistry*, **1999**, 74, 116.

Doan, P. E.; Nelson, M. J.; Jin, H.; and Hoffman, B. M.; An Implicit TRIPLE Effect in Mims Pulsed ENDOR: A Sensitive New Technique for Determining Signs of Hyperfine Couplings;*Journal of the American Chemical Society*, **1996**, 118, 7014-7015.

Drago, R. S.; Physical Methods for Chemists; 2nd ed.; Saunders College Publishing: Ft. Worth, TX, U.S.A., **1992**.

Dufour, É.; Storer, A. C.; and Ménard, R.; Engineering Nitrile Hydratase Activity into a Cysteine Protease by a Single Mutation; *Biochemistry*, **1995**, 34, 16382-16388.

Ellison, J. J.; Nienstedt, A.; Shoner, S. C.; Barnhart, D.; Cowen, J. A.; and Kovacs, J. A.; Reactivity of Five-Coordinate Models for the Thiolate-Ligated Fe Site of Nitrile Hydratase;*Journal of the American Chemical Society*, **1998**, 120, 5691-5700.

Endo, I.; Nojiri, M.; Tsujimura, M.; Nakasako, M.; Nagashima, S.; Yohda, M.; and Odaka, M.; Fe-Type Nitrile Hydratase; *Journal of Inorganic Biochemistry*, **2001**, 83, 247-253.

Endo, I. and Odaka, M.; What Evidences Were Elucidated about Photoreactive Nitrile Hydratase?;*Journal of Molecular Catalysis B: Enzymatic*, **2000**, 10, 81-86.

Enemark, J. H. and Feltham, R. D.; Principles of Structure, Bonding, and Reactivity for Metal Nitrosyl Complexes; *Coordination Chemistry Reviews*, **1974**, 13, 339-406.

Evans, S. V.; Legzdins, P.; Rettig, S. J.; Sánchez, L.; and Trotter, J.; Crystal Structures of Organotungsten Complexes Formed by Sequential Insertion of Elemental Sulfur into Tungsten-Carbon Bonds; *Organometallics*, **1987**, 6, 7-9.

Fallon, G. D. and Gatehouse, B. M.; Crystal and Molecular Structure of an Octahedral Iron(III) Complex with a Sulphur-Containing Schiff-Base Ligand: Bis(2-aminoethylthiosalicylideneiminato)iron(III) Chloride; *Journal of the Chemical Society, Dalton Transactions*, **1975**, 1344-1347.

Fallon, R. D.; Stieglitz, B.; and Turner, I., Jr.; A *Pseudomonas putida* Capable of Stereoselective Hydrolysis of Niriles; *Applied Microbiology and Biotechnology*, **1997**, 47, 156-161.

Flint, D. H.; *Escherichia coli* Contains a Protein That Is Homologous in Function and N-terminal Sequence to the Protein Encoded by the *nifS* Gene of *Azotobacter vinelandii* and That Can Participate in the Synthesis of the Fe-S Cluster of Dihydroxy-acid Dehydratase; *Journal of Biological Chemistry*, **1996**, 271, 16068-16074.

Floriani, C.; Gambarotta, S.; Chiesi-Villa, A.; and Guastini, C.; Reaction of Elemental Sulphur with Bis(pentamethylcyclopentadienyl)-Vanadium Derivatives: Disulphido and μ-Sulphido Complexes. Crystal Structures of $[V(\eta\text{-}C_5Me_5)_2(S_2)]$ and $[V_2(\eta\text{-}C_5Me_5)_2Cl_2(\mu\text{-}S)_2]$; *Journal of the Chemical Society, Dalton Transactions*, **1987**, 2099-2103.

Fomitchev, D. V.; Coppens, P.; Li, T.; Bagley, K. A.; Chen, L.; and Richter-Addo, G. B.; Photo-Induced Metastable Linkage Isomers of Ruthenium Nitrosyl Porphyrins; *Chemical Communications*, **1999**, 2013-2014.

Goh, L. Y.; Hambley, T. W.; and Robertson, G. B.; Chemistry of $[CpCr(CO)_3]_2$. Synthesis of $Cp_2Cr_2(CO)_4S$, $Cp_2Cr_2(CO)_4S_2$, and $Cp_2Cr_2(CO)_5S_2$. Crystal

Structure and Reactivity of $Cp_2Cr_2(CO)_4S_2$ and $Cp_2Cr_2(CO)_5S_2$; *Organometallics*, **1987**, 6, 1051-1057.

Goodman, D. C.; Tuntulani, T.; Farmer, P. J.; Darensbourg, M. Y.; and Reibenspies, J. H.; Axial Ligation of Diazacyclooctane-Nickel and -Zinc Complexes; *Angewandte Chemie, International Edition in English*, **1993**, 32, 116-119.

Gormley, F. K.; Gronbach, J.; Draper, S. M.; and Davis, A. P.; Benzylic Oligothioethers as Ditopic Ligands for Group 6 Transition Metal Carbonyls; *Journal of the Chemical Society, Dalton Transactions*, **2000**, 173-179.

Govindaswamy, N.; Quarless, D. A., Jr.; and Koch, S. A.; New Amine Trithiolate Tripod Ligand and Its Iron(II) and Iron(III) Complexes;*Journal of the American Chemical Society*, **1995**, 117, 8468-8469.

Grant, D. H.; Paramagnetic Susceptibility by NMR; *Journal of Chemical Education*, **1995**, 72, 39-40.

Grapperhaus, C. A. and Darensbourg, M. Y.; Oxygen Capture by Sulfur in Nickel Thiolates; *Accounts of Chemical Research*, **1998**, 31, 451-459.

Grapperhaus, C. A.; Bellefeuille, J. A.; Reibenspies, J. H.; and Darensbourg, M. Y.; Synthesis and Dimer Cleavage Reactions of the N_2S Thiolate Bridged Dimer $[(mmp\text{-}dach)_2Ni_2]Cl_2$; *Inorganic Chemistry*, **1999**, 38, 3698-3703.

Gray, H. B.; Malmström, B. G.; and Williams, R. J. P.; Copper Coordination in Blue Proteins; *Journal of Biological Inorganic Chemistry*, **2000**, 5, 551-559.

Greenwood, N. N. and Gibb, T. C.; Mössbauer Spectroscopy; 1st ed.; Chapman & Hall Ltd.:, **1971**.

Gritzner, G. and Kuta, J.; Recommendations on Reporting Electrode Potentials in Nonaqueous Solvents; *Pure & Applied Chemistry*, **1984**, 56, 461-466.

Hagadorn, J. R.; Que, L., Jr.; and Tolman, W. B.; N-Donor Effects on Carboxylate Binding in Mononuclear Iron(II) Complexes of a Sterically Hindered Benzoate Ligand; *Inorganic Chemistry*, **2000**, 39, 6086-6090.

Hagen, K. S.; Reynolds, J. G.; and Holm, R. H.; Definition of Reaction Sequences Resulting in Self-Assembly of $[Fe_4S_4(SR)_4]^{2-}$ Clusters from Simple Reactants; *Journal of the American Chemical Society*, **1981**, 103, 4054-4063.

Hann, E. C.; Eisenberg, A.; Fager, S. K.; Perkins, N. E.; Gallagher, F. G.; Cooper, S. M.; Gavagan, J. E.; Stieglitz, B.; Hennessey, S. M.; and DiCosimo, R.; 5-Cyanovaleramide Production Using Immobilized*Pseudomonas chloro-raphis* B23; *Bioorganic and Medicinal Chemistry*, **1999**, 7, 2239-2245.

Hauser, C.; Glaser, T.; Bill, E.; Weyhermüller, T.; and Wieghardt, K.; The Electronic Structures of an Isostructural Series of Octahedral Nitrosyliron Complexes $\{Fe\text{-}NO\}^{6,7,8}$ Elucidated by Mössbauer Spectroscopy; *Journal of the American Chemical Society*, **2000**, 122, 4352-4365.

Heinrich, L.; Li, Y.; Vaissermann, J.; Chottard, G.; and Chottard, J.-C.; A Pentacoordinated Di-N-Carboxamidodithiolato-O-Sulfinato-Iron(III) Complex Related to the Metal Site of Nitrile Hydratase; *Angewandte Chemie, International Edition in English*, **1999**, 38, 3526-3528.

Holleman, A. F. and Wiberg, E.; Lehrbuch der Anorganischen Chemie; 34th ed.; Walter de Gruyter: Berlin, Germany, **1995**.

Honda, J.; Teratani, Y.; Kobayashi, Y.; Nagamune, T.; Sasabe, H.; Hirata, A.; Ambe, F.; and Endo, I.; Light-Induced Oxidation of Iron Atoms in a Photosensitive Nitrile Hydratase; *FEBS Letters*, **1992**, 301, 177-180.

Huang, W.; Jia, J.; Cummings, J.; Nelson, M.; Schneider, G.; and Lindqvist, Y.; Crystal Structure of Nitrile Hydratase Reveals a Novel Iron Centre in a Novel Fold; *Structure*, **1997**, 5, 691-699.

Hubin, T. J.; McCormick, J. M.; Alcock, N. W.; and Busch, D. H.; Topologically Constrained Manganese(III) and Iron(III) Complexes of Two Cross-Bridged Tetraazamacrocycles; *Inorganic Chemistry*, **2001**, 40, 435-444.

Hung, Y.; Martin, L. Y.; Jackels, S. C.; Tait, A. M.; and Busch, D. H.; Ring Size Effects among Metal Complexes with Macrocyclic Ligands: Synthesis, Stereochemistry, Spectrochemistry, and Electrochemistry of Co(III) Complexes with Unsubstituted, Saturated Tetraaza Macrocycles; *Journal of the American Chemical Society*, **1977**, 99, 4029-4039.

Jackson, H. L.; Schweitzer, D.; Rittenberg, D. K.; Kaminsky, W.; Shearer, J.; and Kovacs, J. A.; Manuscript in Preparation.

Jackson, H. L.; Shoner, S. C.; Rittenberg, D. K.; Cowen, J. A.; Lovell, S.; Barnhart, D.; and Kovacs, J. A.; Probing the Influence of Local Coordination Environment on the Properties of Fe-Type Nitrile Hydratase Model Complexes; *Inorganic Chemistry*, **2001**, 40, 1646-1653.

Jäger, E.-G.; Schuhmann, K.; and Görls, H.; Steric Effects on Base Adduct Formation and Crystal Structures of Diastereomers of a Nickel(II) Schiff Base Complex; *Chemische Berichte / Recueil*, **1997**, 130, 1643-1646.

Jäger, E.-G.; Schuhmann, K.; and Görls, H.; Syntheses, Characterization, Redox Behavior and Lewis Acidity of Chiral Nickel(II) and Copper(II) Schiff Base Complexes; *Inorganica Chimica Acta*, **1997**, 255, 295-305.

Jin, H.; Turner, I. M., Jr.; Nelson, M. J.; Gurbiel, R. J.; Doan, P. E.; and Hoffman, B. M.; Coordination Sphere of the Ferric Ion in Nitrile Hydratase; *Journal of the American Chemical Society*, **1993**, 115, 5290-5291.

Jo, D.-H. and Que, L., Jr.; Tuning the Regiospecificity of Cleavage in Fe(III) Catecholate Complexes: Tridentate Facial versus Meridional Ligands;*Angewandte Chemie, International Edition in English*, **2000**, 39, 4284-4287.

Kaim, W. and Schwederski, B.; Bioanorganische Chemie; 1st ed.; B. G. Teubner: Stuttgart, Germany, **1991**.

Käpplinger, I.; Keutel, H.; and Jäger, E.-G.; Iron(II/III) Complexes of Non-Porphyrin Macrocyclic $[N_4]^{2-}$ Ligands: Structure and Axial Reactivity; *Inorganica Chimica Acta*, **1999**, 291, 190-206.

Karlin, K. D. and Lippard, S. J.; Sulfur-Bridged Binuclear Iron(II) Complexes: Effect of Ligand Constraints on Their Physical Properties, Reactions with Carbon Monoxide, and Alkyl Isocyanides; *Journal of the American Chemical Society*, **1976**, 98, 6951-6957.

Katayama, Y.; Matsushita, Y.; Kaneko, M.; Kondo, M.; Mizuno, T.; and Nyunoya, H.; Cloning of Genes Coding for The Three Subunits of Thiocyanate Hydrolase of *Thiobacillus thioparus* THI 115 and Their Evolutionary Relationships to Nitrile Hydratase; *Journal of Bacteriology*, **1998**, 180, 2583-2589.

Katayama, Y.; Narahara, Y.; Inoue, Y.; Amano, F.; Kanagawa, T.; and Kuraishi, H.; A Thiocyanate Hydrolase of *Thiobacillus thioparus*: A Novel Enzyme Catalyzing The Formation of Carbonyl Sulfide from Thiocyanate; *Journal of Biological Chemistry*, **1992**, 267, 9170-9175.

Kemper, M. A.; Stout, C. D.; Lloyd, S. E. J.; Prasad, G. S.; Fawcett, S.; Armstrong, F. A.; Shen, B.; and Burgess, B. K.; Y13C *Azotobacter vinelandii* Ferredoxin I: A Designed [Fe-S] Ligand Motif Contains a Cysteine Persulfide; *Journal of Biological Chemistry*, **1997**, 272, 15620-15627.

Kennepohl, P.; Schweitzer, D.; Jackson, H.; Kovacs, J.; and Solomon, E.; Studies of the Electronic Structure of Nitrile Hydratase Model Compounds; Manuscript in Preparation.

Kirby, A. J.; Mechanism and Stereoelectronic Effects in the Lysozyme Reaction; *CRC Critical Reviews in Biochemistry*, **1987**, 22, 283-315.

Kobayashi, M. and Shimizu, S.; Metalloenzyme Nitrile Hydratase: Structure, Regulation, and Application to Biotechnology; *Nature Biotechnology*, **1998**, 16, 733-736.

Kobayashi, M.; Goda, M.; and Shimizu, S.; The Catalytic Mechanism of Amidase also Involves Nitrile Hydrolysis; *FEBS Letters*, **1998**, 439, 325-328.

Kobayashi, M.; Komeda, H.; Yanaka, N.; Nagasawa, T.; and Yamada, H.; Nitrilase from *Rhodococcus rhodochrous* J1; *The Journal of Biological Chemistry*, **1992**, 267, 20746-20751.

Kobayashi, M.; Suzuki, T.; Fujita, T.; Masuda, M.; and Shimizu, S.; Occurrence of Enzymes Involved in Biosynthesis of Indole-3-Acetic Acid from Indole-3-Acetonitrile in Plant-Associated Bacteria, *Agrobacterium* and *Rhizobium*; *Proceedings of the National Academy of Science of the United States of America*, **1995**, 92, 714-718.

Koch, W. O.; Schünemann, V.; Gerdan, M.; Trautwein, A. X.; and Krüger, H.-J.; Evidence for an Unusual Thermally Induced Low-Spin (S = 1/2) = Intermediate-Spin (S = 3/2) Transition in a Six-Coordinate Iron(III) Complex: Structure and Electronic Properties of a (1,2-Benzenedithiolato)iron(III) Complex Containing *N*,*N*'-Dimethyl-2,11-diaza[3.3](2,6)pyridinophane as Ligand; *Chemistry - A European Journal*, **1998**, 4, 686-691.

Kolthoff, I. M.; Meehan, E. J.; Tsao, M. S.; and Choi, Q. W.; Oxidation of n-Octyl Mercaptan by Ferricyanide in Acetone-Water Solution; *Journal of Physical Chemistry*, **1962**, 66, 1233-1237.

Kopf, M.-A.; Varech, D.; Tuchagues, J.-P.; Mansuy, D.; and Artaud, I.; New Intermediate-Spin Chloroiron(III) Complex with a Mixed Nitrogen-Sulfur

Coordination Sphere; *Journal of the Chemical Society, Dalton Transactions*, **1998**, 991-998.

Krüger, H.-J.; Peng, G.; and Holm, R. H.; Low-Potential Nickel(III,II) Complexes: New Systems Based on Tetradentate Amidate-Thiolate Ligands and the Influence of Ligand Structure on Potentials in Relation to the Nickel Site in [NiFe]-Hydrogenases; *Inorganic Chemistry*, **1991**, 30, 734-742.

Kung, I.; Schweitzer, D.; Shearer, J.; Taylor, W. D.; Jackson, H. L.; Lovell, S.; and Kovacs, J. A.; How Do Oxidized Thiolate Ligands Affect the Electronic and Reactivity Properties of a Nitrile Hydratase Model Compound?; *Journal of the American Chemical Society*, **2000**, 122, 8299-8300.

Lam, B. M. T.; Halfen, J. A.; Young, V. G., Jr.; Hagadorn, J. R.; Holland, P. L.; Lledós, A.; Cucurull-Sánchez, L.; Novoa, J. J.; Alvarez, S.; and Tolman, W. B.; Ligand Macrocycle Structural Effects on Copper-Dioxygen Reactivity; *Inorganic Chemistry*, **2000**, 39, 4059-4072.

Lange, B. A.; Libson, K.; Deutsch, E.; and Elder, R. C.; Synthesis of a S-Bonded Sulfinic Acid Complex of Cobalt(III) by an Oxidative Route. A Structural Trans Effect in (2-Sulfinatoethylamine-*N*,*S*)bis(ethylenediamine)cobalt(III) Perchlorate Nitrate; *Inorganic Chemistry*, **1976**, 15, 2985-2989.

Leblanc, J.-C.; Moise, C.; Volpato, F.; Brunner, H.; Gehart, G.; Wachter, J.; and Nuber, B.; Comparative Studies in the $Cp_2M(\eta^2\text{-}S_2)H$ Series (Cp = t-Bu-C_5H_4, C_5Me_4Et; M = Nb, Ta) on the Reactivity of Hydride and Disulfide Ligands; *Journal of Organometallic Chemistry*, **1995**, 485, 237-242.

Lee, Y. B.; Goo, Y. M.; Lee, Y. Y.; and Lee, J. K.; Hydrolysis of Various Nitrile Compounds to the Amides by Catalysis of 2-Mercaptoethanol in a Phosphate Buffer; *Tetrahedron Letters*, **1989**, 30, 7439-7440.

Legras, J. L.; Kaakeh, M. R.; Arnaud, A.; and Galzy, P.; Degradation of Cyanoglucosides by *Brevibacterium sp.* R 312 Strain; *Journal of General and Applied Microbiology*, **1989**, 35, 451-461.

Legzdins, P. and Sánchez, L.; Insertion of Elemental Sulfur into Tungsten-Carbon Bonds; *Journal of the American Chemical Society*; **1985**, 107, 5525-5526.

Leonard, K.; Plute, K.; Haltiwanger, R. C.; and Rakowski DuBois, M.; Reactions of Metal-Disulfur Complexes with Nucleophiles and Electrophiles; *Inorganic Chemistry*, **1979**, 18, 3246-3251.

Liang, H.-C.; Karlin, K. D.; Dyson, R.; Kaderli, S.; Jung, B.; and Zuberbühler, A. D.; Dioxygen-Binding Kinetics and Thermodynamics of a Series of Dicopper(I) Complexes with Bis[2-(2-pyridyl)ethyl]amine Tridentate Chelators Forming Side-On Peroxo-Bridged Dicopper(II) Adducts; *Inorganic Chemistry*, **2000**, 39, 5884-5894.

Liochev, S. I. and Fridovich, I.; A Mechanism for Complementation of the *sodA sodB* Defect in *Escherichia coli* by Overproduction of the *rbo* Gene Product (Desulfoferrodoxin) from *Desulfoarculus baarsii*; *Journal of Biological Chemistry*, **1997**, 272, 25573-25575.

Lippard, S. J. and Berg, J. M.; Principles of Bioinorganic Chemistry; 1st ed.; University Science Books: Mill Valley, CA, U.S.A., **1994**.

Lombard, M.; Fontecave, M.; Touati, D.; and Nivière, V.; Reaction of the Desulfoferrodoxin from *Desulfoarculus baarsii* with Superoxide Anion. Evidence for a Superoxide Reductase Activity; *Journal of Biological Chemistry*, **2000**, 275, 115-121.

Luh, T.-Y. and Ni, Z.-J.; Transition-Metal-Mediated C-S Bond Cleavage Reactions; *Synthesis*, **1990**, 89-103.

Lumry, R. and Eyring, H.; Conformation Changes of Proteins;*Journal of Physical Chemistry*, **1954**, 58, 110-120.

Lyon, E. J.; Georgakaki, I. P.; Reibenspies, J. H.; and Darensbourg, M. Y.; Coordination Sphere Flexibility of Active Site Models for Fe-Only Hydrogenase: Studies in Intra- and Intermolecular Diatomic Ligand Exchange; *Journal of the American Chemical Society*; **2001**, 123, 3268-3278.

Maddrell, S. J.; Turner, N. J.; Kerridge, A.; Willetts, A. J.; and Crosby, J.; Nitrile Hydratase Enzymes in Organic Synthesis: Enantioselective Synthesis of the Lactone Moiety of the Mevinic Acids; *Tetrahedron Letters*, **1996**, 37, 6001-6004.

Mahadevan, V.; Henson, M. J.; Solomon, E. I.; and Stack, T. D. P.; Differential Reactivity between Interconvertible Side-On Peroxo and Bis-μ-oxodicopper Isomers Using Peralkylated Diamine Ligands;*Journal of the American Chemical Society*, **2000**, 122, 10249-10250.

Maier-Greiner, U. H.; Obermaier-Skrobranek, B. M. M.; Estermaier, L. M.; Kammerloher, W.; Freund, C.; Wülfing, C.; Burkert, U. I.; Matern, D. H.; Breuer, M.; Eulitz, M.; Küfrevioglu, Ö. I.; and Hartmann, G. R.; Isolation and Properties of a Nitrile Hydratase from the Soil Fungus *Myrothecium verrucaria* that is Highly Specific for the Fertilizer Cyanamide and Cloning of its Gene; *Proceedings of the National Academy of Science of the United States of America*, **1991**, 88, 4260-4264.

Malmström, B. G.; Rack-Induced Bonding in Blue-Copper Proteins; *European Journal of Biochemistry*, **1994**, 223, 711-718.

March, J.; Advanced Organic Chemistry; 4th ed.; John Wiley & Sons: New York, NY, U.S.A., **1992**.

Marini, P. J.; Murray, K. S.; and West, B. O.; Iron Complexes of N-Substituted Thiosalicylideneimines. Part 1. Synthesis and Reactions with Oxygen and Carbon Monoxide; *Journal of the Chemical Society, Dalton Transactions*, **1983**, 143-151.

Marlin, D. S. and Mascharak, P. K.; Coordination of Carboxamido Nitrogen to Tervalent Iron: Insight into a New Chapter of Iron Chemistry; *Chemical Society Reviews*, **2000**, 29, 69-74.

Marlin, D. S.; Olmstead, M. M.; and Mascharak, P. K.; Carboxamido Nitrogens Are Good Donors for Fe(III): Syntheses, Structures, and Properties of Two Low-Spin Nonmacrocyclic Iron(III) Complexes with Tetracarboxamido-N Coordination; *Inorganic Chemistry*, **1999**, 38, 3258-3260.

Marlin, D. S.; Olmstead, M. M.; and Mascharak, P. K.; Chemistry of Iron(III) Complexes of *N*,*N*'-bis(2-hydroxyphenyl)-pyridine-2,6-dicarboxamide: Seven-coordinate Iron(III) Complexes Ligated to Deprotonated Carboxamido Nitrogens; *Inorganica Chimica Acta*, **2000**, 297, 106-114.

Márquez, V. E.; Anacona, J. R.; Hurtado, R. J.; Díaz de Delgado, G.; and Roque, E. M.; Reactivity of a Binuclear Nickel(II) Sulfur Bridged Complex with Alkylating Agents, Crystal Structure of $[Ni(L)Br(\mu\text{-}Br)]_2$ (L = 2,6-Bis-[(benzyl)mercaptomethyl]pyridine); *Polyhedron*, **1999**, 18, 1903-1908.

Meagher, K. K.; Bocarsly, A. B.; Bernasek, S. L.; and Ramanarayanan, T. A.; Interaction of Neopentylthiol with Clean and Oxygen-Modified Fe(100) Surfaces; *Journal of Physical Chemistry B*, **2000**, 104, 3320-3326.

Meehan, E. J.; Kolthoff, I. M.; and Kakiuchi, H.; Reaction between Ferricyanide and 2-Mercaptoethanol; *Journal of Physical Chemistry*, **1962**, 66, 1238-1241.

Meth-Cohn, O. and Wang, M.-X.; An In-Depth Study of the Biotransformation of Nitriles into Amides and/or Acids Using *Rhodococcus rhodochrous* AJ270; *Journal of the Chemical Society, Perkin Transactions I*, **1997**, 1099-1104.

Miessler, G. L. and Tarr, D. A.; Inorganic Chemistry; 1st ed.; Prentice Hall: Englewood Cliffs, NJ, U.S.A., **1991**.

Migot, J.-L.; Sala-Pala, J.; and Guerchais, J.-E.; Niobium Organometallic Chemistry X. Synthesis of New (η^2-Disulfido) Complexes; Comparison of Their Reactivity with that of (η^2-Dioxo) Derivatives; *Journal of Organometallic Chemistry*, **1983**, 243, 427-436.

Mirza, S. A.; Day, R. O.; and Maroney, M. J.; Oxidation of a Dimeric Nickel Thiolate Complex with O_2; *Inorganic Chemistry*, **1996**, 35, 1992-1995.

Morikita, T.; Hirano, M.; Sasaki, A.; and Komiya, S.; C-S, C-H, and N-H Bond Cleavage of Heterocycles by a Zero-Valent Iron Complex, $Fe(N_2)(depe)_2$ [depe = 1,2-Bis(diethylphosphino)ethane]; *Inorganica Chimica Acta*, **1999**, 291, 341-354.

Mulay, L. N. and Boudreaux, E. A.; Theory and Applications of Molecular Diamagnetism; 1st ed.; John Wiley & Sons: New York, NY, U.S.A.,**1976**.

Mullen, G. E. D.; Went, M. J.; Wocadlo, S.; Powell, A. K.; and Blower, P. J.; Electron Transfer Induced C-S Bond Cleavage in Rhenium and Technetium Thioether Complexes: Structural and Chemical Evidence for π Back-Donation to C-S σ^* Orbitals; *Angewandte Chemie, International Edition in English*, **1997**, 36, 1205-1207.

Murakami, T.; Nojiri, M.; Nakayama, H.; Odaka, M.; Yohda, M.; Dohmae, N.; Takio, K.; Nagamune, T.; and Endo, I.; Post-Translational Modification is

Essential for Catalytic Activity of Nitrile Hydratase; *Protein Science*, **2000**, 9, 1024-1030.

Nagamune, T.; Honda, J.; Kobayashi, Y.; Sasabe, H.; Endo, I.; Ambe, F.; Teratani, Y.; and Hirata, A.; Mössbauer, Electron Paramagnetic Resonance, and Magnetic Susceptibility Studies of Photosensitive Nitrile Hydratase from *Rhodococcus* sp. N-771; *Hyperfine Interactions*, **1992**, 71, 1271-1274.

Nagamune, T.; Kurata, H.; Hirata, M.; Honda, J.; Koike, H.; Ikeuchi, M.; Inoue, Y.; Hirata, A.; and Endo, I.; Purification of Inactivated Photoresponsive Nitrile Hydratase; *Biochemical and Biophysical Research Communications*, **1990**, 168, 437-442.

Nagasawa, T.; Nanba, H.; Ryuno, K.; Takeuchi, K.; and Yamada, H.; Nitrile Hydratase of *Pseudomonas chlororaphis* B23. Purification and Characterization; *European Journal of Biochemistry*, **1987**, 162, 691-698.

Nagasawa, T.; Ryuno, K.; and Yamada, H.; Nitrile Hydratase of *Brevibacterium* R312; *Biochemical and Biophysical Research Communications*, **1986**, 139, 1305-1312.

Nagasawa, T.; Shimizu, H.; and Yamada, H.; The Superiority of the Third-Generation Catalyst, *Rhodococcus rhodochrous* J1 Nitrile Hydratase, for Industrial Production of Acrylamide; *Applied Microbiology and Biotechnology*, **1993**, 40, 189-195.

Nagasawa, T.; Takeuchi, K.; and Yamada, H.; Characterization of a New Cobalt-Containing Nitrile Hydratase Purified from Urea-Induced Cells of *Rhodococcus rhodochrous* J1; *European Journal of Biochemistry*, **1991**, 196, 581-589.

Nagasawa, T.; Takeuchi, K.; and Yamada, H.; Occurrence of a Cobalt-Induced and Cobalt-Containing Nitrile Hydratase in *Rhodococcus rhodochrous* J1; *Biochemical and Biophysical Research Communications*; **1988**, 155, 1008-1016.

Nagashima, S.; Nakasako, M.; Dohmae, N.; Tsujimura, M.; Takio, K.; Odaka, M.; Yohda, M.; Kamiya, N.; and Endo, I.; Novel Non-Heme Iron Center of Nitrile Hydratase with a Claw Setting of Oxygen Atoms; *Nature Structural Biology*, **1998**, 5, 347-351.

Nawaz, M. S.; Chapatwala, K. D.; and Wolfram, J. H.; Degradation of Acetonitrile by *Pseudomonas putida*; *Applied and Environmental Microbiology*, **1989**, 55, 2267-2274.

Nelson, M. J.; Jin, H.; Turner, I. M., Jr.; Grove, G.; Scarrow, R. C.; Brennan, B. A.; and Que, L., Jr.; A Novel Iron-Sulfur Center in Nirile Hydratase from *Brevibacterium sp.*; *Journal of the American Chemical Society*; **1991**, 113, 7072-7073.

Nivorozhkin, A. L.; Uraev, A. I.; Bondarenko, G. I.; Antsyshkina, A. S.; Kurbatov, V. P.; Garnovskii, A. D.; Turta, C. I.; and Brashoveanu, N. D.; Iron Complexes with an N/S Chromophore Relevant to the Active Site of the Hydrolytic Metalloenzyme Nitrile Hydratase; *Chemical Communications*, **1997**, 1711-1712.

Noguchi, T.; Honda, J.; Nagamune, T.; Sasabe, H.; Inoue, Y.; and Endo, I.; Photosensitive Nitrile Hydratase Intrinsically Possesses Nitric Oxide Bound to the Non-Heme Iron Center: Evidence by Fourier Transform Infrared Spectroscopy; *FEBS Letters*, **1995**, 358, 9-12.

Noguchi, T.; Hoshino, M.; Tsujimura, M.; Odaka, M.; Inoue, Y.; and Endo, I.; Resonance Raman Evidence that Photodissociation of Nitric Oxide from the

Non-Heme Iron Center Activates Nitrile Hydratase from *Rhodococcus* sp. N-771; *Biochemistry*, **1996**, 35, 16777-16781.

Nojiri, M.; Nakayama, H.; Odaka, M.; Yohda, M.; Takio, K.; and Endo, I.; Co-Substituted Fe-Type Nitrile Hydratase of *Rhodococcus sp.* N-771; *FEBS Letters*, **2000**, 465, 173-177.

Nojiri, M.; Yohda, M.; Odaka, M.; Matsushita, Y.; Tsujimura, M.; Yoshida, T.; Dohmae, N.; Takio, K.; and Endo, I.; Functional Expression of Nitrile Hydratase in *Escherichia coli*: Requirement of a Nitrile Hydratase Activator and Post-Translational Modification of a Ligand Cysteine; *Journal of Biochemistry (Tokyo)*, **1999**, 125, 696-704.

Noveron, J. C.; Herradora, R.; Olmstead, M. M.; and Mascharak, P. K.; Low-Spin Iron(III) Complexes with N,S Coordination: Syntheses, Structures, and Properties of Bis(N-2-mercaptophenyl-2'-pyridylmethyl-eniminato)iron(III) Tetraphenylborate and Bis(N-2-mercapto-2-methyl-propyl-2'-pyridylmethyleniminato)iron(III) Tetraphenylborate; *Inorganica Chimica Acta*, **1999**, 285, 269-276.

Noveron, J. C.; Olmstead, M. M.; and Mascharak, P. K.; A Synthetic Analogue of the Active Site of Fe-Containing Nitrile Hydratase with Carboxamido N and Thiolato S as Donors: Synthesis, Structure, and Reactivities; *Journal of the American Chemical Society*, **2001**, 123, 3247-3259.

Noveron, J. C.; Olmstead, M. M.; and Mascharak, P. K.; Co(III) Complexes with Carboxamido N and Thiolato S Donor Centers: Models for the Active Site of Co-Containing Nitrile Hydratases; *Journal of the American Chemical Society*, **1999**, 121, 3553-3554.

Noveron, J. C.; Olmstead, M. M.; and Mascharak, P. K.; Effect of Carboxamido N Coordination to Iron on the Redox Potential of Low-Spin Non-Heme Iron

Centers with N,S Coordination: Relevance to the Iron Site of Nitrile Hydratase; *Inorganic Chemistry*, **1998**, 37, 1138-1139.

O'Connor, C. J.; Magnetochemistry - Advances in Theory and Experimentation; *Progress in Inorganic Chemistry*, **1982**, 29, 203-283.

Odaka, M.; Fujii, K.; Hoshino, M.; Noguchi, T.; Tsujimura, M.; Nagashima, S.; Yohda, M.; Nagamune, T.; Inoue, Y.; and Endo, I.; Activity Regulation of Photoreactive Nitrile Hydratase by Nitric Oxide; *Journal of the American Chemical Society*, **1997**, 119, 3785-3791.

Odaka, M.; Noguchi, T.; Nagashima, S.; Yohda, M.; Yabuki, S.; Hoshino, M.; Inoue, Y.; and Endo, I.; Location of the Non-Heme Iron Center on the a Sub-unit of Photoreactive Nitrile Hydratase from *Rhodococcus* sp. N-771; *Biochemical and Biophysical Research Communications*; **1996**, 221, 146-150.

Pantoliano, M. W.; Whitlow, M.; Wood, J. F.; Dodd, S. W.; Hardman, K. D.; Rollence, M. L.; and Bryan, P. N.; Large Increases in General Stability for Subtilisin BPN' through Incremental Changes in the Free Energy of Unfolding; *Biochemistry*, **1989**, 28, 7205-7213.

Payne, M. S.; Wu, S.; Fallon, R. D.; Tudor, G.; Stieglitz, B.; Turner, I. M., Jr.; and Nelson, M. J.; A Stereoselective Cobalt-Containing Nitrile Hydratase; *Biochemistry*, **1997**, 36, 5447-5454.

Peters, J. W.; Stowell, M. H. B.; Soltis, S. M.; Finnegan, M. G.; Johnson, M. K.; and Rees, D. C.; Redox-Dependent Structural Changes in the Nitrogenase P-Cluster; *Biochemistry*, **1997**, 36, 1181-1187.

Pianzzola, M. J.; Soubes, M.; and Touati, D.; Overproduction of the *rbo* Gene Product from *Desulfovibrio* Species Suppresses All Deleterious Effects of Lack of Superoxide Dismutase in *Escherichia coli*; *Journal of Bacteriology*, **1996**, 178, 6736-6742.

Piersma, S. R.; Nojiri, M.; Tsujimura, M.; Noguchi, T.; Odaka, M.; Yohda, M.; Inoue, Y.; and Endo, I.; Arginine 56 Mutation in the β Subunit of Nitrile Hydratase: Importance of Hydrogen Bonding to the Non-Heme Iron Center; *Journal of Inorganic Biochemistry*, **2000**, 80, 283-288.

Ploegman, J. H.; Drent, G.; Kalk, K. H.; and Hol, W. G. J.; The Structure of Bovine Liver Rhodanese: II. The Active Site in the Sulfur-Substituted and the Sulfur-Free Enzyme; *Journal of Molecular Biology*, **1979**, 127, 149-162.

Quickenden, T. I. and Marshall, R. C.; Magnetochemistry in SI Units; *Journal of Chemical Education*, **1972**, 49, 114-116.

Ramakrishna, C. and Desai, J. D.; Superiority of Cobalt-Induced Acrylonitrile Hydratase of *Arthrobacter sp.* IPCB-3 for Conversion of Acrylonitrile to Acrylamide; *Biotechnology Letters*, **1993**, 15, 267-270.

Ramírez, E. C. and Whitaker, J. R.; Cystine Lyases in Plants: A Comprehensive Review; *Journal of Food Biochemistry*, **1998**, 22, 427-440.

Rat, M.; Alves de Sousa, R.; Vaissermann, J.; Leduc, P.; Mansuy, D.; and Artaud, I.; Clean Oxidation of Thiolates to Sulfinates in a Four-Coordinate Co(III) Complex with a mixed carboxamido N-thiolato S donor set: Relevance to Nitrile Hydratase; *Journal of Inorganic Biochemistry*, **2001**, 84, 207-213.

Richter-Addo, G. B. and Legzdins, P.; Metal Nitrosyls; 1st ed.; Oxford University Press: New York, NY, U.S.A., **1992**.

Root, M. J.; Adzamli, I. K.; and Deutsch, E.; Intramolecular Redox Decomposition of $[(en)_2Co(SCH_2CH_2NH_2)]^{2+}$ and Related Complexes; *Inorganic Chemistry*, **1981**, 20, 4017-4019.

Rowland, J. M.; Thornton, M. L.; Olmstead, M. M.; and Mascharak, P. K.; Structure Variation Due to Ligand Flexibility: Syntheses and Structures of

the Copper(II) Complexes [Cu(APPy)] and [$Cu_2(AEPy)_2$] Where $APPyH_2$ = Bis[3-(2-pyridinecarboxamido)propyl]-methylamine and $AEPyH_2$ = Bis[3-(2-pyridinecarboxamido)ethyl]-methylamine; *Inorganic Chemistry*, **2001**, 40, 1069-1073.

Scarrow, R. C.; Brennan, B. A.; Cummings, J. G.; Jin, H.; Duong, D. J.; Kindt, J. T.; and Nelson, M. J.; X-ray Spectroscopy of Nitrile Hydratase at pH 7 and 9; *Biochemistry*, **1996**, 35, 10078-10088.

Scarrow, R. C.; Strickler, B. S.; Ellison, J. J.; Shoner, S. C.; Kovacs, J. A.; Cummings, J. G.; and Nelson, M. J.; X-ray Spectroscopy of Nitric Oxide Binding to Iron in Inactive Nitrile Hydratase and a Synthetic Model Compound; *Journal of the American Chemical Society*, **1998**, 120, 9237-9245.

Schneider, J. L.; Carrier, S. M.; Ruggiero, C. E.; Young, V. G., Jr.; and Tolman, W. B.; Influences of Ligand Environment on the Spectroscopic Properties and Disproportionation Reactivity of Copper-Nitrosyl Complexes; *Journal of the American Chemical Society*, **1998**, 120, 11408-11418.

Schubert, E. M.; Utilizing the Evans Method with a Superconducting NMR Spectrometer; *Journal of Chemical Education*, **1992**, 69, 62.

Schubert, M. P.; A New Complex of Cobalt and Cysteine and its Behavior with Hydrogen Peroxide; *Journal of the American Chemical Society*, **1933**, 55, 3336-3342.

Schweitzer, D.; Ellison, J. J.; Shoner, S. C.; Lovell, S.; and Kovacs, J. A.; A Synthetic Model for the NO-Inactivated Form of Nitrile Hydratase; *Journal of the American Chemical Society*, **1998**, 120, 10996-10997.

Schweitzer, D.; Rittenberg, D. K.; and Kovacs, J. A.; Manuscript in Preparation.

Schweitzer, D.; Shearer, J.; Rittenberg, D. K.; Shoner, S. C.; Ellison, J. J.; Loloee, R.; Lovell, S.; Barnhart, D.; and Kovacs, J. A.; Enhancing Reactivity via Ligand Constraints; Submitted for Publication.

Schweitzer, D.; Taylor, W. D.; and Kovacs, J. A.; Synthetic Models of the Active Site of Nitrile Hydratase; *Journal of Inorganic Biochemistry*, **1999**, 74, 291.

Sellmann, D.; Kunstmann, H.; Moll, M.; and Knoch, F.; Transition Metal Complexes with Sulfur Ligands; *Inorganica Chimica Acta*, **1988**, 154, 157-167.

Sheldrick, G. M.; SHELXL97, A Program for the Refinement of Crystal Structures. University of Göttingen, Germany.

Shoner, S. C.; Barnhart, D.; and Kovacs, J. A.; A Model for the Low-Spin, Non-Heme, Thiolate-Ligated Iron Site of Nitrile Hydratase; *Inorganic Chemistry*, **1995**, 34, 4517-4518.

Sloan, C. P. and Krueger, J. H.; Oxidation of Coordinated Cysteine. Formation of Sulfinato- and Sulfenatocobalt(III) Complexes; *Inorganic Chemistry*, **1975**, 14, 1481-1485.

Smee, J. J.; Goodman, D. C.; Reibenspies, J. H.; and Darensbourg, M. Y.; Models for Terminal Ni(S-Cysteine) Modification in [NiFe]Hydrogenases by Iodoacetamide and Iodoacetate; *European Journal of Inorganic Chemistry*, **1999**, 539-546.

Song, L.-C.; Hu, Q.-M.; and Qin, X.-D.; Synthesis of $(\eta^5\text{-}R^1C_5H_4)(CO)_2Mo(\eta^2\text{-}S_2R)$ via Reaction of $(\mu\text{-}RS)(\mu\text{-}p\text{-}MeC_6H_4SO_2S)Fe_2(CO)_6$ with Nucleophiles $(\eta^5\text{-}R^1C_5H_4)(CO)_3MoSeNa$. Crystal Structure of $(\eta^5\text{-}MeO_2CC_5H_4)(CO)_2Mo(\eta^2\text{-}S_2Bu^t)$; *Journal of Chemical Research, Synopsis*, **1999**, 84-85.

Sono, M.; Roach, M. P.; Coulter, E. D.; and Dawson, J. H.; Heme-Containing Oxygenases; *Chemical Reviews*, **1996**, 96, 2841-2887.

Sorrell, T. N.; Allen, W. E.; and White, P. S.; Sterically Hindered [Tris(imidazolyl)phosphine]copper Complexes: Formation and Reactivity of a Peroxo-Dicopper(II) Adduct and Structure of a Dinuclear Carbonate-Bridged Complex; *Inorganic Chemistry*, **1995**, 34, 952-960.

Sugiura, Y.; Kuwahara, J.; Nagasawa, T.; and Yamada, H.; Nitrile Hydratase: The First Non-Heme Iron Enzyme with a Typical Low-Spin Fe(III)-Active Center; *Journal of the American Chemical Society*; **1987**, 109, 5848-5850.

Sun, T. F.; Schouten, J. A.; Trappeniers, N. J.; and Biswas, S. N.; Measurements of the Densities of Liquid Benzene, Cyclohexane, Methanol, and Ethanol as Functions of Temperature at 0.1 MPa; *Journal of Chemical Thermodynamics*, **1988**, 20, 1089-1096.

Surdhar, P. S. and Armstrong, D. A.; Redox Potentials of Some Sulfur-Containing Radicals; *Journal of Physical Chemistry*, **1986**, 90, 5915-5917.

Surdhar, P. S. and Armstrong, D. A.; Reduction Potentials and Exchange Reactions of Thiyl Radicals and Disulfide Anion Radicals;*Journal of Physical Chemistry*, **1987**, 91, 6532-6537.

Timmons, J. H.; Martin, J. W. L.; Martell, A. E.; Rudolf, P. R.; and Clearfield, A.; Crystal and Molecular Structure of (5,5,8,8,13,13,16,16-Octamethyl-1,4,9,12-tetraazacyclohexadeca-1,3,9,11-tetraene)copper(I) Perchlorate. A Model for the Entatic State in Blue Copper Proteins; *Inorganic Chemistry*, **1988**, 27, 1638-1640.

Tsujimura, M.; Dohmae, N.; Odaka, M.; Chijimatsu, M.; Takio, K.; Yohda, M.; Hoshino, M.; Nagashima, S.; and Endo, I.; Structure of the Photoreactive Iron Center of the Nitrile Hydratase from *Rhodococcus* sp. N-771. Evidence

of a Novel Post-Translational Modification in the Cysteine Ligand; *Journal of Biological Chemistry*, **1997**, 272, 29454-29459.

Tyler, L. A.; Noveron, J. C.; Olmstead, M. M.; and Mascharak, P. K.; Co(III) Complexes with Coordinated Carboxamido Nitrogens and Thiolato Sulfurs as Models for Co-Containing Nitrile Hydratase and Their Conversion to the Corresponding Sulfinato Species; *Inorganic Chemistry*, **2000**, 39, 357-362.

Tyler, L. A.; Noveron, J. C.; Olmstead, M. M.; and Mascharak, P. K.; Oxidation of Metal-Bound Thiolato Sulfur Centers in Fe(III) and Co(III) Complexes with Carboxamido Nitrogens and Thiolato Sulfurs as Donors: Relevance to the Active Sites of Nitrile Hydratases; *Inorganic Chemistry*, **1999**, 38, 616-617.

Ueno, T.; Ueyama, N.; and Nakamura, A.; Fe-S Cluster Formation by C-S Bond Cleavage Reaction of Mononuclear Fe(II) Cysteine-Containing Peptide Complexes; *Journal of Inorganic Biochemistry*, **1997**, 67, 262.

Vallee, B. L. and Williams, R. J. P.; Metalloenzymes: The Entatic Nature of their Active Sites; *Proceedings of the National Academy of Science of the United States of America*, **1968**, 59, 498-505.

Van Geet, A. L.; Calibration of the Methanol and Glycol Nuclear Magnetic Resonance Thermometers with a Static Thermistor Probe; *Analytical Chemistry*, **1968**, 40, 2227-2229.

Vogler, C.; Kaim, W.; and Hausen, H.-D.; Zweikernige Bisphosphankupfer(I)-Komplexe mit dem 2,2'-Bipyrimidin-Brückenliganden: Strukturelle Analogie zu "Blauen" Kupferzentren und Reduktion zu Paramagnetischen Spezies; *Zeitschrift für Naturforschung B: A Journal of Chemical Sciences*, **1993**, 48b, 1470-1480.

Vosáhlová, J.; Pavlu, L.; Vosáhlo, J.; and Brenner, V.; Degradation of Bromoxynil, Ioxynil, Dichlobenil, and Their Mixtures by *Agrobacterium radiobacter* 8/4; *Pesticide Science*, **1997**, 49, 303-306.

Wallace, T. J.; Reactions of Thiols with Metals. II. Low-Temperature Oxidation by Soluble Metal Salts; *Journal of Organic Chemistry*, **1966**, 31, 3071-3074.

Warzeska, S. and Krämer, R.; A Dicopper(II) Complex of a New Octaaza Macrocycle: A Receptor in the Entatic State; *Chemical Communications*, **1996**, 499-500.

White, D. J.; Cronin, L.; Parsons, S.; Robertson, N.; Tasker, P. A.; and Bisson, A. P.; Control of Copper(II) Coordination Geometry via Supramolecular Assembly of Ligands in the Solid State; *Chemical Communications*, **1999**, 1107-1108.

Williams, R. J. P.; Energised (Entatic) States of Groups and of Secondary Structures in Proteins and Metalloproteins; *European Journal of Biochemistry*, **1995**, 234, 363-381.

Wyatt, J. M. and Knowles, C. J.; Microbial Degradation of Acrylonitrile Waste Effluents: the Degradation of Effluents and Condensates from the Manufacture of Acrylonitrile; *International Biodeterioration & Biodegradation*, **1995**, 35, 227-248.

Wyman, D. P. and Kaufman, P. R.; The Chlorination of Active Hydrogen Compounds with Sulfuryl Chloride. I. Ketones; *Journal of Organic Chemistry*, **1964**, 29, 1956-1960.

Xan, J.; Wilson, E. A.; Roberts, L. D.; and Horton, N. H.; The Absorption of Oxygen by Mercaptans in Alkaline Solution; *Journal of the American Chemical Society*, **1941**, 63, 1139-1141.

Yamada, H. and Kobayashi, M.; Nitrile Hydratase and Its Application to Industrial Production of Acrylamide; *Bioscience, Biotechnology, and Biochemistry*, **1996**, 60, 1391-1400.

Yamanari, K.; Kawamoto, T.; Kushi, Y.; Komorita, T.; and Fuyuhiro, A.; Sulfenato and Sulfinato Complex Formation via Oxidation of *OC*-6-3'2-Bis{2-[(2-pyridylmethyl)amino]ethanethiolato}cobalt(III) (1+) Complex by Molecular Dioxygen; *Bulletin of the Chemical Society of Japan*, **1998**, 71, 2635-2643.

Yeh, A. P.; Hu, Y.; Jenney, F. E., Jr.; Adams, M. W. W.; and Rees, D. C.; Structures of the Superoxide Reductase from *Pyrococcus furiosus* in the Oxidized and Reduced States; *Biochemistry*, **2000**, 39, 2499-2508.

Zheng, L. and Dean, D. R.; Catalytic Formation of a Nitrogenase Iron-Sulfur Cluster; *Journal of Biological Chemistry*, **1994**, 269, 18723-18726.

Zheng, L.; White, R. H.; Cash, V. L.; and Dean, D. R.; Mechanism for the Desulfurization of L-Cysteine Catalyzed by the *nifS* Gene Product; *Biochemistry*, **1994**, 33, 4714-4720.